High Resolution Seismic Reflection Profiling at Aberdeen Proving Grounds, Maryland

Richard D. Miller
Jianghai Xia
Joe M. Anderson
David R. Laflen
Sara Marcus

Kansas Geological Survey
1930 Constant Avenue
Lawrence, Kansas 66047

Final Report to

U.S. Army Corps of Engineers
Waterways Experiment Station
Vicksburg, Mississippi

Open-file Report No. 95-22 July 28, 1995

High Resolution Seismic Reflection Profiling at Aberdeen Proving Grounds, Maryland

by
Richard D. Miller
Jianghai Xia
Joe M. Anderson
David R. Laflen
Sara Marcus

of the
Kansas Geological Survey

Final Report
to
U.S. Army Corps of Engineers
Waterways Experiment Station
Vicksburg, Mississippi

Open-file Report No. 95-22
July 28, 1995

SUMMARY

The effectiveness of shallow high resolution seismic reflection (i.e., resolution potential) to image geologic interfaces between about 70 and 750 ft at the Aberdeen Proving Grounds, Maryland (APG), appears to vary locally with the geometric complexity of the unconsolidated sediments that overlay crystalline bedrock. The bedrock surface (which represents the primary geologic target of this study) was imaged at each of three test areas on walkaway noise tests and CDP (common depth point) stacked data. Optimum acquisition equipment and parameters were determined through analysis of walkaway noise tests performed at each of the three test areas. Source testing involved an accelerated weight drop, land air gun, downhole black powder charge, sledge hammer/plate, and high frequency vibrator. Proven high resolution techniques (Steeples and Miller, 1990) were used to design and acquire data on this survey. Production data were collected in a standard CDP format (Mayne, 1962) using roll-along acquisition techniques similar to conventional petroleum exploration data acquisition. Shallow seismic reflection enhanced the resolution, accuracy, and reliability of the horizontal extrapolation of one-dimensional borehole geology to two-dimensional geologic cross-sections.

Interpretations of reflections from unconsolidated lithologic interfaces between the bedrock and ground surface possess varying degrees of resolution and confidence. Reflectors from 70 ft to over 750 ft of depth (depending on the line location) were imaged on data with average practical vertical bed resolution limit of about 15 to 20 ft. CDP stacked sections were correlated with available borehole geology using a combination of stacking velocities and borehole-determined average and interval velocities. Most major clay and sand sequences (i.e., high percentage of clay/sand over at least 20 ft [1/2 wavelength]) identified in boreholes were confidently correlated to coherent reflections on both walkaway data and CDP stacked sections.

Shallow seismic reflection profiles provided for a more detailed and realistic picture of the geometric complexity and variability of the distinct clay sequences (aquatards) previously only inferred from drilling to be present based on sparse drill holes and basewide conceptual models (Swartzel and Miller, 1992). The seismic data also reveal a clear explanation for the difficulties previously noted in correlating individual, borehole-identified sand or clay units over even short distances (Vroblesky and Fleck, 1991). Geologic cross-sections derived from CDP stacked data and borehole logs suggest locally complex geometries and horizontally variable geologic contacts near the western boundary fence west of the three-mile test track

while a much more consistent, uniform subsurface is suggested south of Phillips Airstrip and on Spesutie Island.

This seismic reflection feasibility study included three sites, each with uniquely different primary target depths and surface conditions (Figure 1). Feasibility of the technique and minimum acquisition requirements were determined through evaluation and correlation of walkaway noise tests, CDP survey lines (1.2, 0.5, and 0.3 miles), and a downhole velocity check shot survey. Data processing and analysis revealed several critical attributes of shallow seismic data from APG that need careful consideration and compensation on reflection data sets. The goals of this survey were to determine: 1) the feasibility of the technique, 2) the resolution potential (both horizontal and vertical) of the technique, 3) the optimum source for this site, 4) the optimum acquisition geometries, 5) general processing flow, and 6) a basic idea of the acoustic variability across this site. Shallow seismic reflection effectively imaged the subsurface, to varying degrees, at all three test sites at APG.

The extensive series of source comparisons performed at each of the three sites generally agree—when considering the non-invasive, total energy, spectral requirements, and imaging goals of the area—a high frequency vibratory source seems most effective in the 70 to 750 ft depth range. With the structural complexity and the short wavelength geometric variability observed along the western boundary it seems prudent to acquire multi-fold CDP data using an end-on source/receiver orientation. End-on acquisition generally allows more recording channels to be evenly distributed across a given spread length, thus improving trace-to-trace coherency of rapidly changing interfaces as well as improving accuracy of the velocity function. For target depths between 30 and 70 ft, source and geophone spacing should not exceed 4 ft with a minimum source-to-farthest-offset distance of around 100 ft. To image reflectors between 70 and 300 ft of depth the source and receiver station spacing should not exceed 10 ft, with a source-to-farthest-receiver offset of at least 250 ft. For deeper targets, on Spesutie Island for example, source and receiver station spacing should be on the order of 15 ft with a farthest receiver offset of at least 600 ft. The processing flow that optimizes the signal-to-noise and resolution is fairly similar to those used in petroleum exploration, except for the high level of time and effort required for editing and the lack of wavelet suppression.

From a basewide perspective, the technique proved successful in imaging the bedrock surface and primary sedimentary contacts between 70 and 750 ft at APG. Site-specific capabilities and specifications of the technique at APG must include consideration of near-surface conditions, geologic target depths, and resolution

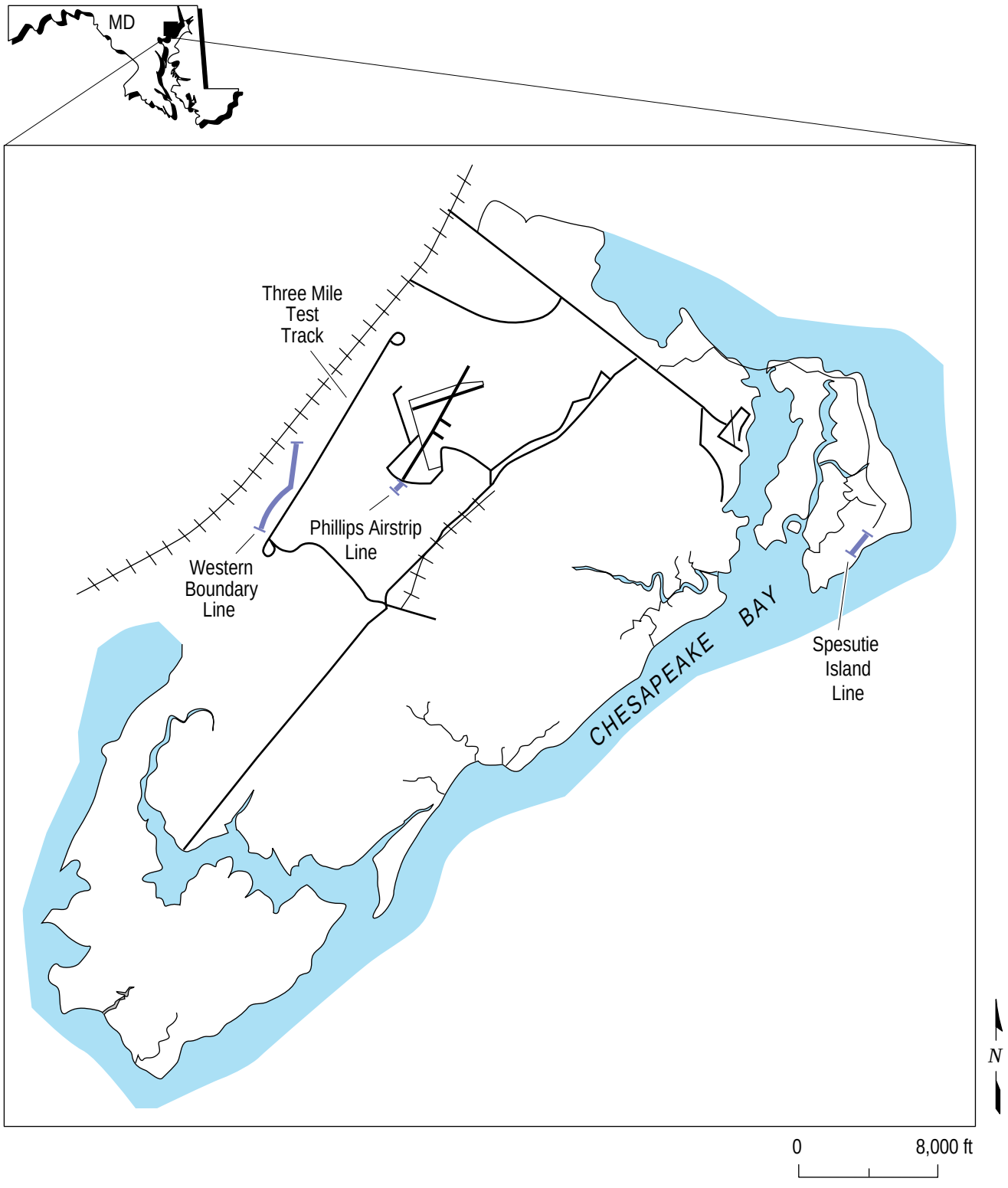

Figure 1. Aberdeen Proving Grounds, Maryland, with general line locations and names.

requirements (vertical and horizontal). At the sites tested in this study the theoretical vertical bed resolution limit (frequency and velocity dependent) was about 10 ft with a practical bed resolution limit on the order of 15 or so feet. Horizontal resolution (depth, frequency, and velocity dependent) is proportional to the radius of the first Fresnel zone, which at a depth of around 150 ft is approximately 50 ft. If interpreted reflections from the three sites are representative of acoustic signatures and reflector geometries at APG, seismic reflection programs, if properly planned and executed, could provide extremely useful information to complement existing geologic data and guide placement of future boreholes and monitor wells. Shallow seismic reflection greatly improved the detail and resolution of geologic cross-sections as well as substantiated speculative well-to-well correlations on cross-sections derived from drilling alone.

INTRODUCTION

The APG compound occupies approximately 123 square miles directly north of Baltimore on the Chesapeake Bay. Geologically, APG is located on the northern edge of the Atlantic Coastal Plain physiographic province. The bedrock surface in this area is composed predominantly of metamorphosed sedimentary and igneous rocks (Owens, 1969). Regionally the bedrock surface is believed to dip to the east beneath APG from a depth of around 200 ft to more than 1000 ft at an average of about 75 ft/mile (Swartzel and Miller, 1992). The sediments that overlie bedrock are Cretaceous clays, silts, sands, and gravels. These infilled sediments begin at the Fall Line and thicken to the southeast, forming a wedge. This wedge of sediments was tailored by transgressive and regressive seas during the Cretaceous. These cyclic seas have resulted in several subparallel clay layers with apparent dip consistent with the bedrock surface. Near-surface and surface materials and topography have been recently altered by glacial and river activities. Knowledge of the consistency, surface topography, and thickness of confining clay layers is critical to the hydrologic understanding of this site.

This feasibility study, which began on December 2, 1994, and continued through December 13, 1994, consisted of two major phases: testing and production. The testing phase was carried out at each of three sites and included source, receiver, and geometry evaluations. Walkaway noise spreads were used as the acquisition format for testing. Analysis of common shot gathers for each unique source, seismograph, receiver, or geometry configuration provided valuable insight into the acoustic nature of the site. A velocity check shot survey conducted in the 170 ft

deep, PVC cased monitor well #WB-MW-15C, located just west of Phillips Field, provided partial one-way and interval travel times important for calibration of normal moveout (NMO) velocities used in time-to-depth conversions of CDP stacked sections. The quality of field testing and analysis allowed optimization of available equipment for the acquisition of production CDP data.

The production phase of the project included four nominal 24-fold CDP lines: two at the western boundary fence (0.6 miles each), one south of Phillips Airstrip (0.3 miles), and one on Spesutie Island (0.5 miles). Acquisition of production data required five days and followed well-established procedures, ever mindful of QA/QC. Based on subtle changes in the near-surface, minor adjustments to some parameters were necessary to maintain the optimum recording window (Hunter et al., 1984). The basic structure of both the acquisition and processing flow was roughly designed around the findings of the preliminary testing. QA/QC were critical and continuous, allowing for adjustments necessary to ensure the highest data quality possible throughout the acquisition and processing phases of the survey.

DATA ACQUISITION

Data for this study were acquired on a 48-channel Geometrics StrataView seismograph. The seismograph amplifies, digitizes the analog signal into a 21-bit word, digitally filters displayed data, and stores the digital information in a demultiplexed SEG2 format. The StrataView has the ability to record an auxiliary pilot trace on channel 1 that can be either saved coincident with the other channels or used for in-field correlation with the other (47 in this case) channels. For the impulsive sources, 1024 samples were recorded at a 1/2 msec sampling interval, providing a 512 msec record with a 1000 Hz Nyquist frequency. For the vibratory source a total of 6144 msec of data were recorded at a 1/2 ms sampling interval. This floating-point seismograph possesses a dynamic range that was more than adequate to record high-quality reflection information in the presence of source-generated and cultural noise at this site.

Walkaway Noise Tests

The 192-trace common shot walkaway noise tests were conducted along segments of three CDP survey lines (Figure 2). Sources and source configurations tested included the Bolt LSS-6 land air gun (500 and 1500 psi with 20 cubic inch chamber), 12 lb sledge hammer and steel plate, rubberband accelerated weight drop (Bison EWG equivalent), IVI MiniVib (several sweeps, in-field correlated against

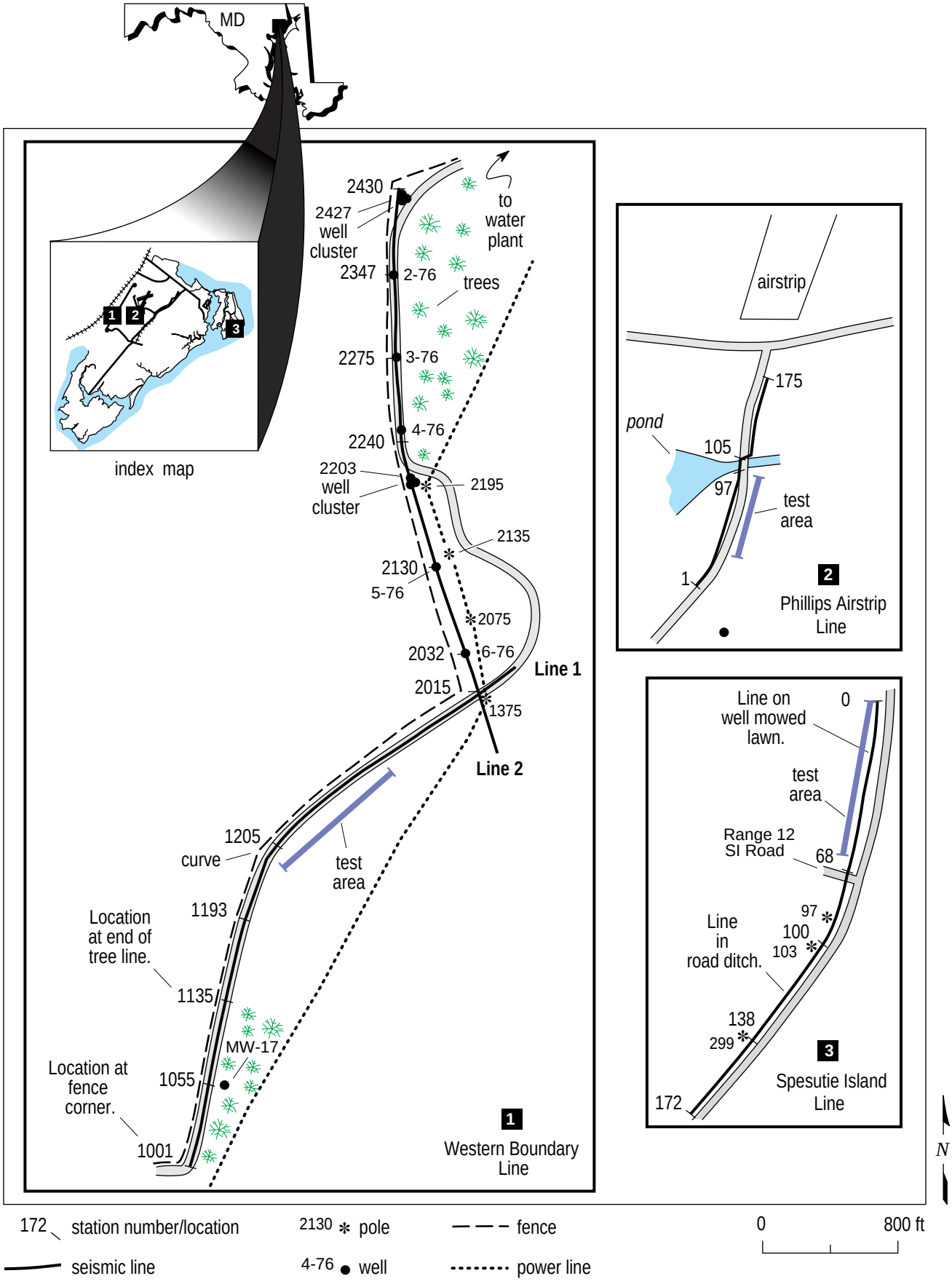

Figure 2. Site maps of each of the CDP lines with station numbers at landmarks and tie points.

drive signal, ground force, and filtered ground force; recorded uncorrelated; and with a taper of .1 sec, 1 sec, 2 sec, and 3 sec) (Table 1), and the 8-gauge auger gun (400 grain black powder) (Healey et al., 1991). Receivers (three Mark Products L28E 40 Hz geophones with 5-inch spikes) were selected based on field conditions, transmitted acoustic frequency band, and previous experience.

On-site testing concentrated on source configuration, source/receiver geometries, and recording parameters. Multiple shots per station were vertically stacked for impulsive sources (i.e., air gun, sledge hammer, and weight drop). The source-to-receiver offsets ranged from 8 to 776 ft with adjacent stations separated by 4 ft. The seismograph's dynamic range was sufficient to negate the effective use of analog filters. The digital acquisition filters would have only been of value when recording stacking sources. The data quality was sufficient to allow selection of optimum parameters and geometries for acquisition of data targeting reflectors between 70 and 750 ft deep.

Production CDP Profiles

Production parameters were designed in accord with analysis of walkaway data. Minimum QA/QC of field data necessitated in-field correlation capabilities, digital display filters, and a real-time noise monitor. Analysis of noise effects during walkaway tests resulted in the designation of a maximum allowable background noise threshold of 0.1 mV peak-to-peak. Identification of various unique reflection arrivals on walkaway data allowed confident selection of equipment, parameters, and geometries to be used for the CDP portion of the survey.

The production portion of the survey took 5 days and included 1171 shot-points acquired along four lines. Using the vibrator as the seismic energy source allowed input power and spectral control while maintaining a relatively undisturbed and uninvaded ground surface. The vibrator's pad was located on the gravel road surface across most of the western boundary line, on the dirt road for the majority of the airstrip line, and in the road ditch or grassy right-of-way for the Spesutie Island line. For each line the pad was seated and coupled to the ground with 3500 lbs of hold down. The three geophones were planted into competent material in a 3 ft in-line array to help attenuate source-generated air-coupled waves as well as cultural noise. Each receiver was monitored intermittently for continuity (≈3,000 ohms) and leakage (>1,000K ohms) and each phone underwent a modified twist and tap test to ensure an optimum plant prior to recording. The seismograph was configured to target reflectors shallower than 250 msec with average velocities

TABLE 1

Sweeps Tested at the Aberdeen Proving Grounds, Maryland

Name	Description
112394s	40 to 500 Hz, taper length 0.1 sec., calibrated at KGS, sweep length 5.0 sec.
120394s	35 to 500 Hz, taper length 0.1 sec., calibrated at site, sweep length 5.0 sec.
120394s1	35 to 500 Hz, taper length 1.0 sec., calibrated at site, sweep length 5.0 sec.
120394s2	35 to 500 Hz, taper length 2.0 sec., calibrated at site, sweep length 5.0 sec.
120394s3	35 to 500 Hz, taper length 3.0 sec., calibrated at site, sweep length 5.0 sec.
120494s	35 to 500 Hz, taper length 0.1 sec., calibrated at site, sweep length 5.0 sec.
120494s1	35 to 500 Hz, taper length 1.0 sec., calibrated at site, sweep length 5.0 sec.
120494s2	35 to 500 Hz, taper length 2.0 sec., calibrated at site, sweep length 5.0 sec.
120494s3	35 to 500 Hz, taper length 1.5 sec., calibrated at site, sweep length 5.0 sec.
120494s4	35 to 350 Hz, taper length 0.1 sec., calibrated at site, sweep length 6.0 sec.
120694s	30 to 400 Hz, calibrated at site, sweep length 5.0 sec.
120694s1	30 to 450 Hz, calibrated at site, sweep length 5.0 sec.
120694s2	25 to 400 Hz, calibrated at site, sweep length 5.0 sec.
120794s	35 to 500 Hz, wide open, no calibration, sweep length 6 sec.

from 3000 to 7000 ft/sec. The analog spectrum was in part shaped by the vibrator sweep and drive force in an attempt to enhance the higher frequency components of the recorded energy. This emphasis on pushing the high side of the spectrum was necessary if there was to be any chance of interpreting unique reflectors from within the clay/sand sequences (i.e., lenses, stringers, etc.) as well as distinguishing weathered-in-place bedrock from the unweathered bedrock surface.

DATA PROCESSING

All data processing was done on an Intel 80486-based microcomputer using *Eavesdropper*, a set of commercially available algorithms. Display parameters were determined based on scale of existing data sets, optimum exaggerations, and workable formats.

Walkaway Noise Tests

Comparisons of various source, receiver, and instrument settings and configurations as well as overall signal-to-noise, frequency content, and velocity structure are the intent of the walkaway noise tests. The level of testing is dependent on the objectives of the project and the degree of difficulty in obtaining the required resolution and signal-to-noise ratio. Processing of data for this test was limited to trace organizing, gain balancing, and digital filtering. Vibrator data comparisons from this study also include in-field vs post-acquisition correlation and the effect of varying sweep specifications and data characteristics. Spectral analysis contributed to optimizing the acquisition specifications. The data are gathered and displayed in a source-to-receiver offset order according the specific source configuration.

Production CDP Lines

The CDP data processing flow was similar to those used in petroleum exploration (Table 2). The main distinctions relate to the conservative use and application of correlation statics, precision required during velocity and spectral analysis, and extra care taken during muting operations. A very low percentage allowable NMO stretch (< 20%) was extremely critical in avoiding wide-angle reflections, maximizing resolution potential, and avoiding distortion in the stacked wavelets (Miller, 1992). Many processing techniques that have not routinely been effective on shallow data sets (including f-k migration, deconvolution, and f-k filtering) were tested to evaluate their potential on this data set.

TABLE 2

General Processing Flow

format from SEG2 to KGSSEGY
spectral analysis (frequency vs amplitude plots)
digital filtering (bandpass with spectrum balance 61-120 240-359,
band reject 170-175 185-190 and 290-295 305 310)
trace balance (50 msec window)
first arrival muting (direct wave and refraction)
surgical muting (removal of groundroll based on trace-by-trace arrival)
assign geometries (input source and receiver locations)
sort into CDPs (re-order traces in common midpoints)
velocity analysis (whole data set analysis on 200 ft/sec increments)
NMO correction (velocity from 4700 ft/s to 5000 ft/s)
static correction (5 msec max shift)
CDP stack
trace balance (50 msec window)
mute up to 30 msec
migration (velocity of 5000 ft/s)
time-variant filtering (50 msec: 70-140 280-400; 150 msec: 30-60 180-240)
display

Processing flow for CDP stacked data. Parameters were determined by analysis for each prior step as well as through iterative analysis of particular operations.

For most basic shallow high resolution seismic reflection data the processing steps/operations are a simple scaling down of established petroleum-based processing techniques and methods. However, processes such as deconvolution have basic assumptions (Yilmaz, 1987) that are violated by most shallow data sets, and this data set is no exception. Migration is another operation that, due to non-conventional scaling (vertical and/or horizontal), many times may appear to be necessary when in actuality geometric distortion may be simple scale exaggeration (Black et al., 1994). Processing/processes used on data for this report has/have been carefully executed with no *a priori* assumptions and designed to simply enhance what can be interpreted on shot gather data, not to create through processing.

Uncompensated variations in the near-surface velocity structure manifests itself as erroneous apparent structures, reduced resolution, and apparent stratigraphic variations. A first arrival statics operation proved effective in reducing long wavelength (several times larger than the length of the spread) artifacts of a horizontally varying near-surface velocity function. Geometric analysis of reflection hyperbola (the basis for the zero-offset corrections necessary in establishing apparent NMO velocities used for common midpoint summation) was adversely affected in places along the western boundary lines by relatively severe inter-spread statics. Some of the apparent non-uniform reflection curvature was a direct result of small scale bed terminations, erosional features, and possibly gradual horizontal lithologic changes. Sub-spread length features can be smoothed or slightly distorted by the hyperbolic zero-offset (NMO) correction and therefore may be slightly de-focused on CDP stacked sections. Iterative surface-consistent statics and velocity analysis effectively reduced much of the zero-offset trace misalignment that resulted from the inter-spread static.

Vibrator

The use of vibratory sources increases the potential for spectral shaping of the recorded wavelet, minimizes the environmental impact, and increases the signal-to-noise ratio, while increasing the complexity of in-field and/or post-acquisition processing when compared to non-coded impulsive sources. Vibratory techniques were first developed over 30 years ago as an alternate method (non-impulsive) of introducing acoustic energy into the ground (Crawford et al., 1961). This oscillatory energy method known as "vibroseis" uses a controlled vibrating source to generate a sinusoidal wavetrain of continuously varying frequency delivered to the ground over a specific time period (Sheriff, 1991). The sweep (sinusoidal source input

function) trace or pilot is correlated with each time series trace. The record time of each data trace is slightly longer than the sweep (pilot) time to allow sufficient "listen" time for two-way travel of the entire sweep. The correlation process effectively produces a time series trace comparable to impulsive source records with respect to full wave field recording.

Both in-field and post-acquisition correlation were equally effective at APG. In-field correlation requires on-site determination of the optimum pilot trace. Once the data have been in-field correlated against the sinusoidal wavetrain (pilot) the process cannot be easily reversed. Since the vibrator is instrumented with one accelerometer on the base plate and one on the mass, three possible pilot trace choices exist: ground force (mathematically determined based on weighted output of base plate accelerometer and mass accelerometer), filtered ground force (tracking filter derived from synthetic), and the synthetic (theoretical drive function). Depending on near-surface conditions and selected parameters, any one of the previous pilot trace options could produce the broadest band, most representative seismogram. Field and post-acquisition testing included combinations of several sweeps correlated to each of the three possible pilot traces.

RESULTS

Walkaway Testing

The walkaway tests were designed to permit evaluation and optimization of source configuration, source/receiver geometry, seismograph settings, receiver type and configuration, and line location (i.e., road ditch vs road surface vs grassy lawns). Walkaways were conducted using all available equipment at each of the three sites (Figure 2). Two source locations were occupied off one end of a fixed 96-channel spread providing 192 unique receiver offset distances, each with receiver station spacing of 4 ft. The total spread length for all walkway tests was 764 ft, with the smallest source-to-receiver distance being 8 ft. The resulting shot gathers provide ample coherency and energy penetration to adequately image the reflectors of interest.

Western Boundary

Testing along the western boundary fence was concentrated in the road ditch immediately east and at the foot of the road grade (Figure 2). The location was selected to allow a uniform source setting, as close to native (undisturbed) near-surface conditions as possible, and to minimize surface-to-water table depth. The

test line was within 500 ft of high tension power lines (providing strong 60 Hz, 120 Hz, 180 Hz, and 240 Hz components to the spectra) and the three-mile test track, both formidable noise sources. The three 40 Hz geophones were deployed in tightly clustered groups to ensure accurate recording of the full wavefield. Each source was provided a plot of land previously undisturbed by other sources. The ground surface in the test area was dry with coarsely mowed vegetation.

The 12 lb sledge hammer impacting a steel plate provided relative low source energy, resulted in minimal surface disturbance, minimized access problems, and is cost effective. A single impact of the 12 lb sledge produced a seismogram that possesses several interpretable close offset (< 200 ft) reflections (Figure 3). The dominant frequency of reflections between 70 and 140 msec is around 125 Hz. Source-generated linear noise is very apparent (i.e., ground roll, air coupled wave, refraction, and direct wave). At longer offsets the power lines become an overwhelming contributor to the time series plot. The horizontal arrival pattern and spectral properties of this 60 Hz, 120 Hz, and 180 Hz noise prohibits most slope and frequency attenuating techniques. Extreme care must be exercised to ensure flat arrivals from powerline noise do not contribute to and are not mistaken for apparent reflection arrivals. The stacking of several sledge hammer shots sufficiently improves the data quality that reflections from 70 msec (approximately 100 ft) to over 130 msec (approximately 350 ft) become easily interpretable (Figure 4). The dominant frequency of stacked sledge hammer data is around 120 Hz with an upper corner frequency of about 180 Hz. The high amplitude ground roll, direct wave, and refractions generated by this weight drop source all but eliminate hopes of recording and enhancing reflections from interfaces shallower than 100 ft.

Compared with data from the sledge hammer, data from the rubber band accelerated weight drop (RAWD) (equivalent to the Bison Elastic Wave Generator (EWG)) have less coherent interpretable reflection arrivals and more groundroll. A single shot with RAWD contains noticeable source-generated, pre-first arrival noise (Figure 5). A four-shot vertical stack provides only a slight improvement in the signal-to-noise ratio (Figure 6). Based on normal moveout velocity and arrival times, apparent reflection events deeper than about 150 msec must be multiple reflections or out-of-the-plane events. Evident on all shot gather data recorded at the western boundary is the high amplitude bedrock reflection at offsets greater than about 350 ft. At offset distances this large, reflected arrivals are approaching wide angle. The non-unique wavelet characteristics of wide angle reflections inhibit interpretation of reflectors separated by less than 1/2 wavelength using wavelet

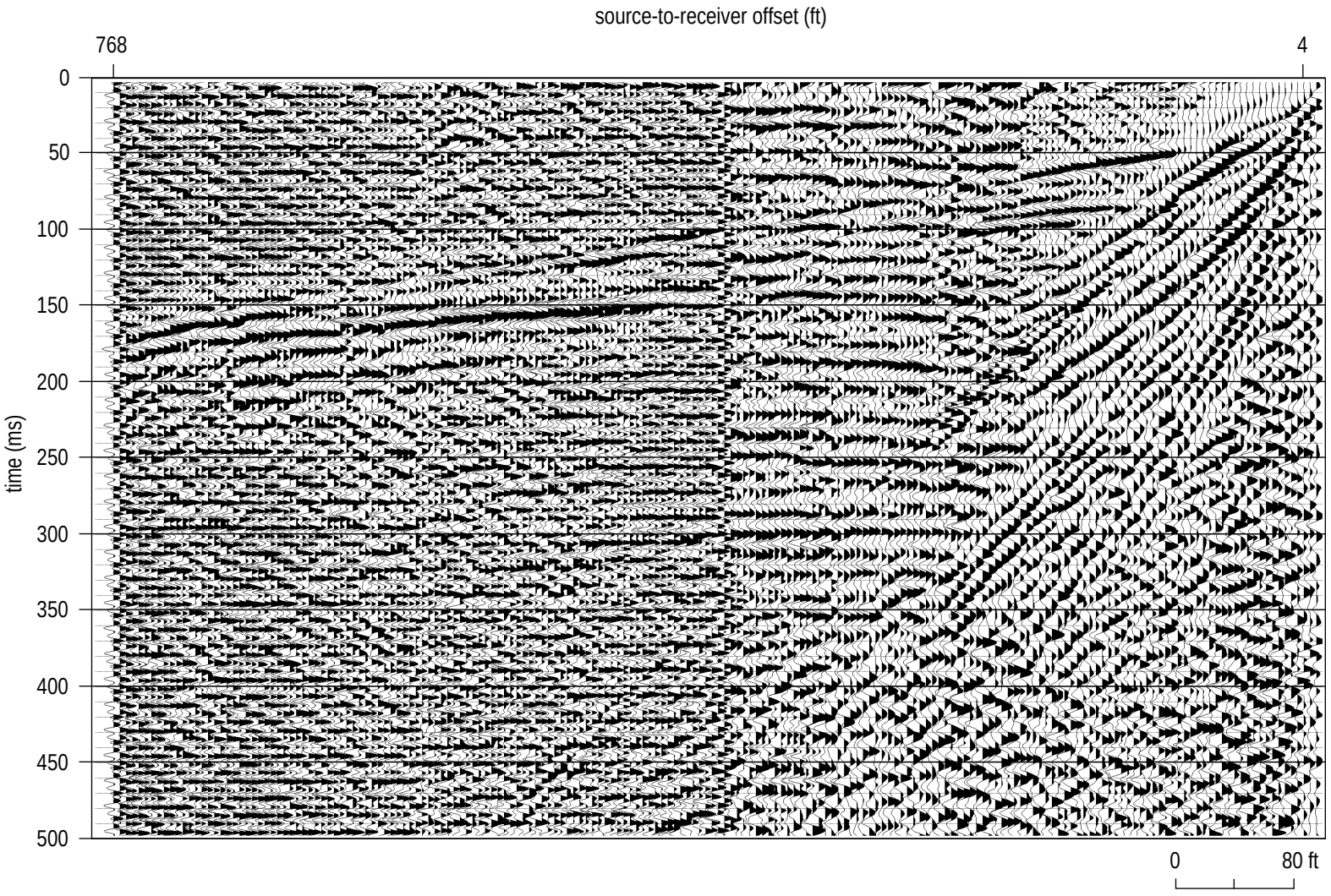

Figure 3. Single impact from a 12 lb sledge hammer on a steel plate near the western boundary.

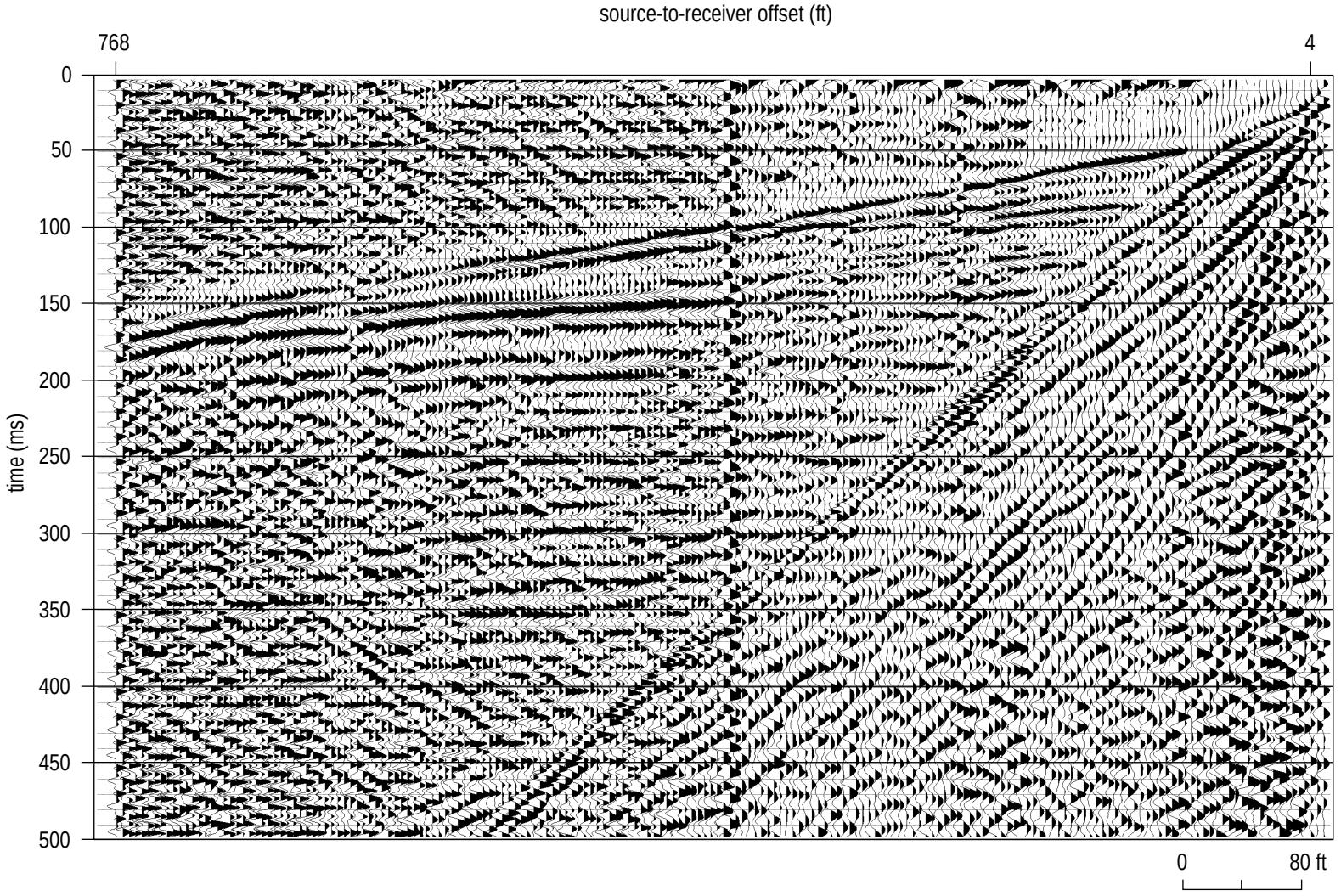

Figure 4. Four-shot vertical stack of a 12 lb sledge hammer on a steel plate near the western boundary.

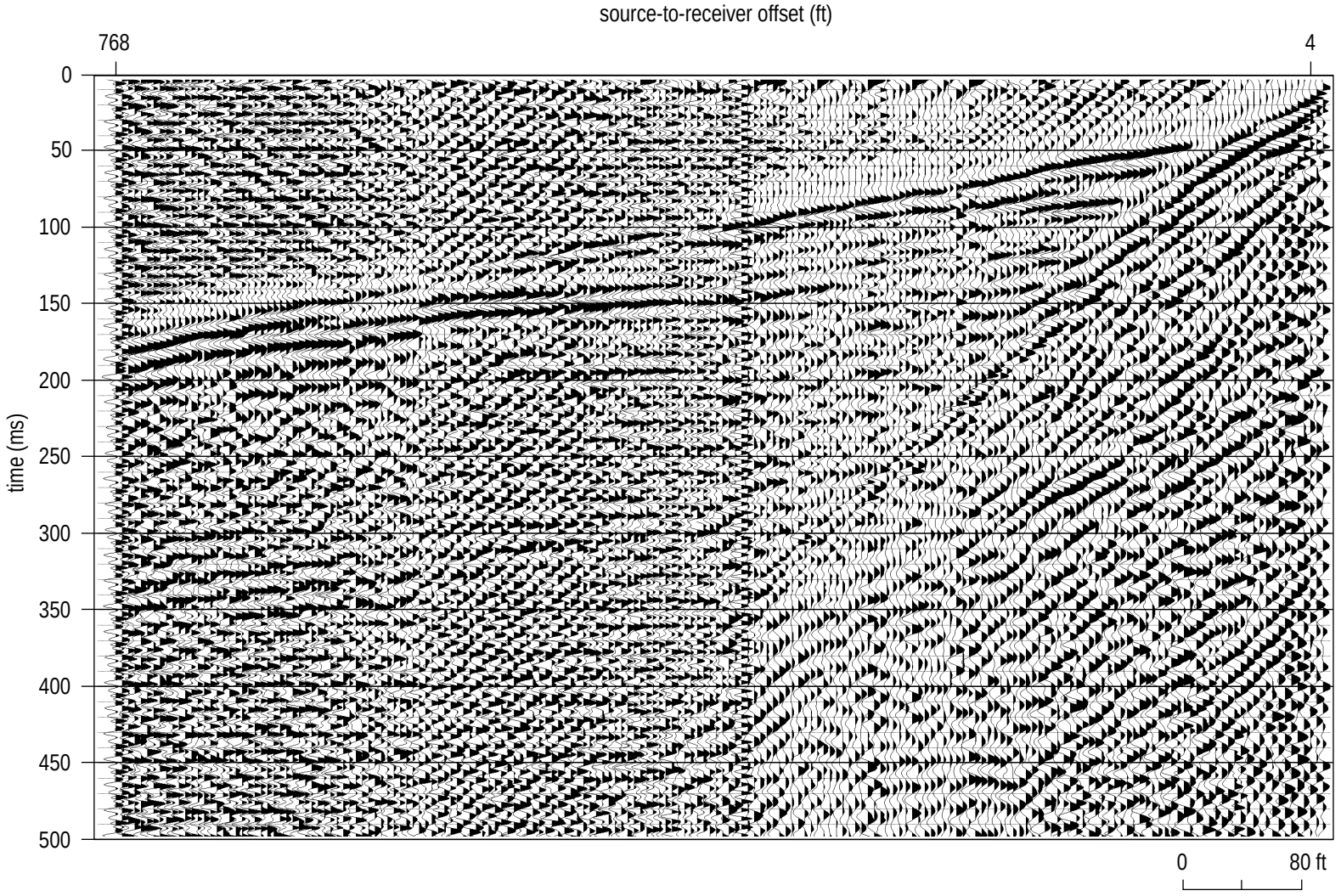

Figure 5. Single impact of a rubber band accelerated weight drop (RAWD), EWG equivalent, near the western boundary.

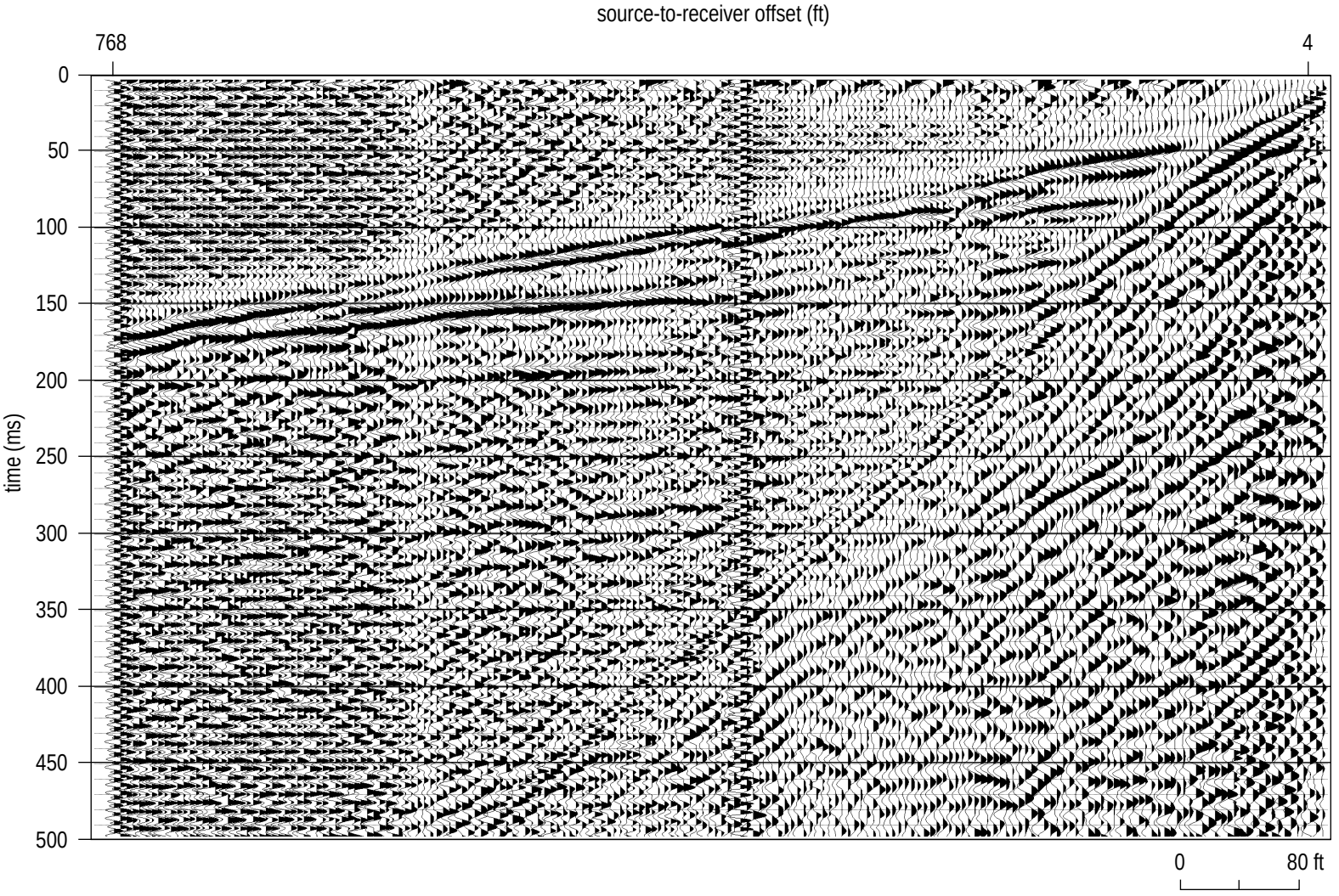

Figure 6. Four-shot vertical stack of RAWD near the western boundary.

interference criteria and therefore reduces the resolution potential (Pullan and Hunter, 1985). High amplitude coherent noise contaminates a large portion of the data recorded from RAWD.

The auger gun represents the only explosive and/or invasive source used on this study. The auger gun was never intended to represent a viable source at this site due to unexploded ordinance (UXO) concerns. Since the auger gun is not designed as a vertical stacking source, only single shot records were recorded for each offset. Reflections are very coherent with a dominant frequency of about 100 to 120 Hz. The upper corner frequency of the reflection pass band is about 200 Hz. First order (primary) reflections can be interpreted on auger gun data from about 60 msec to 140 msec (Figure 7). Reflection energy possesses a slightly broader bandwidth than the weight drop sources. The coherent hyperbolic events that arrive after the 140 msec bedrock reflection are multiple reflections. The strong curved arrival with a vertical incidence time of about 270 msec is modeled to be a first-order multiple from the source to bedrock back to the water table or ground surface back down to bedrock and then up to the receivers. This record clearly demonstrates the origin of the apparent sub-bedrock reflectors evident to varying degrees on all data recorded at APG.

The Bolt LSS-6 air gun is a one-ton truck-mounted compressor, diesel power plant, and air gun system designed to release between 500 and 1500 psi of air into a submerged 20 cubic inch chamber (chamber size is selectable) through a high-velocity shuttle valve. The air gun data were saturated with both coherent and random noise (Figure 8). The 500 psi data possess a good quality bedrock reflection at offsets greater than 300 ft but have little in the way of high signal-to-noise energy arriving at closer offsets. Overall data quality improves when four shots are vertically stacked (Figure 9). Some suggestion of coherent reflections are evident at two-way times between 80 and 140 msec and source offsets from 200 to 350 ft on vertically stacked data where none were evident on single shot data. Increasing the gun pressure to 1500 psi dramatically improves the interpretability (in this case signal-to-noise ratio) of reflected energy (Figure 10). Frequency content of the 1500 psi air gun shot is much more consistent with other sources tested than the 500 psi shot. The signal-to-noise ratio within the optimum reflection window allows the interpretation of at least 5 unique reflection arrivals. Four shots vertically stacked does little to improve the signal-to-noise ratio (Figure 11). Multiple reflections are obvious at times greater than 150 msec and offsets beyond 300 ft. The frequency content of the

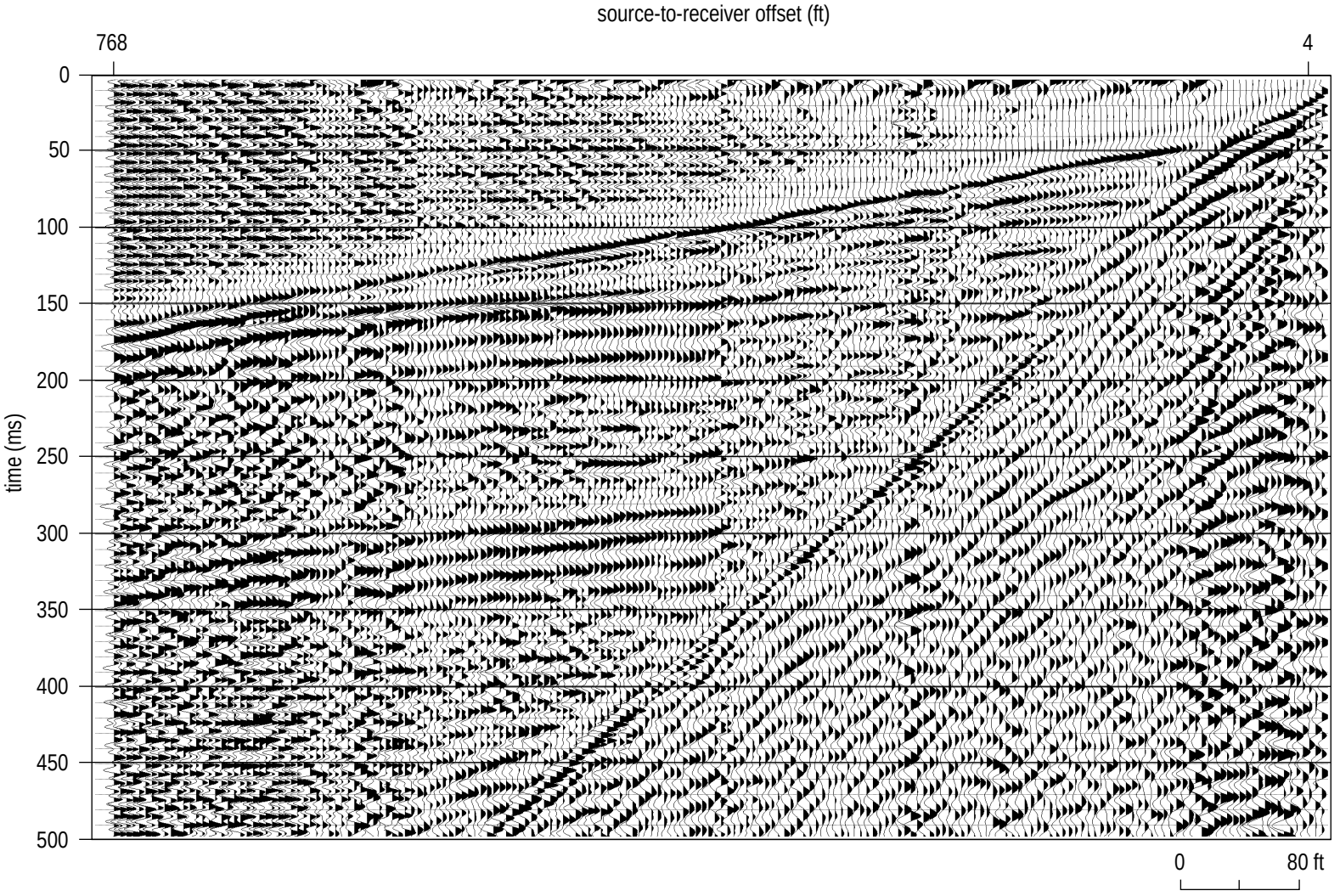

Figure 7. 8-gauge auger gun shot gather with 400 grain black powder near the western boundary.

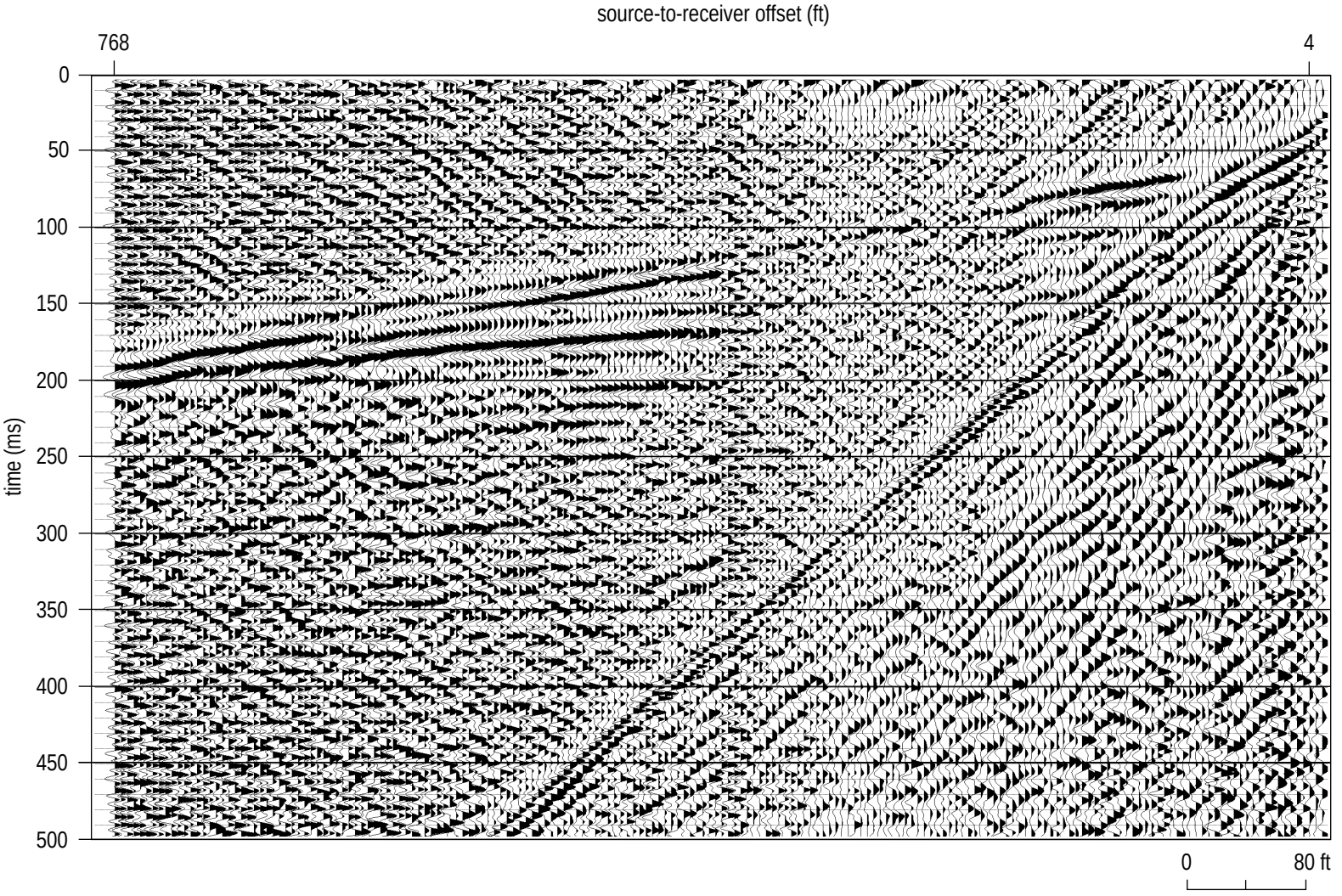

Figure 8. Single 500 psi air gun shot near the western boundary.

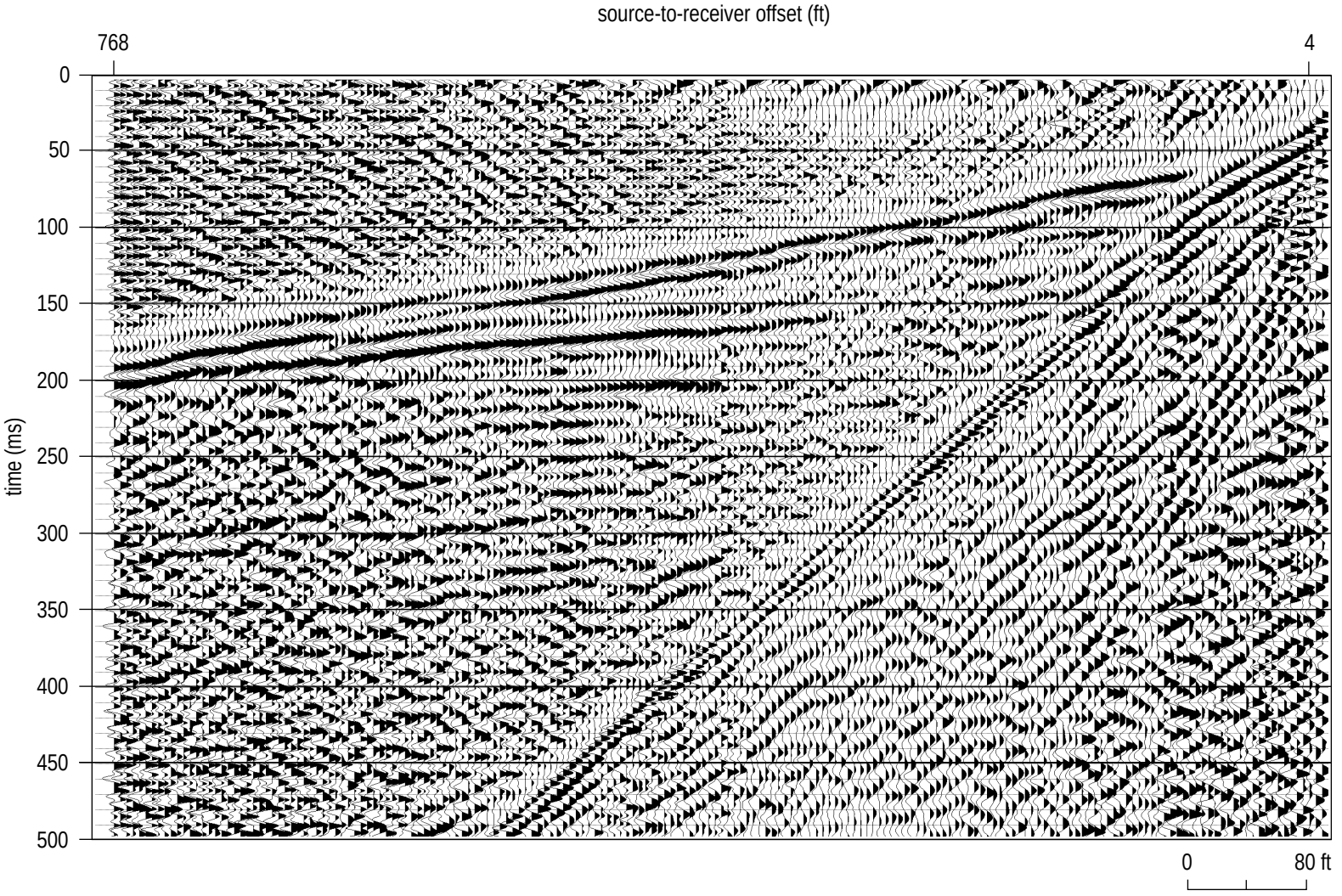

Figure 9. Four-shot vertical stack of 500 psi air gun shot near the western boundary.

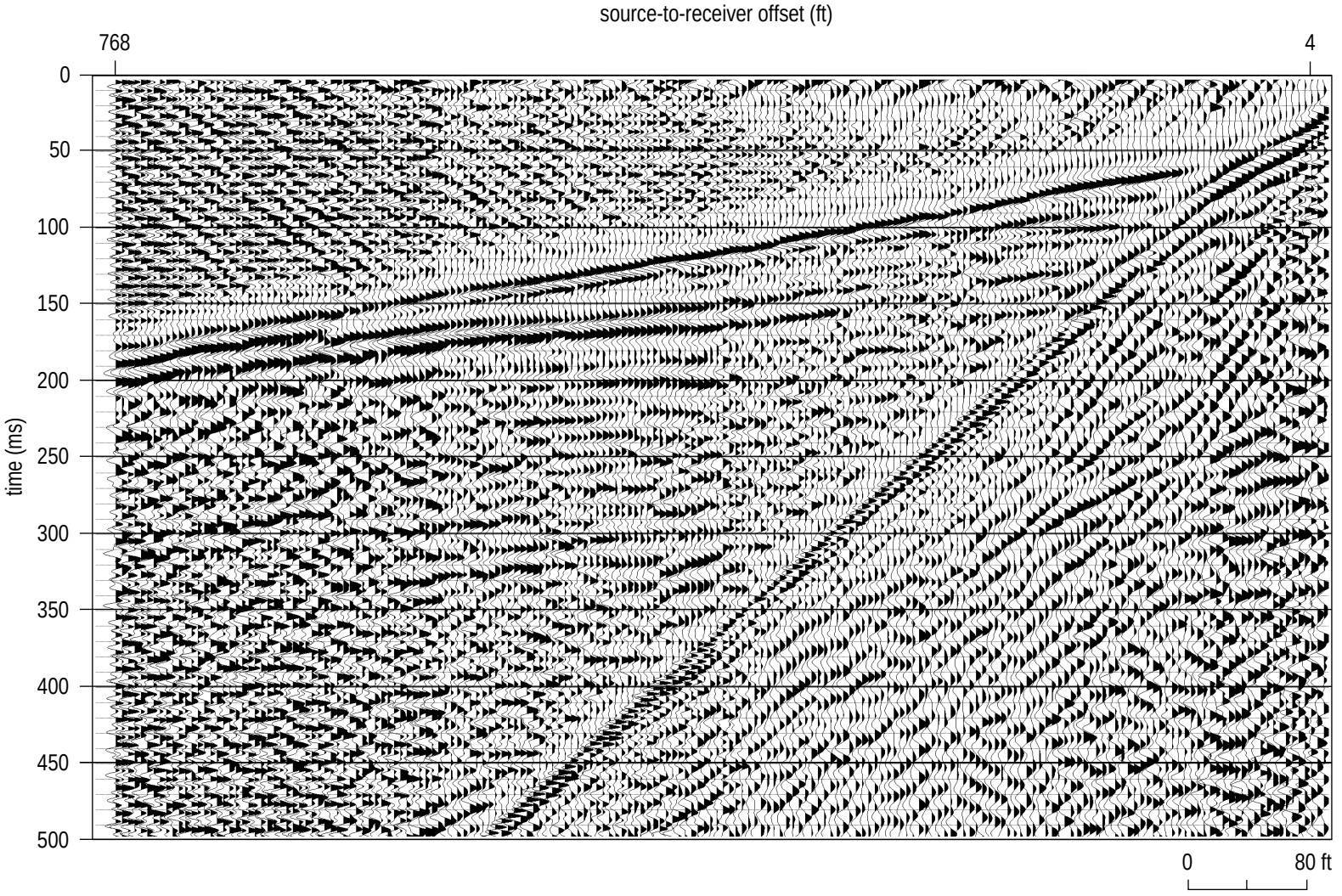

Figure 10. Single 1500 psi air gun shot gather near the western boundary.

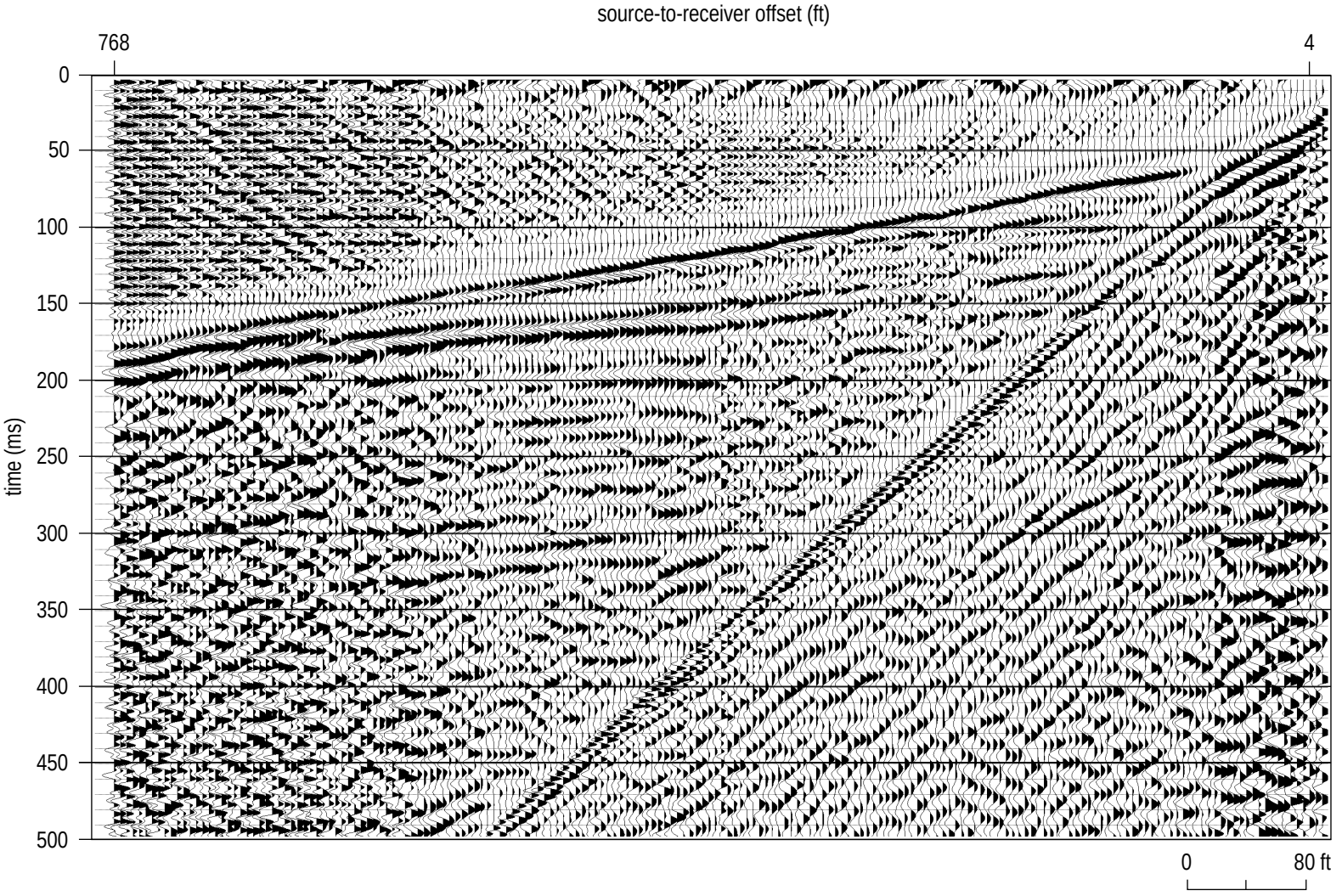

Figure 11. Four-shot vertical stack of 1500 psi air gun shot gather near the western boundary.

stacked wavelets is only slightly degraded and therefore it can be ascertained that the air gun produces a repeatable source wavelet.

The vibratory technique underwent the highest level of scrutiny and greatest amount of parameter testing. This was based solely on the significantly larger number of factors that influence and control overall quality of recorded and correlated data. Vibrator sweep testing included subtle changes in peak force and beginning/ending frequency values. These small changes greatly affected the signal-to-noise and dramatically varied the appearance of correlated records.

Comparing the ground force correlation of sweep 120394s with sweep 112394s, the frequency pass band is much higher and total number of visible reflections are greater with 112394s (Figures 12 and 13). The apparent ringiness of the reflection arrivals on sweep 112394s is most likely a combination of narrow bandwidth and interference from thin bed sequences. Sweep 112394s possesses the highest amplitude and confidence reflections at zero offset times less than 60 msec. A reflection from about 80 msec is much more pronounced on sweep 112394s. The dominant frequency of reflections from 112394s is around 150 Hz with the upper corner of the reflected energy pass band around 180 Hz. The most notable difference between sweep 112394s and 120394s is the high frequency event immediately above the bedrock reflection that appears to diverge from the bedrock reflection wavelet on sweep 112394s at offsets greater than 300 ft. The ground force correlation with sweep 112394s produces a higher quality record than when correlated with sweep 120394s.

Comparing records generated with ground force, filtered ground force, and the synthetic correlated with sweep 120394s, the synthetic appears more representative of transmitted and recorded energy than either of the ground force pilots (Figures 12, 14, and 15). The frequency content and signal-to-noise ratio is markedly better when the synthetic is correlated to 120394s. Conventional wisdom suggests the ground force (which should represent the wavetrain that is actually introduced into the ground) should correlate with recorded data better than the synthetic. Based on this comparison, it would be prudent to always test this theory when using high frequency vibratory sources at APG.

With the apparent improvement noted by correlating sweep 120394s with the synthetic, the same was tested on sweep 112394s. It is evident that sweep 112394s correlated with the ground force produces a slightly better shot gather (Figures 13 and 16). Several pros and cons can be noted when comparing the two records. Analysis of the shallowest reflections on shot gathers produced by correlating 112394s with the synthetic (Figure 16) reveals a very clean single peak reflection

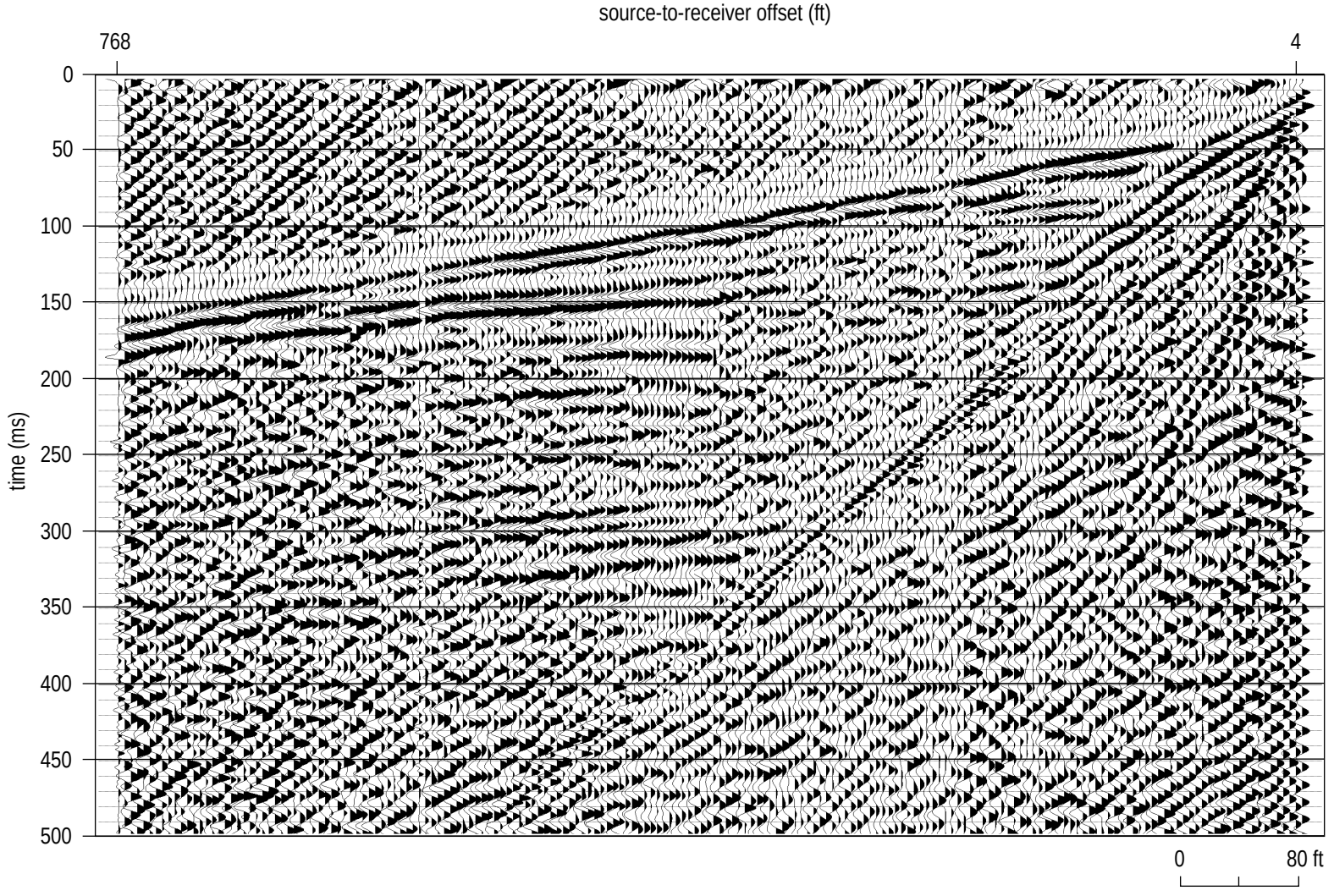

Figure 12. Ground force correlation of vibratory sweep 120394s near the western boundary.

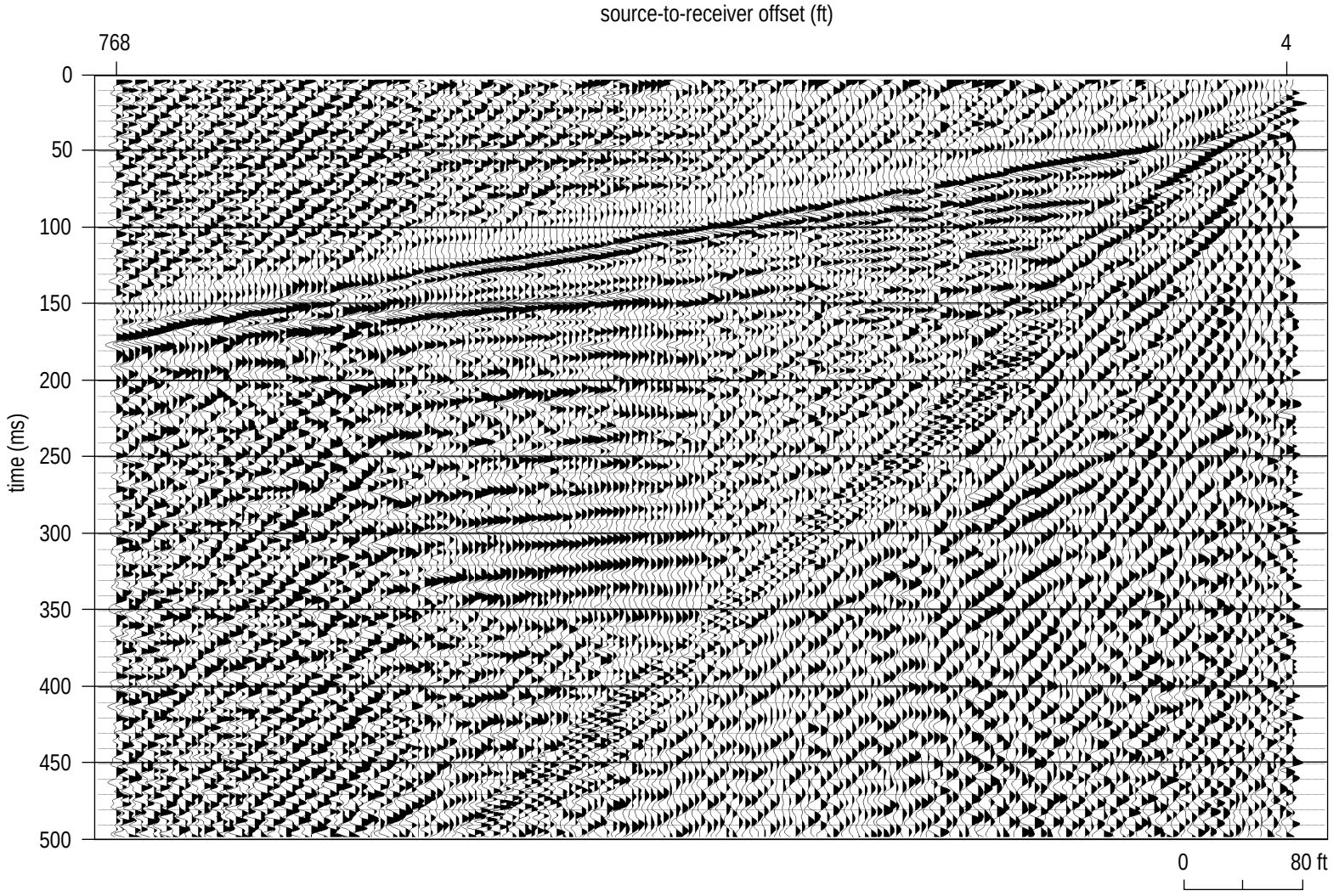

Figure 13. Ground force correlation of vibratory sweep 112394s near the western boundary.

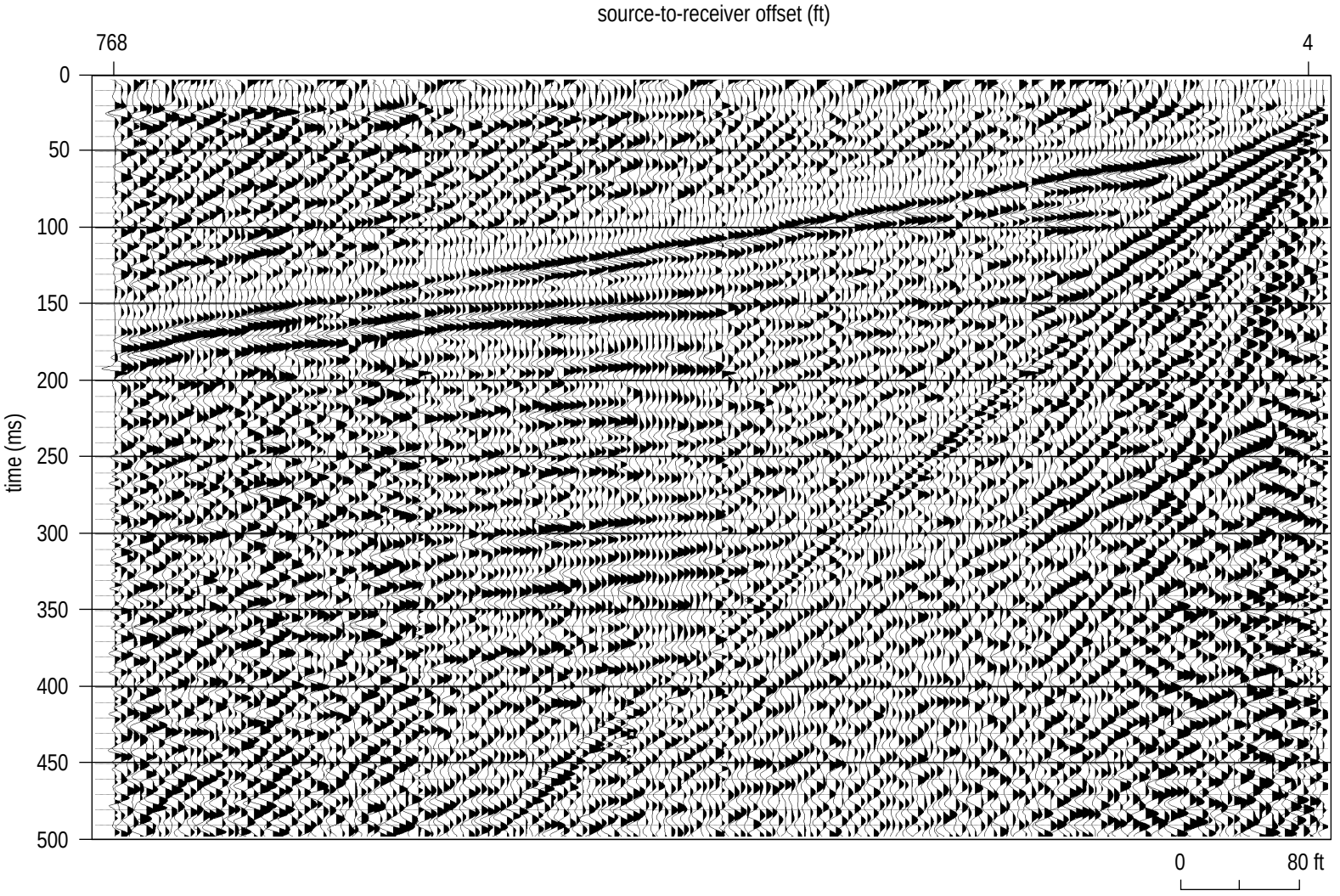

Figure 14. Filtered ground force correlation of vibratory sweep 120394s near the western boundary.

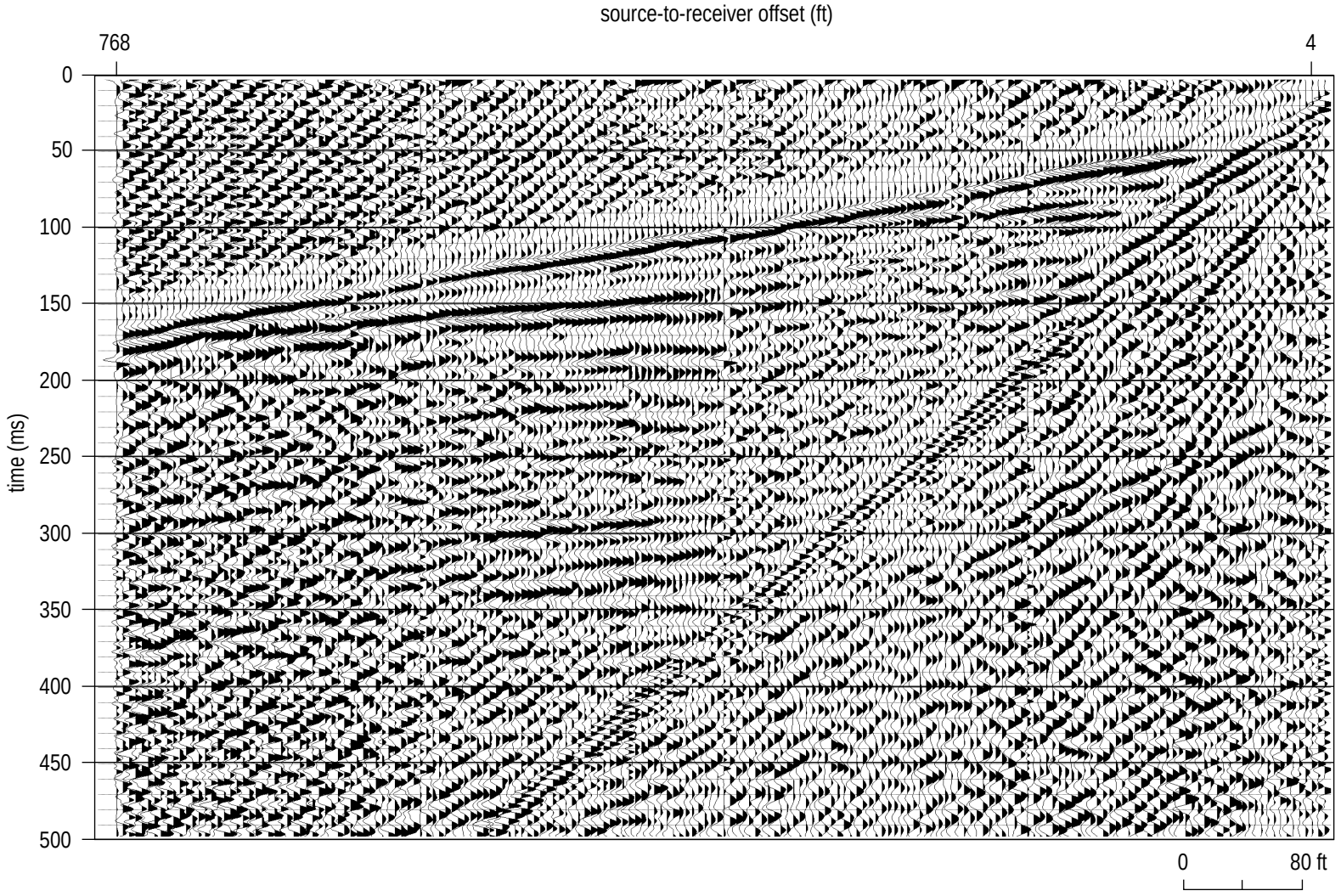

Figure 15. Synthetic correlation of vibratory sweep 120394s near the western boundary.

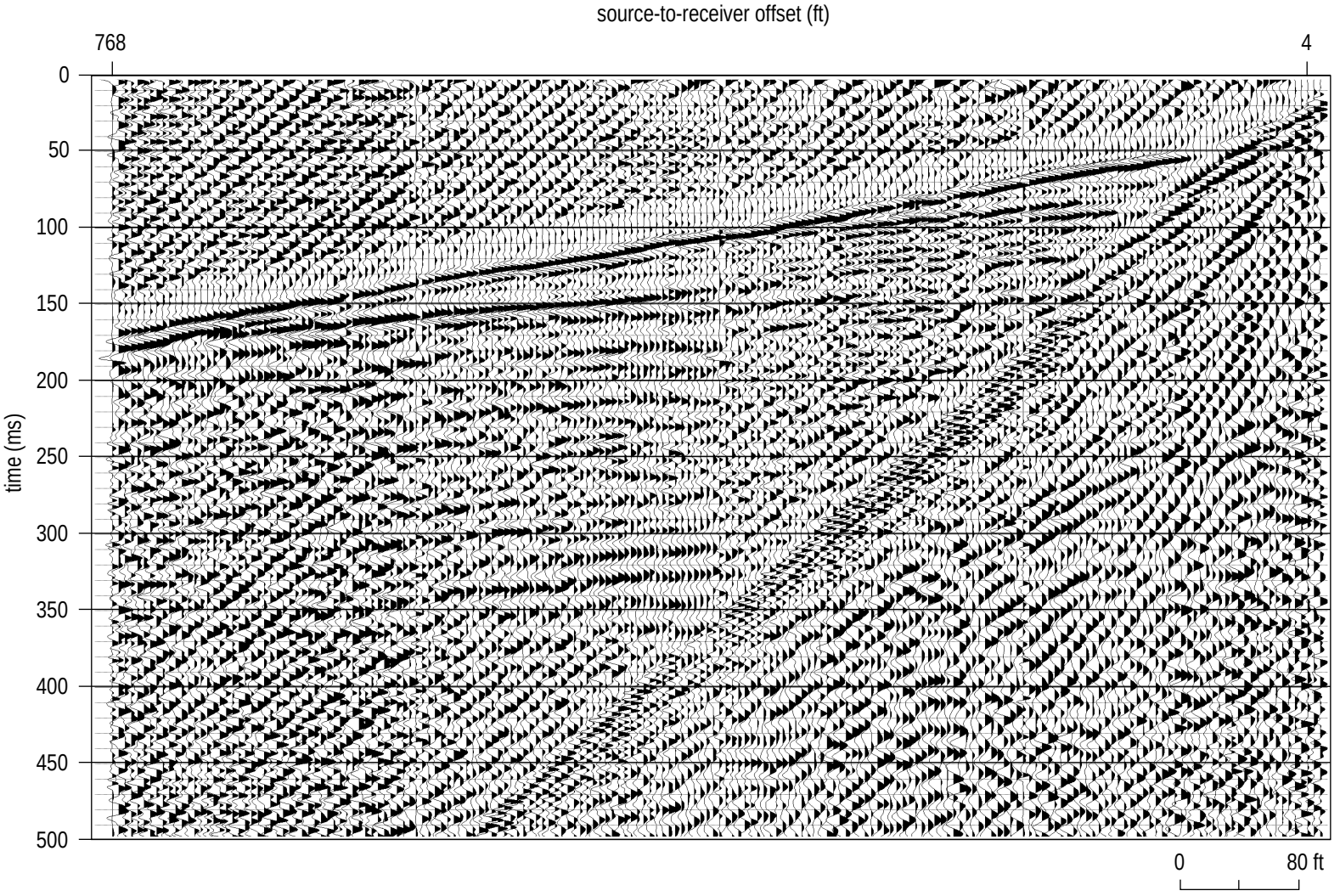

Figure 16. Synthetic correlation of vibratory sweep 112394s near the western boundary.

wavelet at about 65 or 70 msec. At the same time and offset distance on shot gathers correlated with the ground force the reflection wavelet is a doublet. A slightly shallower event appearing to interfere with the refraction can be interpreted on ground force records at smaller source offsets (Figure 13). At longer offsets the bedrock reflection on synthetic correlated data is a clean, high amplitude doublet. The bedrock reflection on ground force data is slightly higher frequency as evidenced by the horizontally intermittent event that appears to interfere with the well-defined bedrock reflection wavelet. Several subtle wavelet features are more prominent and the vertical bed resolution is slightly improved on the ground force correlated shot gather in comparison to the synthetic correlated gathers.

Wavelet shaping through sweep tapering was tested to determine if a non-linear sweep amplitude could counter the high-cut nature of the earth. Attempts to shape the amplitude spectra by attenuating the low frequency components of sweep 120394s with a 0.125, 1, 2, and 3 second taper (amplitude ramp) narrowed the effective bandwidth, causing the recorded reflection wavelets to ring (Figures 12, 17, 18, and 19).

The final vibrator test run prior to commencing the production portion of the survey was designed to determine if vibrator calibration adversely affected the transmission of a broad band sweep. A 35 to 500 Hz sweep delivered to the ground with no amplitude limiting (site-specific calibration) of the vibrator resulted in a correlated record with all the prominent reflections interpreted on sweep 112394s, but with a lower dominant frequency (Figures 20 and 21). The dominant frequency of recorded reflections using sweep 112394s is about 20 percent higher than sweep 120794s.

Everything considered, the four-shot vertical stack of the 12 lb sledge hammer (Figure 4), 1500 psi air gun shot (Figure 10), and the 5-second vibrator sweep 112394s (Figure 13) were the "best" shot gathers recorded at the western boundary. It is clear that the vibrator and the sledge hammer out-performed the air gun when evaluated according to frequency content and bandwidth, signal-to-noise ratio, and number of interpretable reflections. A possible reflection on vibrator data at around 55 to 60 msec is not well differentiated on sledge hammer data. Thin bed interference interpreted in the bedrock reflection wavelet at a source offset of around 350 to 400 ft on the vibrator walkaway is not as distinct on the sledge hammer gather. Production data from the western boundary were acquired using sweep 112394s stored uncorrelated with an 8 ft station spacing, source-to-nearest offset of 24 ft, and farthest offset of 400 ft.

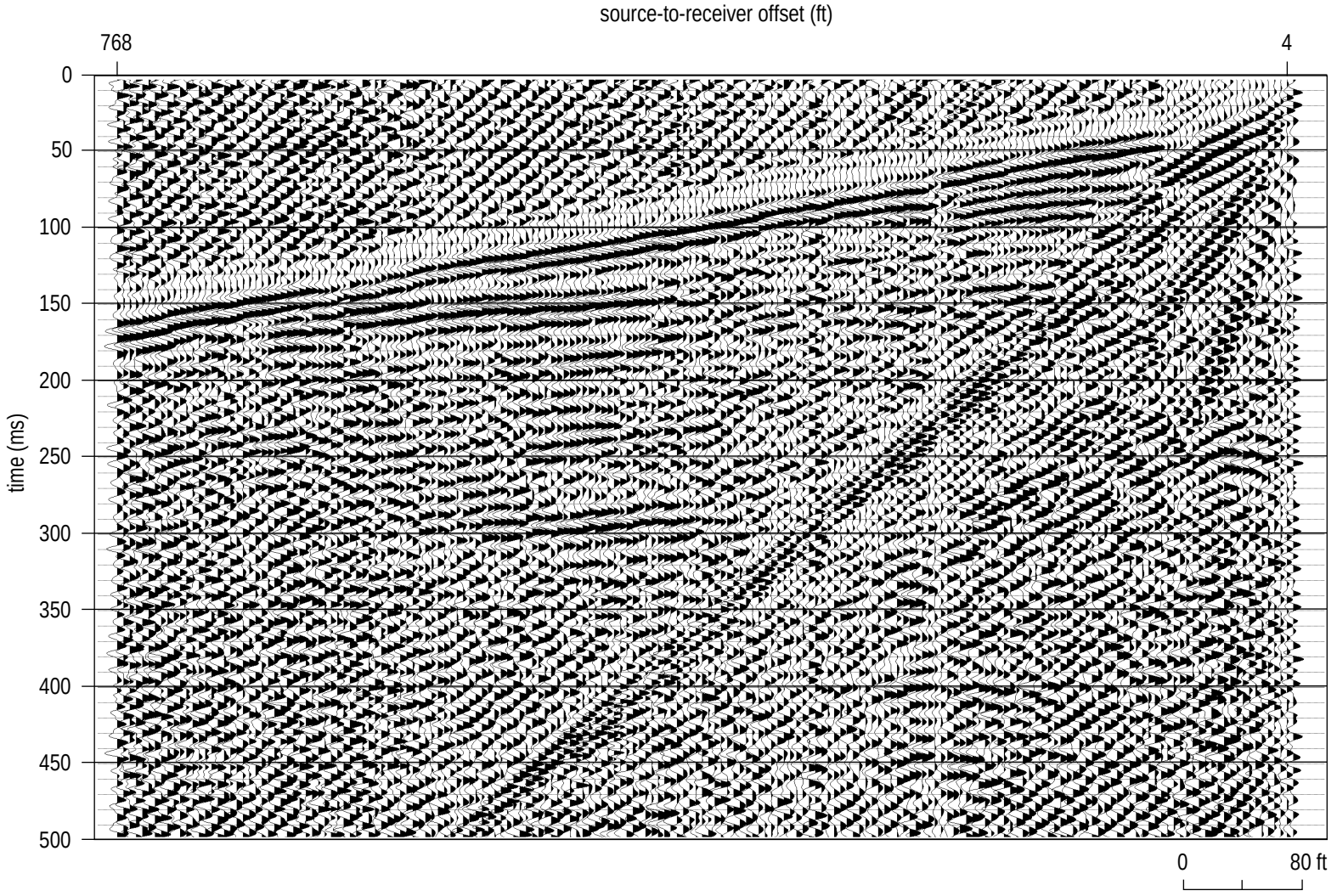

Figure 17. Ground force correlation of vibratory sweep 120394s with 1 second taper near the western boundary.

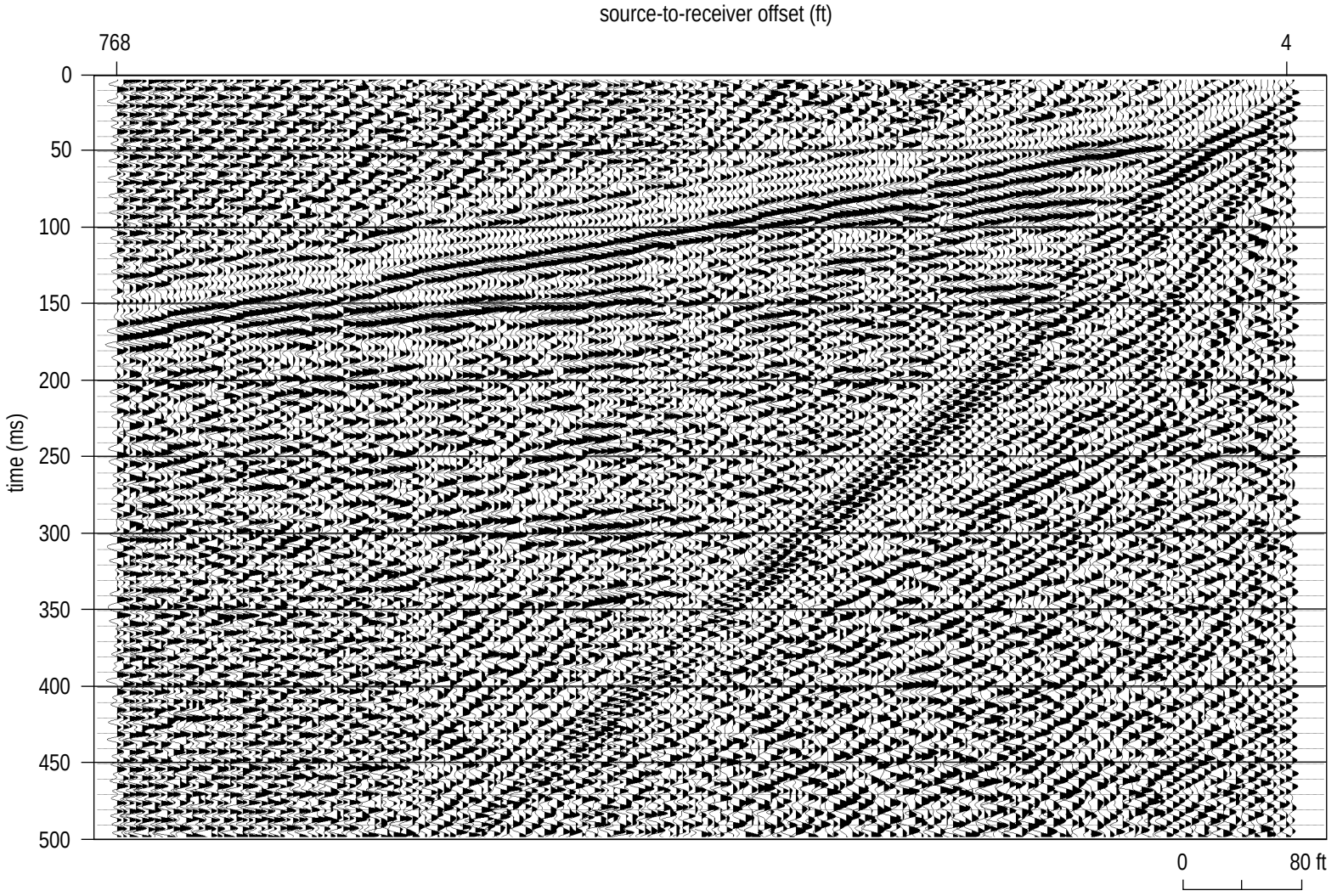

Figure 18. Ground force correlation of vibratory sweep 120394s with 2 second taper near the western boundary.

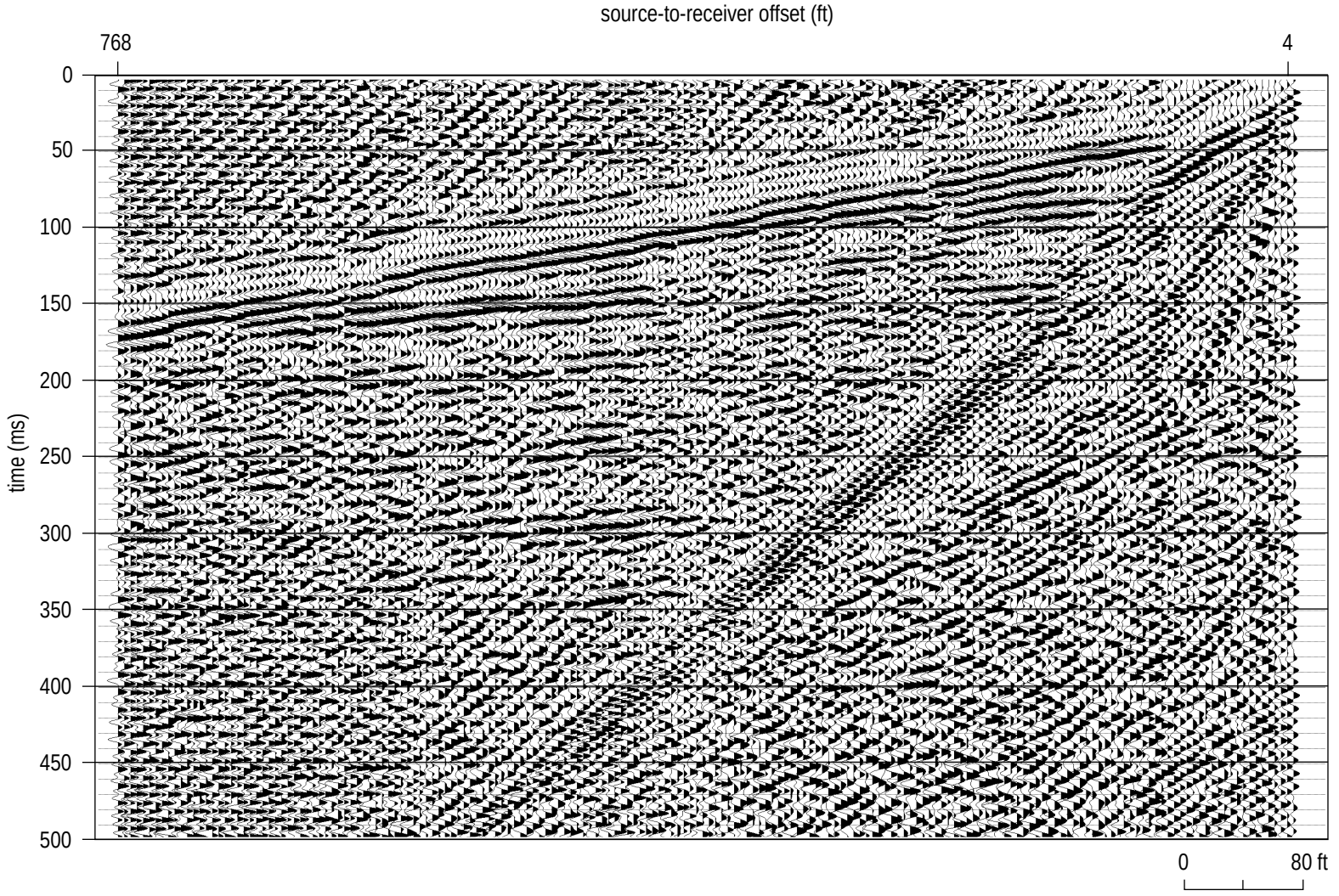

Figure 19. Ground force correlation of vibratory sweep 120394s with 3 second taper near the western boundary.

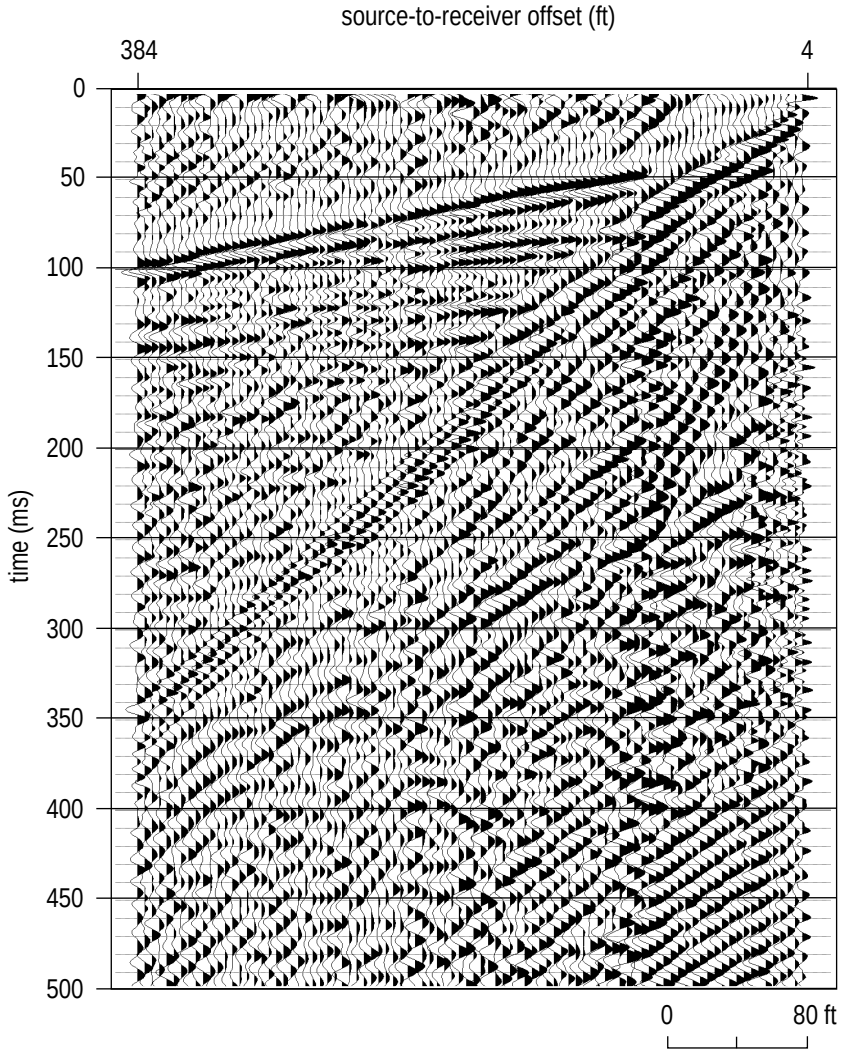

Figure 20. Ground force correlation of vibratory sweep 120794s with no calibration near the western boundary.

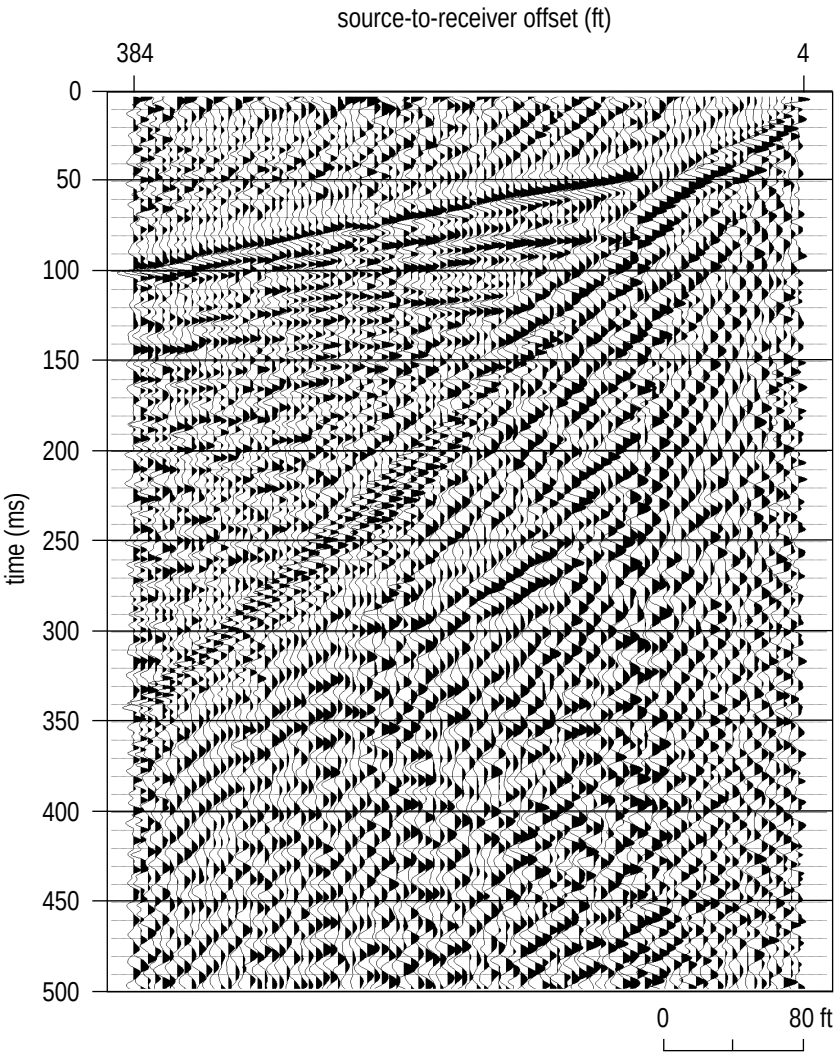

Figure 21. Ground force correlation of vibratory sweep 112394s near the western boundary.

Phillips Airstrip

The test spread for the airstrip was located along the north-south dirt road directly off the end of the north-south runway (Figure 1). The 96 receiver stations started at the creek and ran south on a mowed grassy strip about 50 ft east of the road. Each of the sources occupied space previously undisturbed by any other source. The near-surface was damp with spotty grass vegetation covering a relatively loose clay type near-surface soil.

The 12 lb sledge hammer provided sufficient energy to record reflections from the over 300 ft deep bedrock surface. Unlike the sledge hammer data from the western boundary, stacking four shots does not appear to dramatically improve the signal-to-noise ratio (Figures 22 and 23). The crossover between the direct wave and refraction appears to occur at a source offset of about 300 ft. Therefore, the high amplitude event at about 35 to 40 msec (zero offset time) must be a reflection at source offsets less than about 100 ft. At offsets between 100 ft and about 200 ft there is a mathematical chance (although extremely minute) that the event could be a refraction with a 100 ft source offset representing the critical distance. The apparent 35 msec reflection at offsets between 35 and 90 ft is the shallowest reflection identified during these tests. The dominant frequency of the sledge hammer data is about 100 to 110 Hz with the upper corner of the reflection bandwidth at about 130 Hz. The bandwidth on the sledge hammer data is not broad enough to maintain a clean minimum phase wavelet throughout the depth range of interest.

Increasing the impact mass of the sledge hammer by using the RAWD only slightly improved the overall resolution or signal-to-noise ratio. As with the sledge hammer source, increasing the number of impacts from one to four had little effect on signal-to-noise ratio (Figures 24 and 25). Some improvement in the signal-to-noise ratio resulted from increasing the impact energy of a single hit as evidenced by comparing the sledge hammer with RAWD (Figures 22 and 24). The dominant and upper corner frequency of the RAWD does appear to be 5 to 10% higher than the sledge hammer. The RAWD is very repeatable as evidenced by the consistency in the reflection wavelets between a single vs four vertically stacked shots (Figures 24 and 25). The source vehicle noise, clearly evident pre-first arrivals, interferes to some degree with reflected energy from the shallower parts of the section.

The 8-gauge auger gun produced a relatively high frequency, broadband reflection wavelet with minimum phase characteristics. The auger gun produced a record with a high signal-to-noise ratio (relative to other sources at this site) and significant amplitude variations over the time/depth window of interest

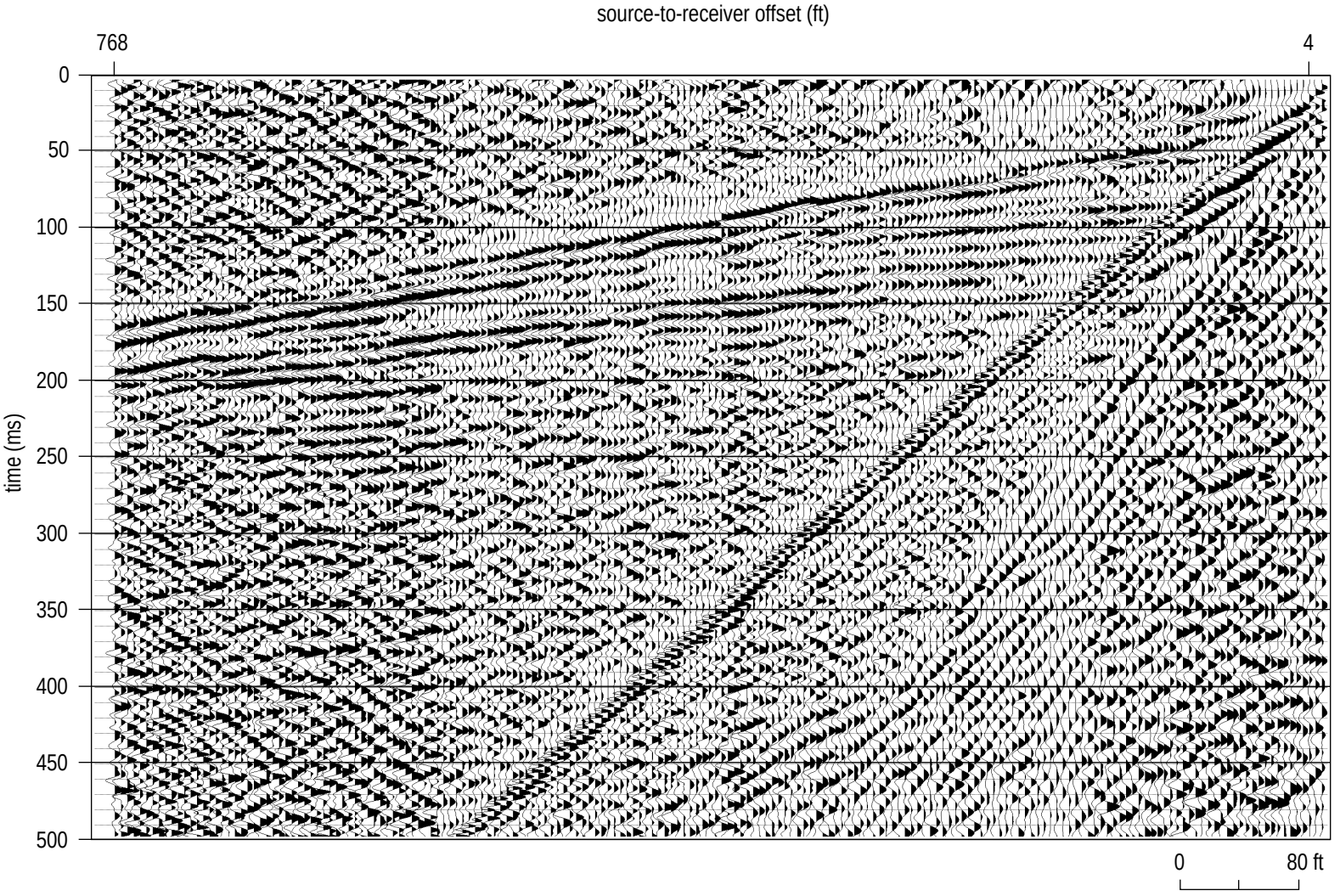

Figure 22. Single impact from a 12 lb sledge hammer on a steel plate along the airstrip line.

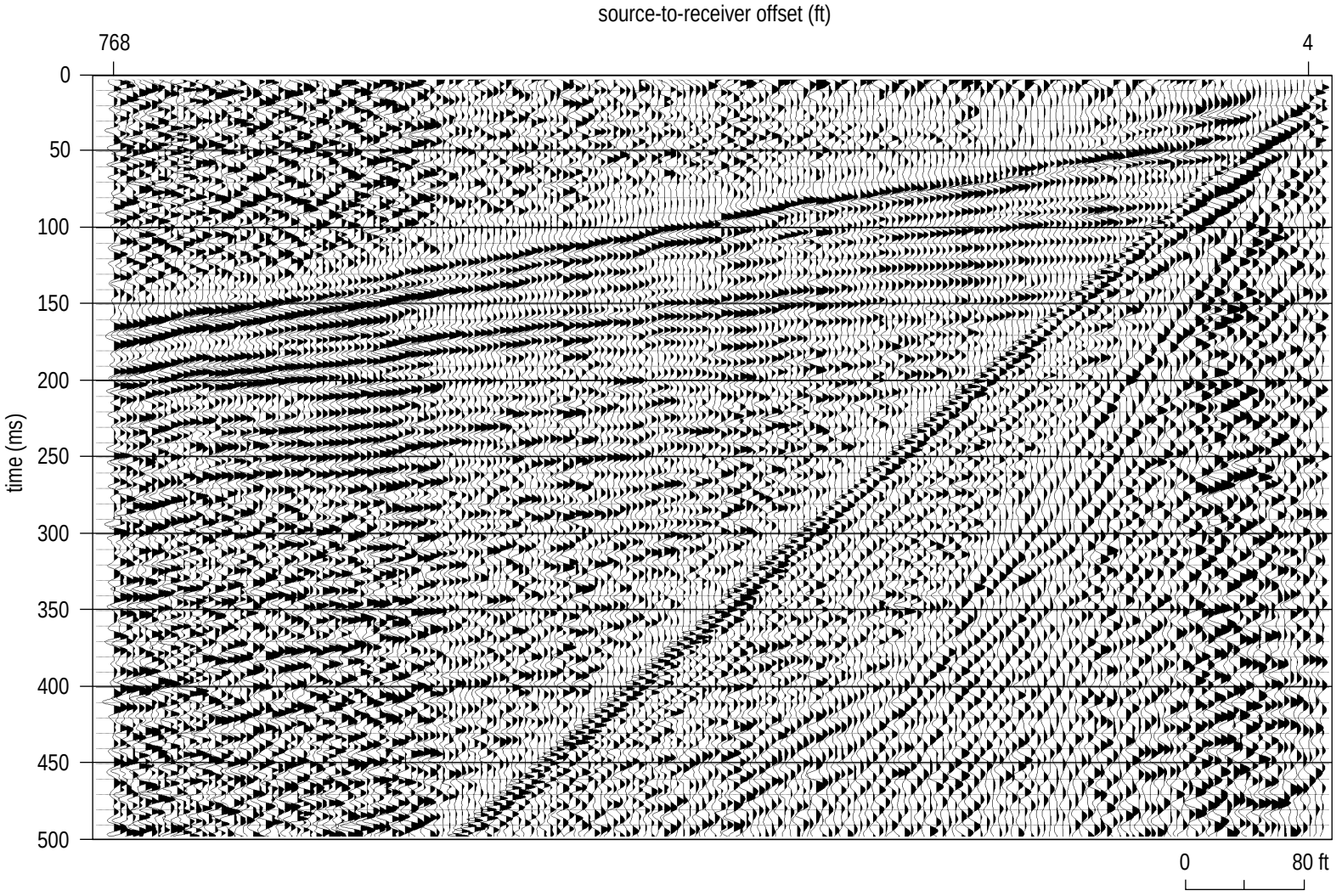

Figure 23. Four-shot vertical stack of a 12 lb sledge hammer on a steel plate along the airstrip line.

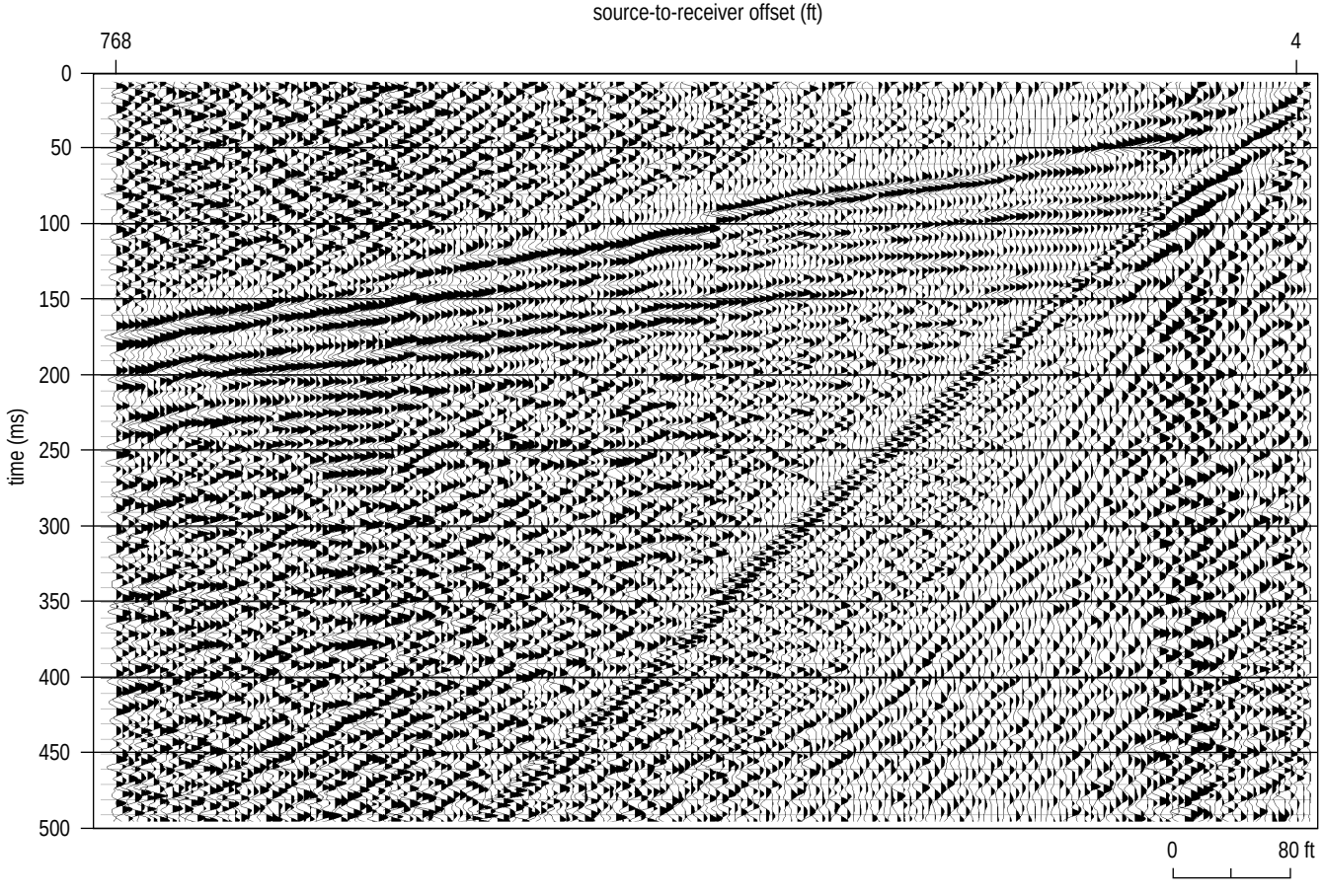

Figure 24. Single impact of RAWD along the airstrip line.

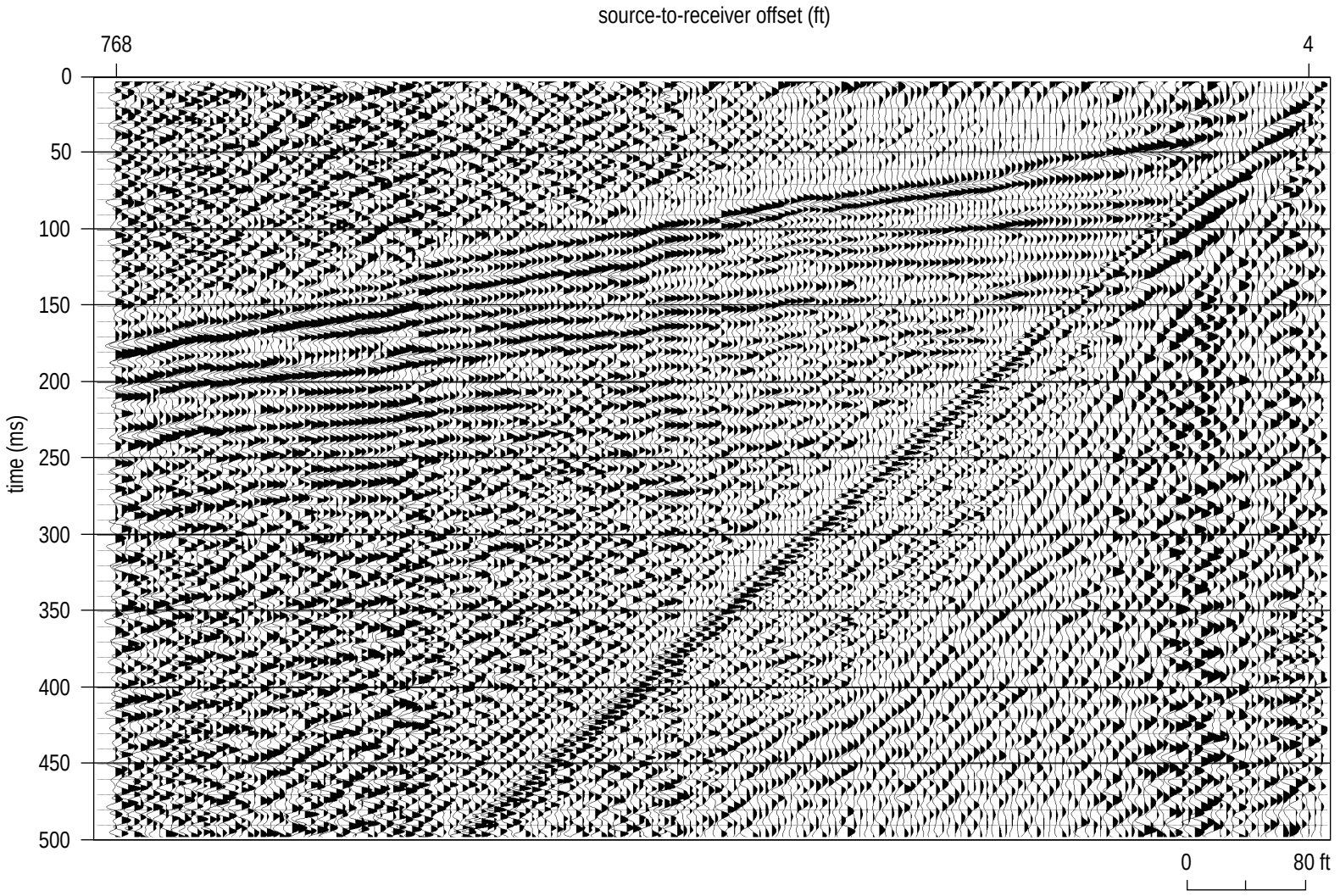

Figure 25. Four-shot vertical stack of RAWD along the airstrip line.

(Figure 26). The dominant frequency is about 140 Hz with an upper corner frequency of the reflection pass band of nearly 175 Hz. This downhole explosive source clearly provided an increase in the resolution potential of apparent reflections arriving between 35 and 140 msec. Increasing the acquisition low-cut filter narrowed bandwidth sufficiently to cause the reflected wavelets to "ring" (Figure 27). The acquisition low-cut dramatically focused and separated individual reflections recorded between 35 and 70 msec at offsets between 30 and 100 ft. The auger gun required extra site clearances and is therefore not considered practical for production surveys at APG.

The air gun was fired at 500 psi and 1500 psi gun pressures with a single and four vertically stacked shots recorded for each pressure. The 500 psi single shot and four vertically stacked shots generated reflection wavelets with a dominant frequency of about 100 Hz and an upper corner frequency of the reflection bandwidth around 130 Hz (Figures 28 and 29). With the exception of low amplitude engine and compressor noise evident within 200 ft of the source, vertical stacking does little to enhance interpreted reflections. Increasing the gun pressure to 1500 psi dramatically improves the overall signal-to-noise and resolution (Figures 30 and 31). The dominant frequency of the 1500 psi reflection energy is around 125 Hz with an upper corner of about 145 Hz. The bandwidth is relatively broad as evidenced by the tight doublets, each representative of a unique reflecting interface.

The 1500 psi air gun shot compares favorably to the 8-gauge auger gun data (Figures 31 and 26). A slight delay is evident in the air gun data due to electronic pre-trigger settings on the gun. Shallow events are very well defined and the signal-to-noise ratio is equivalent to the auger gun, but the air gun does not possess the high frequency energy (> 150 Hz) evident on auger gun data. The 1500 psi air gun shot was clearly superior to the sledge hammer and RAWD. The suggestion (based on comparison of sledge hammer and RAWD seismograms from the airstrip) that vertically stacking multiple shots does not significantly improve the signal-to-noise ratio but increasing single shot energy levels does is consistent with air gun data.

The vibrator provided a very good ratio of signal-to-noise with at least seven unique reflecting events identifiable at source offsets between 50 and 300 ft. Comparison of sweep 112394s with sweep 120494s (which was produced from vibrator calibration at the airstrip site) indicates that 112394s results in a broader recorded reflection bandwidth and better resolution potential (Figures 32 and 34). Ground force correlations appear to maximize bandwidth and reduce the time duration of reflected wavelet for sweep 112394s (Figure 32 compared with Figure 33). The

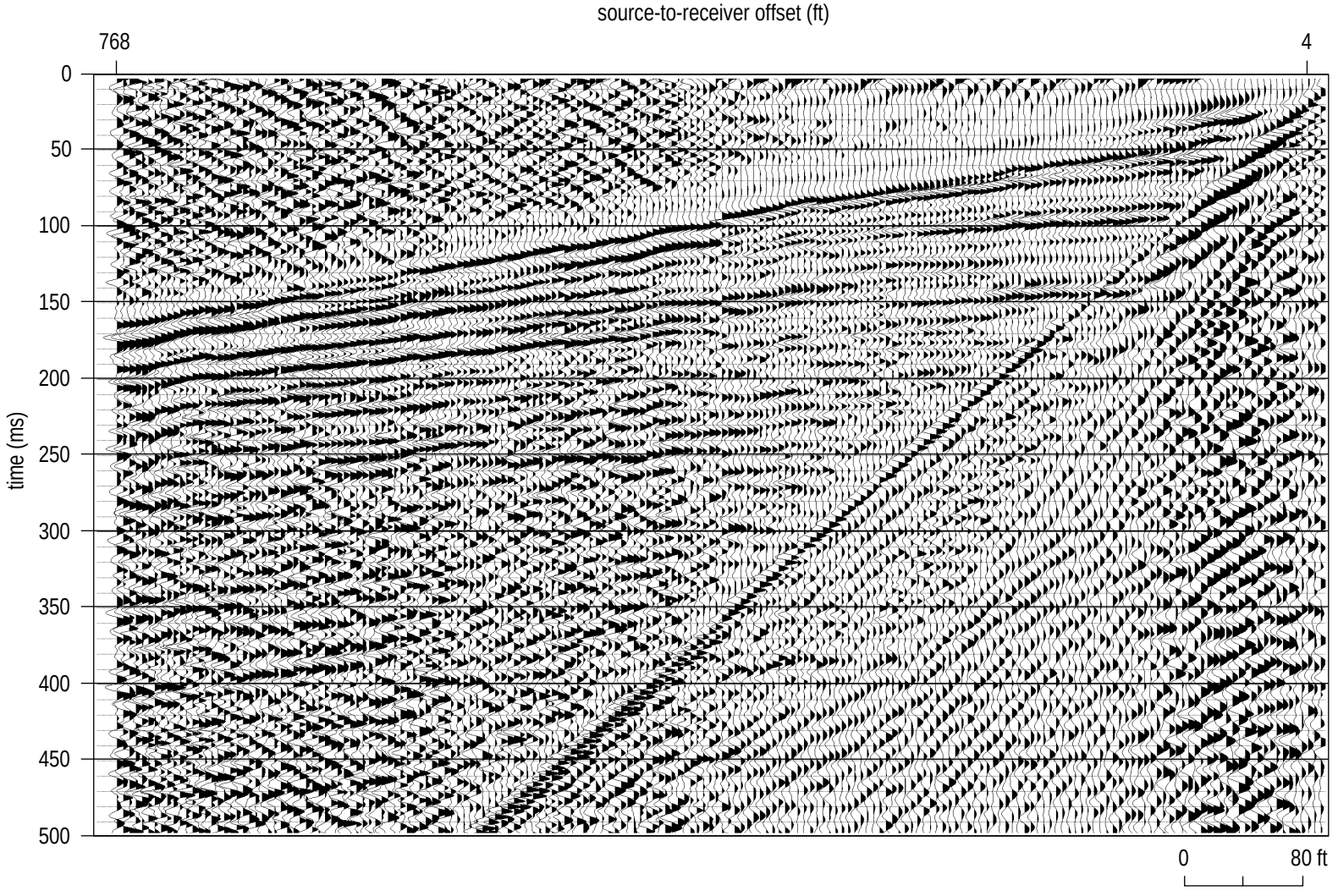

Figure 26. 8-gauge auger gun 400 grain black powder shot gather along the airstrip line.

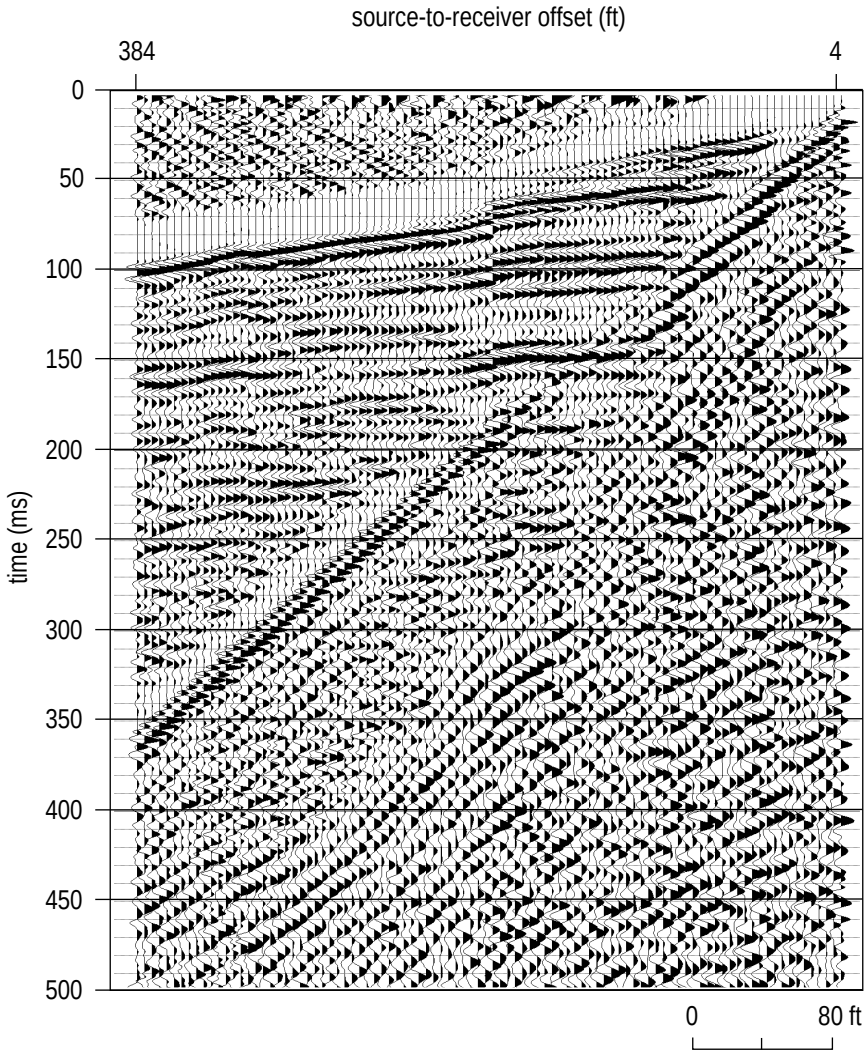

Figure 27. 8-gauge auger gun 400 grain black powder shot gather with 100 Hz acquisition filter along the airstrip line.

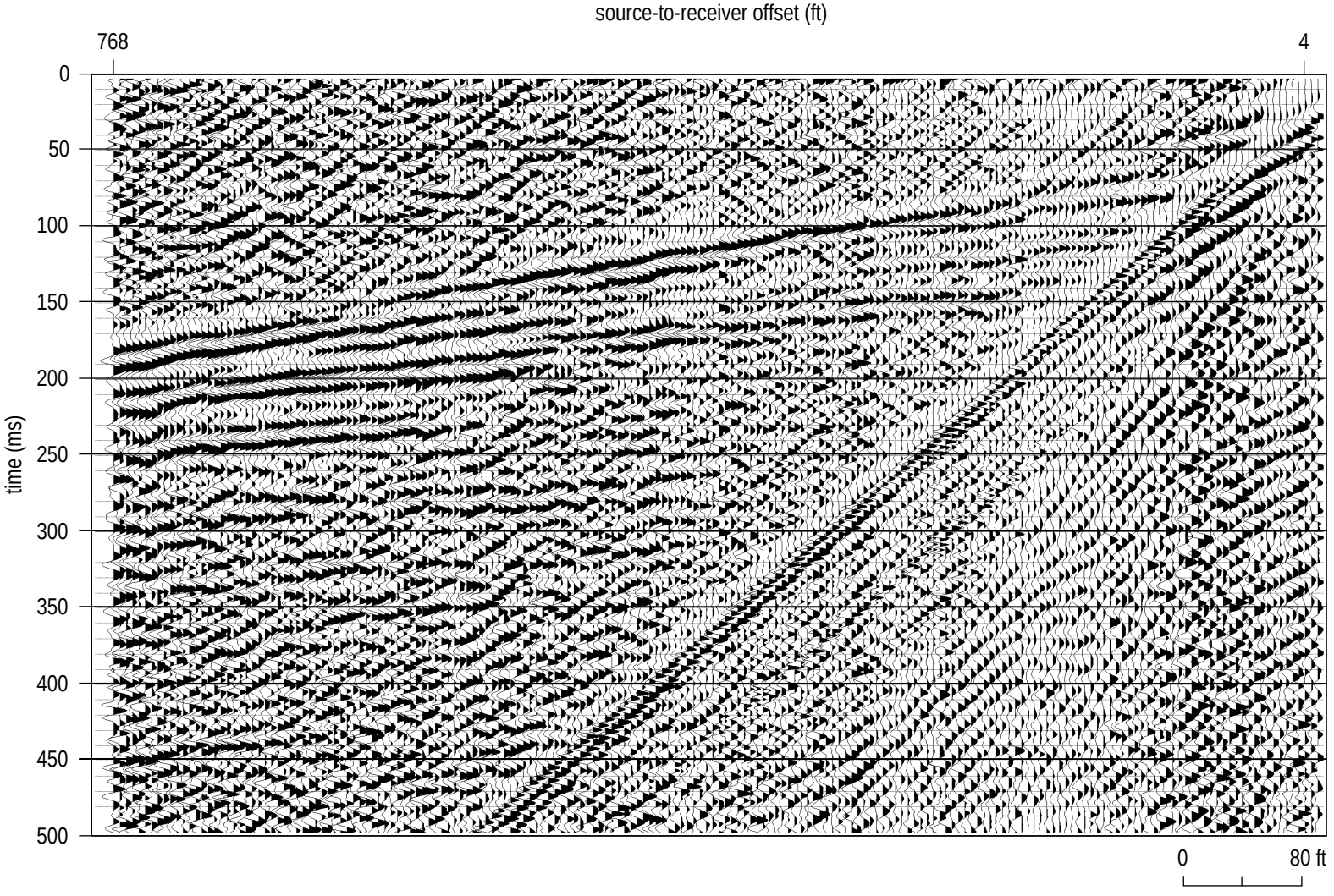

Figure 28. Single 500 psi air gun shot along the airstrip line.

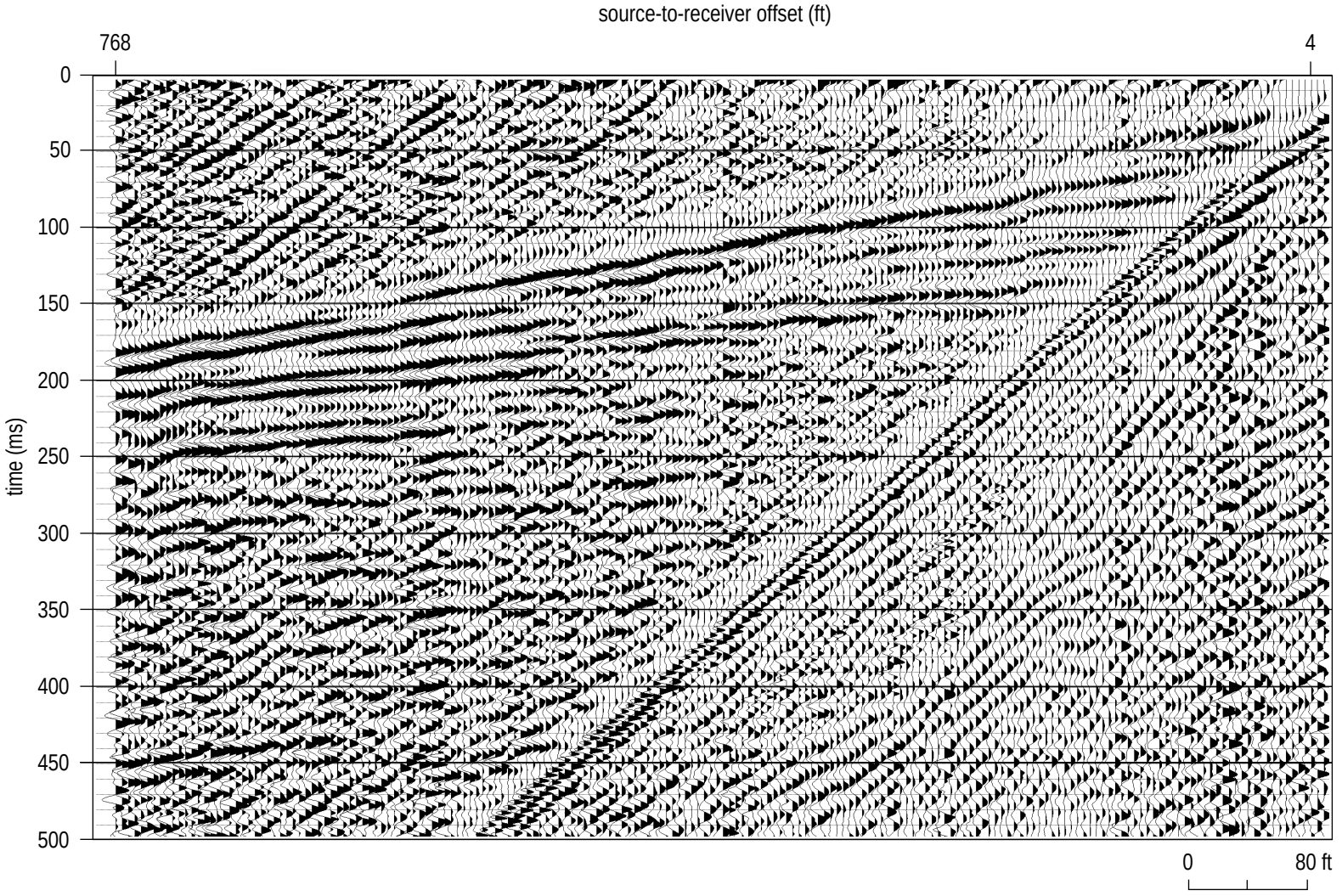

Figure 29. Four-shot vertical stack of 500 psi air gun shot along the airstrip line.

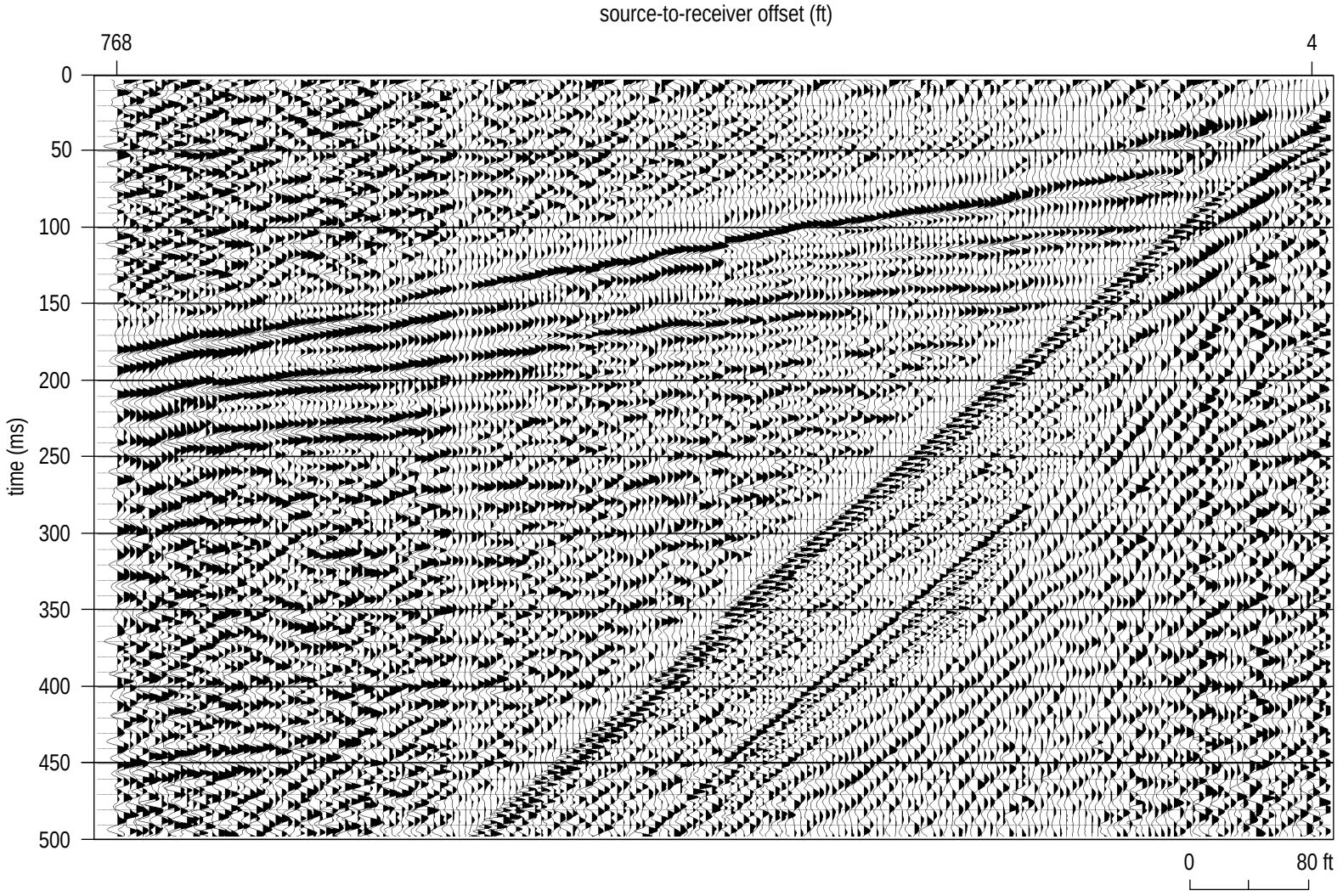

Figure 30. Single 1500 psi air gun shot along the airstrip line.

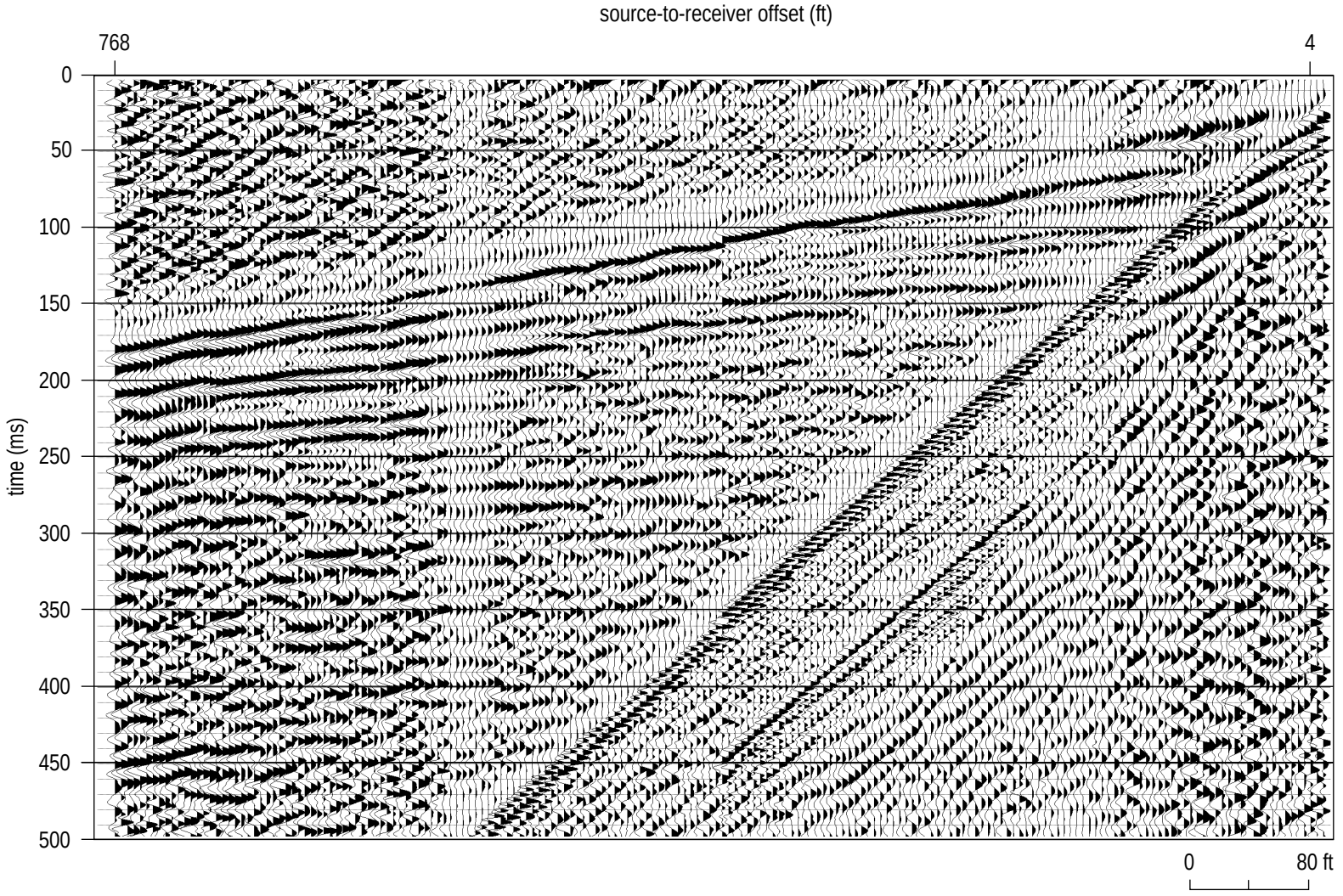

Figure 31. Four-shot vertical stack of 1500 psi air gun shot along the airstrip line.

opposite (correlation with the synthetic vs the ground force) is true for sweep 120494s where the synthetic obviously increases the reflection bandwidth, therefore reducing the time duration of the reflection wavelet (Figure 34 compared with Figure 35). The cause of this extreme inconsistency is neither evident nor has it been fully investigated as to what physically contributes to this difference.

Calibration of the vibrator is apparently as significant (if not more significant) to the shaping of the recorded wavelet as post-acquisition processing (which includes pilot trace correlation). Sweep 112394s correlated with the ground force results in the highest resolution and best signal-to-noise vibrator record at this site (Figure 32). The dominant reflection frequency is around 140 Hz with the upper corner of the reflection bandwidth at about 170 Hz. The ground force correlation of sweep 112394s possesses at least eight unique interpretable reflection events from 30 to 140 msec. Little difference is evident in correlated data regardless of whether pad placement is on the packed dirt road or the softer, grassy strip about 30 to 50 ft from the road (Figures 34 and 36). The outcome of correlation with ground force vs synthetic seems as well somewhat independent of soil/near-surface conditions (Figures 36 and 37).

The use of a sweep taper to shape the spectrum was effective in narrowing the bandwidth sufficiently to cause reflection wavelets to "ring." Analysis of data correlated with and without a time-varying linear amplitude taper applied to the synthetic drive signal showed how ineffective source-controlled spectral shaping is at this site (Figures 35, 38, 40, and 42). The apparent narrow band nature of ground force correlated data without tapering (Figure 34) was negatively impacted by the source amplitude alterations (Figures 39, 41, and 43). When a 3 second amplitude taper is applied to sweep 120494s (the peak force is linearly increased from zero at 30 Hz to full power at 265 Hz), very little difference is evident regardless of whether correlation is with the synthetic or the ground force (Figures 42 and 43). Varying the wavetrain frequency components of the drive signal dramatically changed the bandwidth.

Focusing on optimization of recorded seismic reflection data while considering all site restrictions and resolution requirements, a single impact from RAWD (Figure 24), a single 1500 psi air gun shot (Figure 30), and the 5-second vibrator sweep 112394s correlated to ground force (Figure 33) provided the "best" shot gathers south of Phillips Field. It is clear that the vibrator and air gun outperformed the weight drop sources (RAWD and sledge hammer) when the shot gathers are compared for frequency content and bandwidth, signal-to-noise ratio, and number of

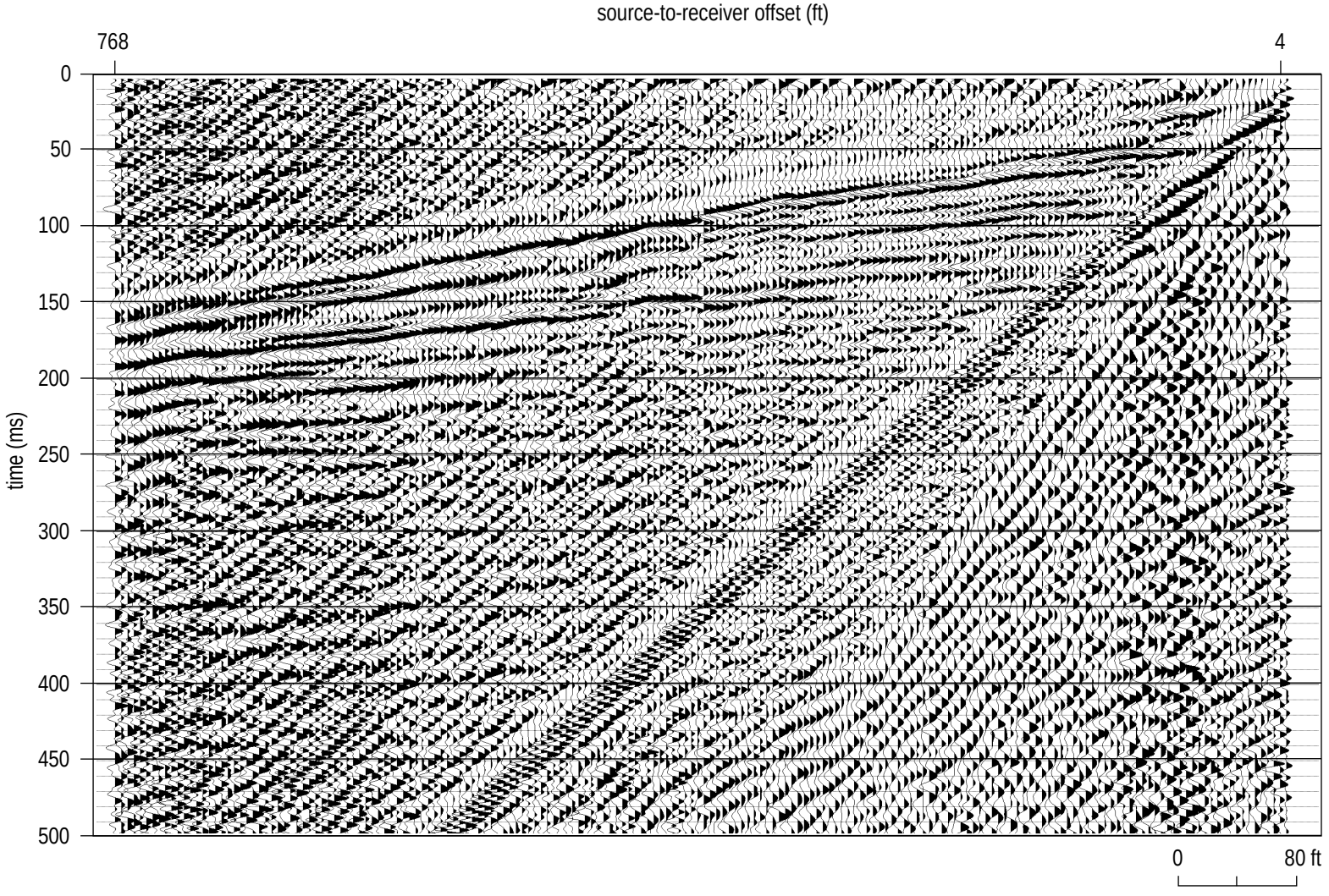

Figure 32. Ground force correlation of vibratory sweep 112394s along the airstrip line.

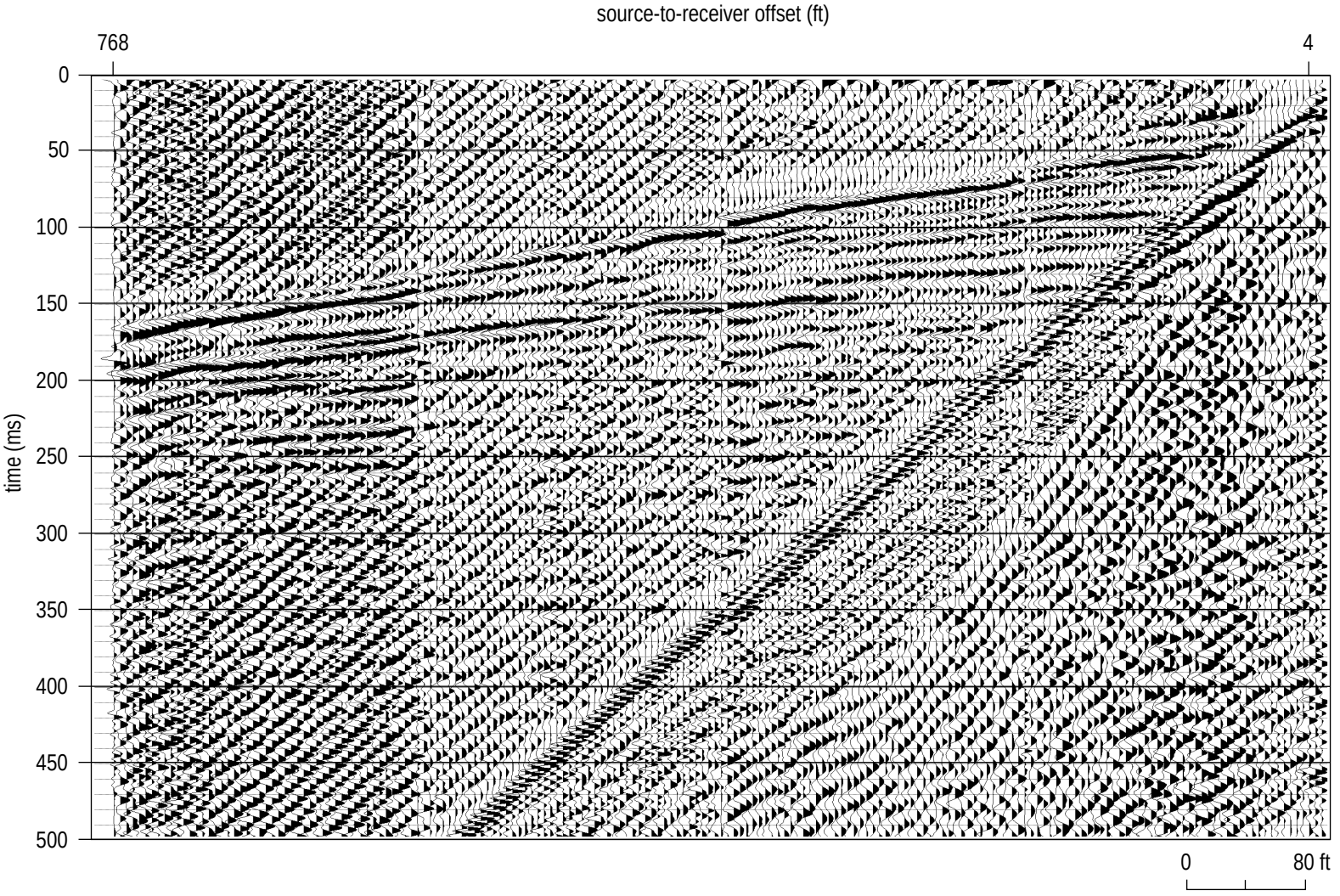

Figure 33. Synthetic correlation of vibratory sweep 112394s along the airstrip line.

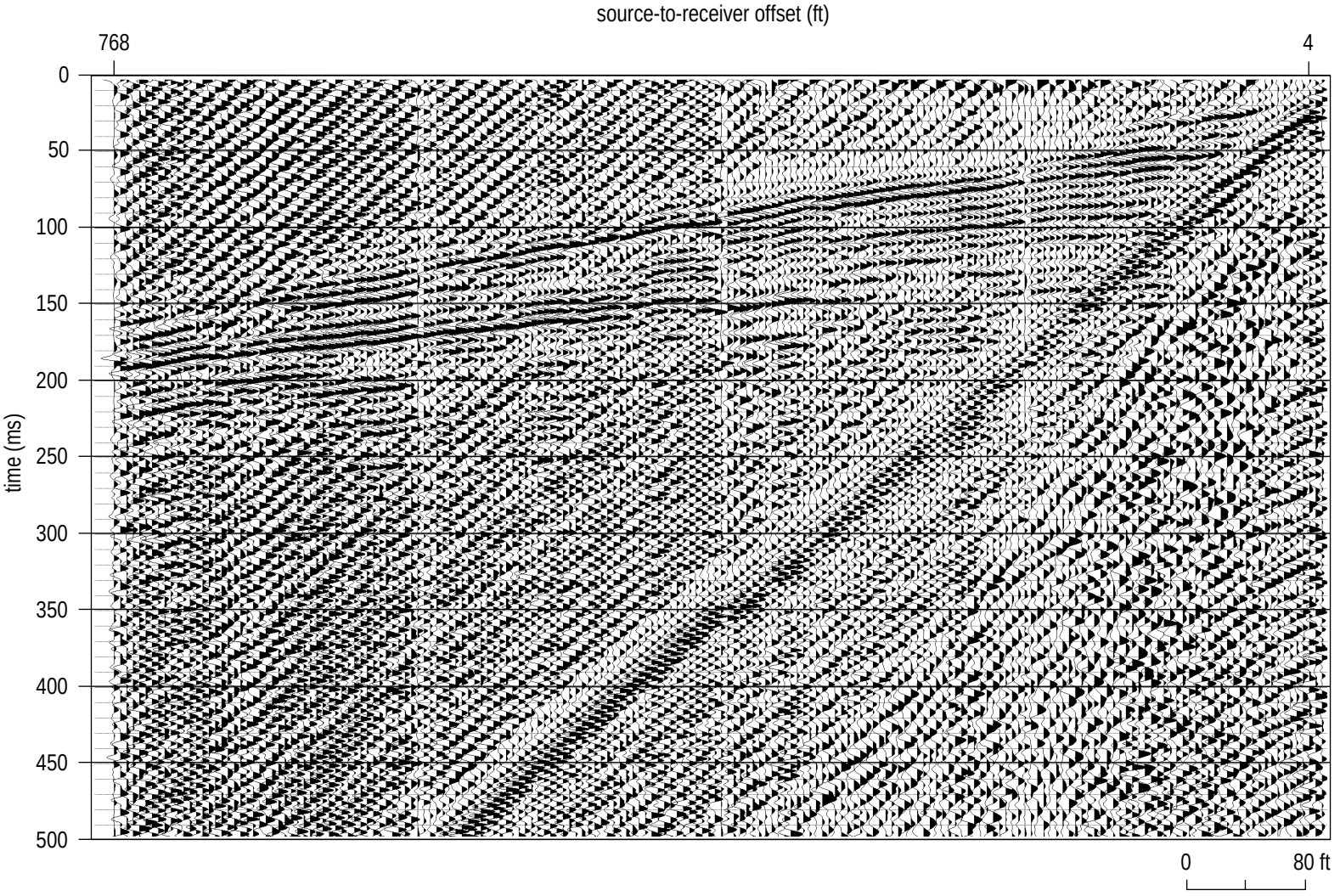

Figure 34. Ground force correlation of vibratory sweep 120494s along the airstrip line.

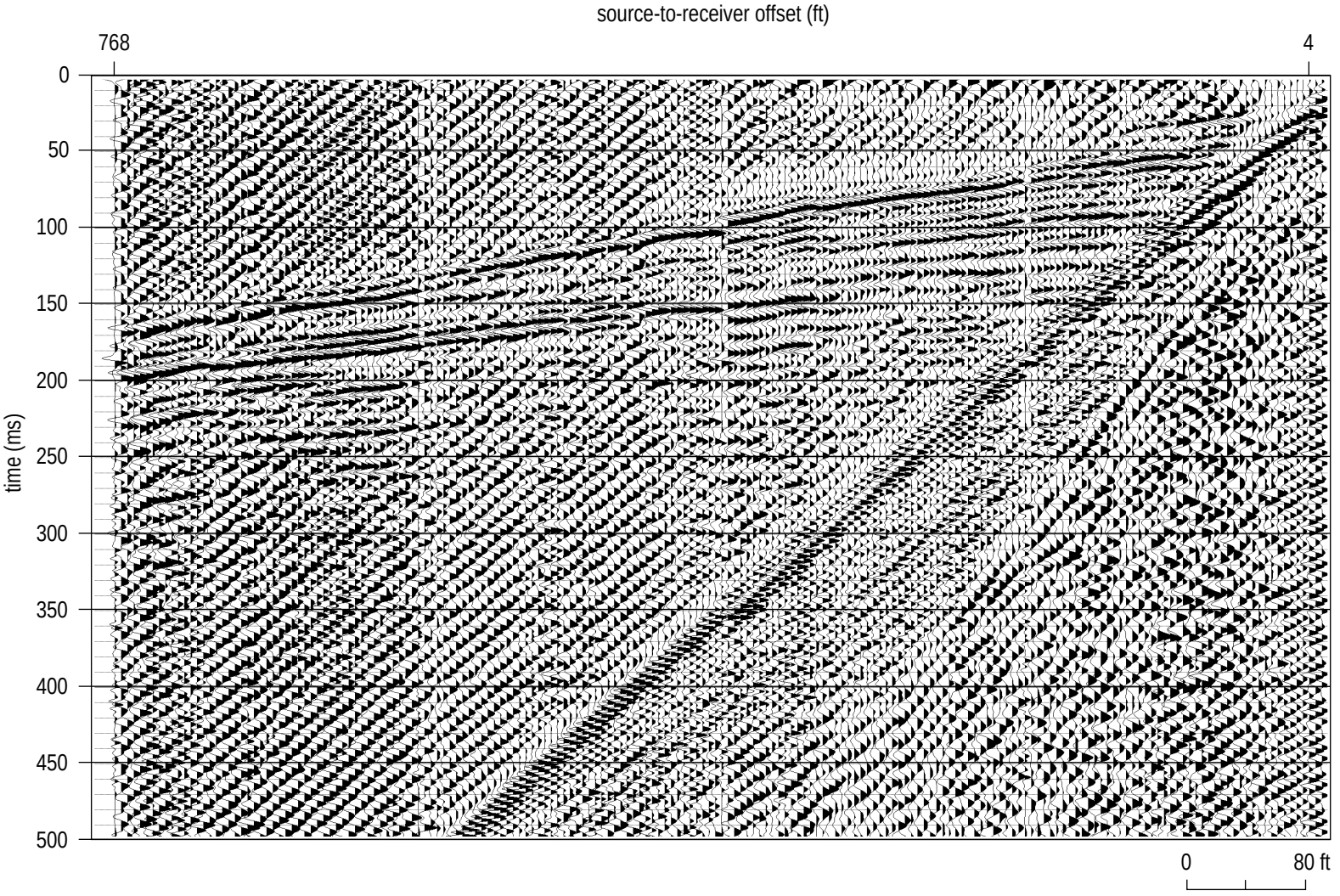

Figure 35. Synthetic correlation of vibratory sweep 120494s near the airstrip line.

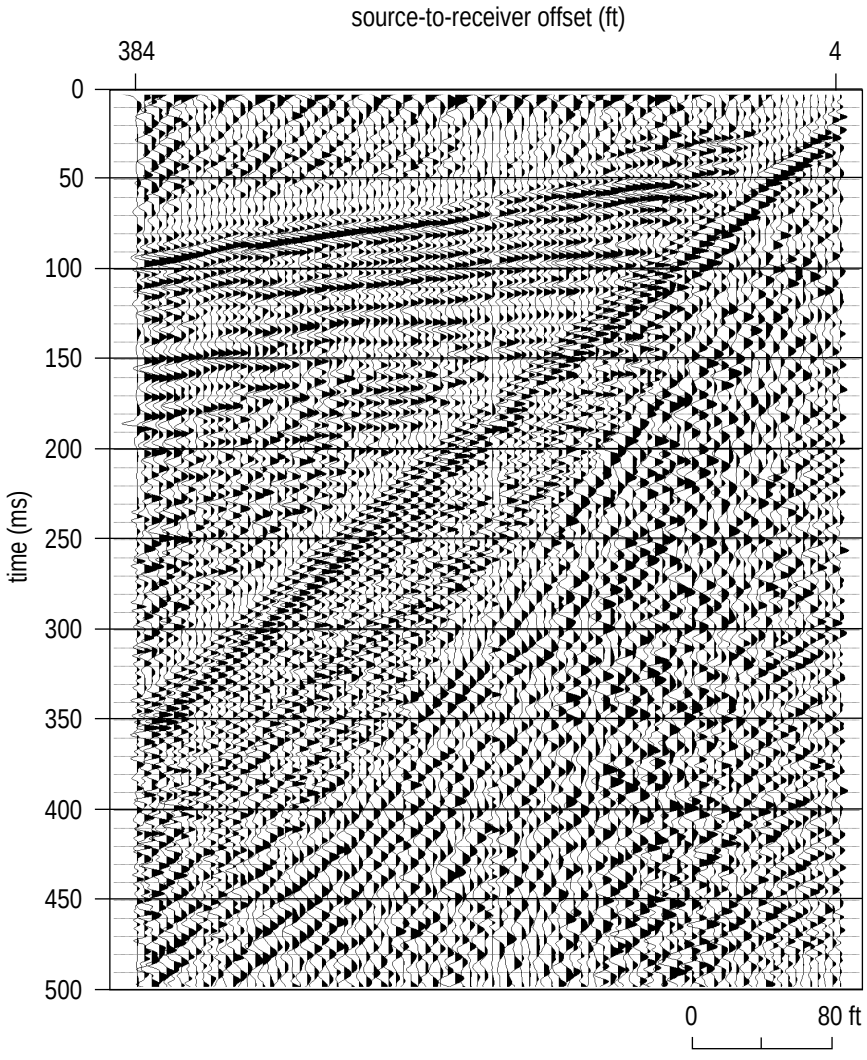

Figure 36. Ground force correlation of vibratory sweep 120494s4 on dirt road along the airstrip line.

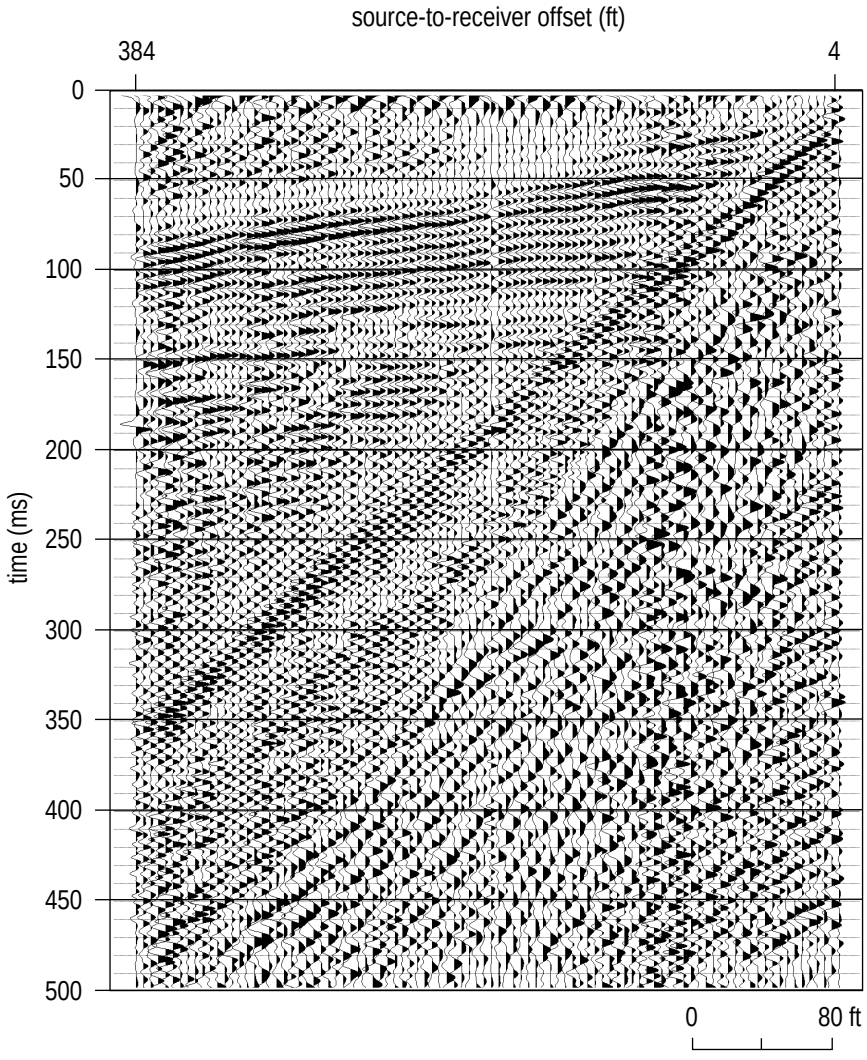

Figure 37. Synthetic correlation of vibratory sweep 120494s4 on dirt road along the airstrip line.

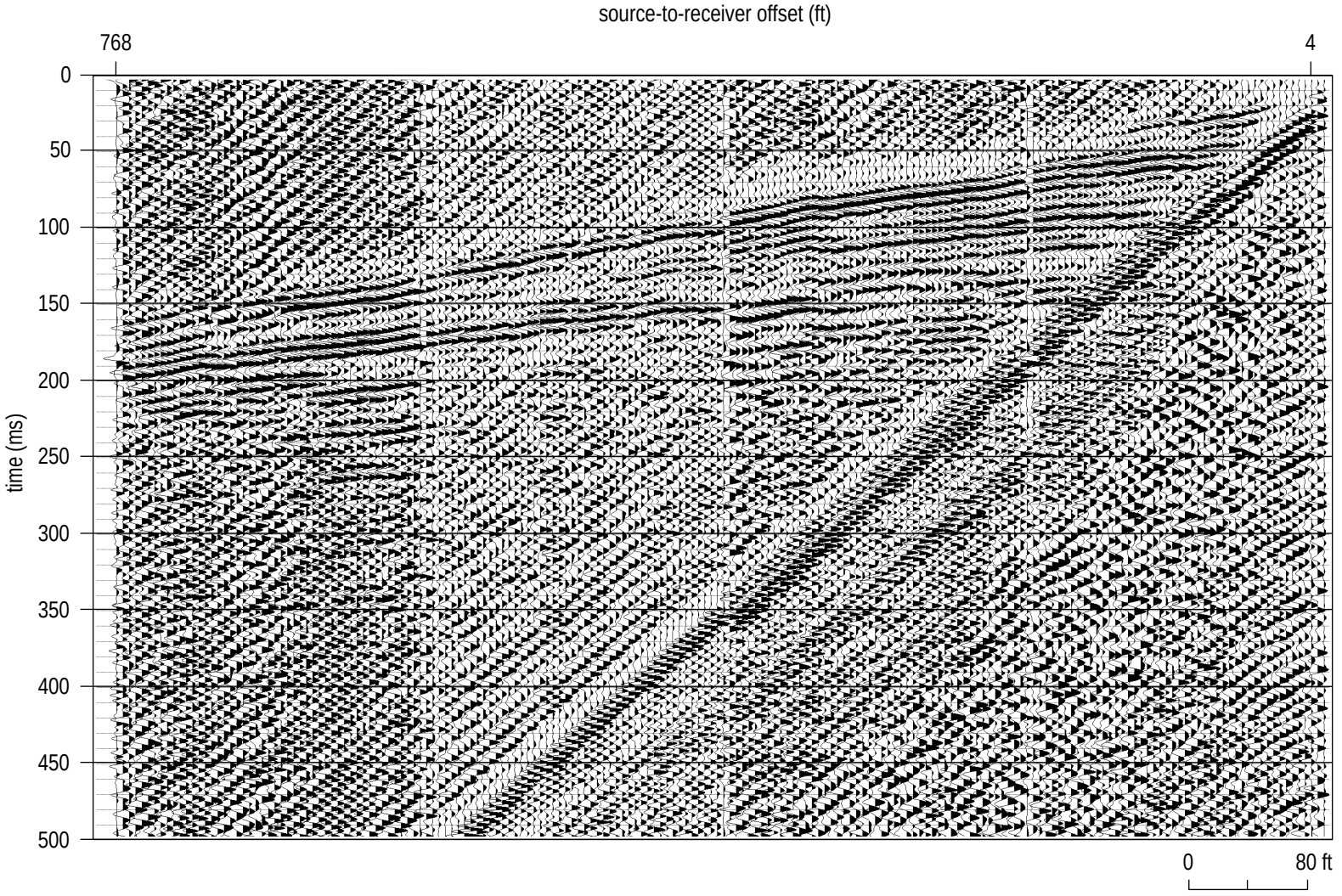

Figure 38. Synthetic correlation of vibratory sweep 120494s with 1 second taper along the airstrip line.

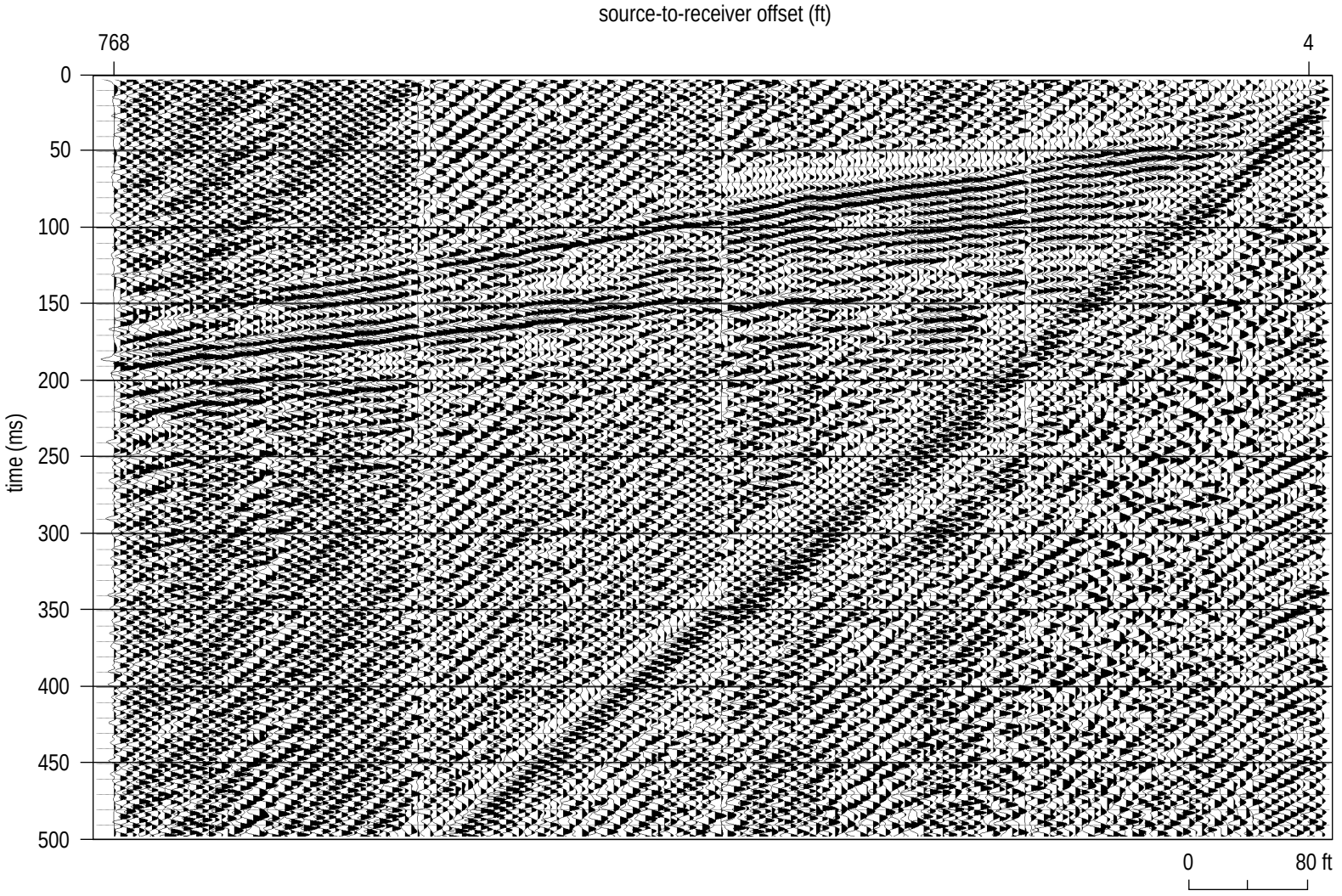

Figure 39. Ground force correlation of vibratory sweep 120494s with 1 second taper along the airstrip line.

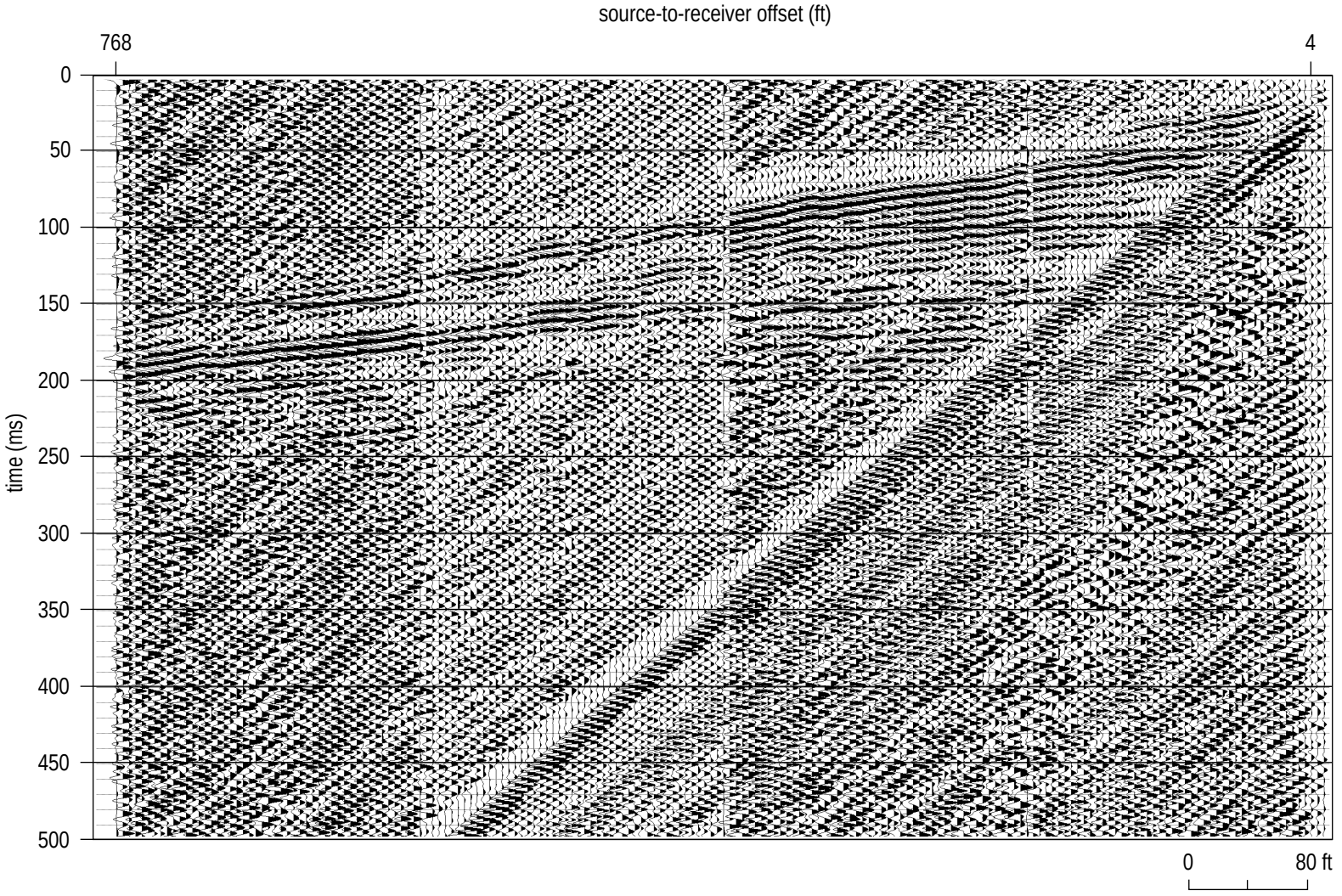

Figure 40. Synthetic correlation of vibratory sweep 120494s with 2 second taper along the airstrip line.

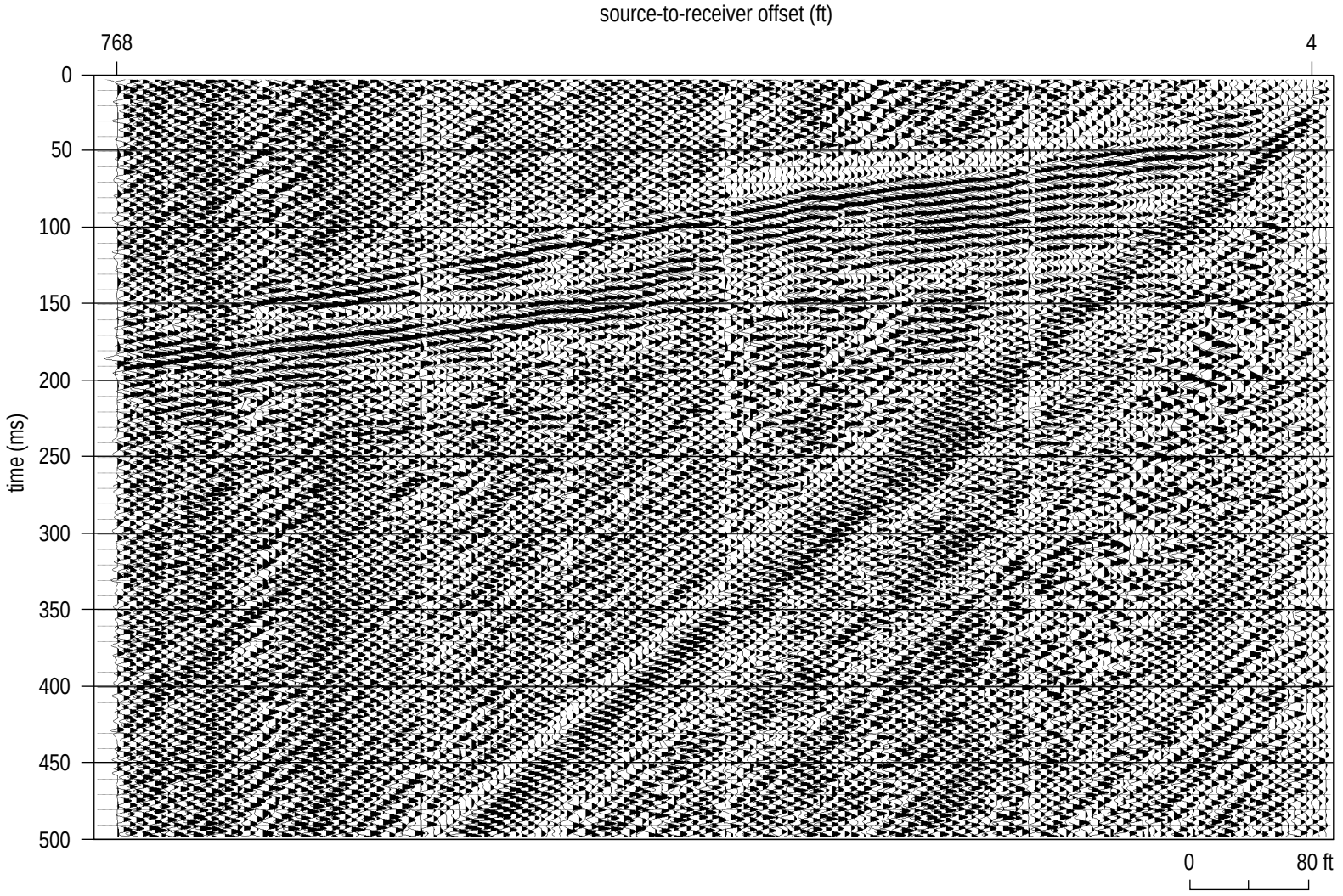

Figure 41. Ground force correlation of vibratory sweep 120494s with 2 second taper along the airstrip line.

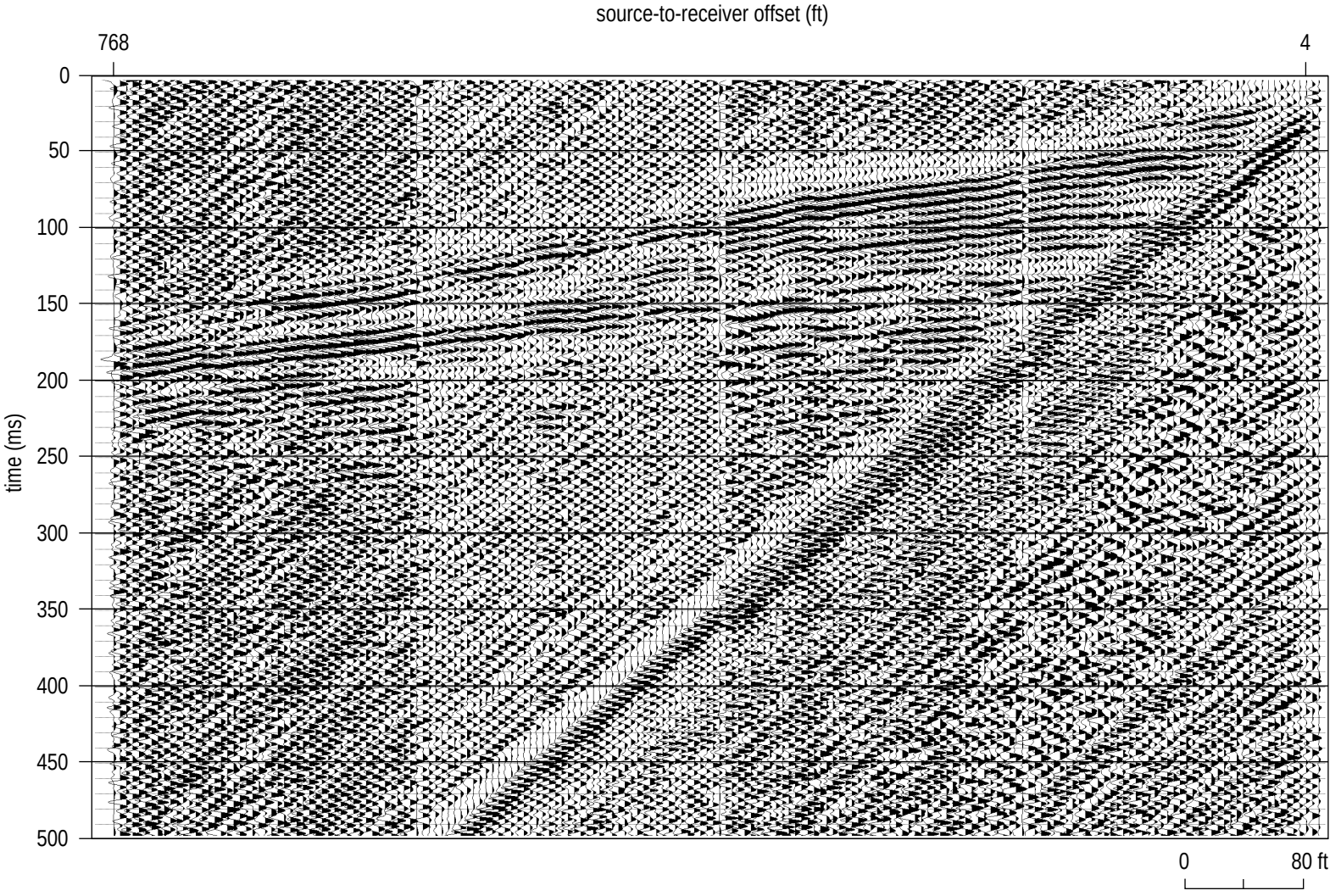

Figure 42. Synthetic correlation of vibratory sweep 120494s with 3 second taper along the airstrip line.

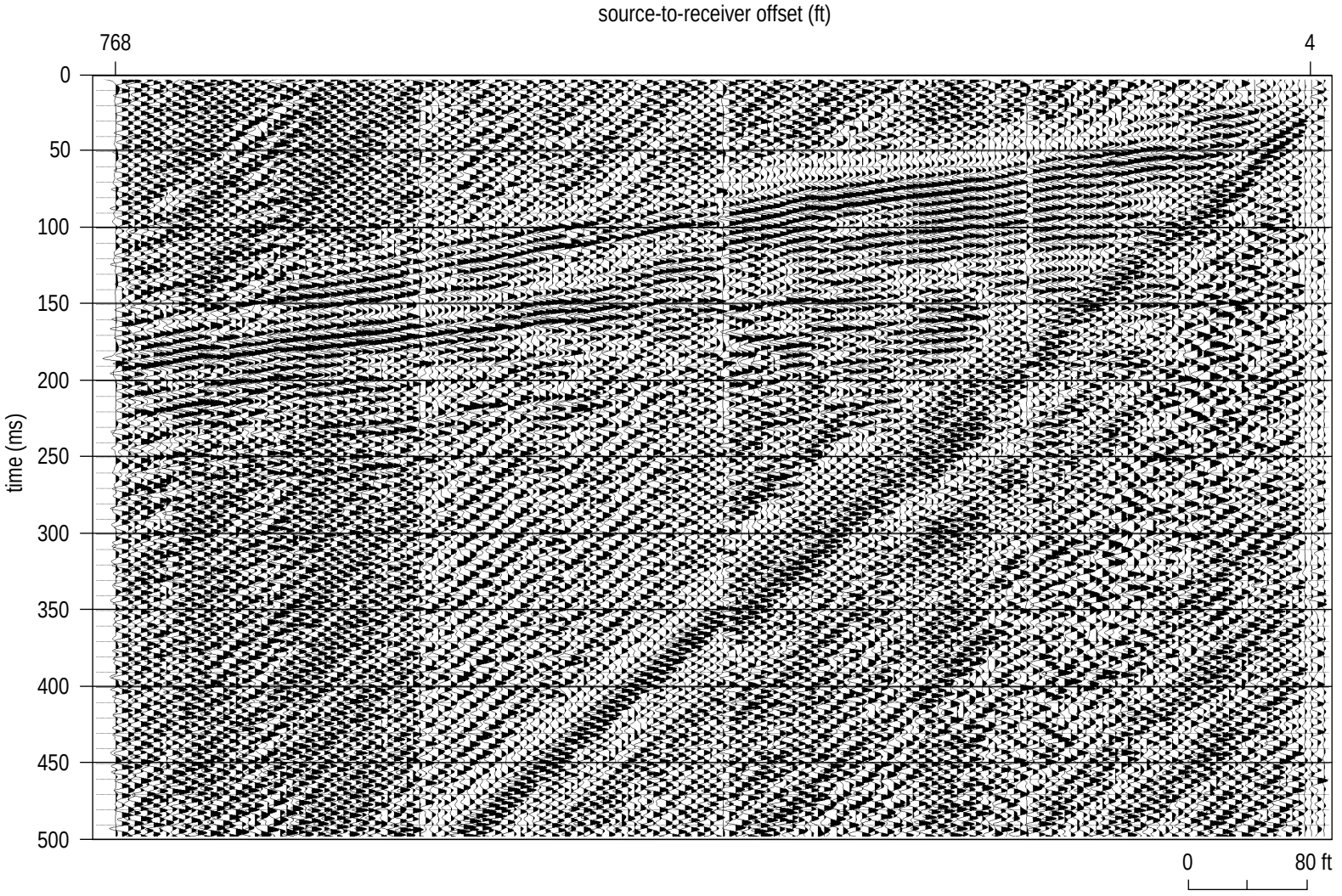

Figure 43. Ground force correlation of vibratory sweep 120494s with 3 second taper along the airstrip line.

interpretable reflections. The vibrator data seemed to possess several more reflections between 35 and 140 msec with better resolution potential than the air gun. The coherency and overall signal-to-noise ratio of very shallow reflections (35 to 70 msec at offsets less than 100 ft) were clearly superior on the vibrator data when correlated with the ground force. Multiples were not nearly as evident on test data from the airstrip as from the western boundary. Production data from the airstrip were acquired using sweep 112394s stored in an uncorrelated format with an 8 ft station spacing, source-to-nearest offset of 8 ft, and farthest offset of 384 ft.

Spesutie Island

The walkaway data at Spesutie Island were collected along the northern end of the production line (Figure 2). The walkaway spread was deployed in a mowed area about 30 ft west of the main north-south access road, extending from Range 12 S.I. road north to the westward bend in the north-south access road. The two source locations were off the north end of the spread and separated by 384 ft. In the test area the grass was well established and manicured with no obvious surface disturbance. Each source occupied ground that had not been disturbed by other seismic sources. Based on the results of line clearances, this area had at one time been either an active range or near enough to receive shrapnel from targets or ordnance. Aside from the occasional artillery blast, the area was very quiet with only intermittent road traffic.

The near-surface geology at Spesutie Island is slightly different than at the airstrip, as evidenced by comparison of the first arrivals at offsets less than 100 ft. The sledge hammer data at Spesutie Island have a much narrower frequency band than at the airstrip. The similarity in refraction and reflection frequency bands renders digital filtering ineffective in separating the ringy refraction from low amplitude, shallow reflections. Four-shot vertical stacks with the 12 lb sledge hammer did little to improve the signal-to-noise ratio of the data sets (Figures 44 and 45). After careful examination it becomes evident that vertical stacking at this site actually decreased the resolution potential by reducing the dominant frequency. This decreased resolution potential is likely the result of plastic deformation from repetitive hammer/plate impacts. The dominant reflection frequency is about 100 Hz with an upper corner frequency of around 150 Hz. The majority of the reflected energy has a strong 100 Hz component.

The RAWD generated a substantial refraction ring at offsets from 50 to 275 ft. This ring is not unusual for surface weight drop sources. As with the sledge

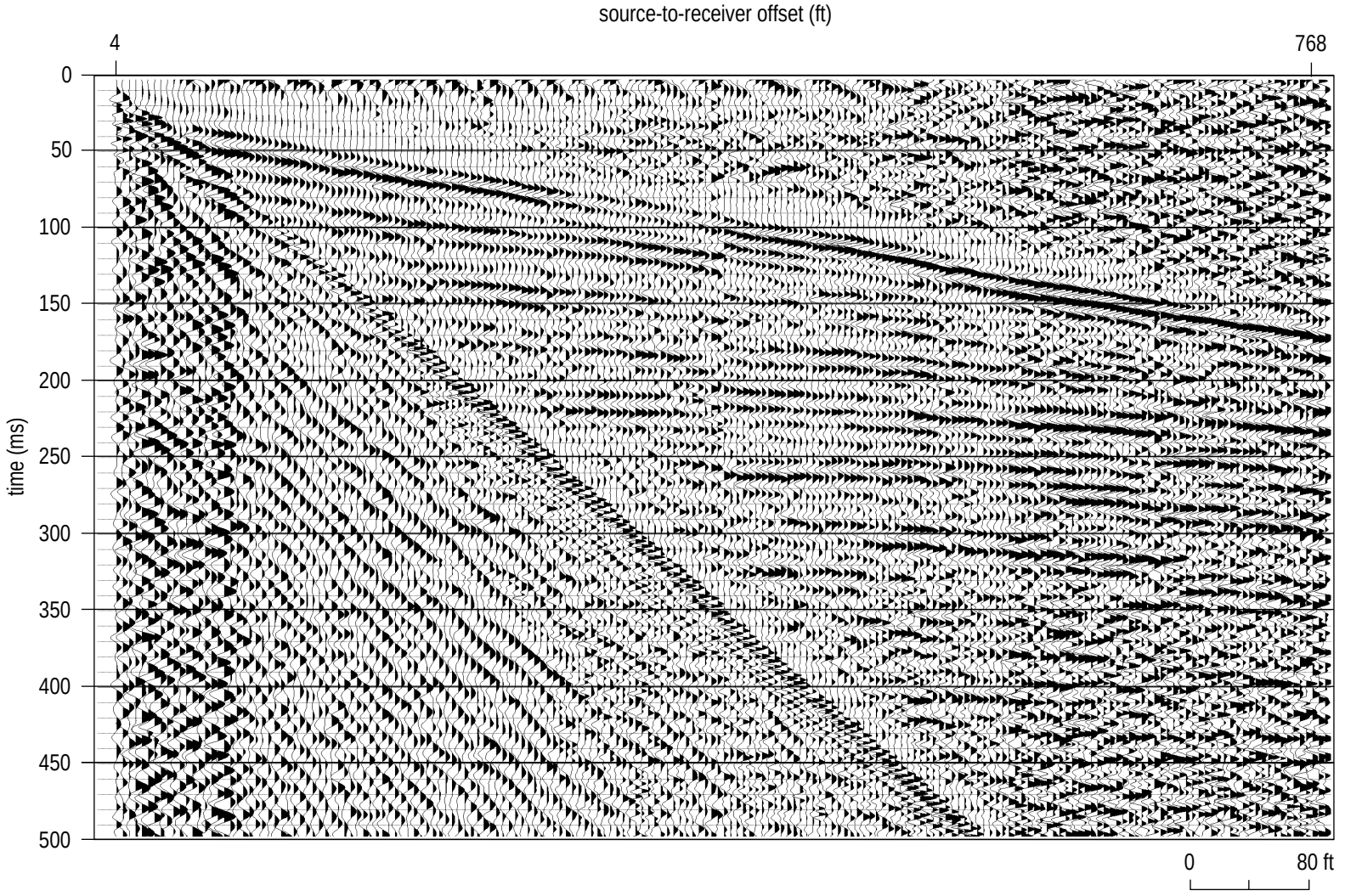

Figure 44. Single impact from a 12 lb sledge hammer on a steel plate at Spesutie Island.

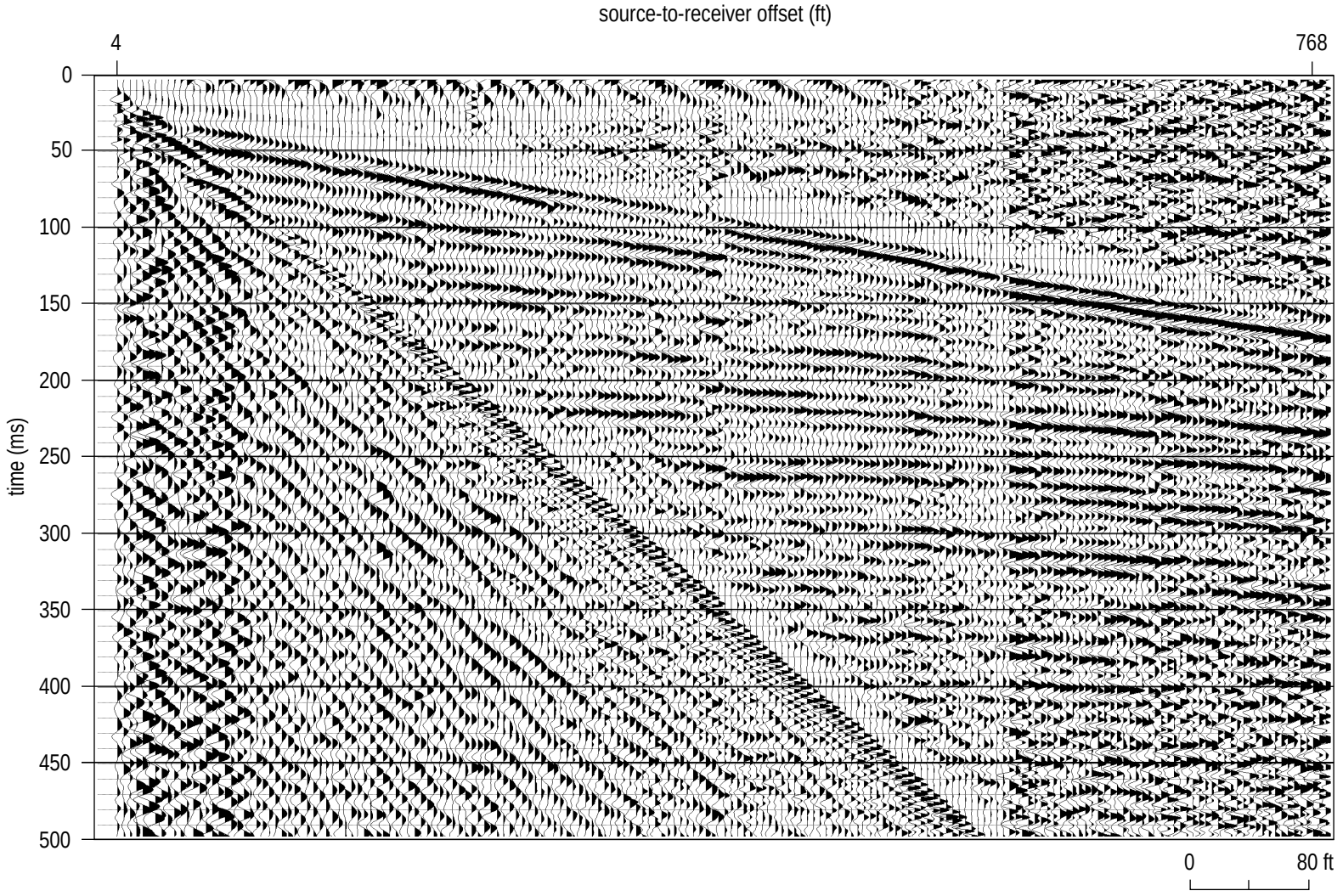

Figure 45. Four-shot vertical stack of a 12 lb sledge hammer on a steel plate at Spesutie Island.

hammer data, little improvement is noted by vertically stacking impacts (Figures 46 and 47). The reduction in resolution potential by subtle misalignment of repetitive impacts is not nearly as evident with the RAWD as with the sledge hammer. The difference observed in stacking potential is likely related to the use of a hammer switch for time zero control on the sledge and the contact closure method used with RAWD. The dominant frequency of RAWD reflection data appears to be about 90 Hz with the upper corner frequency near 130 Hz. Coherent arrivals at offsets greater than 300 ft and at time depths greater than 300 msec are multiples. RAWD data do have a significantly larger percentage of multiples to primary reflections than does sledge hammer data.

Due to the 8-gauge auger gun's invasive and explosive nature, it was tested at Spesutie Island in this potential UXO encounter area for comparison purposes only. Auger gun data at this site provides a substantially higher resolution potential and signal-to-noise ratio than any of the weight drop sources tested. Reflections from zero offset times between 40 and 70 msec are interpretable at source offsets greater than 100 ft and less than 200 ft (Figure 48). Multiples are evident below 300 msec, as was the case with RAWD. By comparing the 200 msec reflection on the auger gun data with the same reflection on RAWD data, the broader reflected energy band-width becomes evident (Figures 48 and 46). The auger gun reflection wavelet is much closer to a minimum phase pulse as opposed to the mixed phase uniform doublet of RAWD. The dominant reflection frequency is about 110 Hz with an upper corner frequency of about 140 Hz. The frequency content and number of identifiable unique reflections at offsets between 50 and 400 ft on the auger gun record is greater than any of the weight drop sources or the air gun.

Signal-to-noise enhancement is possible through repetitive vertical stacking of air gun shots. Unlike the airstrip test area, at Spesutie Island the signal-to-noise ratio of air gun data can be increased without compromising frequency content. Comparison of a single 500 psi shot with a stack of four 500 psi shots from the air gun shows a reduction in high frequency random noise (chatter) at offsets greater than 300 ft while maintaining a dominant frequency of around 100 Hz (Figures 49 and 50). The closer offsets (< 250 ft) are dominated by the same refraction ring noted on RAWD data. Use of a severe low-cut filter did little to "uncover" reflections masked by this overpowering cyclic refraction energy.

Increasing the power of the air gun (i.e., raising the gun pressure to 1500 psi) dramatically changed the characteristics of the reflected wavelets (Figures 51 and 52 compared with Figures 49 and 50). The reflection wavelet (doublet) of the 200 msec

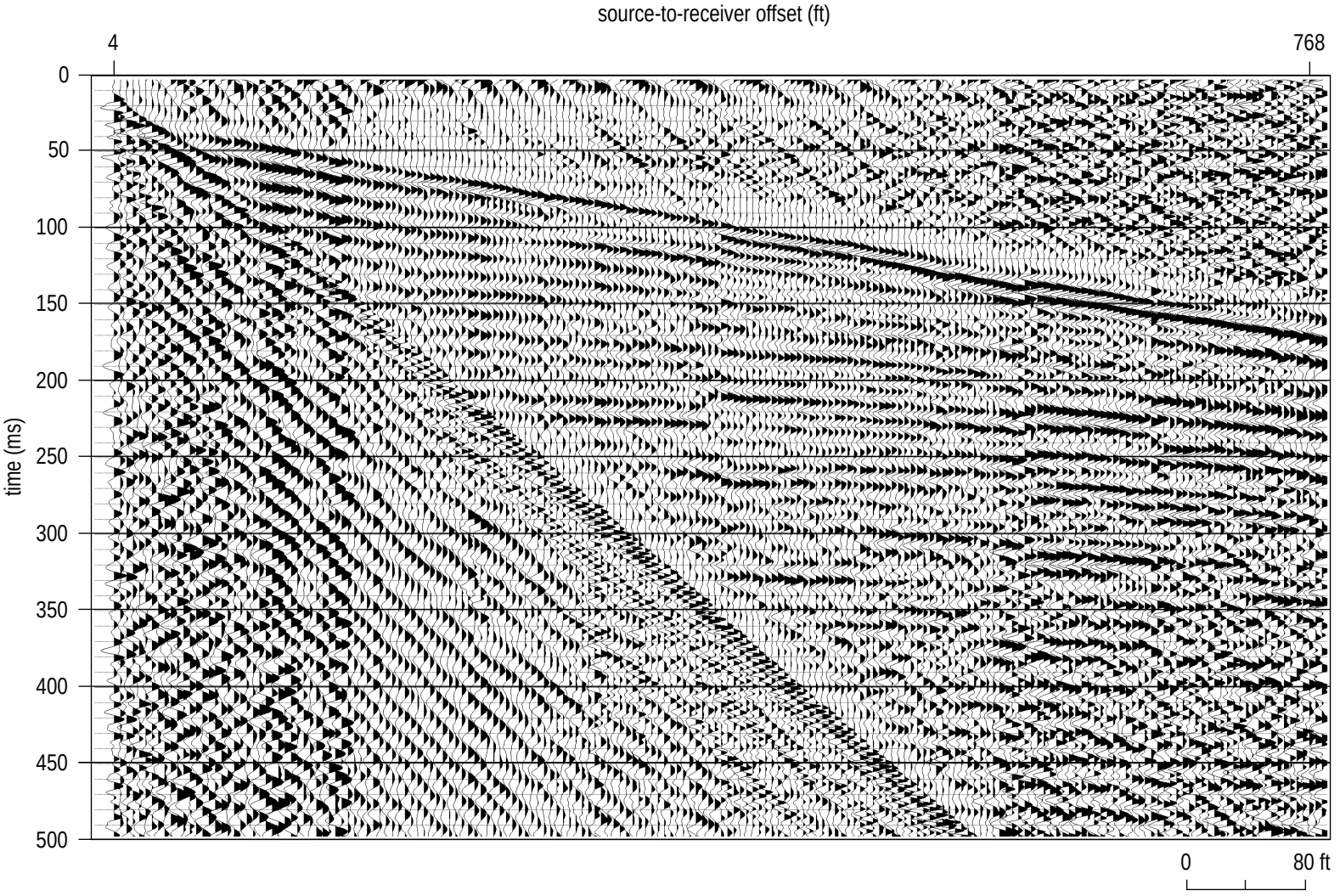

Figure 46. Single impact of RAWD at Spesutie Island.

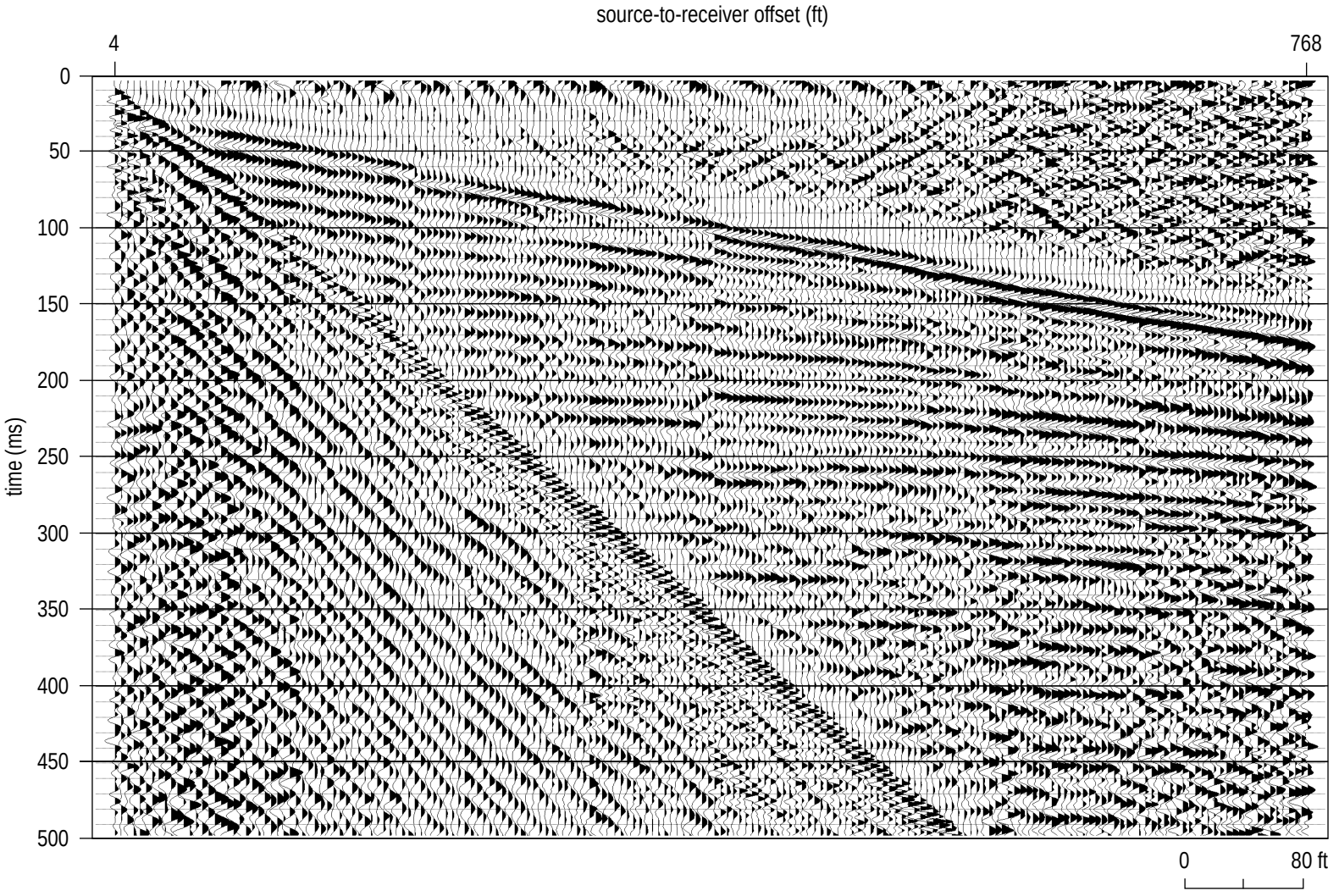

Figure 47. Four-shot vertical stack of RAWD at Spesutie Island.

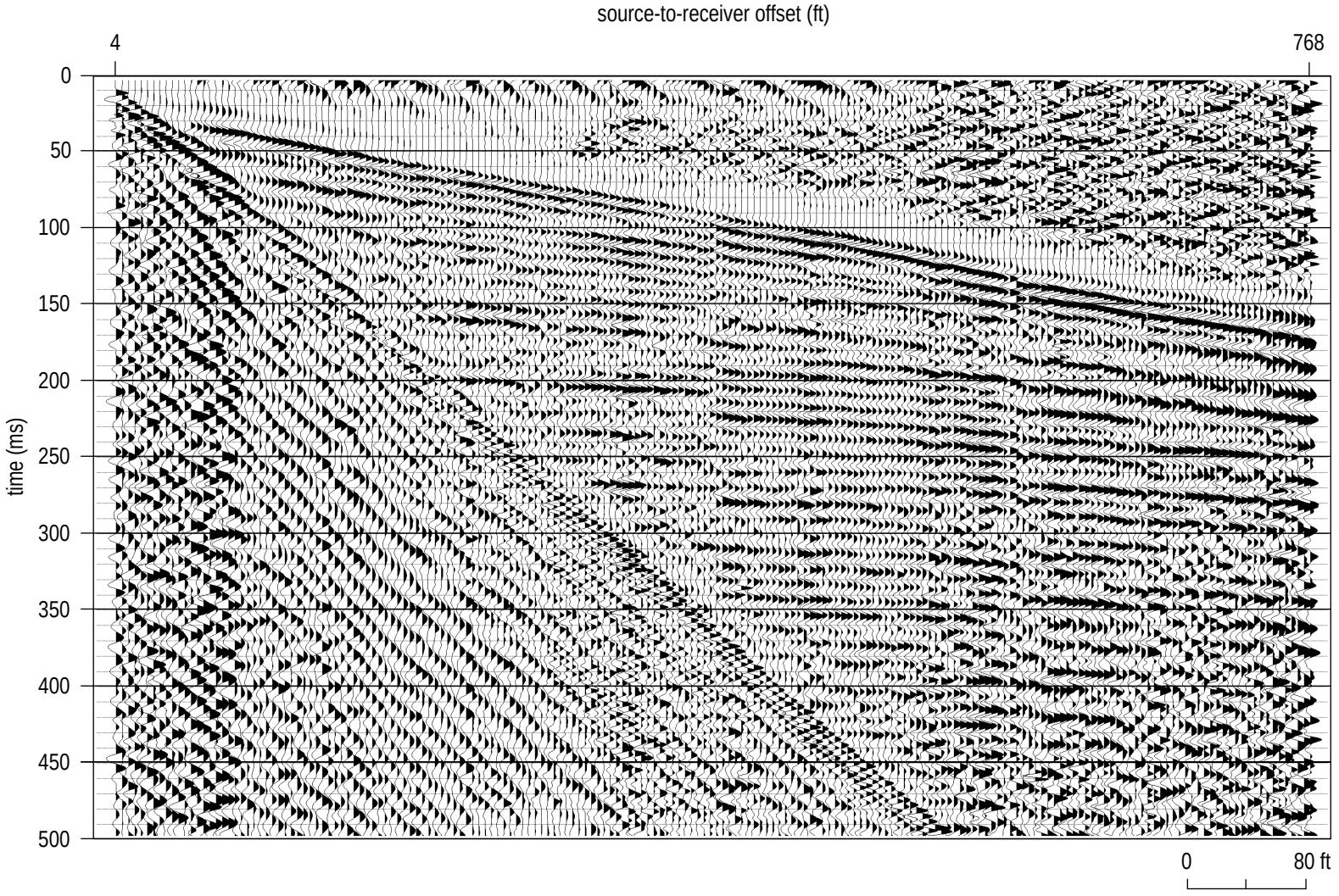

Figure 48. 8-gauge auger gun shot gather at Spesutie Island.

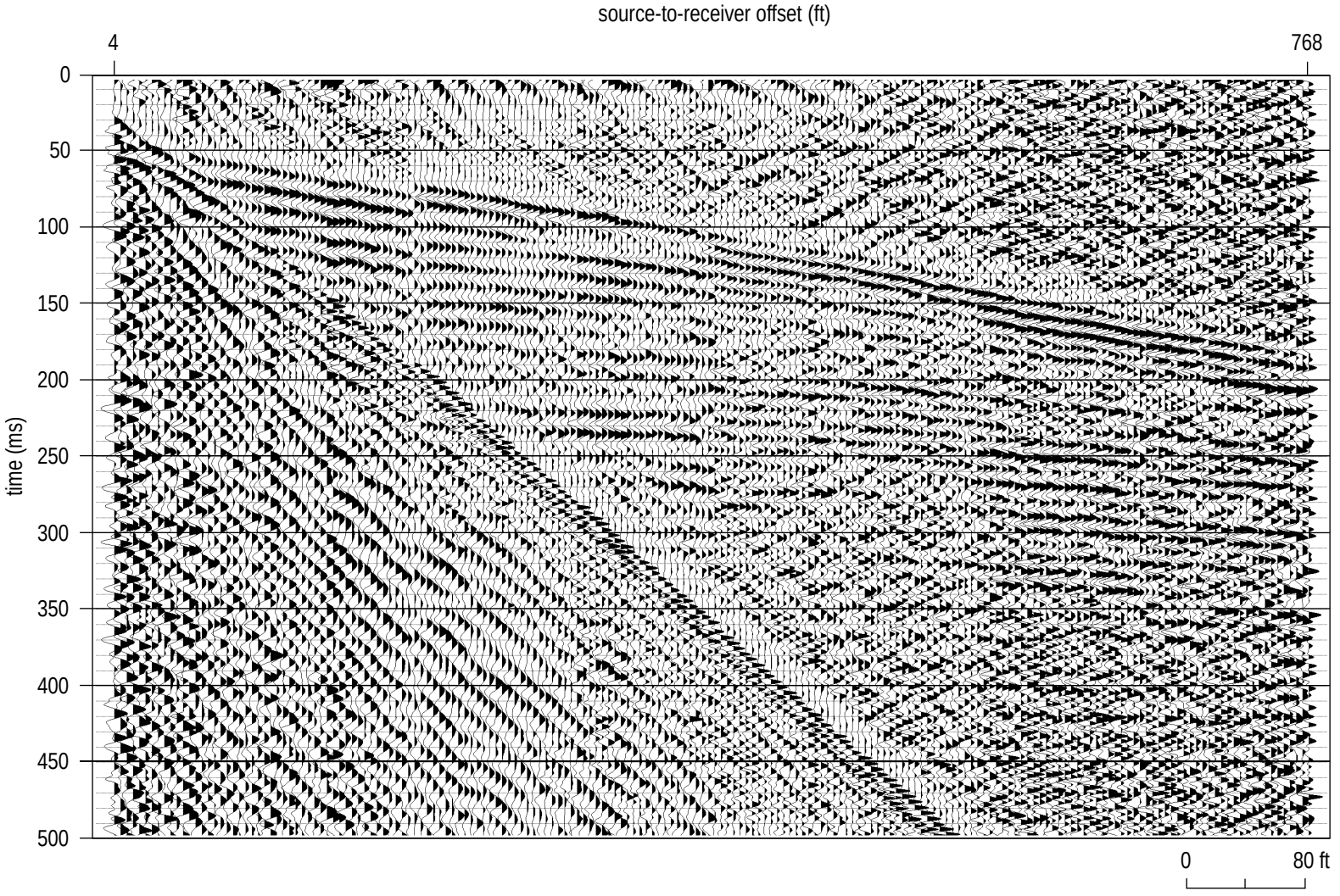

Figure 49. Single 500 psi air gun shot at Spesutie Island.

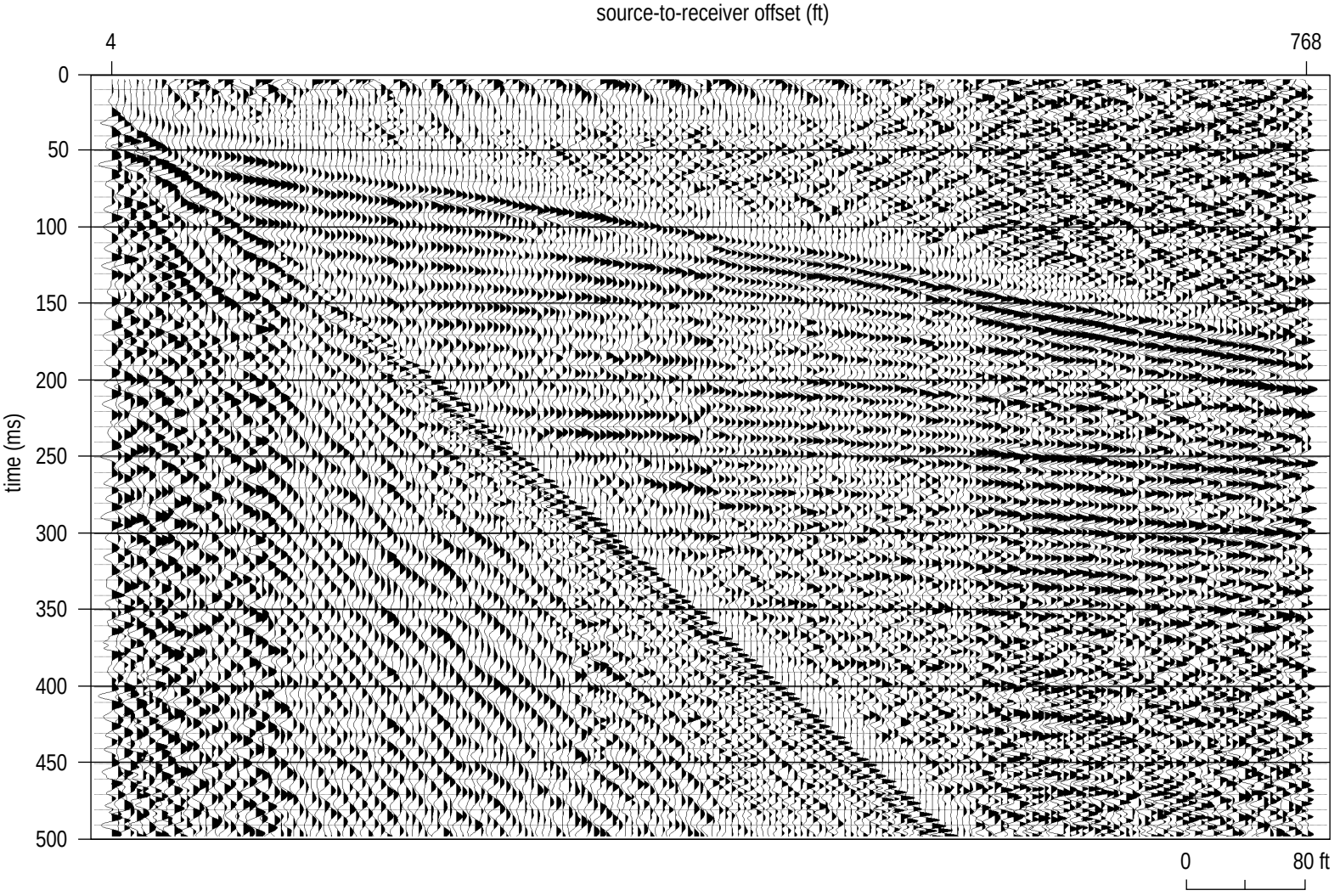

Figure 50. Four-shot vertical stack of 500 psi air gun shot at Spesutie Island.

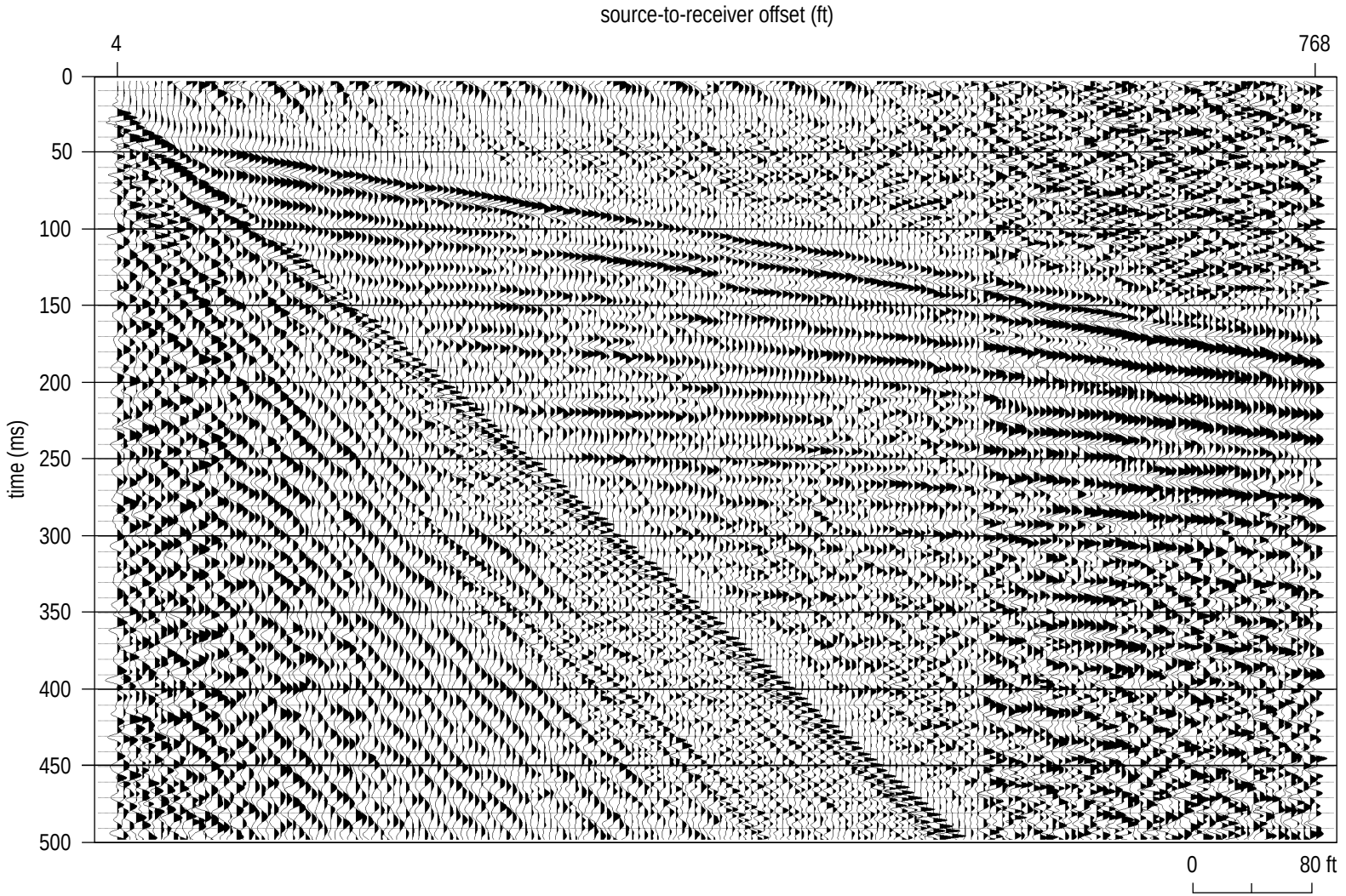

Figure 51. Single 1500 psi air gun shot at Spesutie Island.

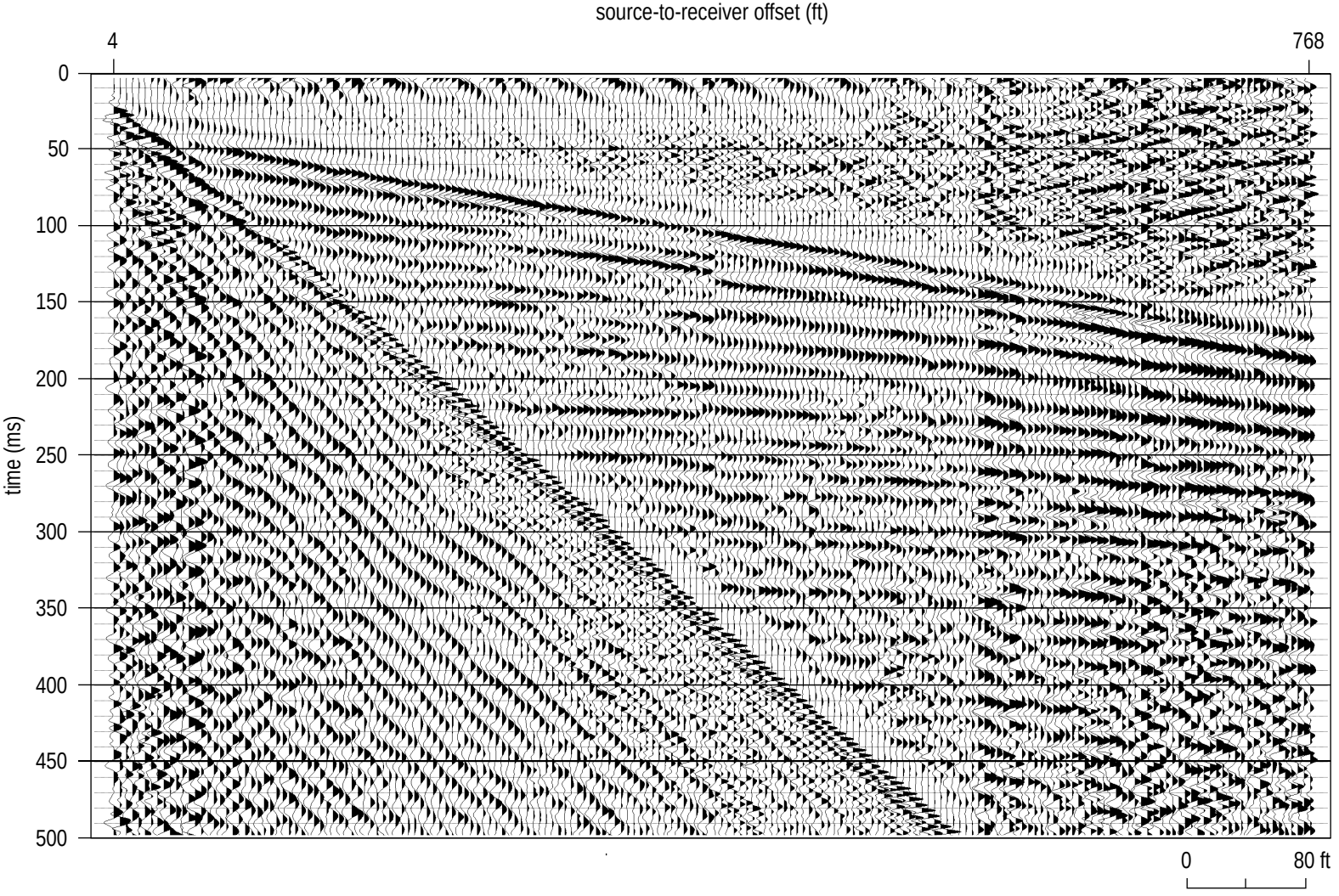

Figure 52. Four-shot vertical stack of 1500 psi air gun shot at Spesutie Island.

event changed polarity from an initial positive peak, or kick, on the 500 psi data to a negative first peak on the 1500 psi shot gather. This is the first and only time on this data set that simply changing a source configuration has resulted in such a dramatic source wavelet change. It is likely the change is related to coupling and source volume. The dominant frequency of the air gun data is about 100 Hz on single shot data and 90 Hz on stacked data with an upper corner on both of around 120 Hz. Unlike other surface impact sources tested at this site, the 1500 psi air gun single shot produced a reflection at about 200 msec, which is very similar to the auger gun reflection at that time.

The vibrator comparison, as at the other two sites, focused on variations in sweep calibrations, the correlation trace, and shaping the amplitude spectra of the drive signal. Consistent with the other test areas, ground force correlation produces the highest frequency reflections and largest signal-to-noise ratio (Figure 53 compared to 54 and Figure 55 compared to 56). However, unlike the other two sites, at Spesutie Island the variability in data quality as a function of which pilot trace was used for the correlation is not nearly as distinct. One very noteworthy difference between the ground force and synthetic shot gathers is the presence of a high frequency event that interferes with the second lobe of the refraction wavelet at offsets between 50 and 100 ft (Figures 55 and 56). This small interference phenomenon is consistent with what appears to be a reflection on the auger gun data (Figure 48). The auger gun data at Spesutie Island is, of course, the highest quality of all data acquired at this site.

Comparisons of sweep 112394s (which has produced the best correlated vibrator records at both the western boundary and airstrip) with sweep 120694s suggest that 120694s (which was site-calibrated) results in higher frequency reflection wavelets and reduced signal-to-noise ratio at time depths greater than about 150 msec. It is very difficult in this comparison format to determine if sweep 120694s correlated to the ground force might produce a "better" stacked section than 112394s. Reflections interpreted between 100 and 200 msec possess slightly higher dominant and corner frequencies on 120694s than 112394s.

Sweep tapering dramatically emphasizes reflections with zero offset times of 45 msec or so. Comparison of sweep 120694s with 0.125, 1, and 2 sec amplitude attenuation shows the clean separation of reflections from the refraction (Figures 56, 57, and 59). The dominant frequency of the reflected wavelet increases with only minimal reduction of bandwidth, as evidenced by a lack of excessive wavelet ring. This was noted as well on the same type of amplitude attenuation of sweeps at the

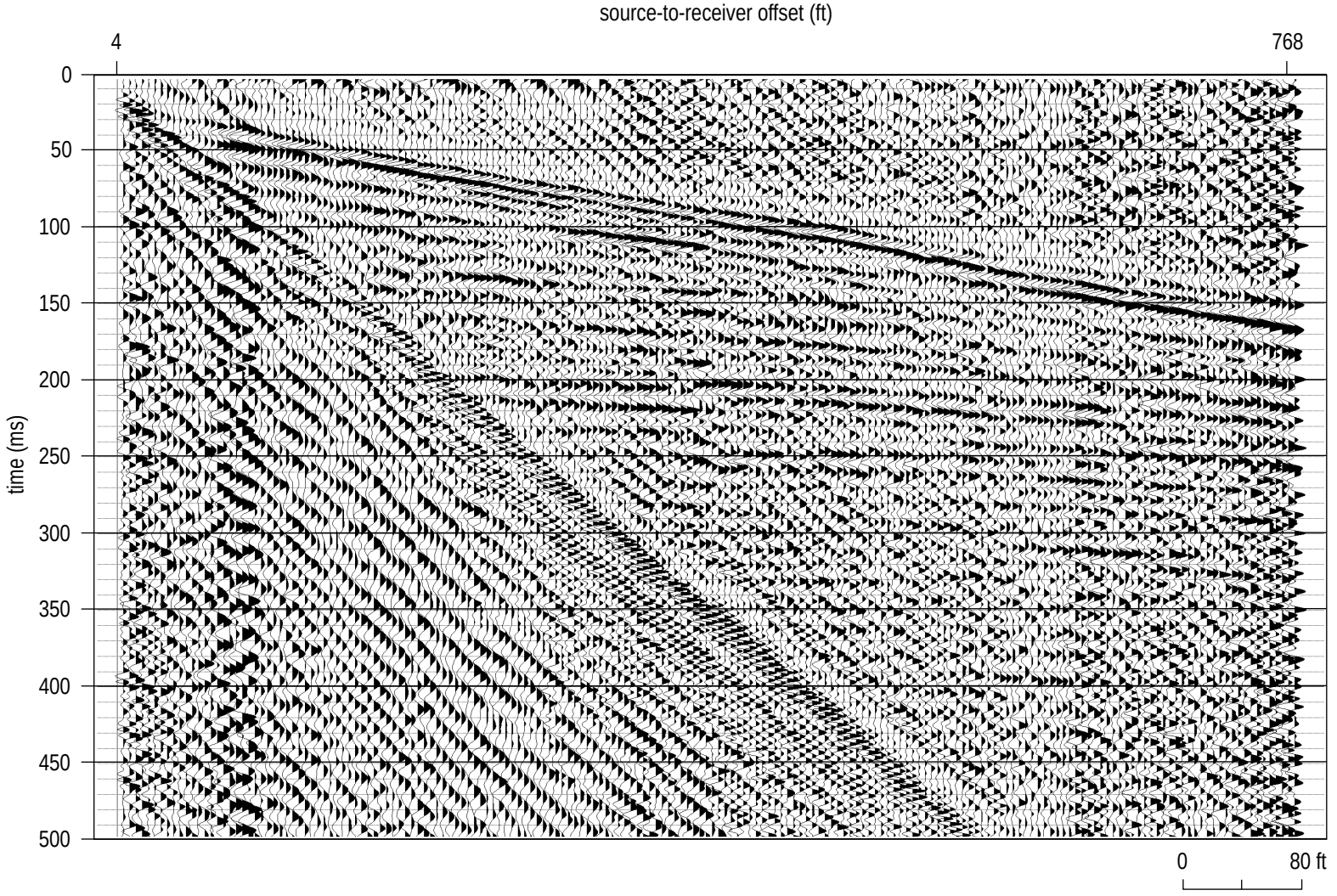

Figure 53. Ground force correlation of vibratory sweep 112394s at Spesutie Island.

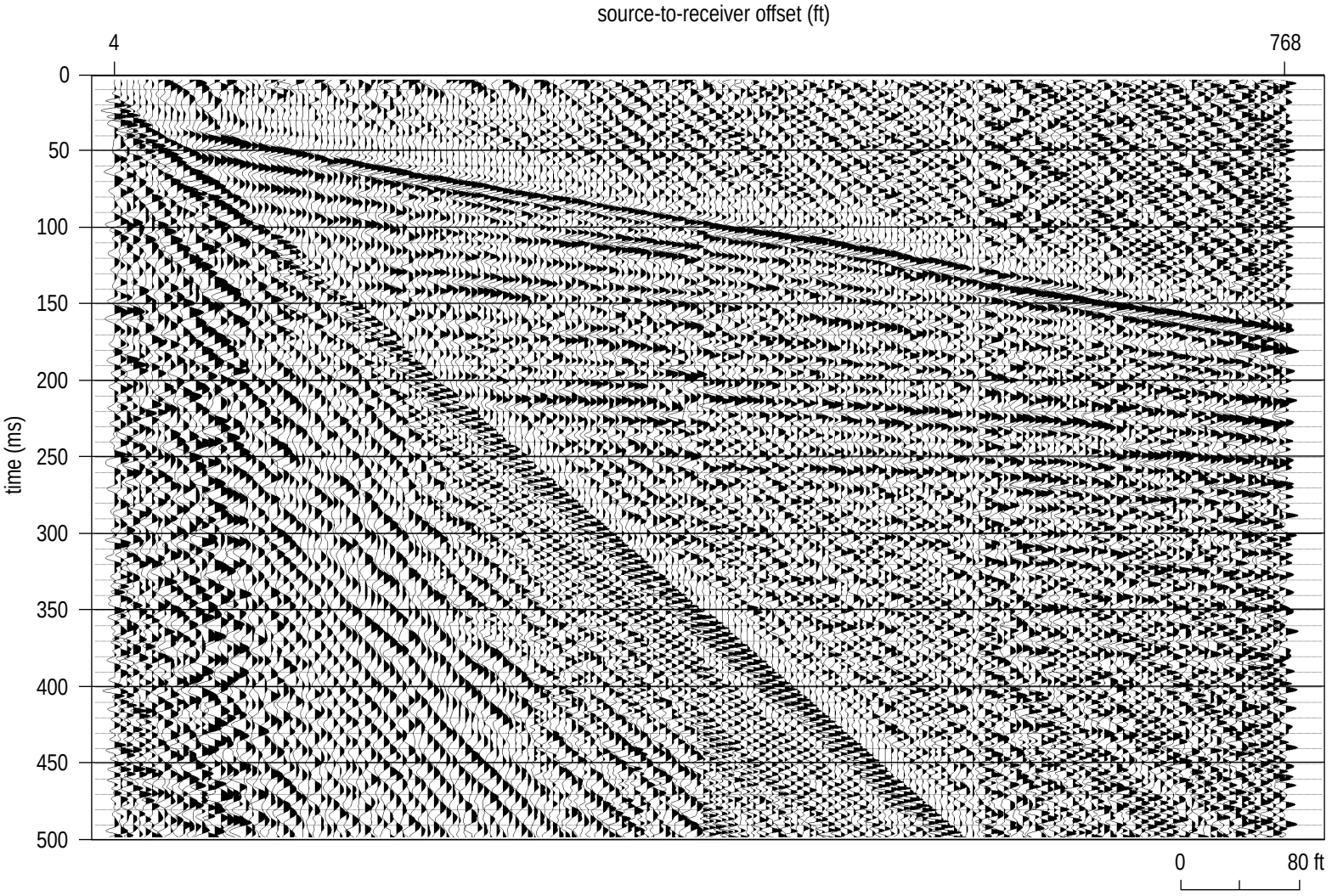

Figure 54. Synthetic correlation of vibratory sweep 112394s at Spesutie Island.

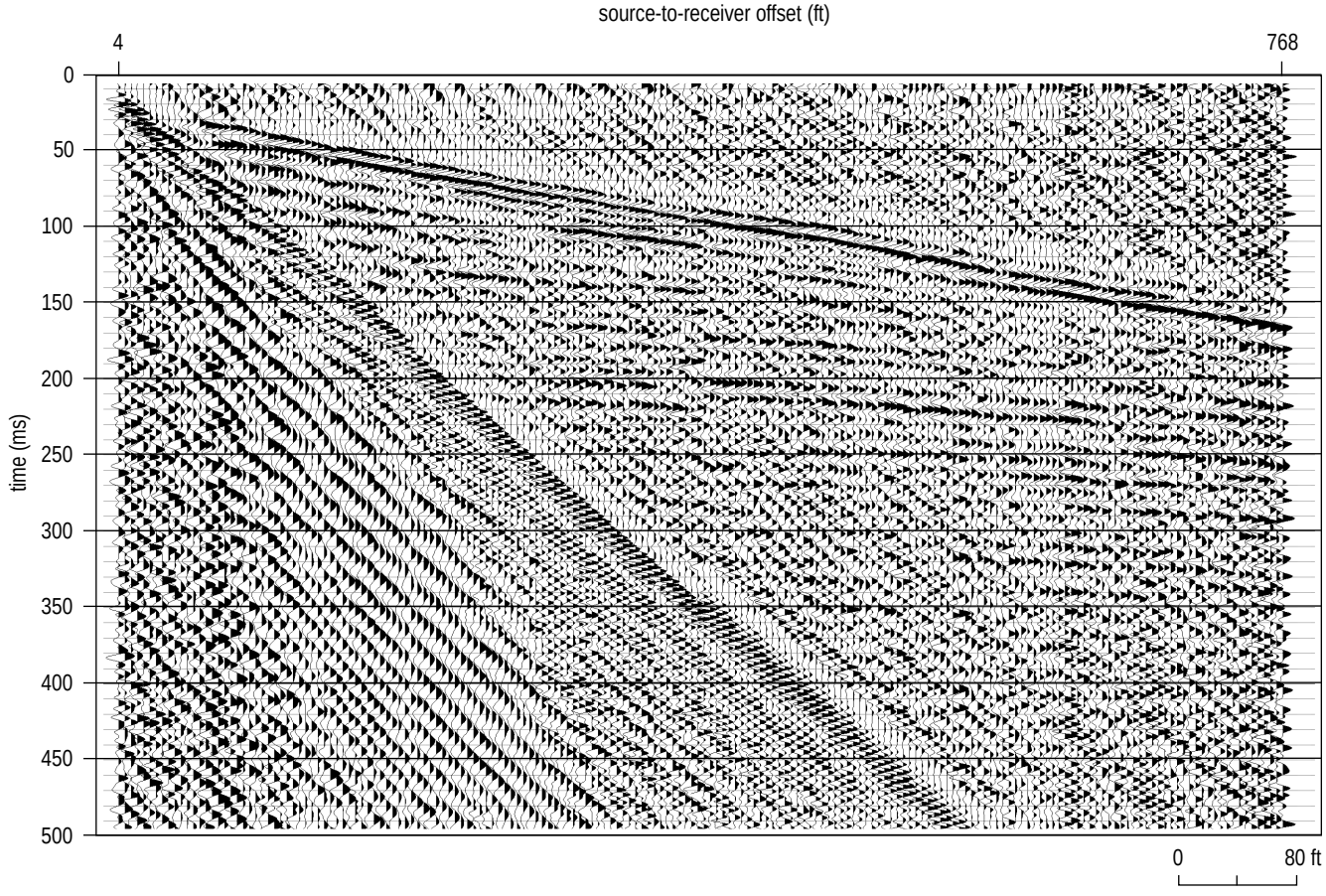

Figure 55. Ground force correlation of vibratory sweep 120694s at Spesutie Island.

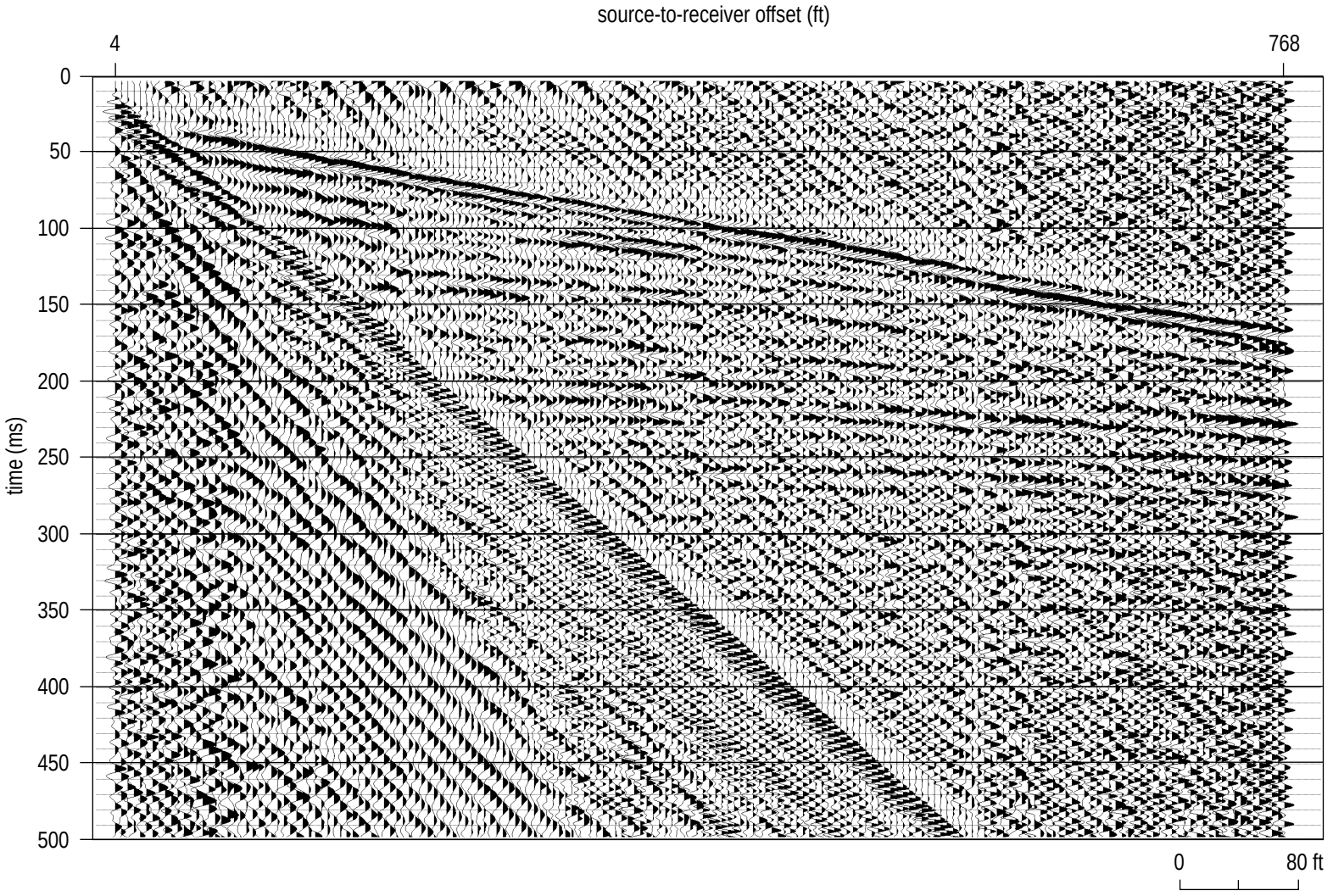

Figure 56. Synthetic correlation of vibratory sweep 120694s at Spesutie Island.

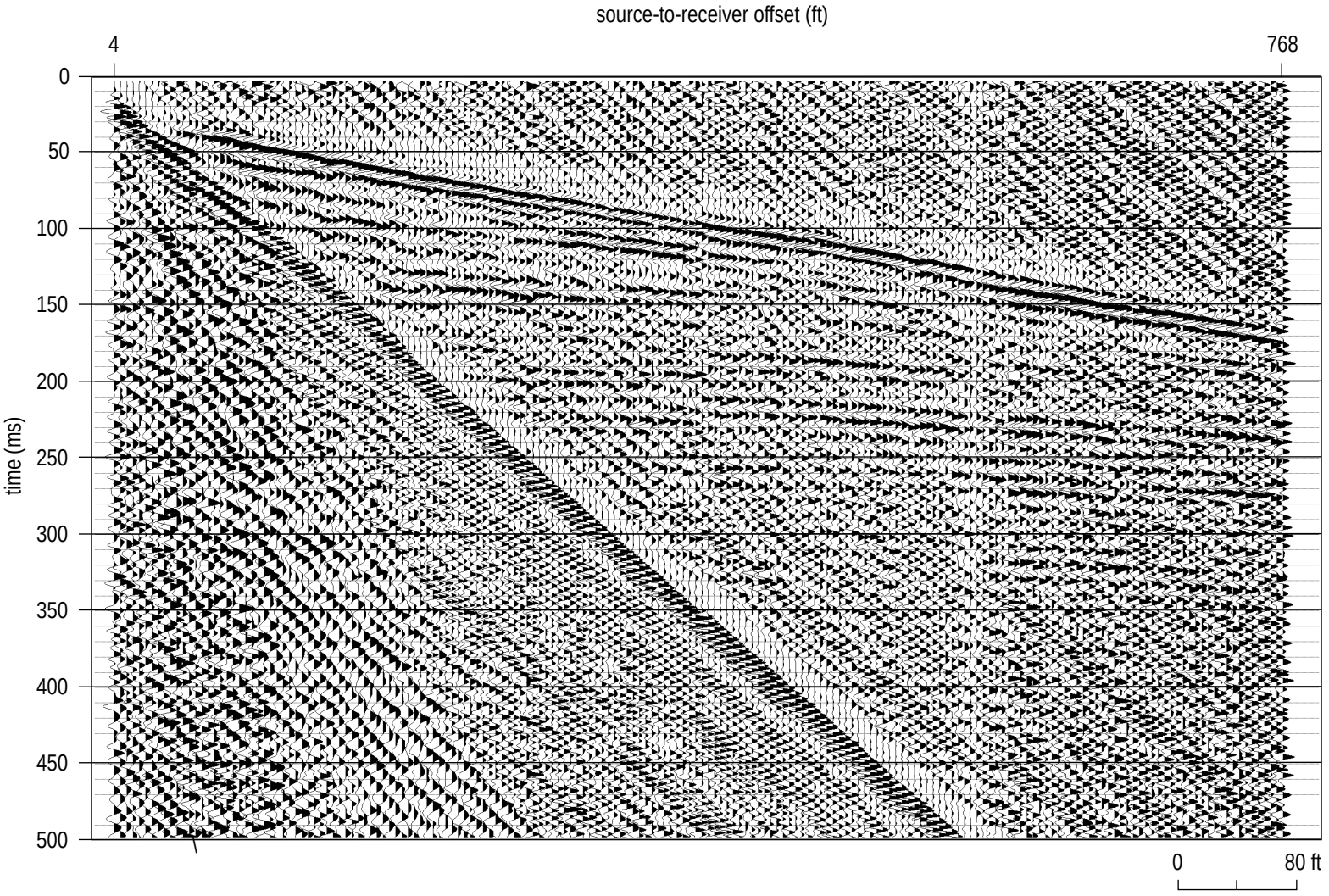

Figure 57. Synthetic correlation of vibratory sweep 120694s with 1 second taper at Spesutie Island.

airstrip. Correlation with the ground force improved the overall quality of the amplitude attenuation test data (Figures 55, 58, and 60).

The ground force correlation minimized the time duration of each individual reflection wavelet and more closely approximated a minimum phase wavelet. The bandwidth of the 120 msec reflection evident with the 2 sec amplitude taper is nearly a spike in time (Figure 60). Comparison of the 120 msec reflection on the 2 second taper data (Figure 60) to the much lower frequency wavelet recorded with a 0.125 sec taper (Figure 55) suggests an increase in dominant frequency without a decrease in the bandwidth. Sweep calibration at this site improved the resolution potential of shallower reflections and was consistent with non-site specific calibration for deeper reflections.

The source with the highest quality seismic reflection shot gather at Spesutie Island is not optimum for the production portion of this survey. The 8-gauge auger gun generated the best signal-to-noise and resolution potential of the sources tested (Figure 48). Focusing on the 65 msec and 200 msec reflections, the auger gun produced the "best" shot gather, followed by the vibrator with ground force correlation of either sweep 120694s (Figure 55) or 112394s (Figure 53), the 1500 psi air gun (Figure 51), and the four-shot stack of the sledge hammer (Figure 45). The auger gun was not considered due to site restrictions. After analysis of frequency content and bandwidth, signal-to-noise ratio, and the sheer number of interpretable reflections, it is clear that the vibrator out-performed the air gun and sledge hammer. The impact sources did not provide sufficient high frequency energy to separate the 65 msec reflection from the ring of the refraction.

The site-calibrated sweep (120694s) resulted in a slight increase in the shallow frequency spectra and possibly better resolution on some of the reflections between 150 and 200 msec. Since the coherency of sweep 112394s is as good or better than the site-calibrated sweep on events deeper than 100 msec, was within a few percent of the frequency content of the site-calibrated sweep, and was far superior at the airstrip and western boundaries, sweep 112394s was selected for the acquisition of production data at Spesutie Island. Multiples were an obvious problem at offsets greater than about 500 ft. With a nearby borehole encountering bedrock at 750 ft, any hyperbolic event at times greater than about 250 msec must be multiple reflections. Production data at Spesutie Island were acquired using sweep 112394s stored uncorrelated with a 16 ft station spacing, source-to-nearest offset of 8 ft, and a farthest offset of 768 ft.

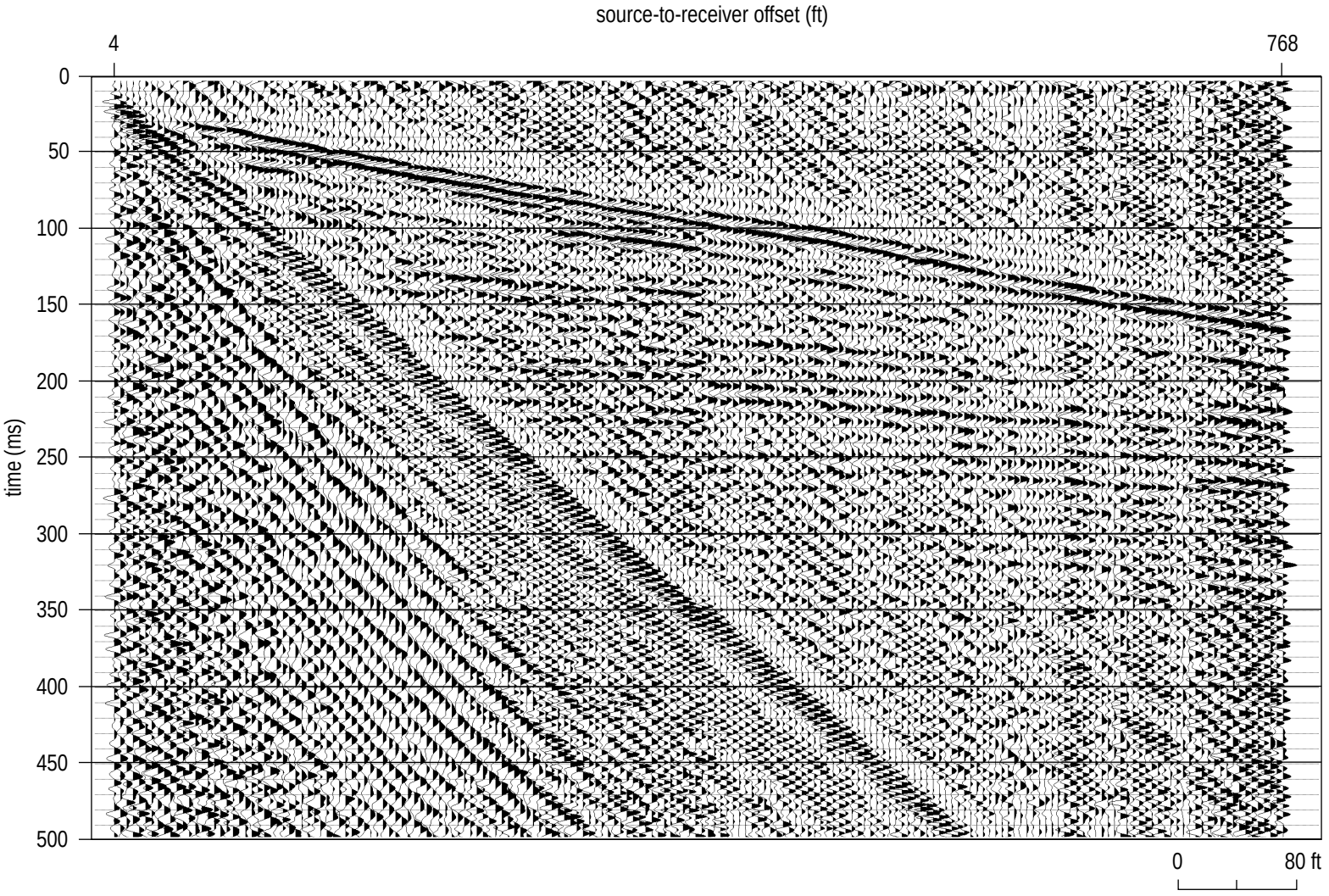

Figure 58. Ground force correlation of vibratory sweep 120694s with 1 second taper at Spesutie Island.

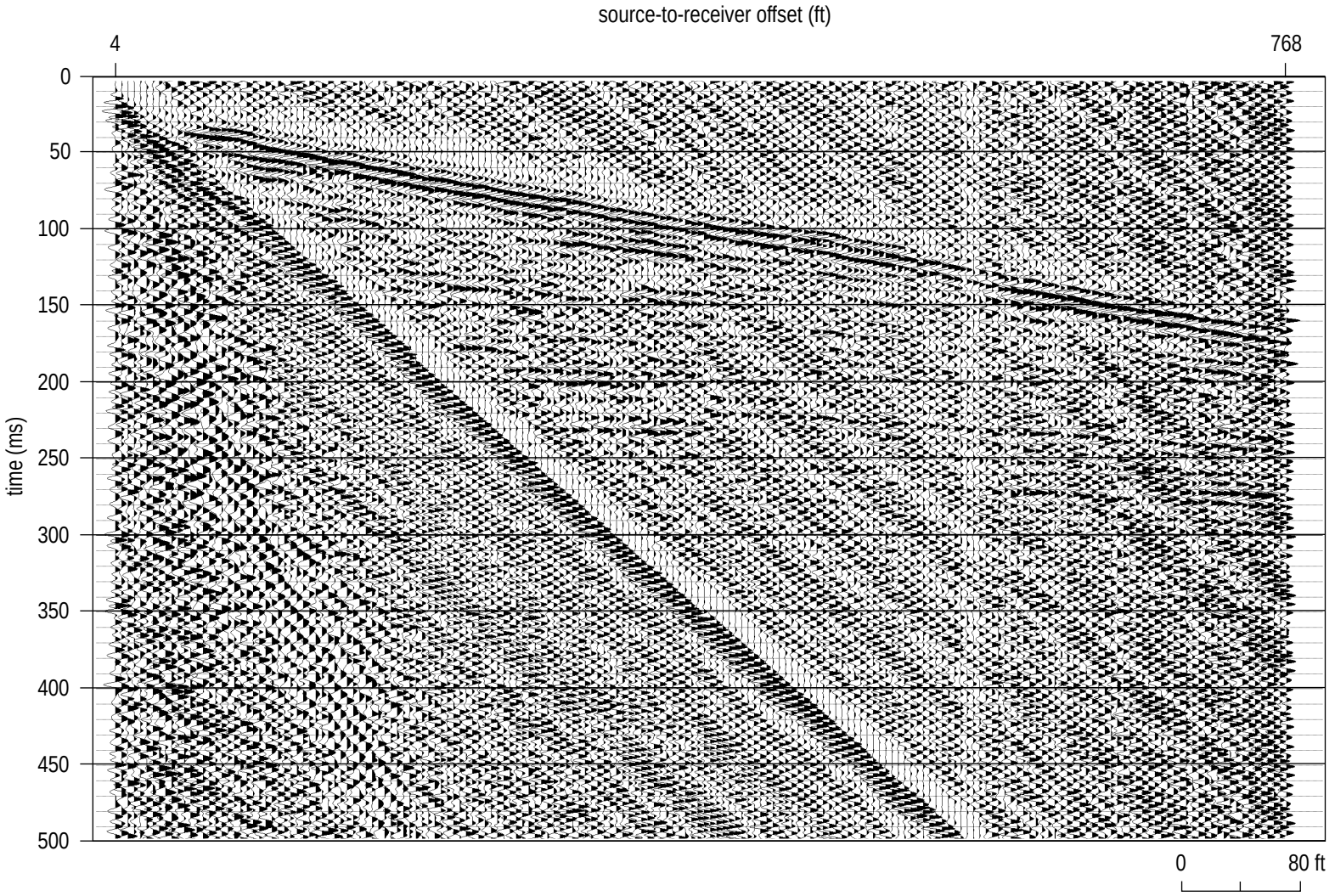

Figure 59. Synthetic correlation of vibratory sweep 120694s with 2 second taper at Spesutie Island.

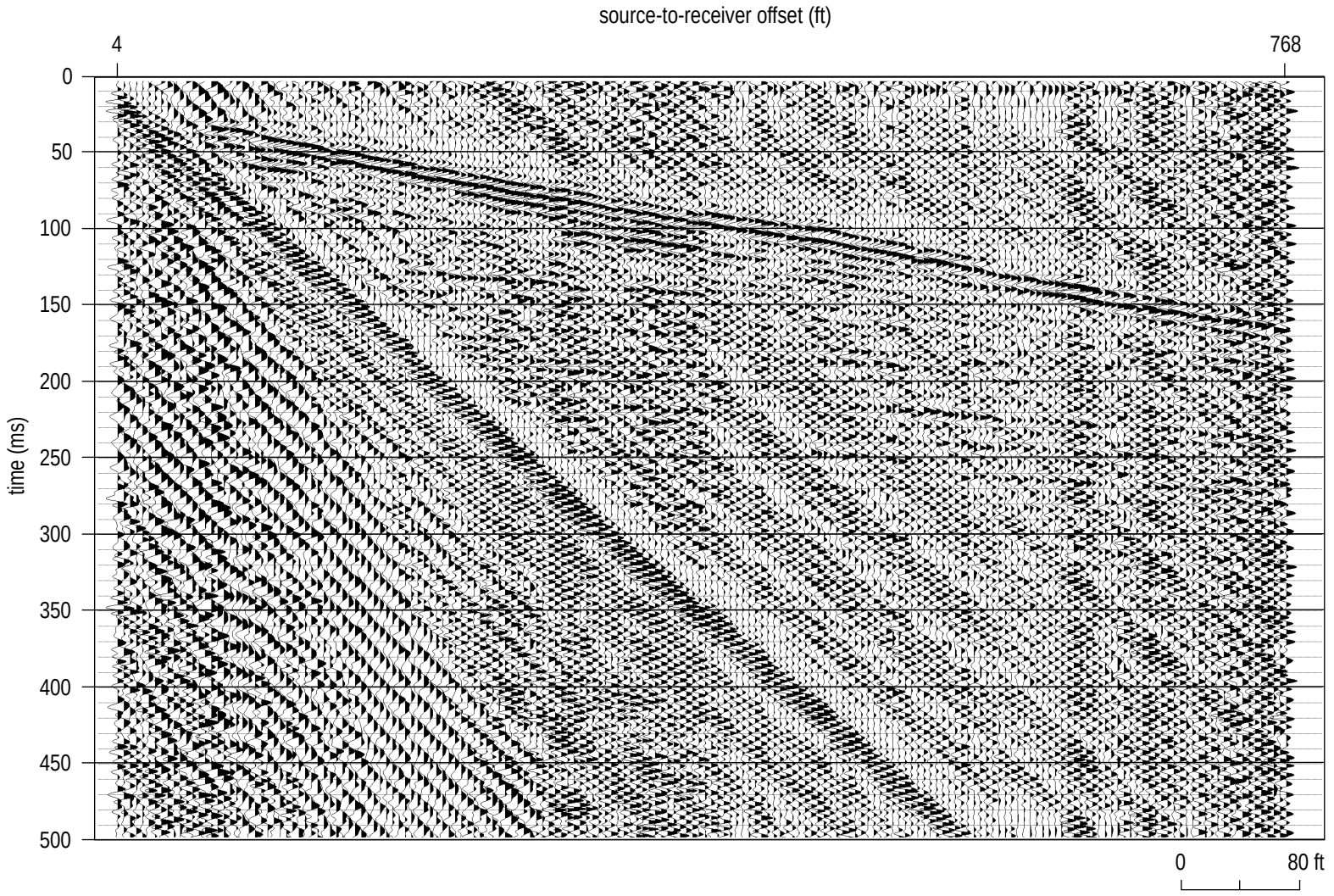

Figure 60. Ground force correlation of vibratory sweep 120694s with 2 second taper at Spesutie Island.

Velocity Check Shot Survey

Accurate time-to-depth conversions, whether extrapolated or determined through borehole studies, are critical for correlation of reflections to reflectors and reflectors to geologic contacts. The optimum method for determining time/depth correlations requires borehole measurements of one-way travel time. Boreholes that were open and of sufficient diameter to accommodate a hydrophone (with minimal peril to phone recovery) at the time of this test were not deep enough to allow sufficient sampling throughout the interval of interest. Based on availability, depth, and diameter, well #WB-MW-15C was measured for one-way acoustic travel time to a depth of 175 ft using a single hydrophone and both the air gun and vibrator as sources.

Five-foot vertical sampling of the borehole with the hydrophone and several source-to-well offset distances was sufficient to determine accurate average and interval velocities in the upper 170 ft near Phillips Field. To ensure a consistent time zero (energy start time), two surface geophones were installed near the edge of the well pad and recorded on two separate channels throughout the check shot survey. The water table (potentiometric surface) at the time of the test was approximately 13.5 ft below the ground surface. The sweep used by the vibrator was calibrated at the well site. The ground surface was very wet and it was lightly raining at the time of the uphole survey.

The seismograph was set up with a sampling interval of 1/2 msec, fully aware at the time that this setting was not nearly fine enough to get reliable interval velocities. The goal of the velocity survey was to determine average velocities from the surface to critical depths. Therefore the 1/2 msec sampling interval was more than sufficient for the purposes of this survey (the 1/2 msec was a necessary trade-off to allow for a 5 second sweep that included frequencies to 500 Hz). Error in the average velocity model is primarily influenced by the accuracy of first arrival picks. For this uphole survey it is estimated that the error in average velocity is less than 5%. The error in interval velocity due to both picking errors and insufficient sampling could be as high as 25 to 30%. Measurements of interval velocities on this survey should be used to distinguish lithologic changes and not for highly accurate applications such as generation of a synthetic seismogram.

The average velocity increases gradually from just below the water table surface to near the bottom of the borehole. Interval velocity curves are relatively smooth and uniform down to a depth of about 110 ft (Figure 61). This upper interval is probably a sand and, based on the relative increase in velocity over the

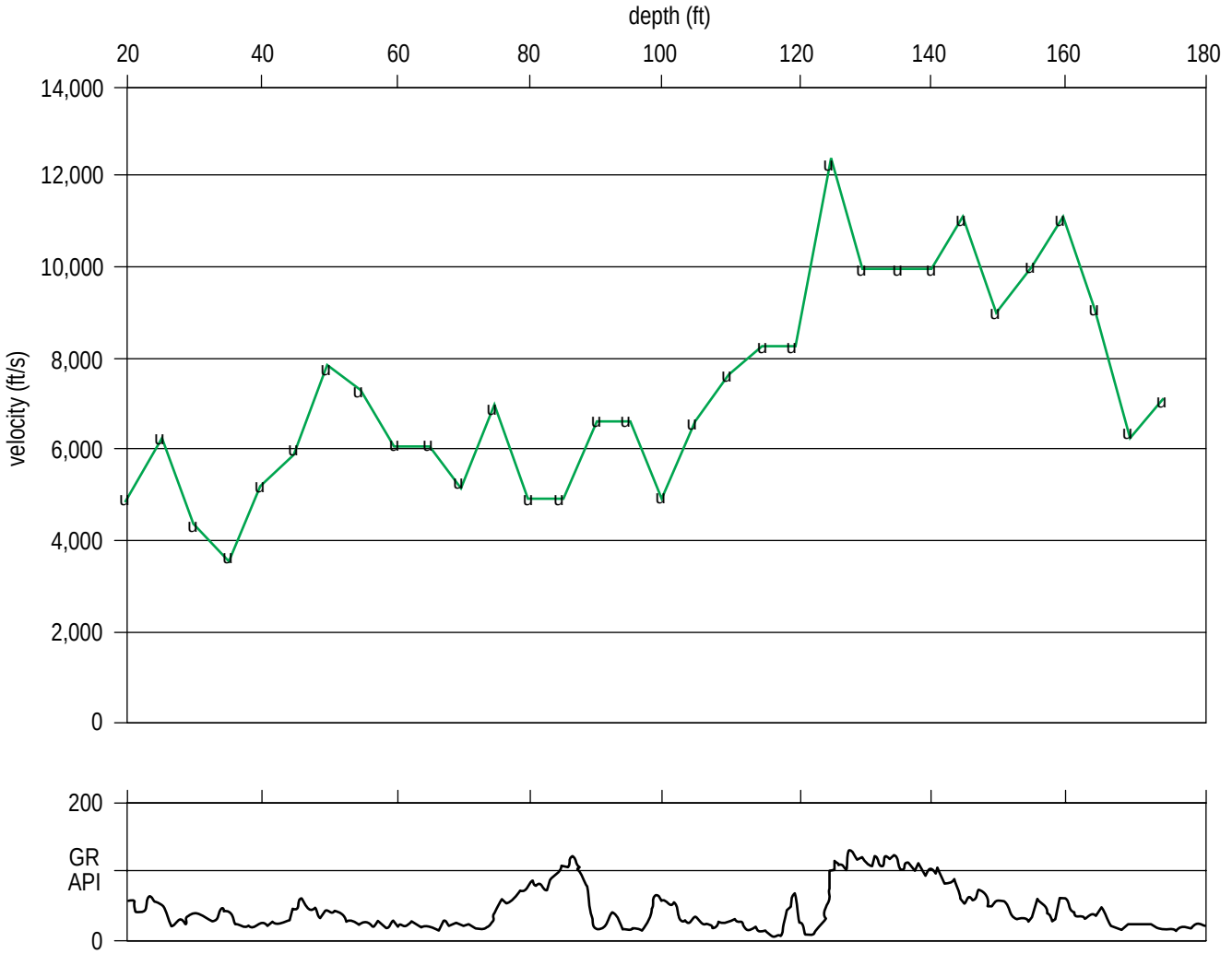

Figure 61. Interval velocities as a function of depth measured in monitor #WB-MW-15C with natural gamma log displayed at the same depth scale.

next 50 ft, the next unit is most likely a clay sequence. It is also clear that between about 165 ft and the bottom of the hole (175 ft) the material probably returns to a sand sequence similar to the first 80 ft or so beneath the water table surface. The average velocity, which provides the most useful information for the interpretation of seismic data, presents a very clear and somewhat expected picture of the average velocity structure within the unconsolidated sequence at this borehole (Figure 62). Considering the depths of the shallowest reflections imaged on this survey, interval velocities from around 4000 to 5000 ft/sec would be reasonable down to about 100 to 125 ft, where the velocity would probably gradually increase to as much as 7000 ft/sec or so at maximum unconsolidated sediment thicknesses (these velocity assumptions are made without the benefit of uphole data below 175 ft). A combination of borehole-derived and extrapolated average velocities, interval velocities, and NMO velocities (determined by curve fitting of reflection hyperbola) are used to make time-to-depth conversions on interpretive geologic cross-sections displayed in this report.

Production CDP Sections

Four CDP profiles were located and designed to evaluate the feasibility and resolution limits of the technique, map the bedrock surface, and differentiate and correlate the major clay/sand contacts as interpreted in boreholes. Two lines were necessary at the western boundary to allow continuous profiling around a sharp bend in the line. The western boundary seismic profiles were located to allow correlation with a series of boreholes that penetrate a majority of the unconsolidated section. The Phillips Field profile was also located in close proximity to a strat-hole with interpreted geology and geophysical logs down to the bedrock surface. The Spesutie Island profile was over some of the thickest unconsolidated sediment sequences at APG and a half-mile west of a strat-hole with geophysical logs. Colors assigned to different geologic contacts on the interpreted CDP stacked sections are not intended to infer or suggest continuity of geology from line to line (with the exception of the yellow bedrock reflection), they are only for site-specific interpretations. The distribution of CDP profiles allowed for an excellent sampling of the various geologic intervals and near-surface settings at APG.

Unequivocal identification of all coherent energy arrivals on field files is essential for accurate interpretations of CDP stacked sections. Reflection events between 45 and 250 msec are identifiable on field files from each line. The reflections have an average dominant frequency of approximately 140 Hz and an apparent

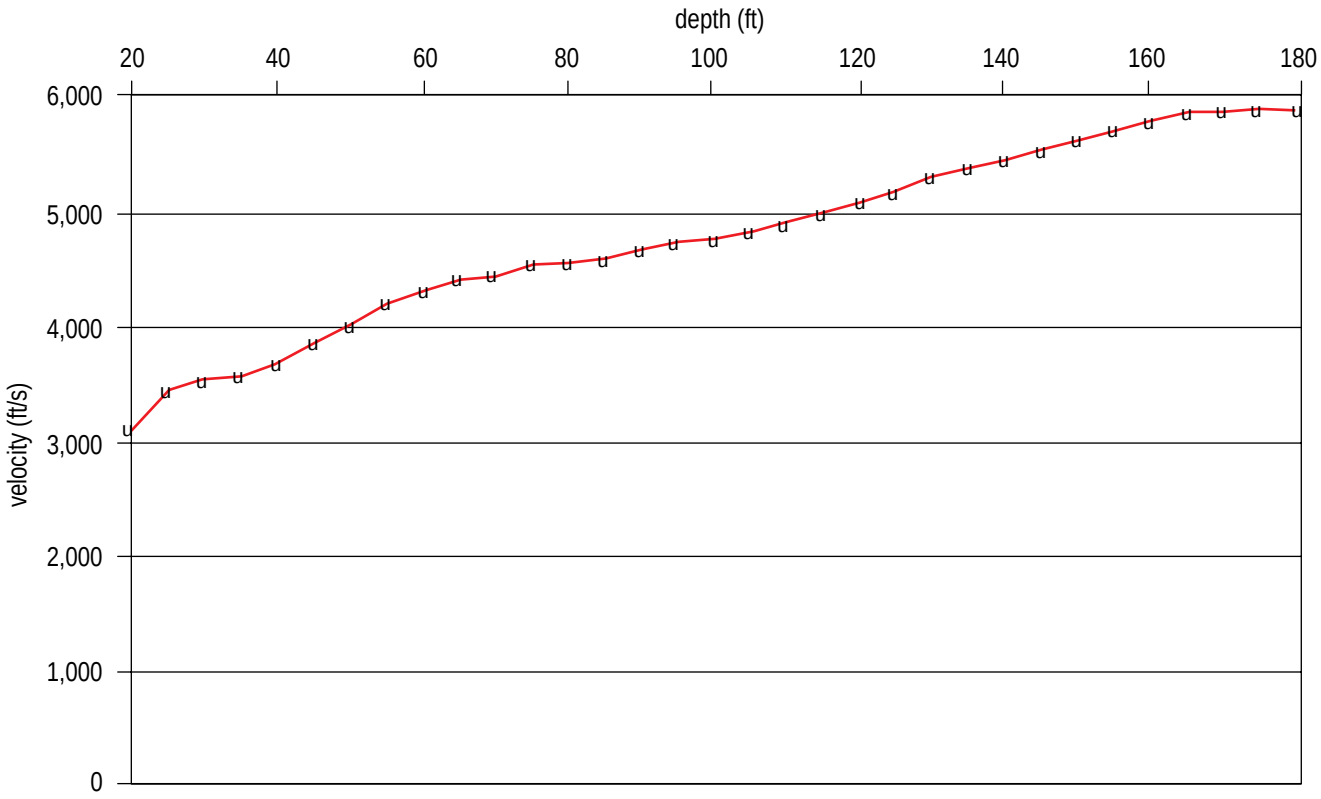

Figure 62. Average velocities as a function of depth measured in monitor well #WB-MW-15C.

NMO velocity ranging from 4000 to 6000 ft/sec. This velocity range equates to reflector depths from about 90 to over 750 ft. The signal-to-noise ratio is sufficient to allow confident identification of reflections on most field files.

The CDP stacked sections represent as accurate a time representation of the unconsolidated sediments as possible using shallow seismic reflection techniques at APG. Transcribing the time domain stacked sections into geologically-oriented depth sections required multiplication of the reflection arrival time (two-way) by the average velocity (to that depth) and then dividing by two. The accuracy of correlating from time domain CDP stacked seismic sections to spatial (depth) domain geologic sections is dependent on the accuracy of both reflection time picking and the average velocity function. Ideally a combination of borehole-measured travel times in conjunction with NMO curve calculated velocities are used to derive a time/depth dependent average velocity function. The generalized geologic cross-sections are the time-to-depth converted interpretations of the CDP stacked sections with lithology inferred from drill information.

Assignment of interval velocities for the direct generation of the geologic cross-sections is the only part of the process from raw field files to generalized geologic cross-sections that requires interpretations and/or assumptions that could alter the accuracy of the geologic model. The interval velocities used to generate the generalized geologic cross-sections were a combination of available shallow borehole velocity measurements and NMO velocities as determined from curve fitting and modeling (Table 3). The interval velocities were extremely reasonable for this geologic setting and were consistent with depth to reflectors calculated directly from CDP stacked sections using average velocity (NMO) values measured in the borehole and estimated from reflection hyperbola.

Interpretation of the reflection sections and generation of a geologic cross-section was accomplished through incorporation of interpreted and modeled shot gathers, borehole information, stacked reflection wavelet characteristics, velocity uphole survey, NMO velocity calculations, and section-wide coherency. The apparent structure as implied by the undulating reflecting surfaces is in part a real representation of the bedding geometries and in part the effects of velocity changes in shallower units. Determining real geometric orientation of the reflectors requires depth calculations from average velocities that change as a function of material properties and thickness of overlying sediments. Reflections above bedrock undulate, changing thickness and, therefore, time-to-depth ratios change slightly across the line. No assignment of lithologic classification has been made on any

TABLE 3
Interpretation Color and Interval Velocity

Line near the western boundary fence

Layer Number	Color of Event	Interval Velocity (ft/s)
1	Green	4100
2	Orange	4200
3	Blue	4400
4	Red	5600
5	Purple	6100
6	Yellow	6400
Bedrock		6800

Secondary events or reflections are shown in gray.

Line on Spesutie Island

Layer Number	Color of Event	Interval Velocity (ft/s)
1	Green	4900
2	Orange	5000
3	Blue	5100
4	Red	5200
5	Purple	5300
6	Aqua	5400
7	Violet	5900
8	Brown	6300
9	Yellow	6400
Bedrock		6800

Secondary events or reflections are shown in gray.

Line near Phillips Airstrip

Layer number	Color of Event	Interval Velocity (ft/s)
1	Green	4700
2	Orange	5000
3	Red	5200
4	Purple	5300
5	Aqua	5900
6	Brown	6300
7	Yellow	6400
Bedrock		6900

Secondary events or reflections are shown in gray.

geologic cross-section; all unit descriptions are based on material type. For the purpose of this report the reflectors will be correlated to material types as identified in boreholes.

Western Boundary Line

Interpretation of shot gathers based on curve fitting, zero offset times, and ray trace modeling correlate quite well to the borehole-derived geologic section. The seismic reflection section dramatically improved the detail and spatial resolution of geologic interpretations based on drilling data alone. Inputting zero offset times and apparent NMO velocities into the ray trace model results in an excellent correlation between the field file and the synthetic (Figures 63 and 64). The subtle undulations in Pre-Cambrian bedrock surface (yellow) interpreted at about 125 msec are probably at least in part related to uncompensated near-surface static. By correlating reflector depths with average borehole geology in the proximity of this field file, it can be inferred that the green event from a depth of about 70 ft is the contact between sand and slightly sandy mixed clay, the orange event from about 105 ft is the contact between the slightly sandy mixed clay and yellow/white sand, the blue event from about 140 ft is the contact between yellow/white sand and slightly sandy mixed clays, the red event from about 175 ft is the contact between the slightly sandy mixed clays and gray/white clay, and the purple event from about 240 ft is the contact between the gray/white clay and saprolite/wood/crusty clay. Reflector depths vary across the line and therefore the correlation of the depth to material types will change depending on location across the 1.3-mile section.

The 24-fold CDP stacked section suggests a geometrically complex and horizontally varying stratigraphy along this line (Figure 65). The section as presented is a combination of the two lines from the western boundary graphically sutured at the intersection of the two lines (CDPs 2750 and 4030, which are equivalent to stations 1375 and 2015, respectively). This presentation format allows easier line-to-line correlation. The series of boreholes (2-76 through 6-76) provide control over the northern half of the section, with MW-17 providing shallow control at the very southern end of the line (MW-17 is of limited value due to its very shallow TD).

The color interpretation of the stacked section is based on reflection coherency and amplitude (Figure 66). The choice of colors was not based on convention. They are, however, consistent with the geologic interpretation of the field file (Figure 63). Reflection interference, out-of-the-plane reflections, and scatter are prevalent across the entire section. A large number of events coherent over distances of 1/4 mile or

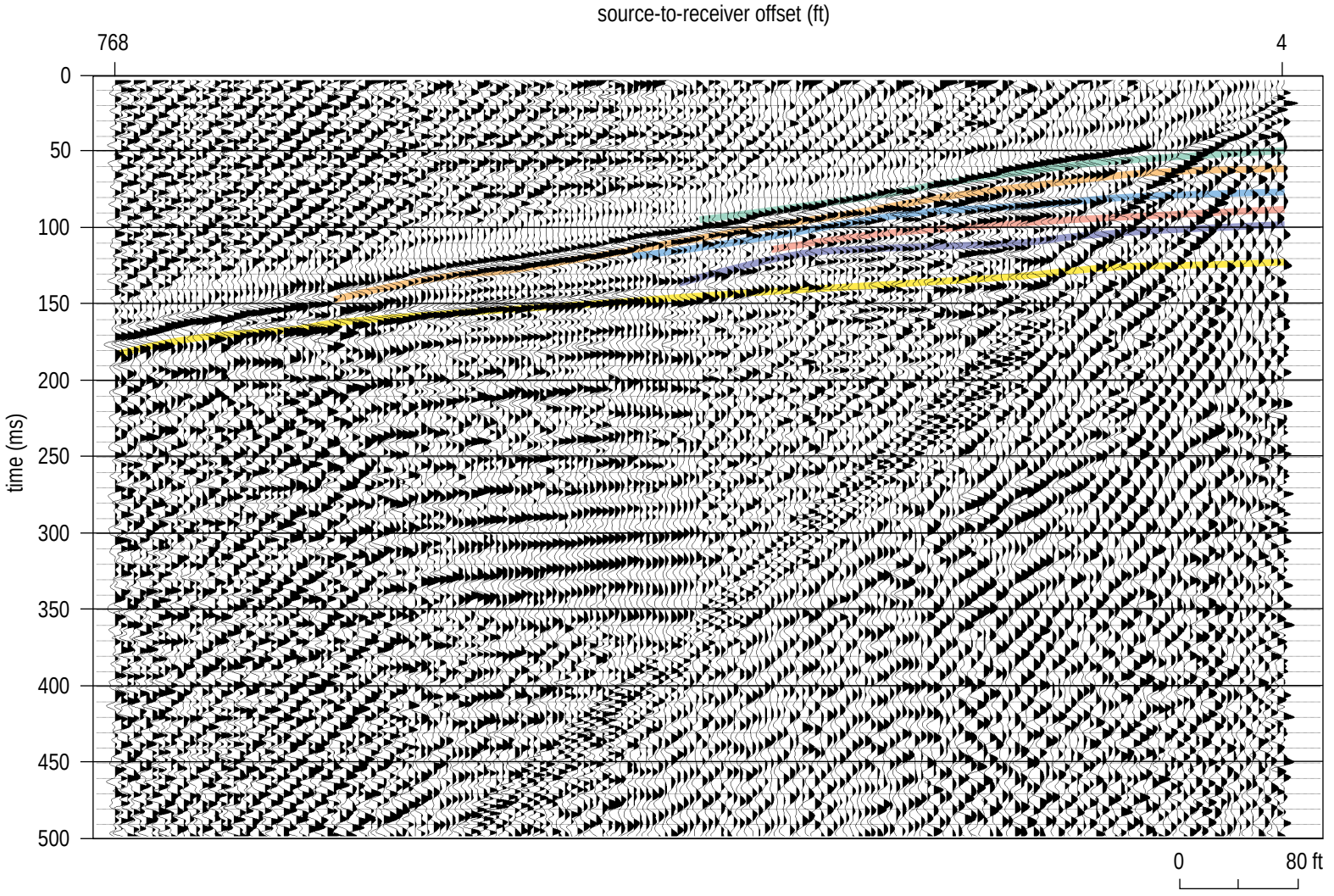

Figure 63. Shot gather with color interpreted reflection hyperbola from south end of the western boundary line.

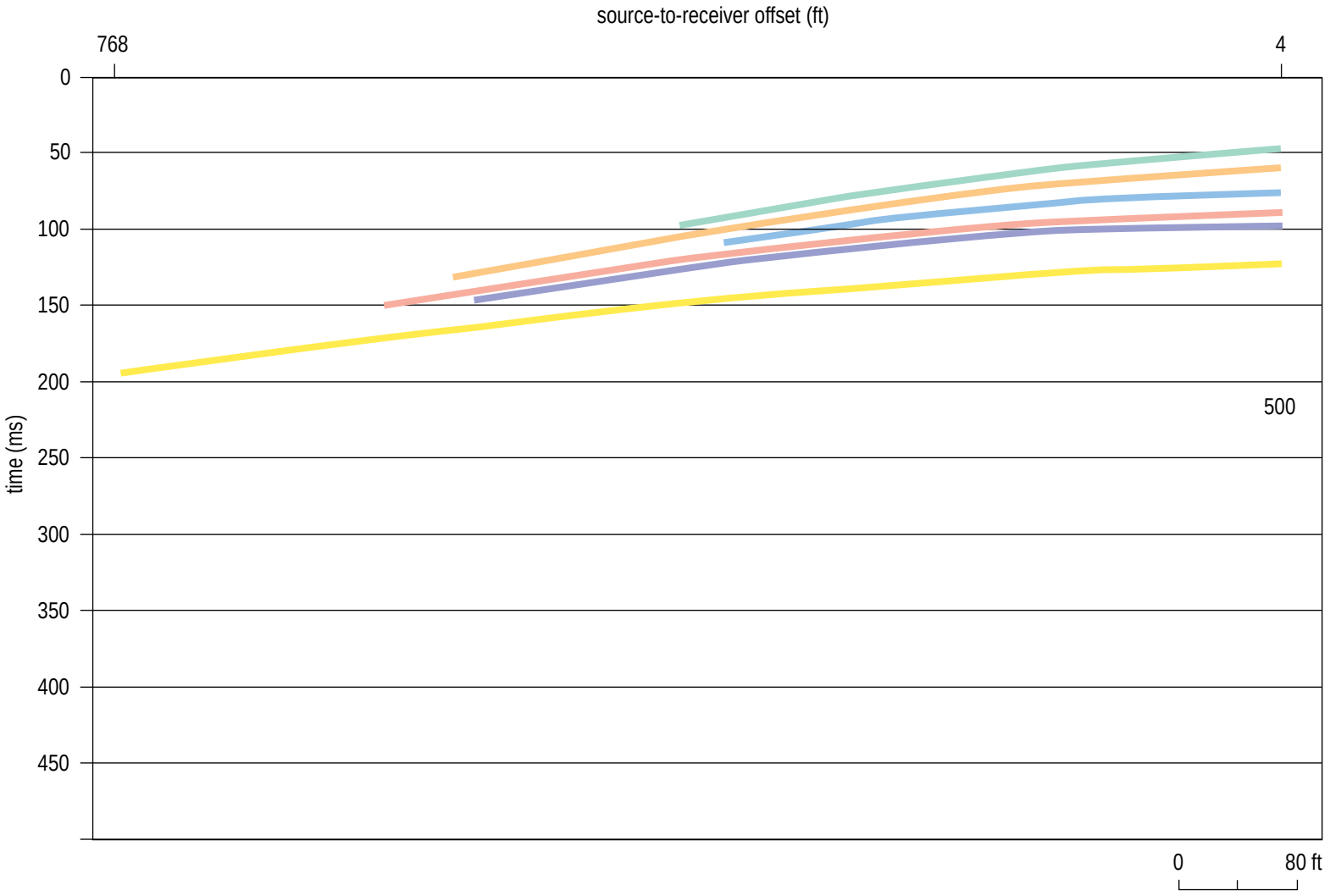

Figure 64. Ray trace model of reflection hyperbola with color correlated with Figure 63 from the south end of the western boundary line.

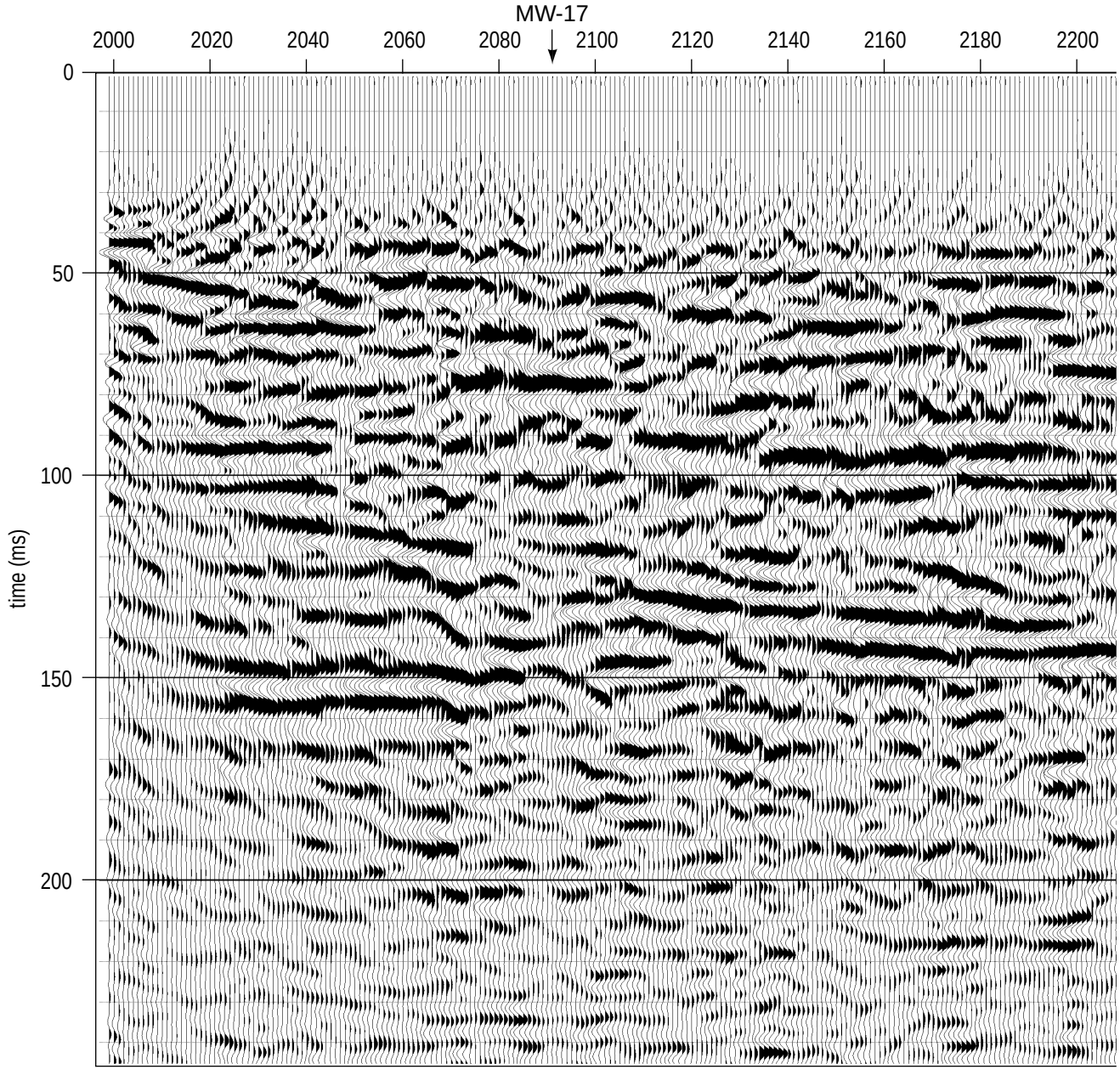

Figure 65a.CDP stacked section from the near the western boundary combining the two profiles at the tie point. CDP numbers are exactly double the equivalent station number.

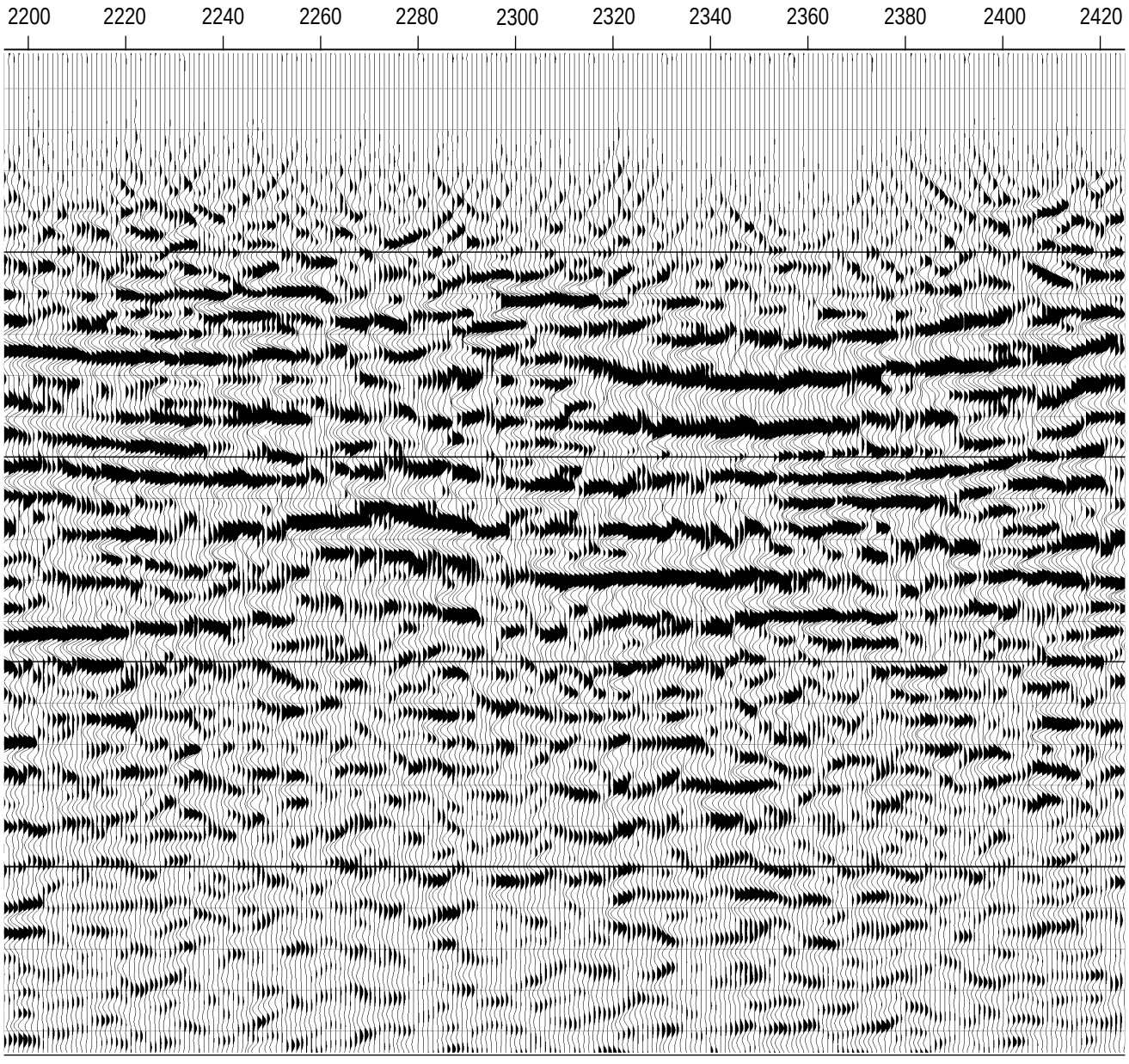

Figure 65b.

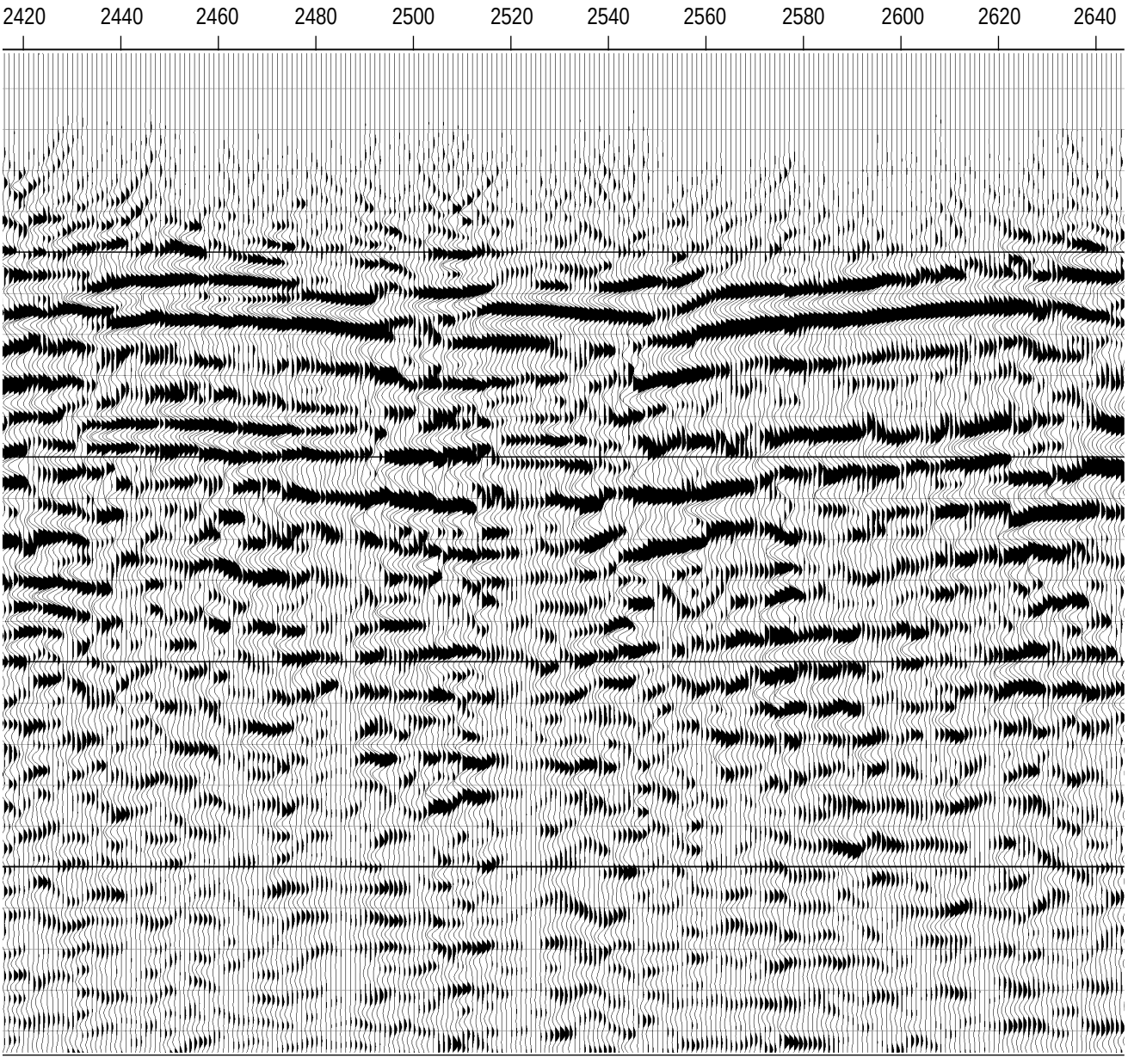

Figure 65c.

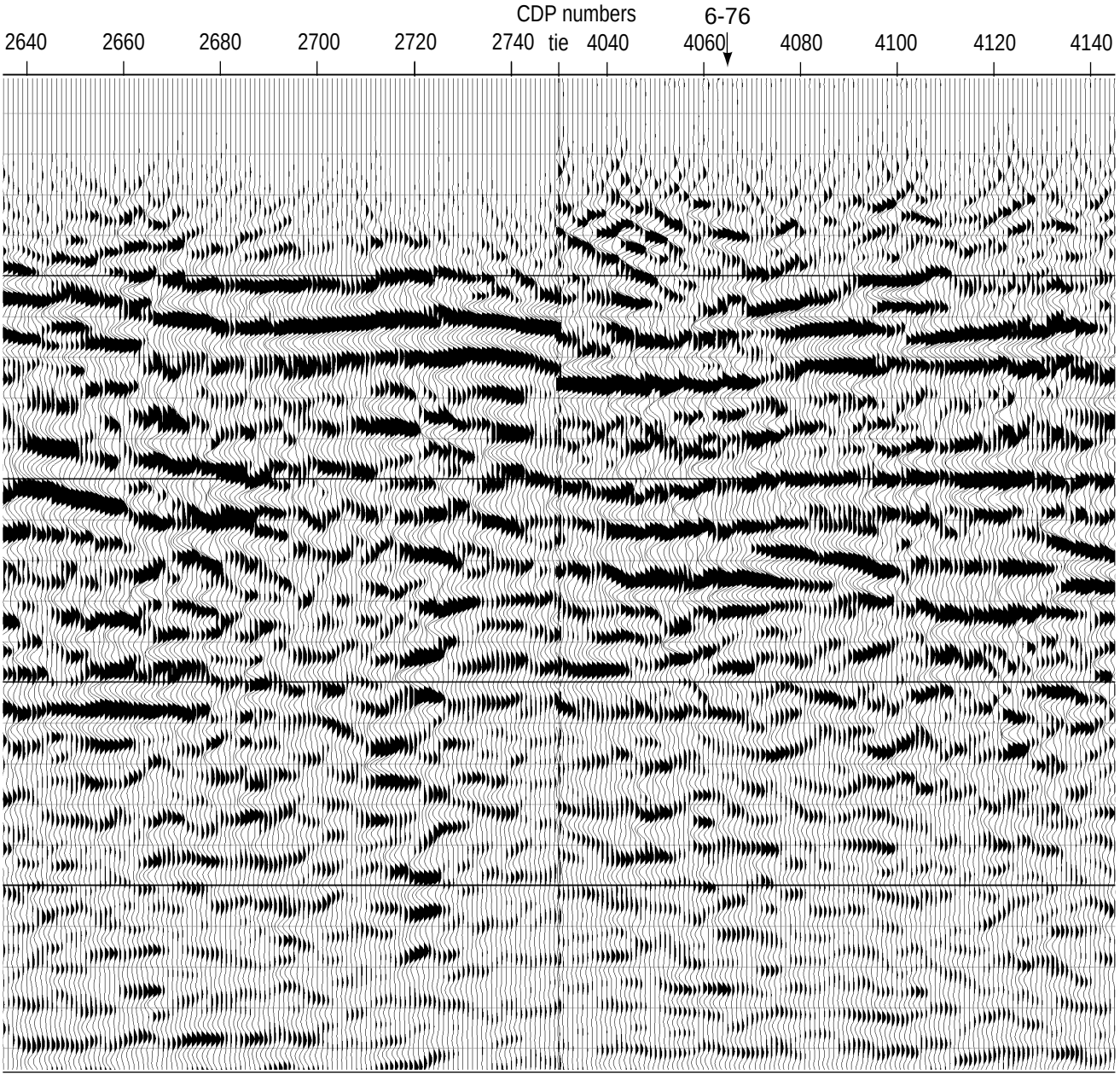
CDP numbers
6-76
2640
2660
2680
2700
2720
2740
tie
4040
4060
4080
4100
4120
4140

Figure 65d.

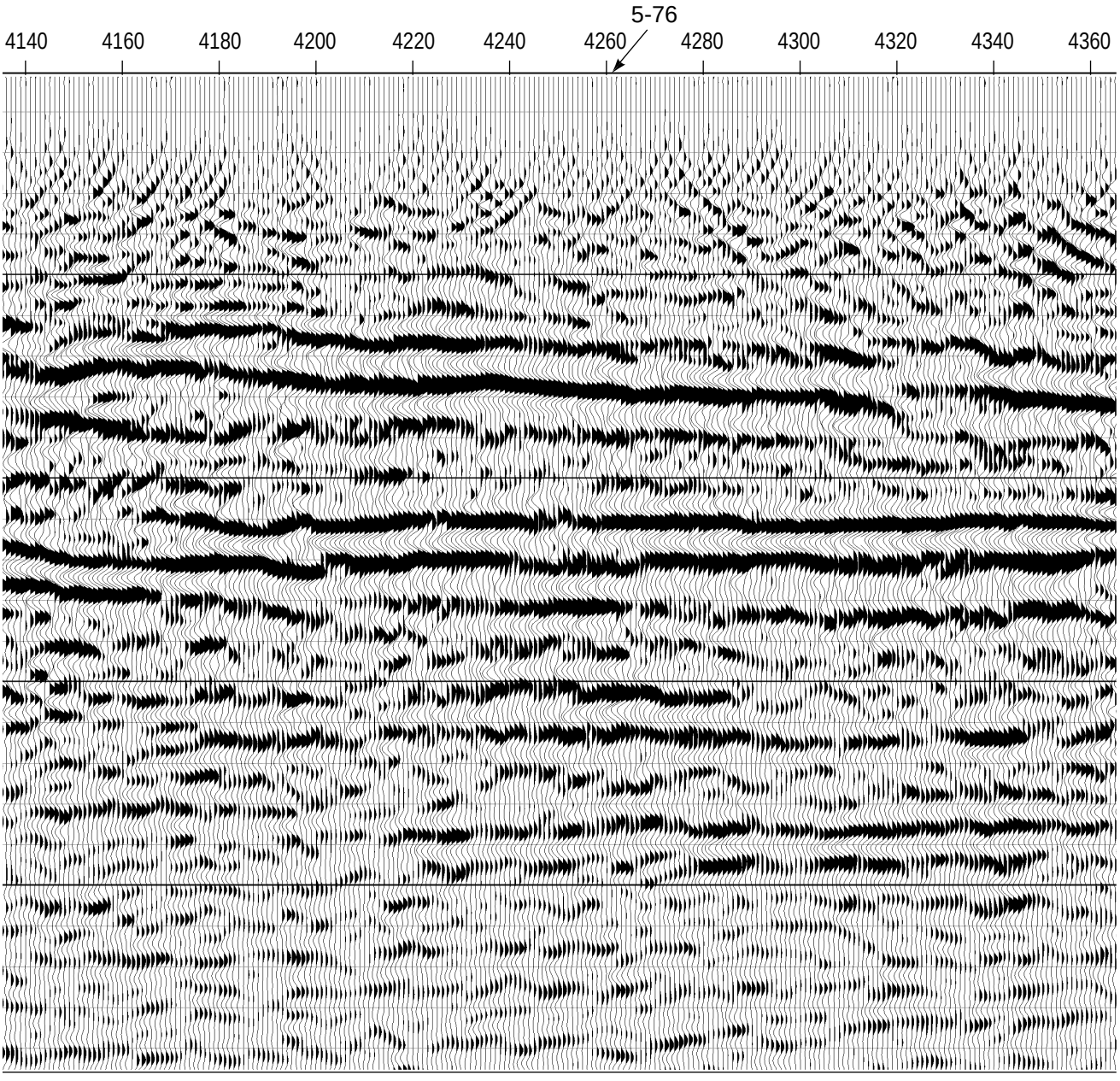
5-76
4140
4160
4180
4200
4220
4240
4260
4280
4300
4320
4340
4360

Figure 65e.

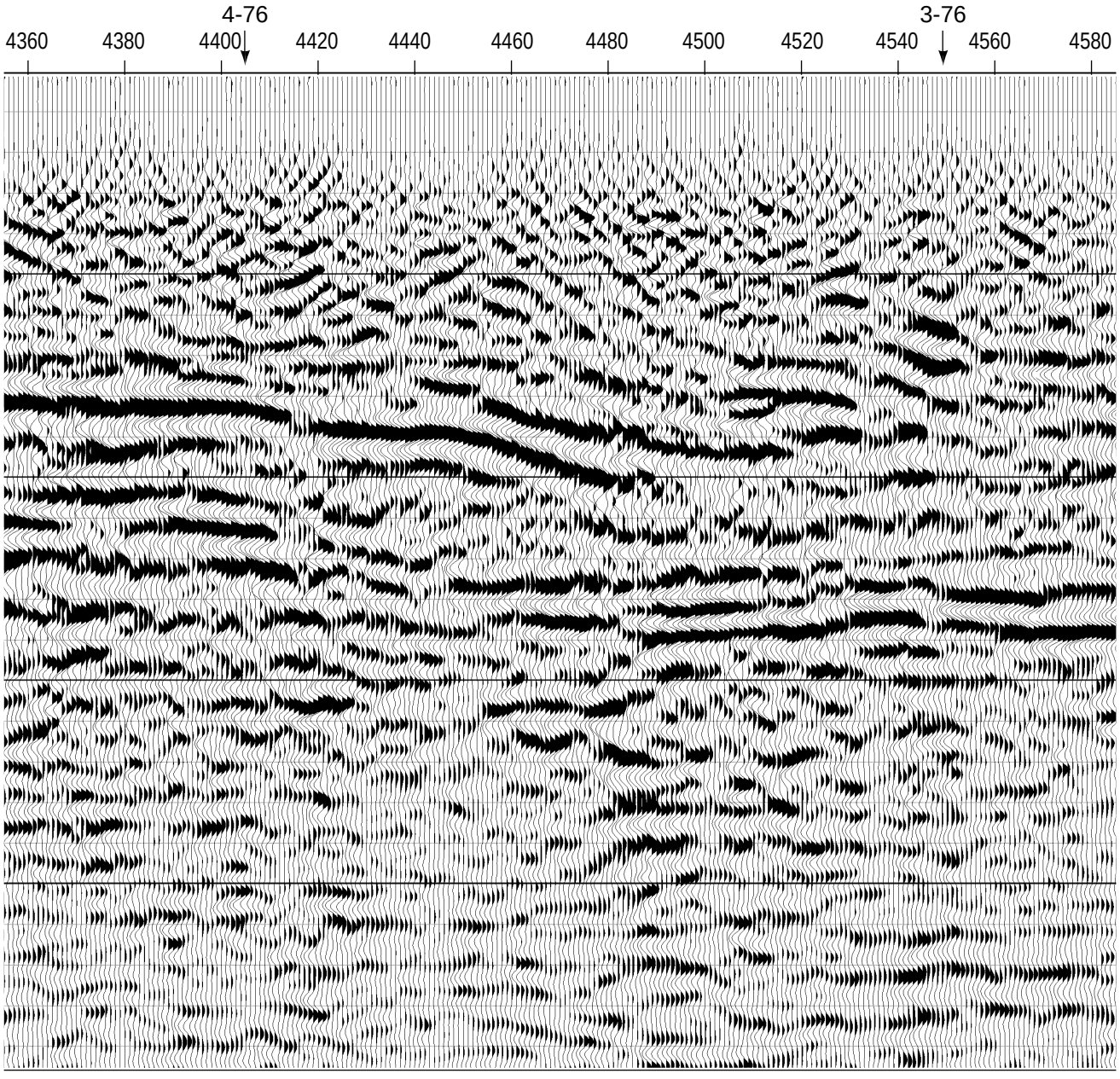
4-76
3-76
4360
4380
4400
4420
4440
4460
4480
4500
4520
4540
4560
4580

Figure 65f.

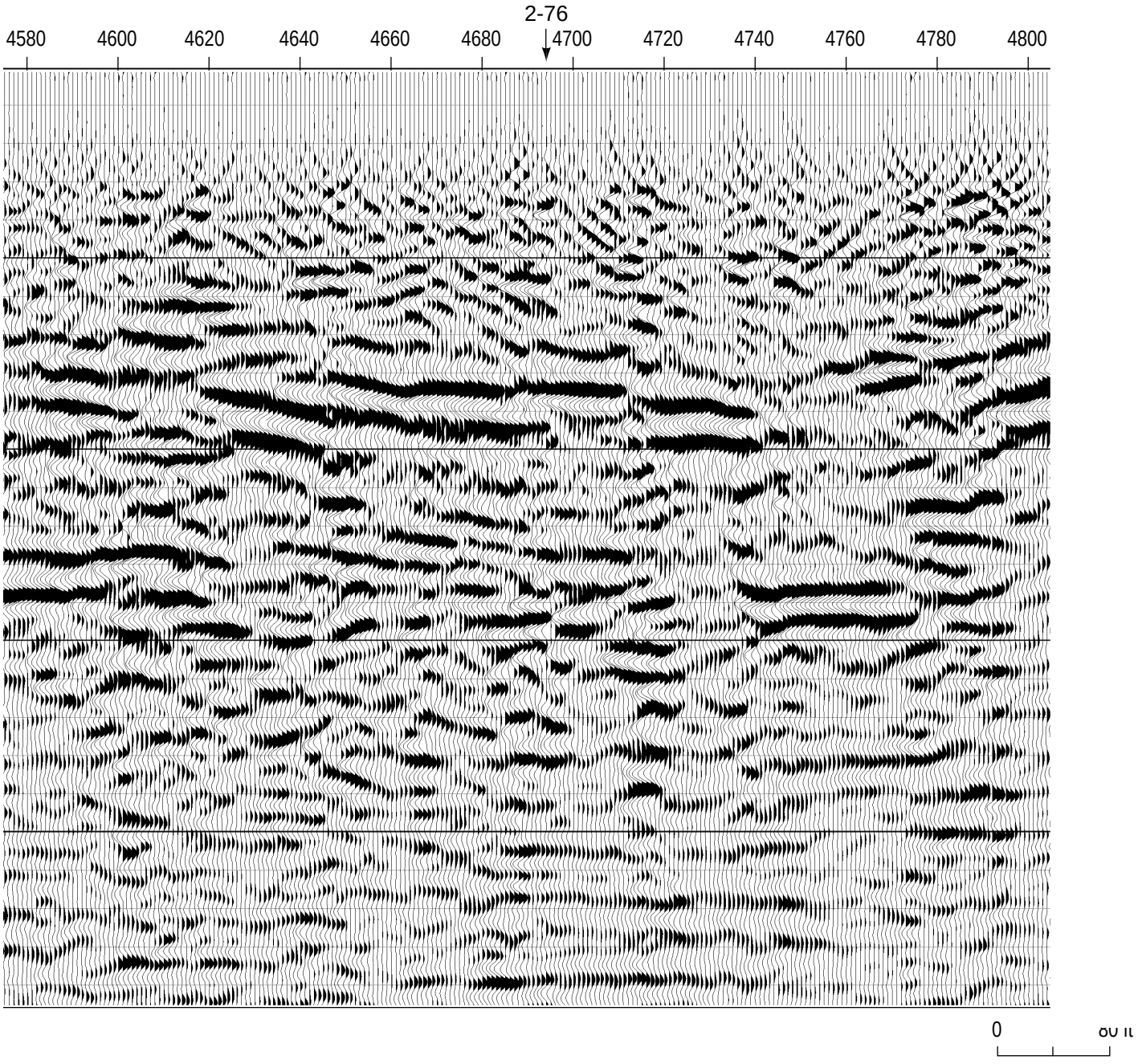
2-76
4580
4600
4620
4640
4660
4680
4700
4720
4740
4760
4780
4800
0

Figure 65g.

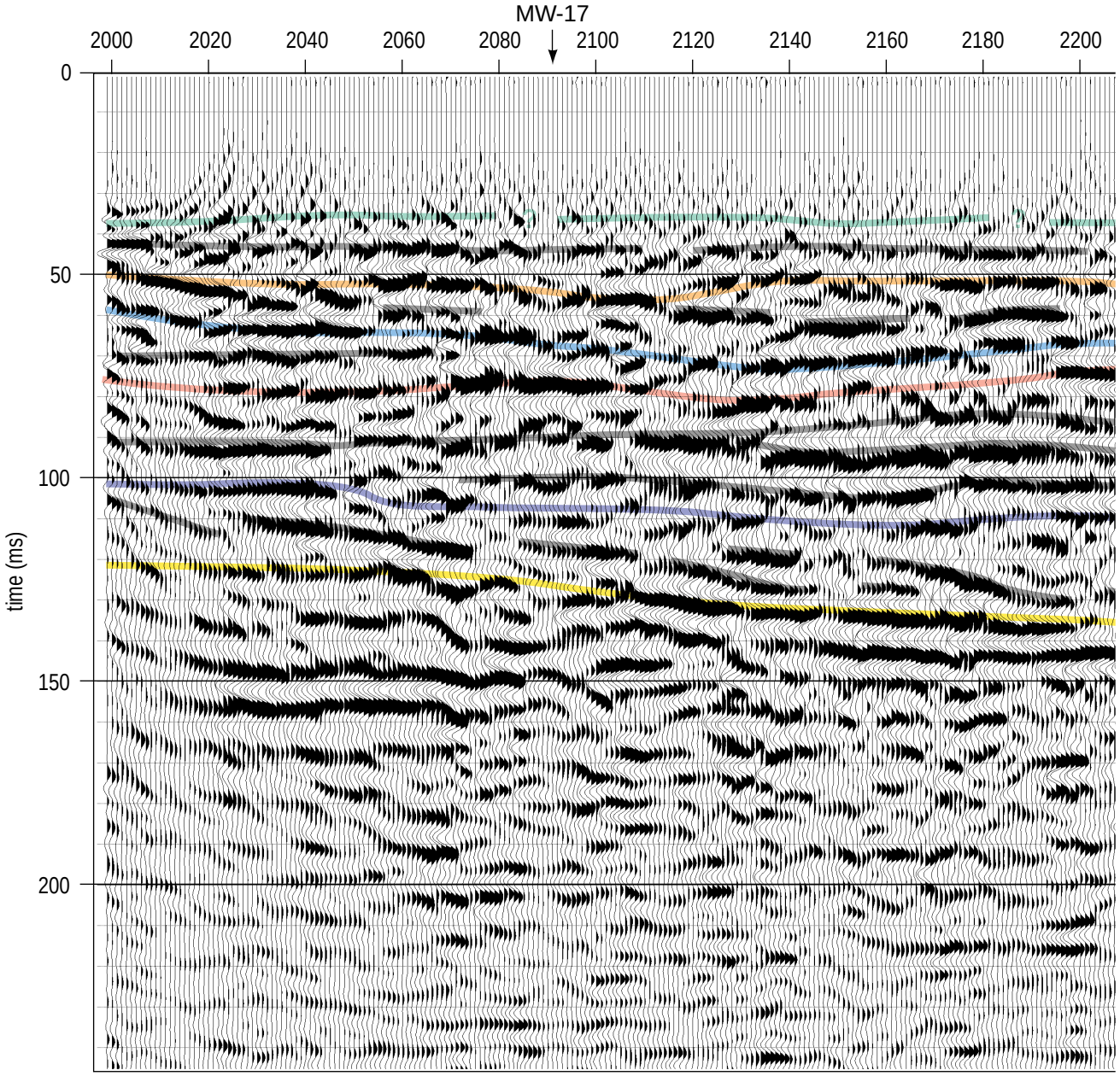

Figure 66a.Color interpreted CDP stacked section including well locations from near the western boundary.

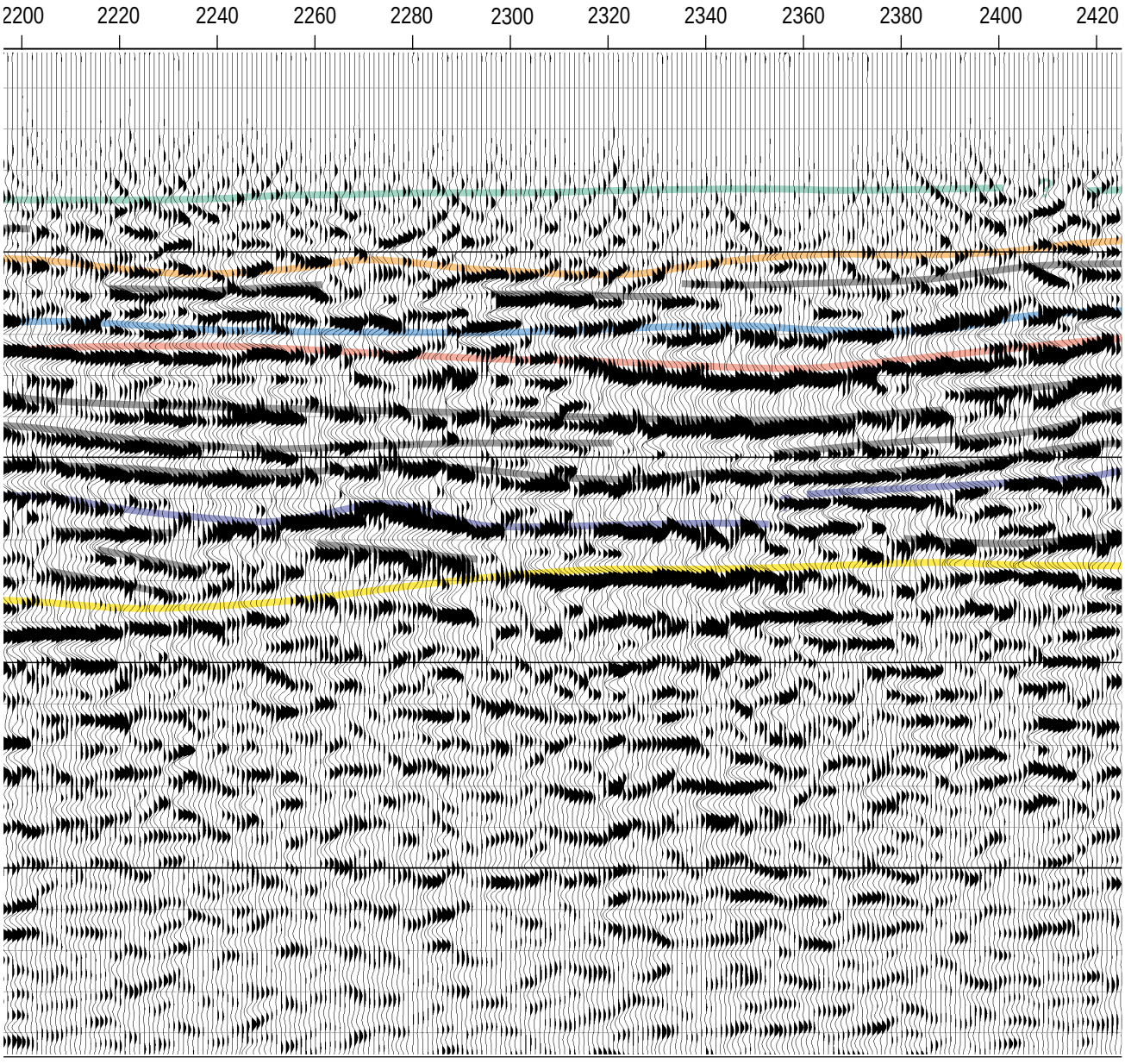

Figure 66b.

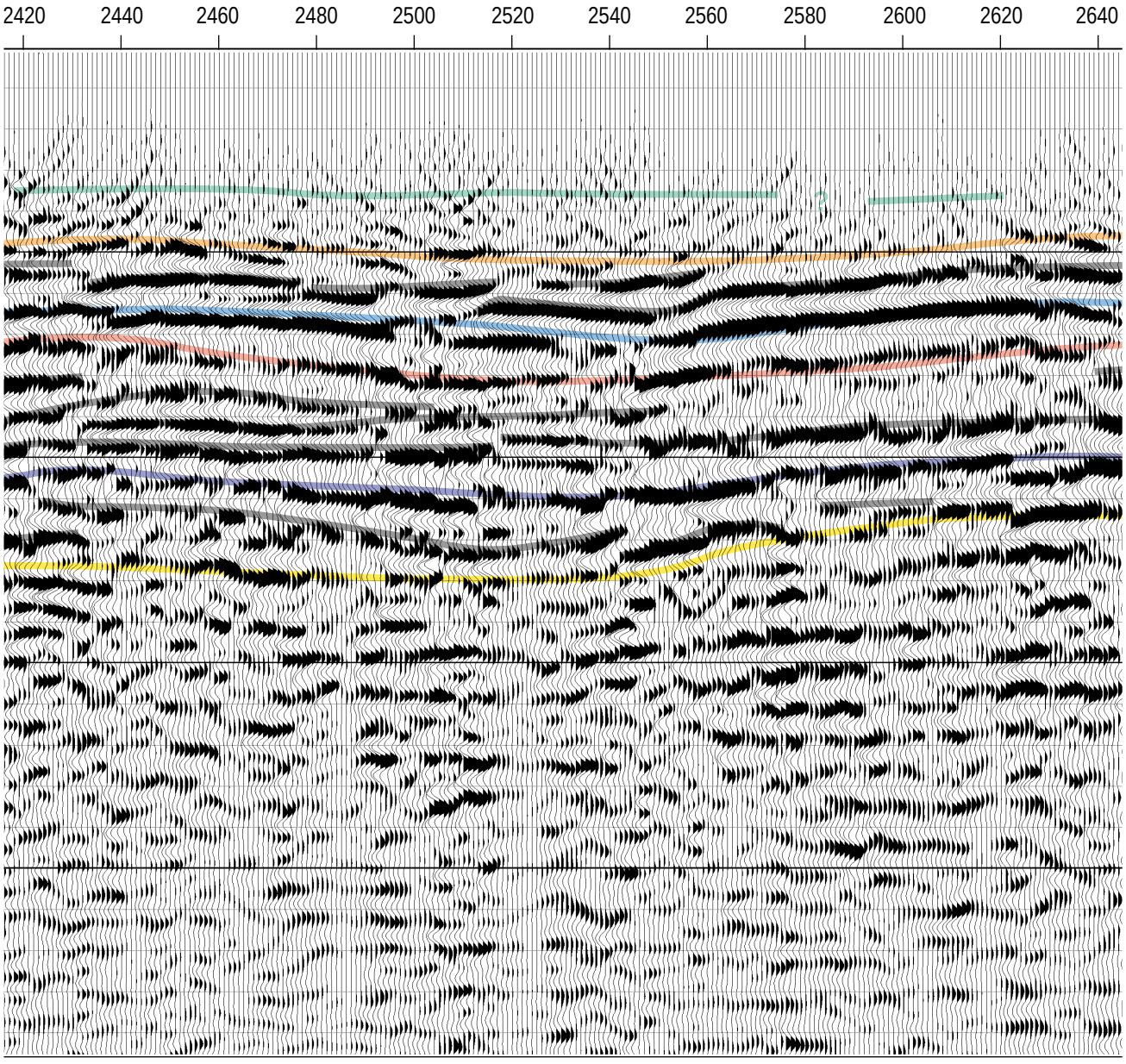

Figure 66c.

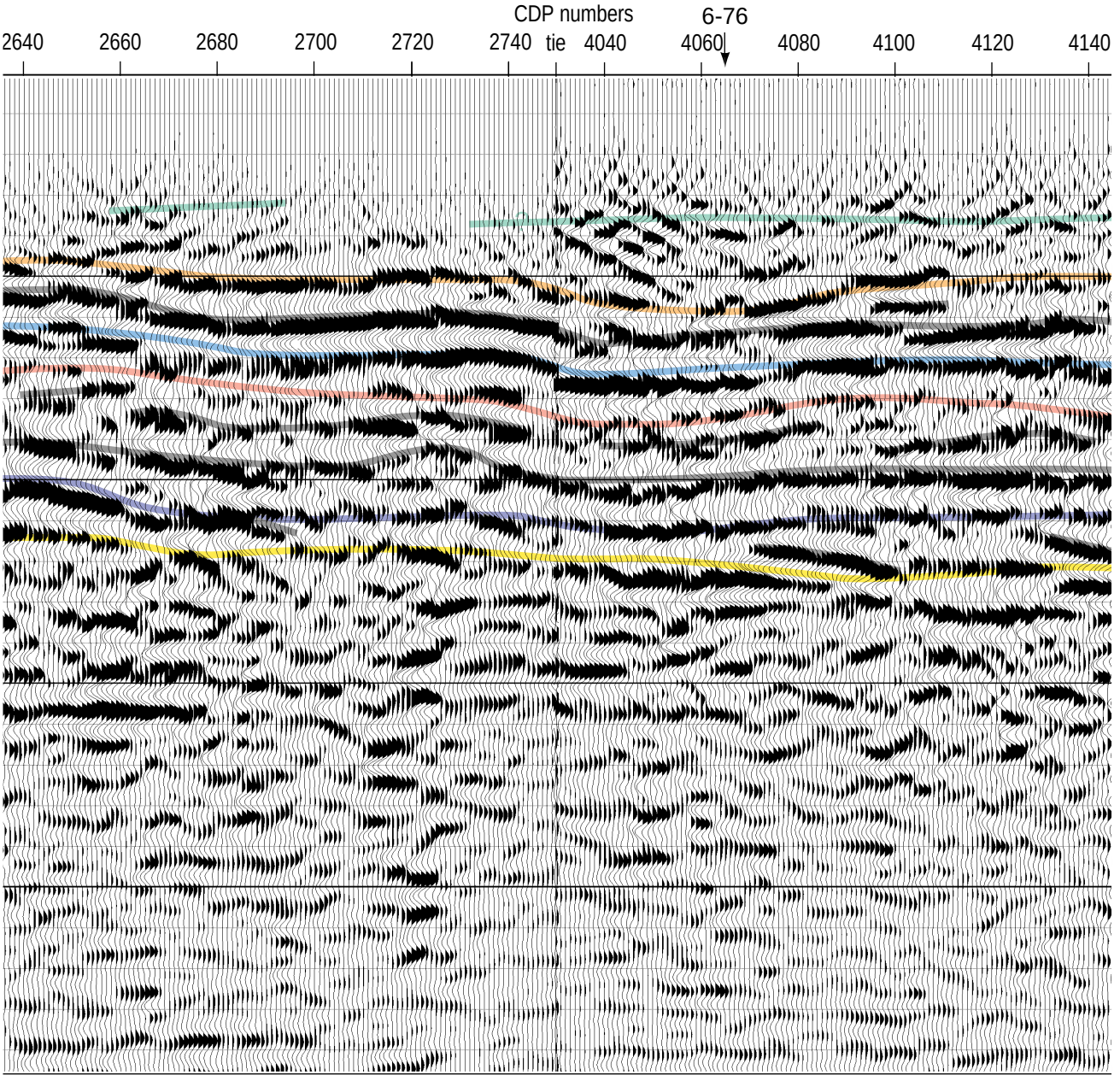
CDP numbers
6-76
2640
2660
2680
2700
2720
2740
tie
4040
4060
4080
4100
4120
4140

Figure 66d.

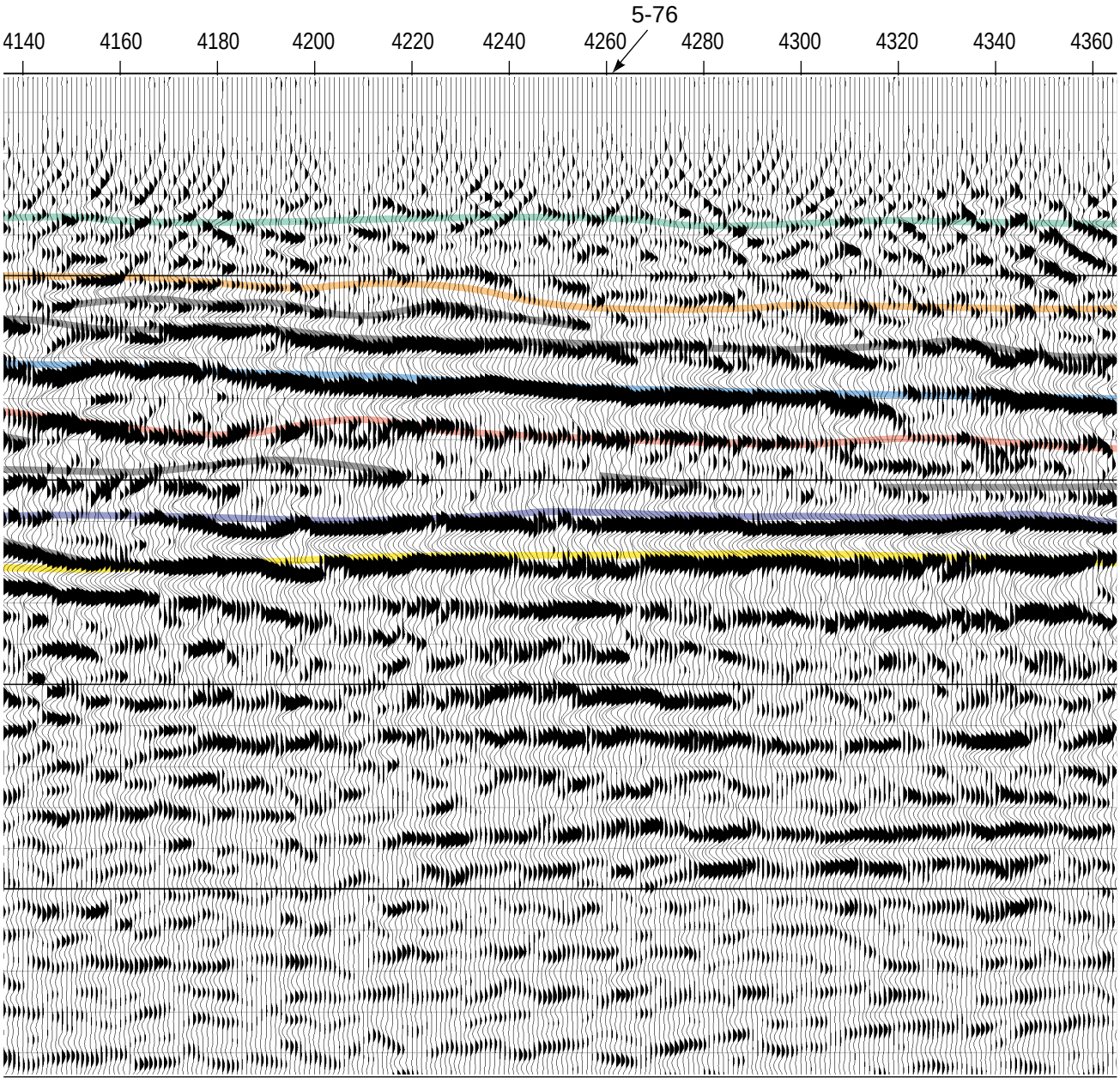
5-76
4140
4160
4180
4200
4220
4240
4260
4280
4300
4320
4340
4360

Figure 66e.

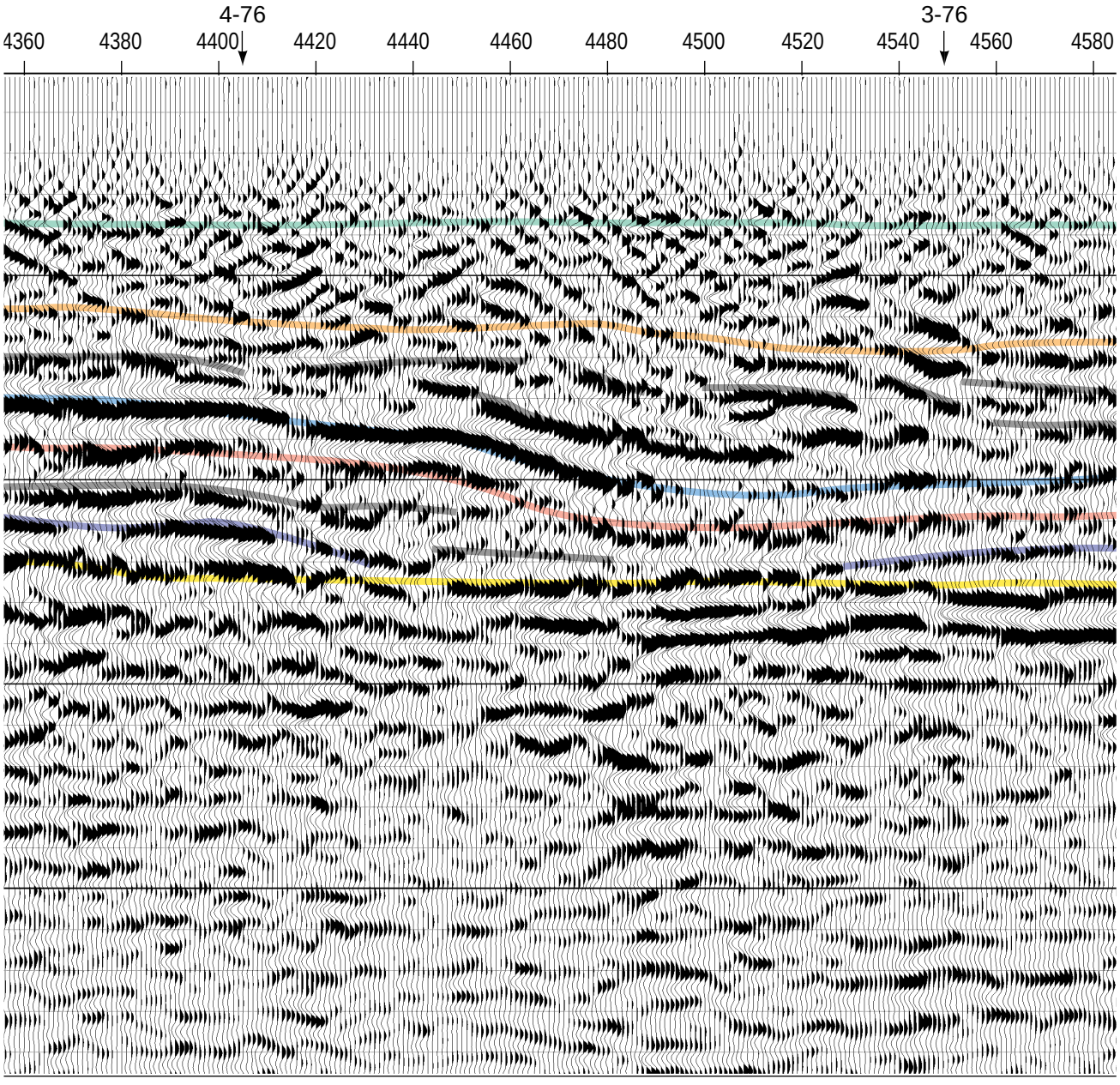
4-76
3-76
4360
4380
4400
4420
4440
4460
4480
4500
4520
4540
4560
4580

Figure 66f.

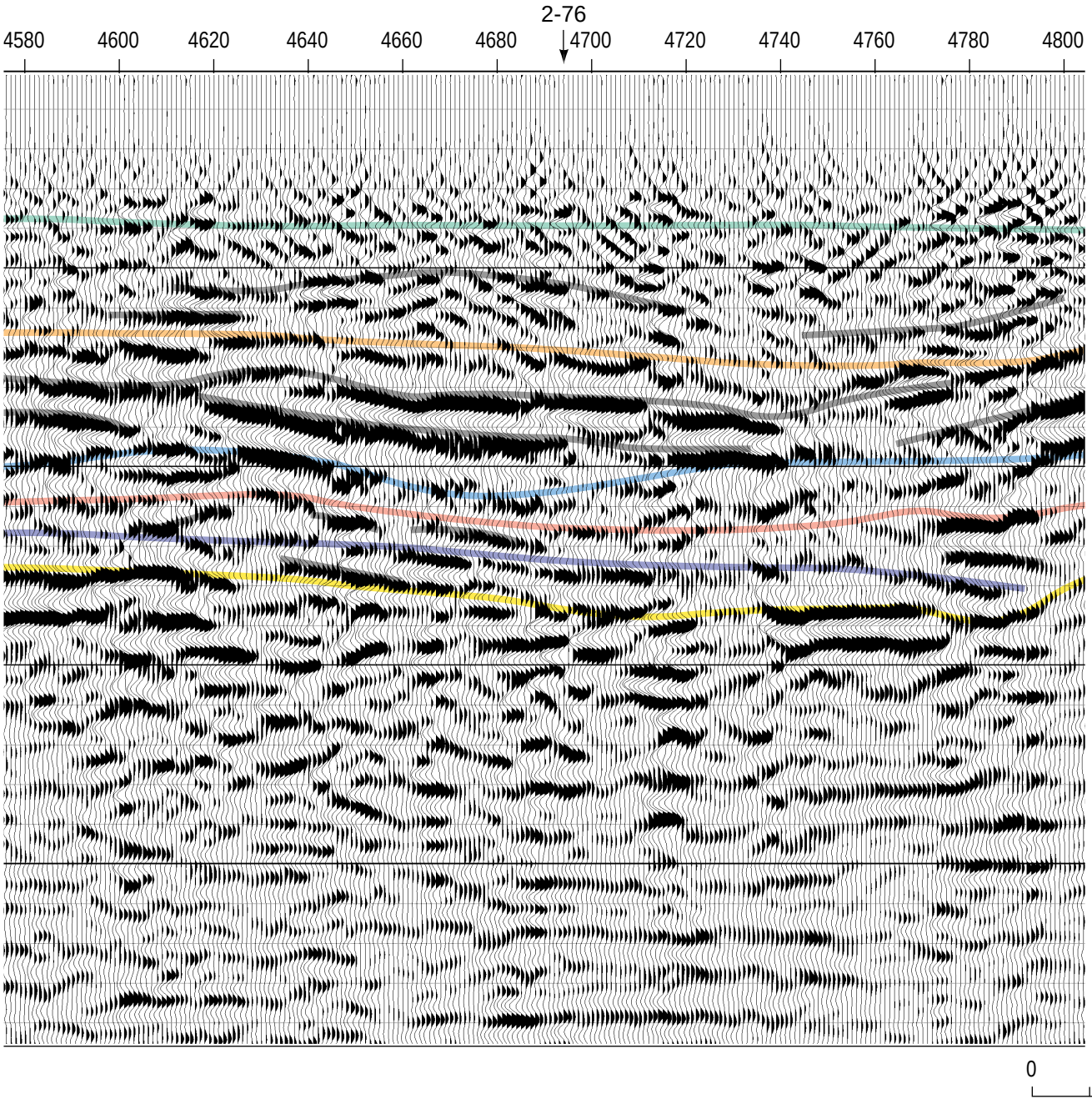
2-76
4580
4600
4620
4640
4660
4680
4700
4720
4740
4760
4780
4800
0

Figure 66g.

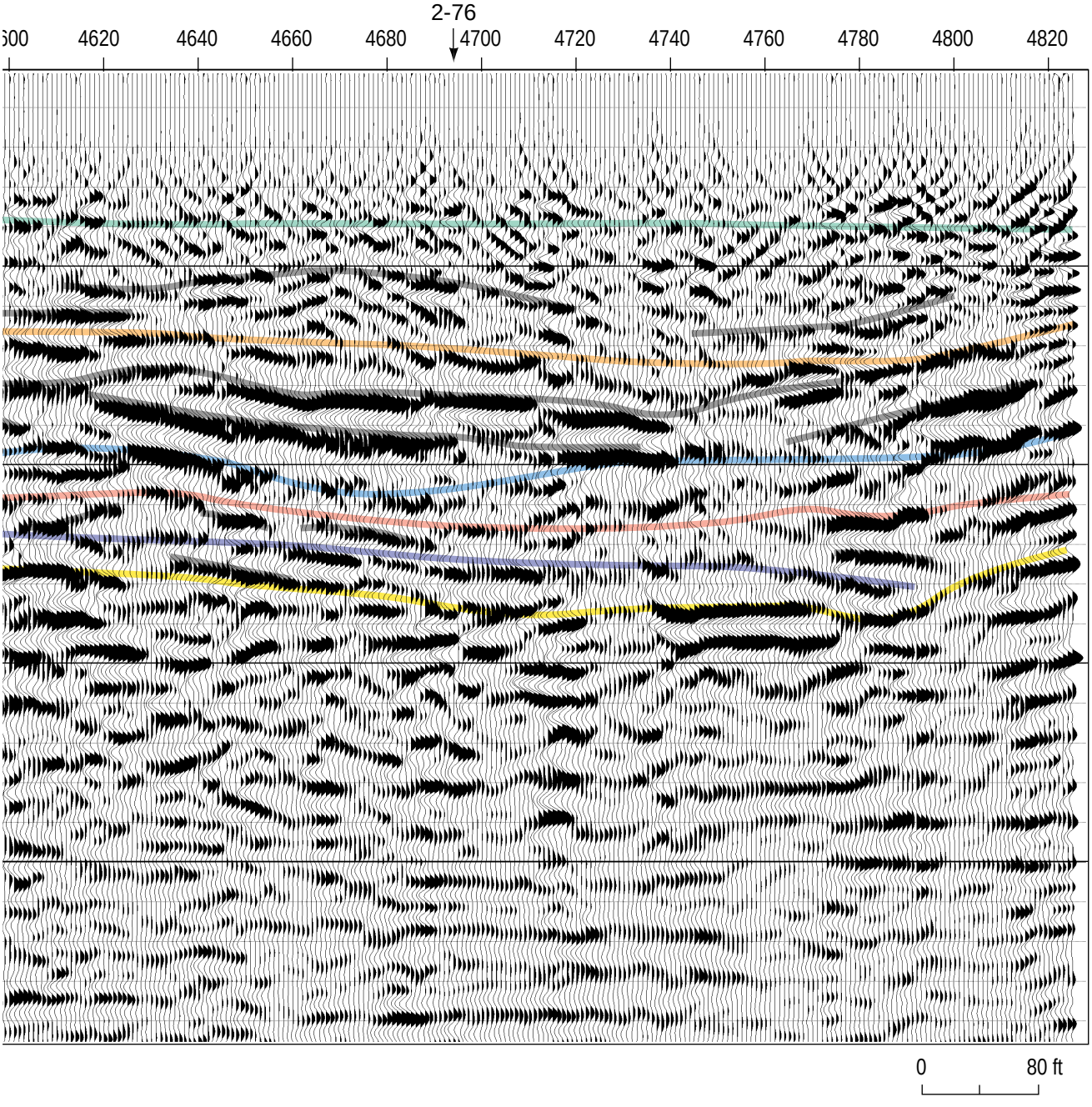
2-76
600
4620
4640
4660
4680
4700
4720
4740
4760
4780
4800
4820
0
80 ft

Figure 66h.

less are considered to be secondary events and are interpreted with the color gray. The determination of a unique color assignment was based on geologic interpretation of well logs and reflection characteristics. The secondary events/reflections are probably from within units identified on borehole logs as mixed clays, yellow and white sand, sandy clay with sand streaks, etc. Interbedded sands and clays could have extremely large acoustic impedance contrasts at their contacts but not represent geologically unique units or material changes. It is also very possible to have units identified on drilling logs as significant changes that show up on CDP stacked sections as very subtle reflection events.

Multiple reflections noted on walkaway shot gathers at times greater than the bedrock reflection are evident on the CDP stacked section and complicate interpretations of the bedrock surface. The general appearance of the bedrock reflection wavelet varies across the 1.2 miles represented on this profile. Interpretation of the bedrock surface was based on several criteria: amplitude, coherency, deepest confirmable reflection, wavelet properties, and in a general sense, drill control. The occasional breaks in coherency—such as at CDPs 2260, 2440, 4070, and 4120—are interpreted as variations in the weathered-in-place bedrock vs the unweathered, interference from beds or material contacts that terminate against the bedrock surface, interference from scatter (either out-of-the-plane or from shallower units), etc.

The only apparent bedrock structure that is probably not real is the relative high between CDPs 2540 and 2680. Skepticism of this topographic high is based on the observation that all reflections above this bedrock high have exactly the same apparent time change in elevation. Assuming an increasing velocity function with depth, an extremely consistent growth structure active throughout the Cretaceous would be required to provide this particular acoustic representation. The apparent bedrock high centered at CDP 2640 is therefore most probably an artifact of a horizontally varying near-surface velocity. This static was compensated for during time-to-depth conversions and is not present on the interpreted line drawing. Ground truth for the bedrock reflection was establish by the only borehole (2-76) along the line that penetrated the bedrock surface with high confidence.

The cyclic depositional environment and variable erosion patterns of the Cretaceous (i.e., transgressive and regressive seas) is clearly represented in the geometric complexity of the reflectors imaged along the western boundary. Within each interpreted unit subtle reflectors are intermittently prevalent. For example, within the gray/white clay unit beginning about 175 ft deep at the southern end of

the CDP stacked section is a relatively strong reflection evident from about CDP 2130 to about CDP 2430 were it appears to terminate against a shallower interface. This is likely an interbedded sand lens with little or no regional significance but locally (i.e., < 1/8 mile) could play a critical role in the hydrologic setting and therefore would need to be considered in the hydrologic model.

Apparent erosional features observed on the bedrock surface and several overlying units around CDP 4460 are suggestive of either a deep channel or several repetitive cut-and-fill episodes in that area. The increased bedrock depth and increased thickness of shallower sediments near the north end of the line are consistent with and greatly enhance the detail of the borehole-derived cross-sectional models. The termination of the deep clay/saprolite/wood fragments unit (between purple and yellow) appears to be erosional in nature. Thin bed interference or extremely short wavelength structures are suggested between boreholes 4-76 and 3-76 at the 170 ft deep sand/clay interface (Figure 66). The scalloped appearance at this sand/clay interface is very similar to that observed on the bedrock surface near borehole 6-76. This could be indicative of smaller sub-channel features or possibly related to the deposition/infill of sand into an existing scour. Interpretations of lenses, small scours, and thin bed interference on seismic data are somewhat speculative at this site, but some degree of confidence can be placed in accurate representations of bed geometries.

The interpreted seismic reflection section presents a very detailed and geometrically complicated picture when examined at the individual reflection level, but once the major material units are identified a relatively uniform, horizontally continuous geologic picture appears. The geologic cross-section derived from the CDP stacked section maps the contacts between "major" material sequences or units. From the seismic cross-section it is possible to ascertain not only the relative structural extremes and continuity of the various clay/sand contacts, but also some speculation is possible as to the presence of sand lenses and clay streaks evidenced by the interpreted secondary units.

The 8:1 vertically exaggerated generalized geologic cross-section was derived from reflection coherency and interval velocities (Figure 67). The assignment of material type (i.e., predominantly clay or predominantly sand) was based on correlation to drill-defined lithology. Some well-to-well material correlations were made in spite of discrepancies in generalized color assignments (e.g., gray and white crusty clay in borehole 6-76 is correlated to white clay in borehole 5-76). If any major unit (clay or sand) acoustically represented on this CDP stacked section were to have

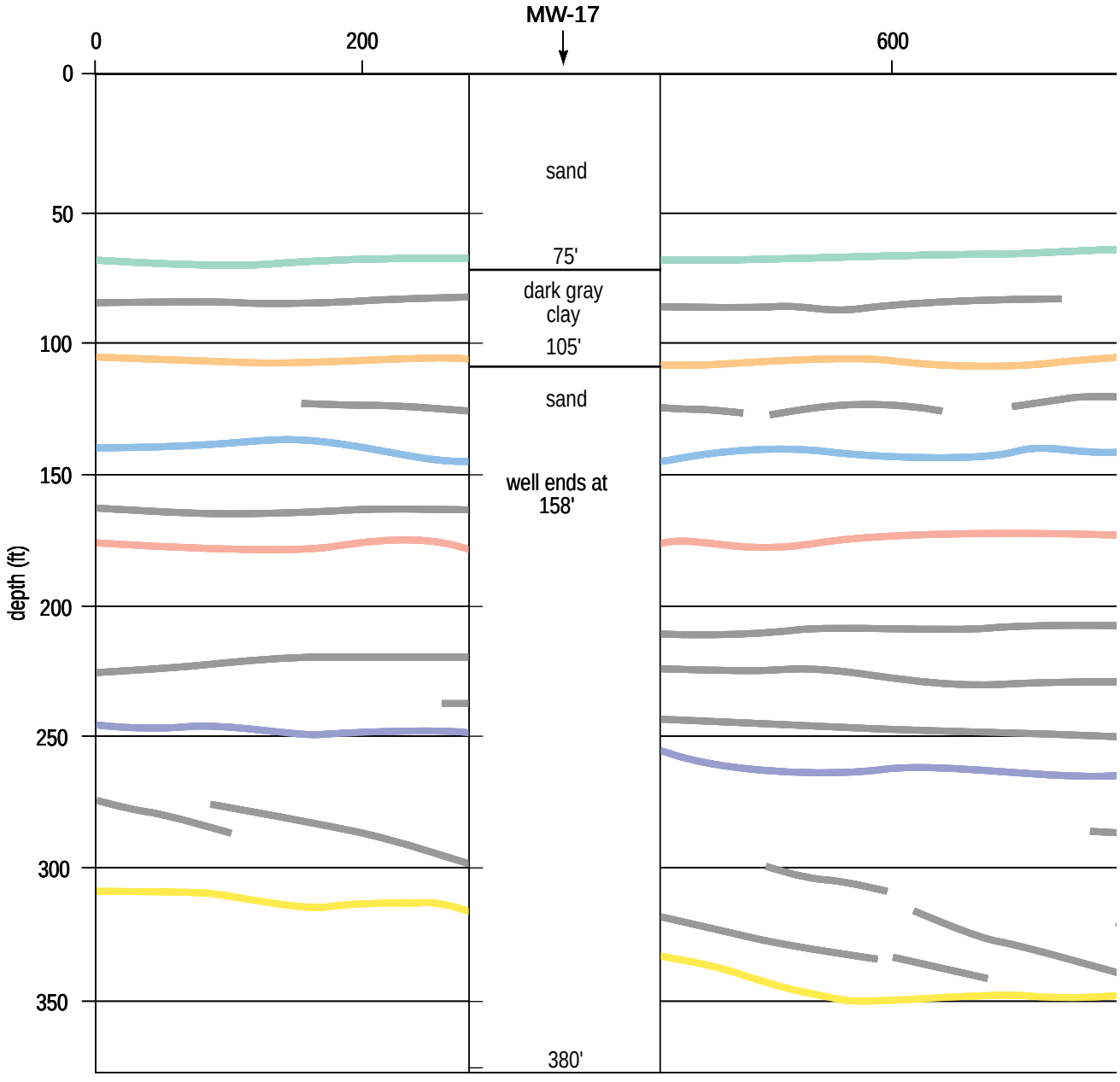

Figure 67a.Generalized geologic cross-section with lithologies interpreted from boreholes along the western boundary.

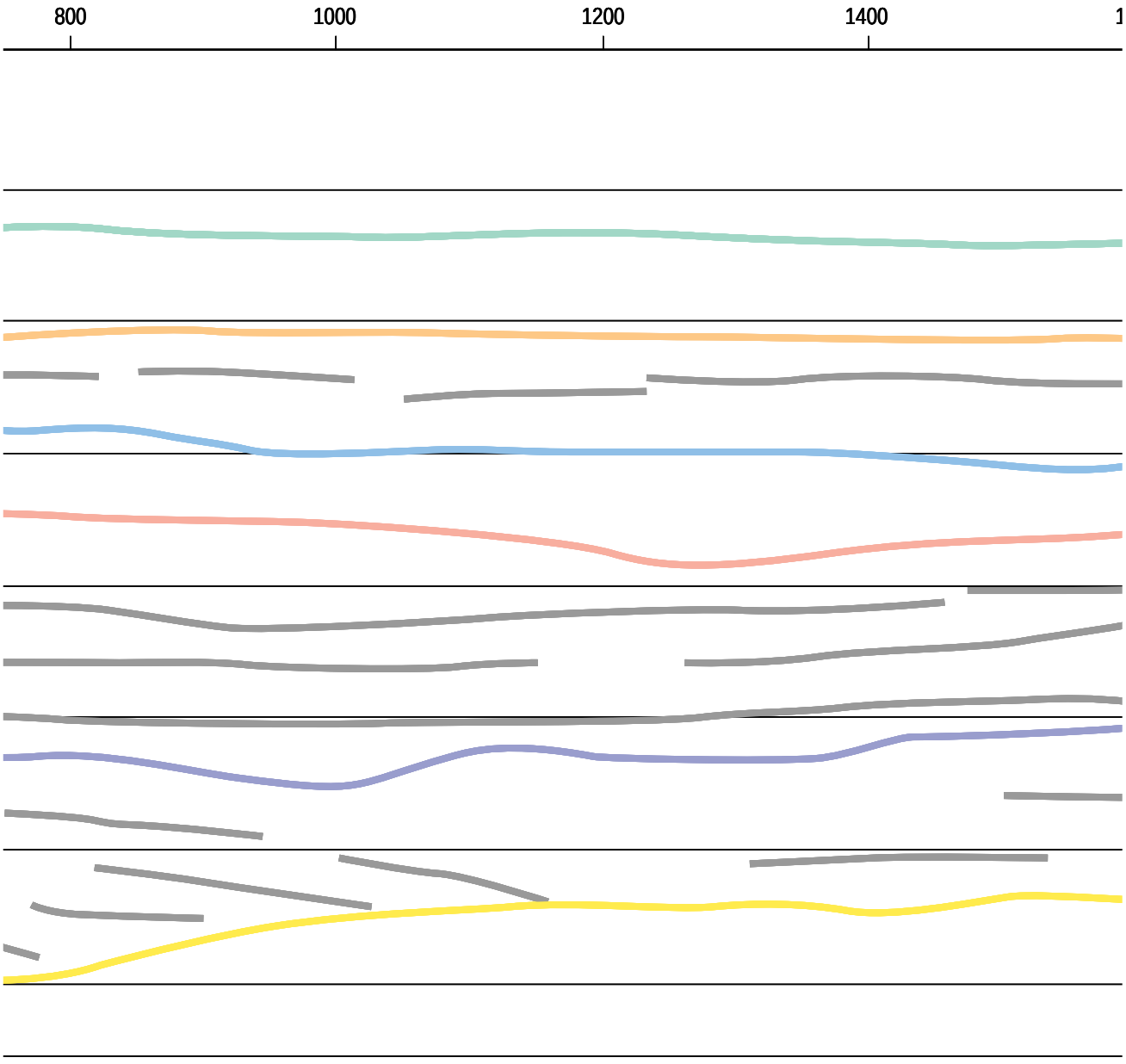

Figure 67b.

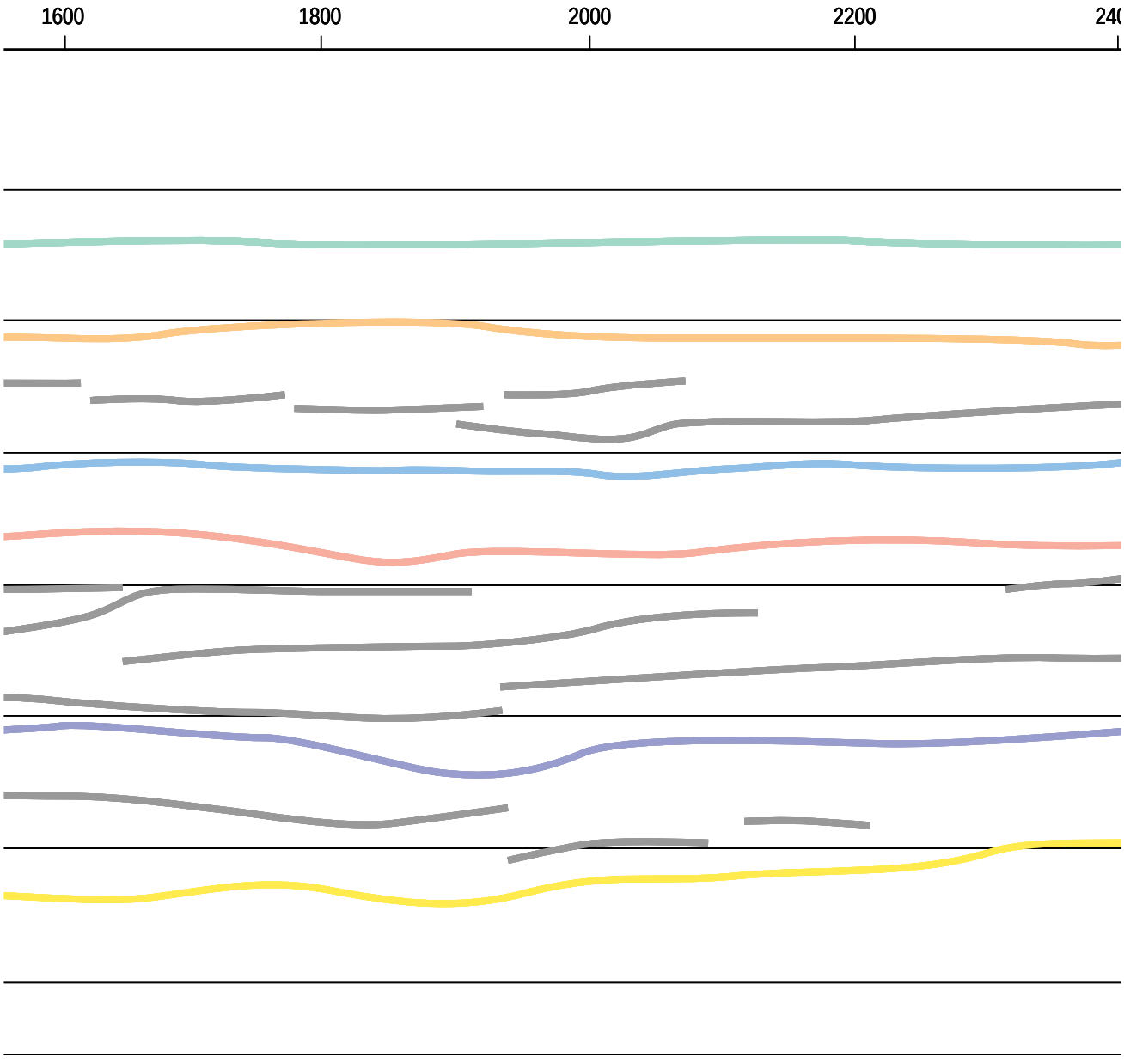

Figure 67c.

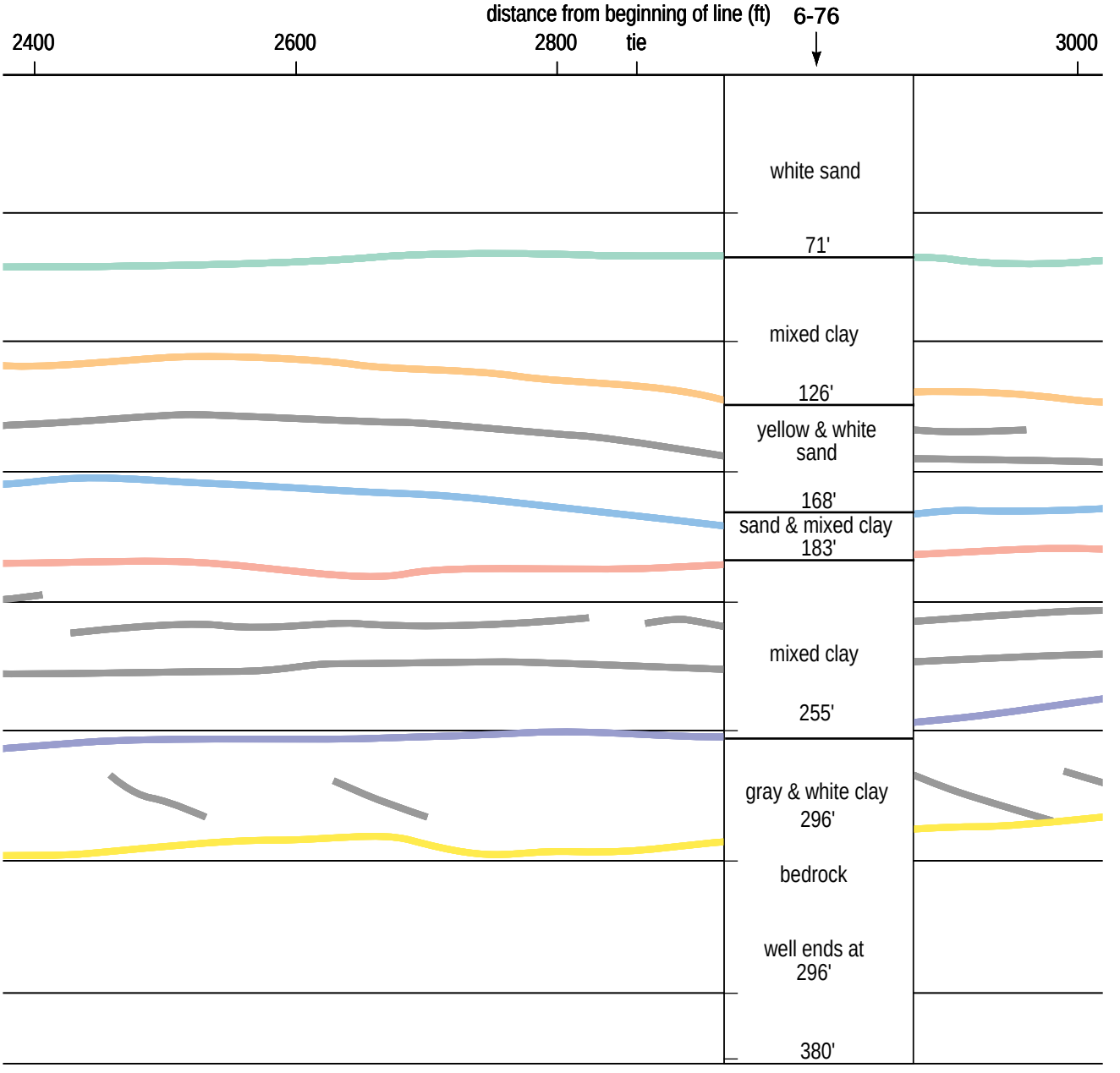
distance from beginning of line (ft)
6-76
2400
2600
2800
tie
3000
white sand
71'
mixed clay
126'
yellow & white sand
168'
sand & mixed clay
183'
mixed clay
255'
gray & white clay
296'
bedrock
well ends at 296'
380'

Figure 67d.

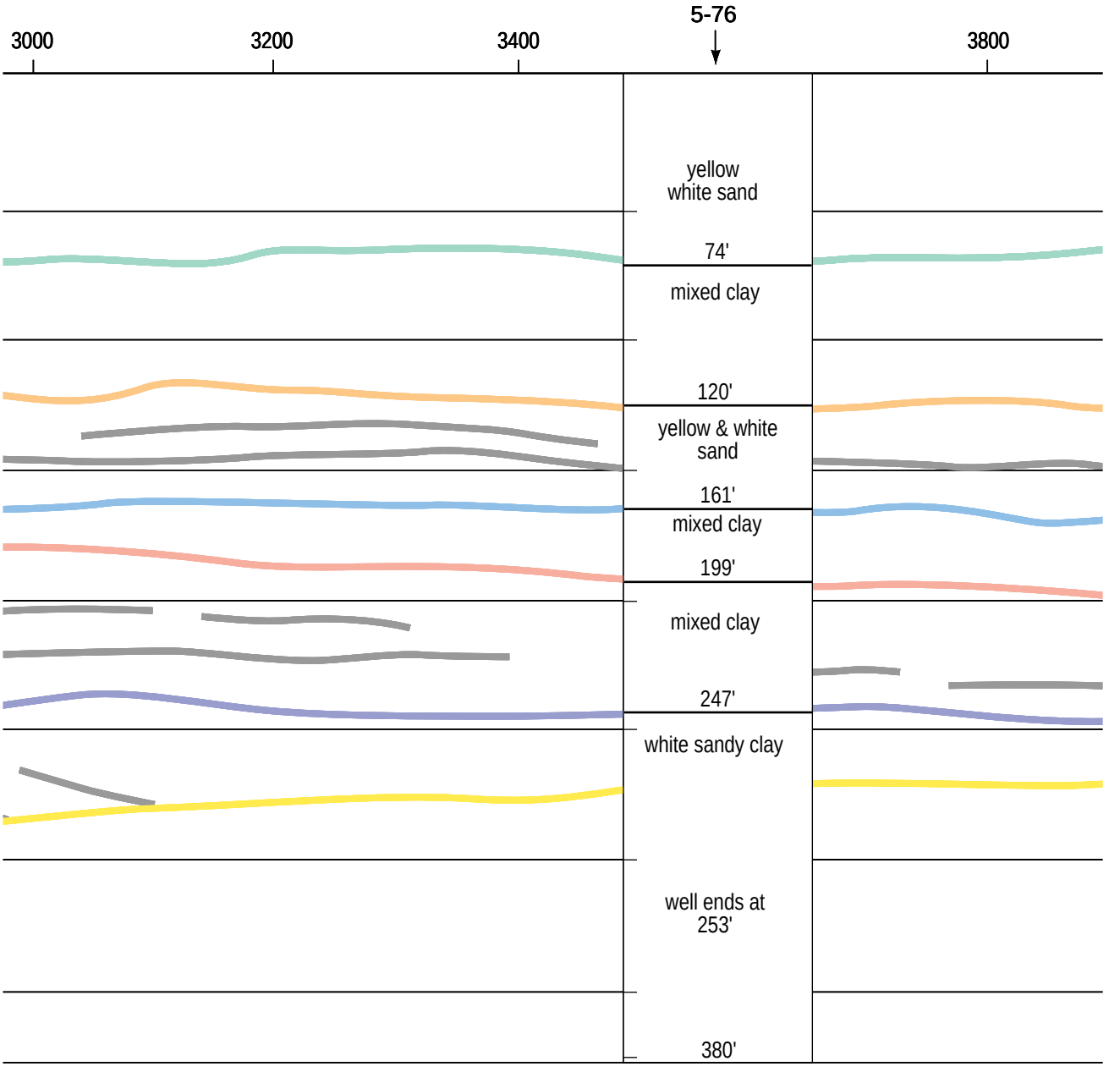
5-76
3000
3200
3400
3800
yellow
white sand
74'
mixed clay
120'
yellow & white
sand
161'
mixed clay
199'
mixed clay
247'
white sandy clay
well ends at
253'
380'

Figure 67e.

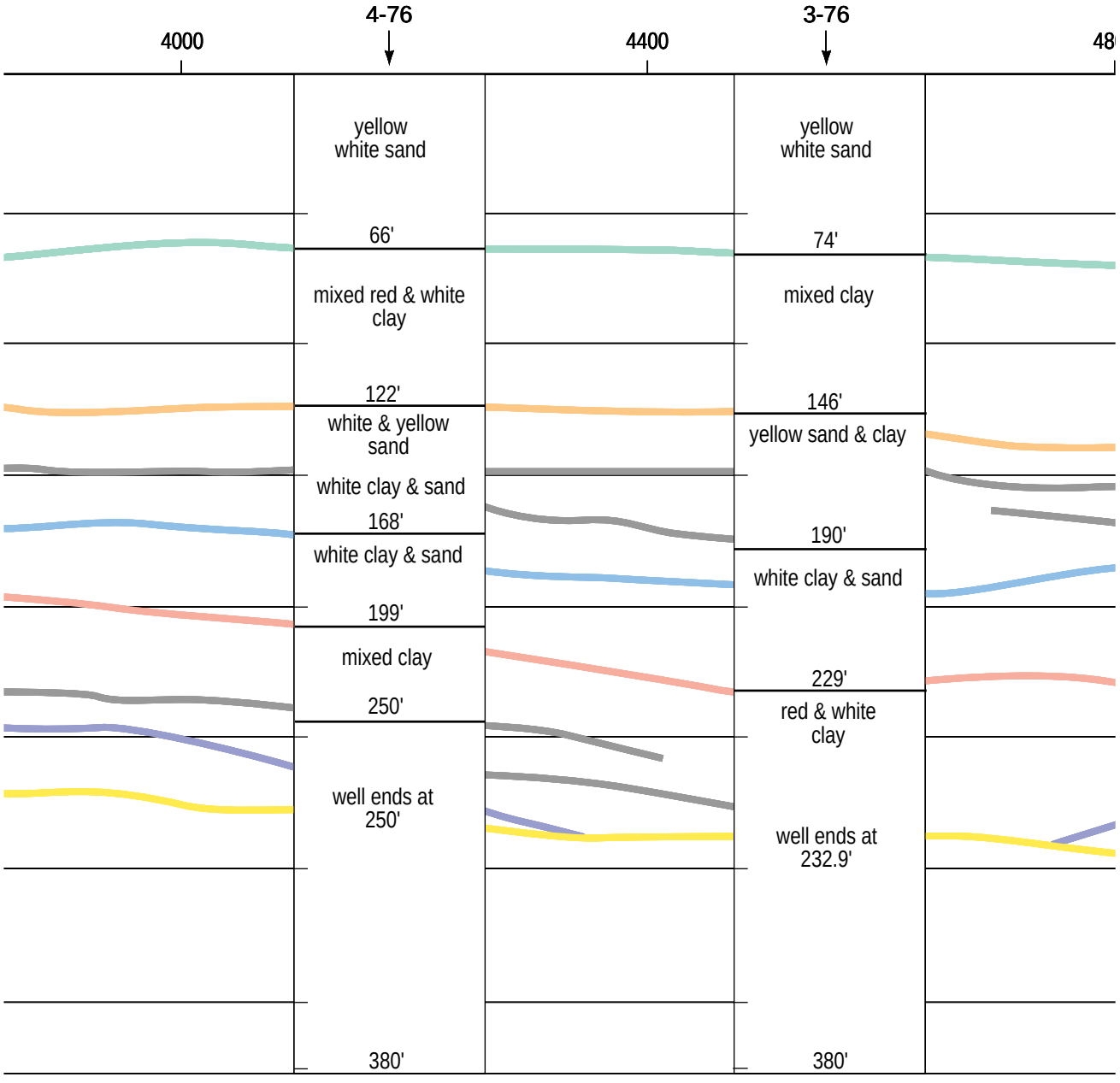
4000
4-76
4400
3-76
48
yellow
white sand
66'
mixed red & white
clay
122'
white & yellow
sand
white clay & sand
168'
white clay & sand
199'
mixed clay
250'
well ends at
250'
380'
yellow
white sand
74'
mixed clay
146'
yellow sand & clay
190'
white clay & sand
229'
red & white
clay
well ends at
232.9'
380'

Figure 67f.

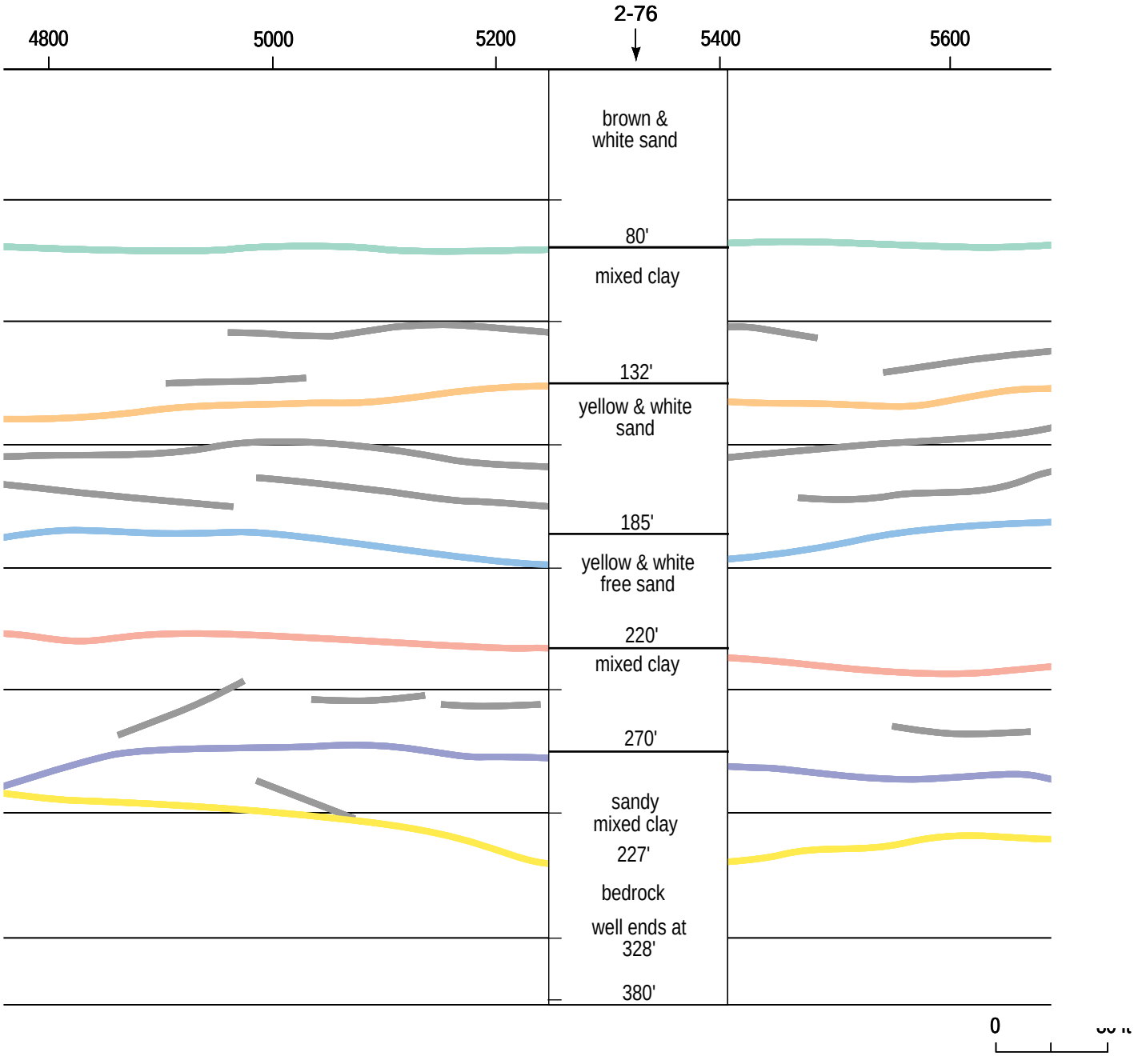
2-76
4800
5000
5200
5400
5600
brown &
white sand
80'
mixed clay
132'
yellow & white
sand
185'
yellow & white
free sand
220'
mixed clay
270'
sandy
mixed clay
227'
bedrock
well ends at
328'
380'
0

Figure 67g.

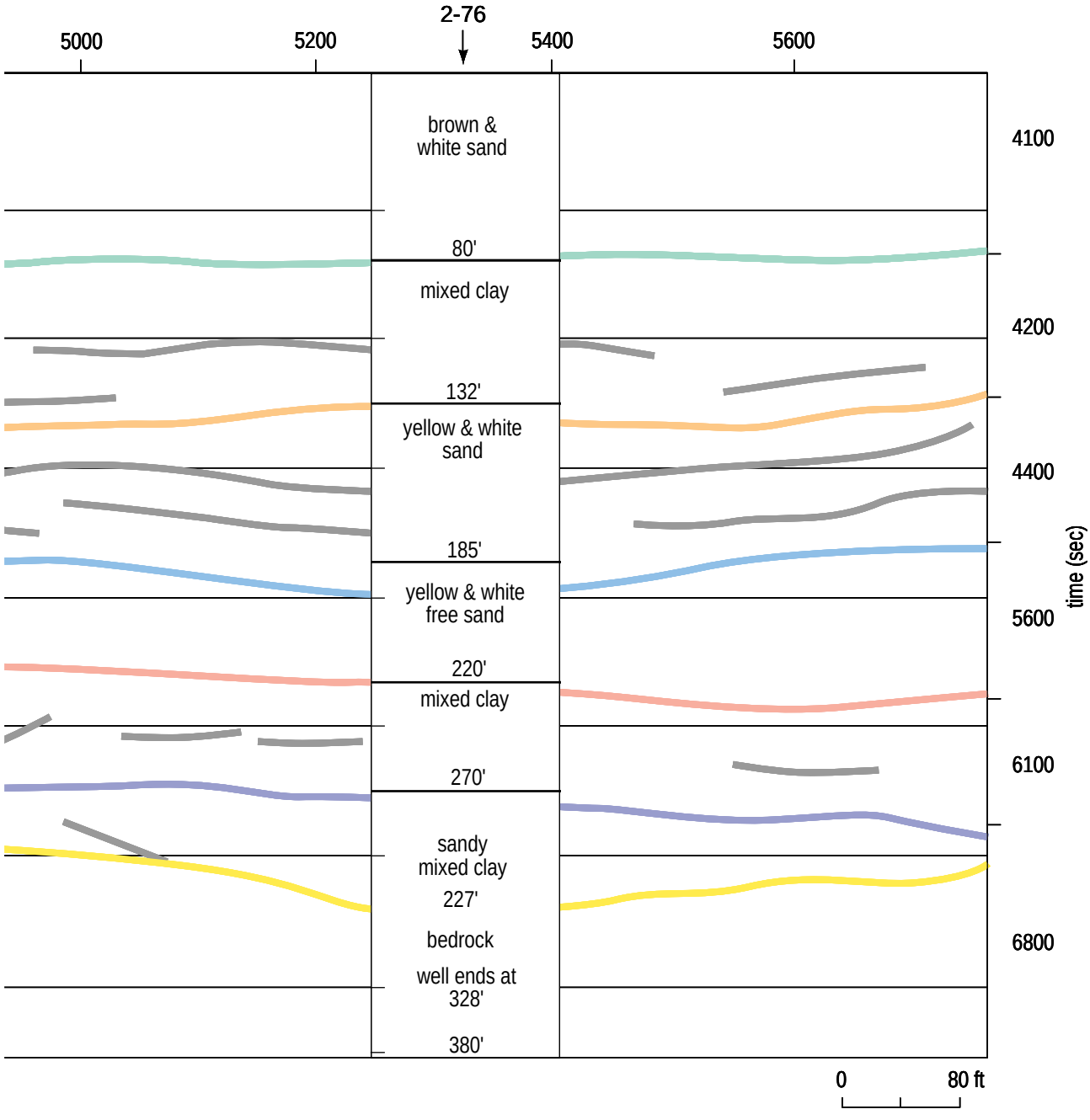
2-76
5000
5200
5400
5600
brown &
white sand
80'
mixed clay
132'
yellow & white
sand
185'
yellow & white
free sand
220'
mixed clay
270'
sandy
mixed clay
227'
bedrock
well ends at
328'
380'
4100
4200
4400
5600
6100
6800
time (sec)
0
80 ft

Figure 67h.

terminated (i.e., pinched out) along the profile, these data possess sufficient resolution to have detected and allowed an accurate interpretation of that feature. Subtle detail impossible to obtain from drill data are interpretable with high confidence on CDP stacked sections. All things considered, the seismic interpretations align extremely well with major geologic units as defined from boreholes. The seismic data are consistent with drill data and provide details about pinch-outs, channels, and bed structures not interpretable from drill data.

Phillips Airstrip Line

Several interpretable reflection events are evident on shot gathers acquired along the approximately north/south road south of Phillips Field (Figure 68). The hyperbolic curvature of the reflections distinguishes them from all other energy. Reflections from 50 to 130 msec are interpreted with an extremely high level of confidence. The intermittent nature of a potential reflection at about 35 msec was sufficient justification to mute it with the refractions and direct wave to maintain and ensure the highest confidence in the origin of all events interpreted on stacked sections. It would, however, be possible to design acquisition parameters at this site to optimize the recording of the 35 msec event as well as most reflections between 35 and about 100 msec. The ray trace model of the reflection hyperbola based on the interpretation of the shot gathers closely matches the recorded reflection geometries (Figure 69). The reflection hyperbola from the airstrip are much more uniform in appearance than those from the western boundary and hence represent a much less geometrically complex reflector environment. The color coding is consistent with the stacked section from the airstrip.

The CDP stacked section depicts a subsurface environment significantly less variable than the western boundary (Figure 70). Data have been elevation corrected to several sloping datums and therefore depth calculations are based on measurements from the ground surface. Reflectors represented on the interpretative geologic cross-section are consistent with a flat datum (Figure 72). A subtle interbed/inter-unit reflection evident between the orange and red reflections (clay unit) seems to thin and possibly terminate from south to north across the expanse of the seismic line (Figure 71). Based on reflection characteristics, the reflector interpretable within the 120 ft deep sand unit is likely a clay stringer. This interpreted clay stringer appears to truncate around CDP 12200.

The sand layer about 115 msec (270 ft) deep is at the practical vertical resolution limit of this data (Figure 71). This subtle thinning layer at its thickest point is

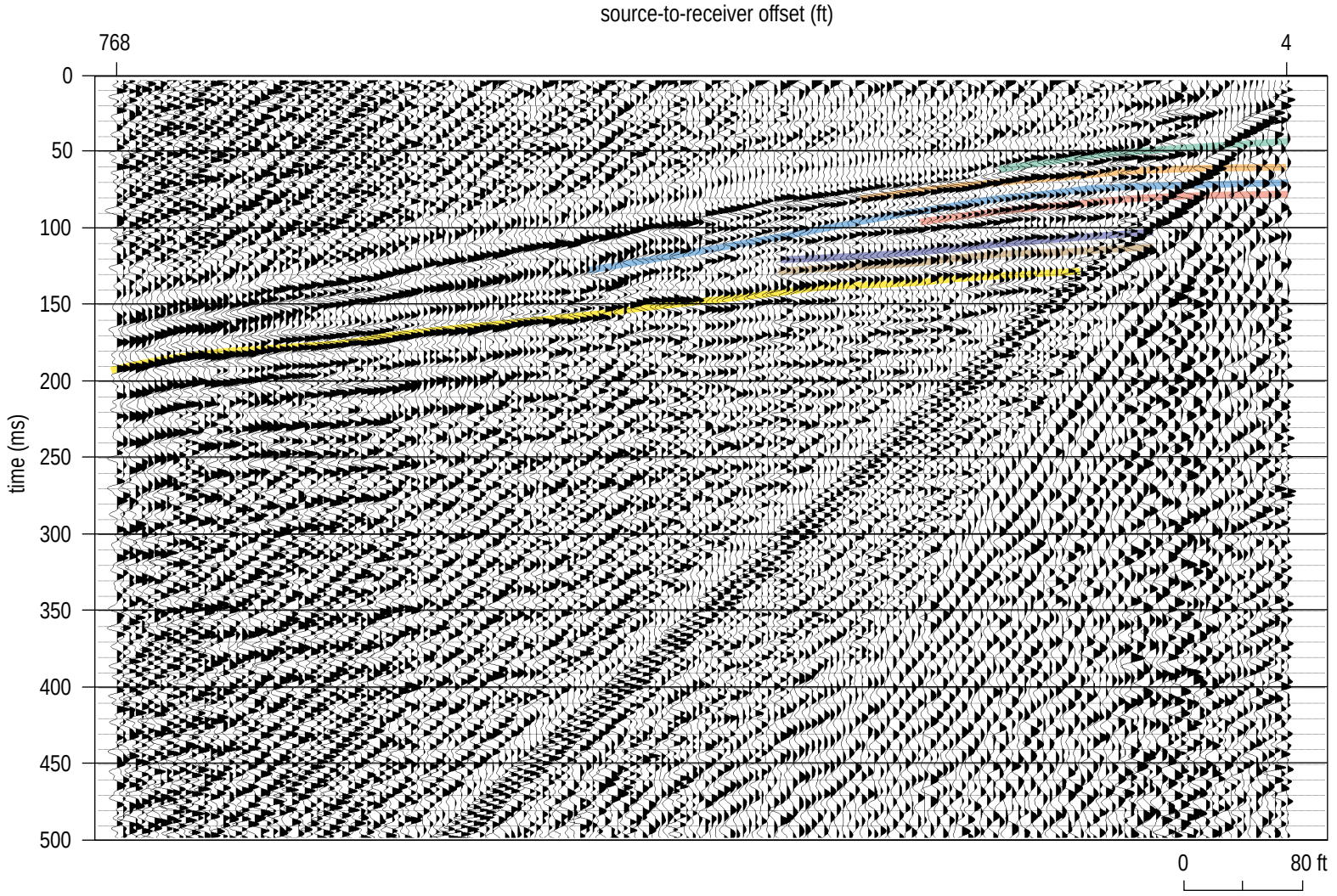

Figure 68. Shot gather with color interpreted reflection hyperbola from the south end of the airstrip line.

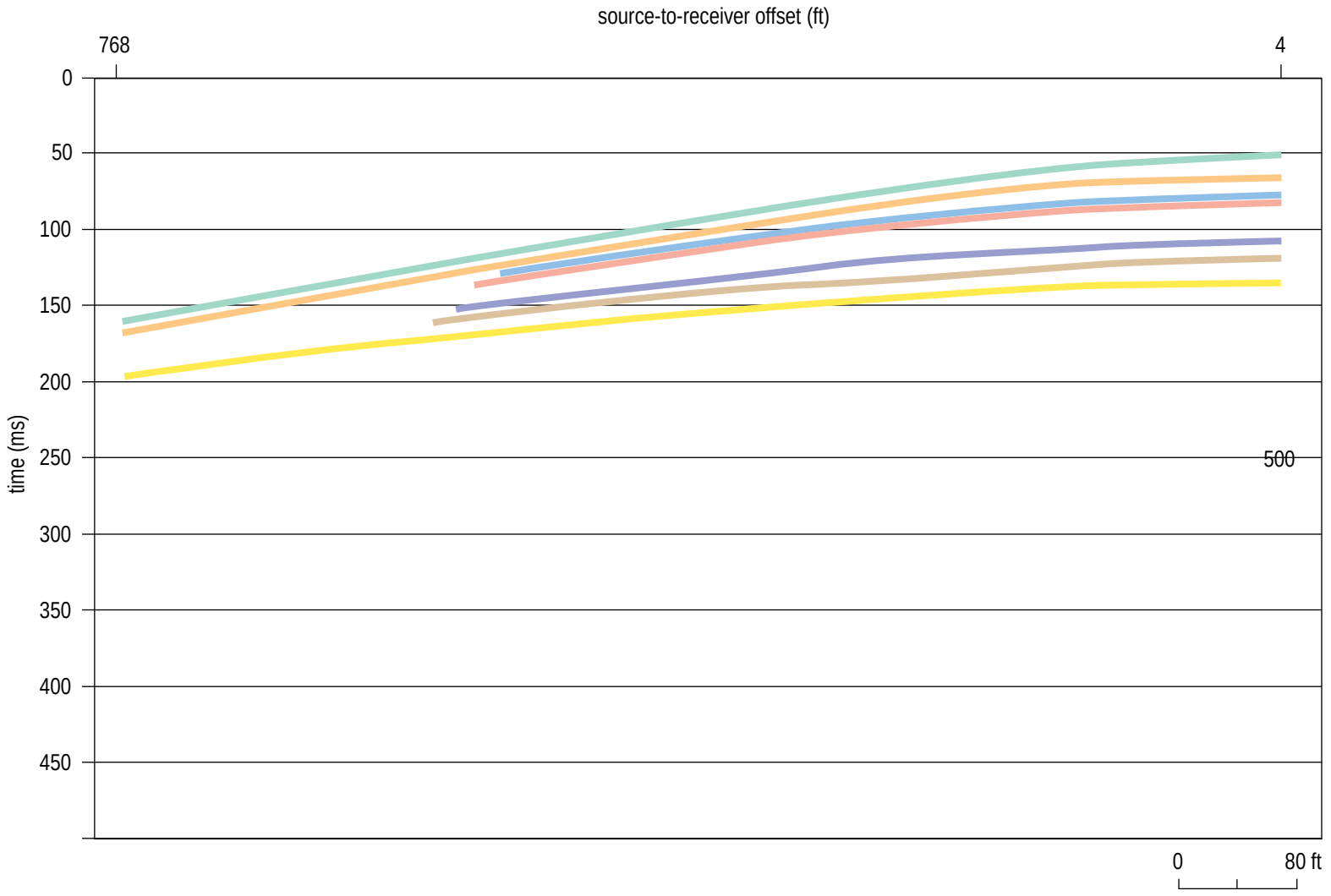

Figure 69. Ray trace model of reflection hyperbola with color correlated to the shot gather from the south end of the airstrip line.

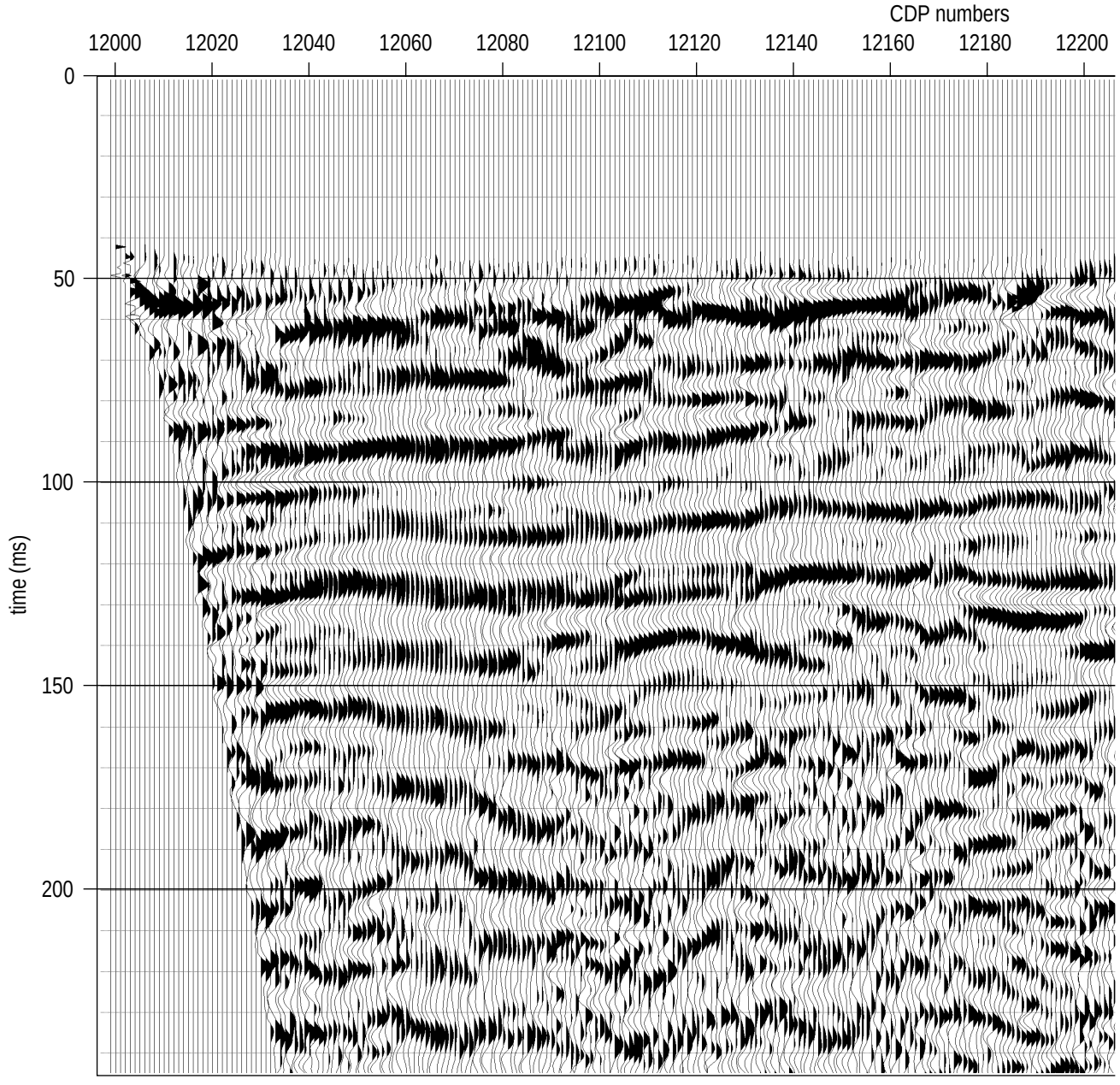

Figure 70a.CDP stacked section from the airstrip line.

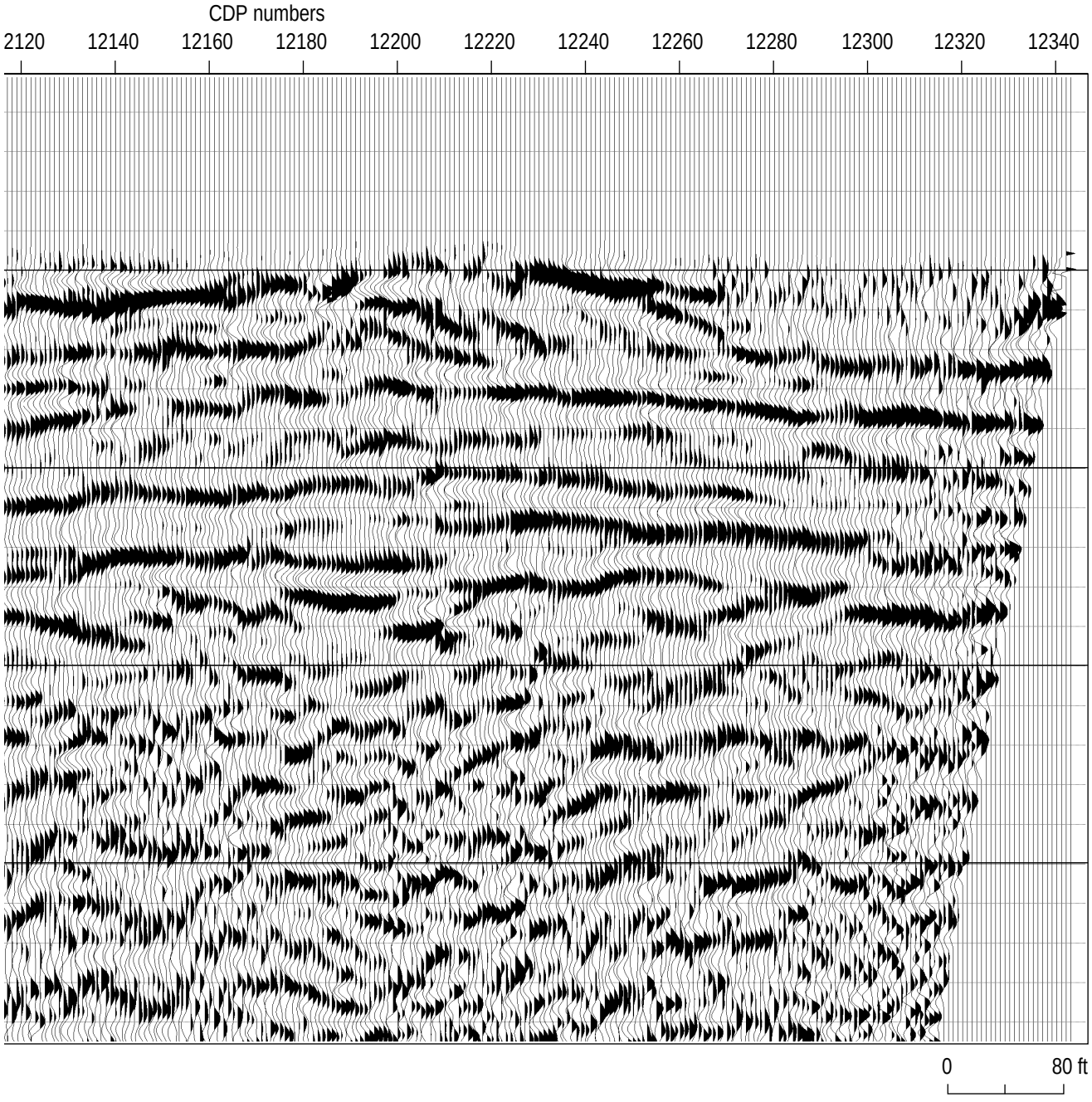
CDP numbers
2120
12140
12160
12180
12200
12220
12240
12260
12280
12300
12320
12340
0
80 ft

Figure 70b.

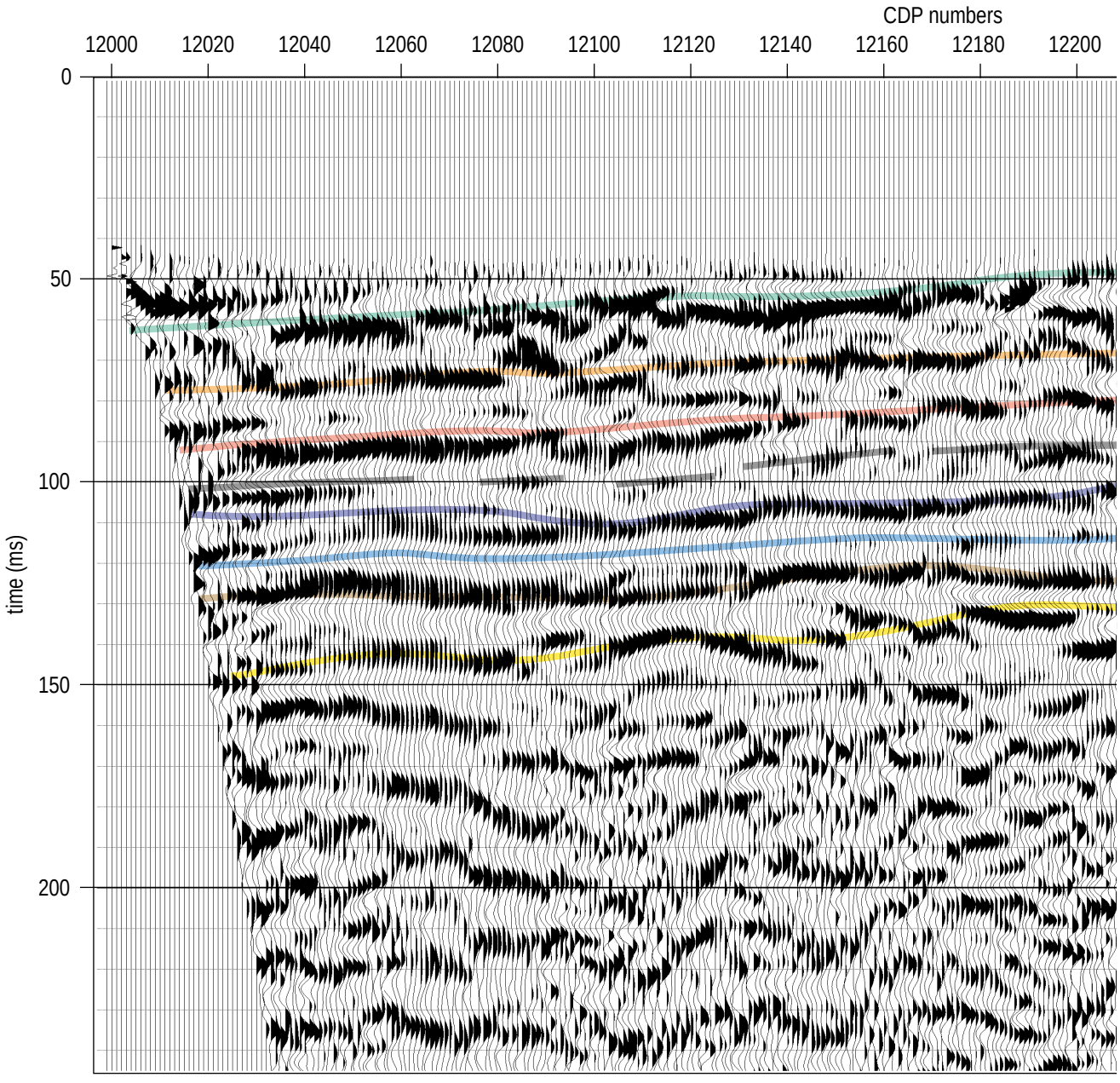

Figure 71a. Colorinterpreted CDP stacked section with colors interpreted as major lithologic changes near the airstrip line.

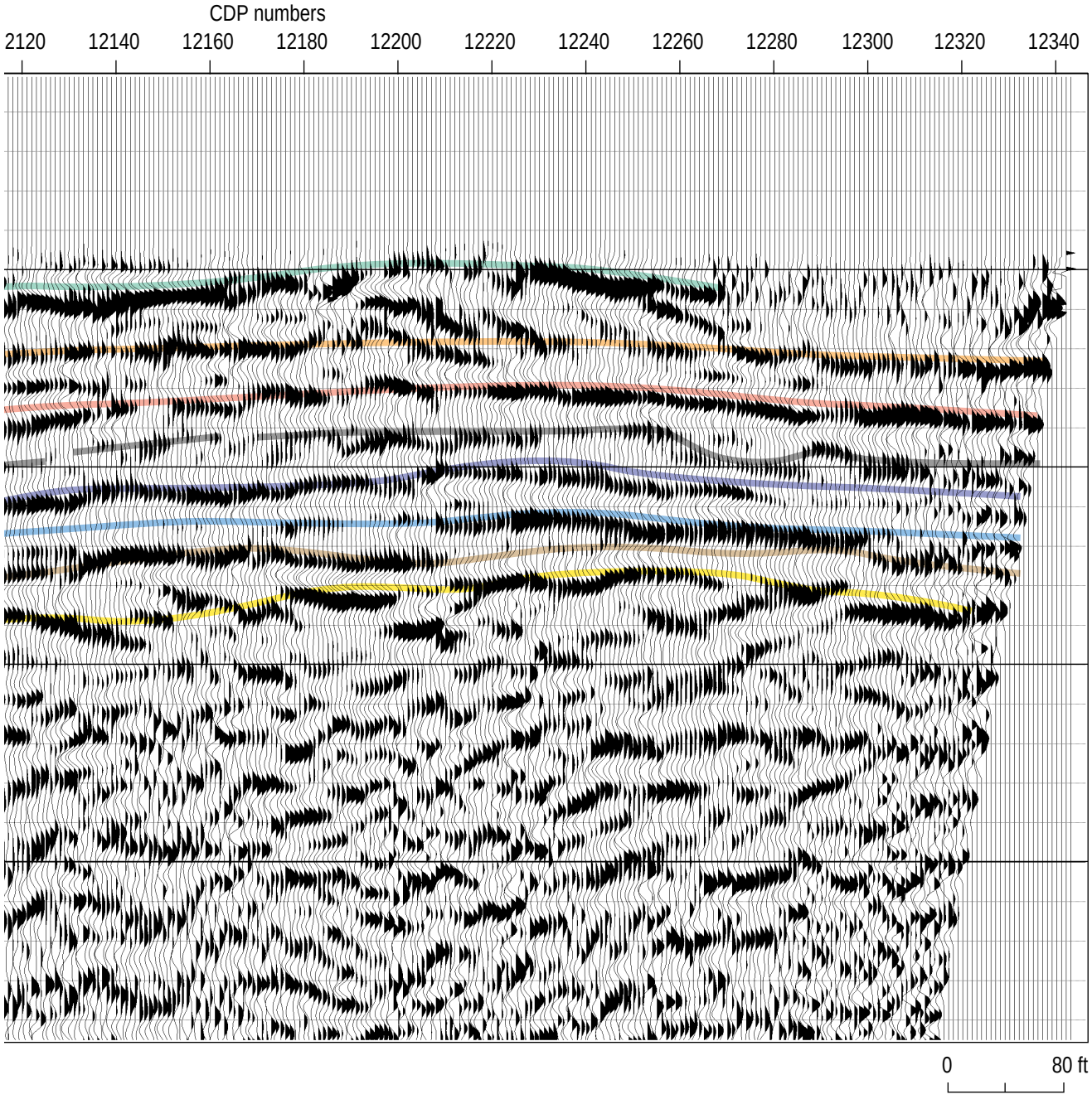
CDP numbers
2120
12140
12160
12180
12200
12220
12240
12260
12280
12300
12320
12340
0
80 ft

Figure 71b.

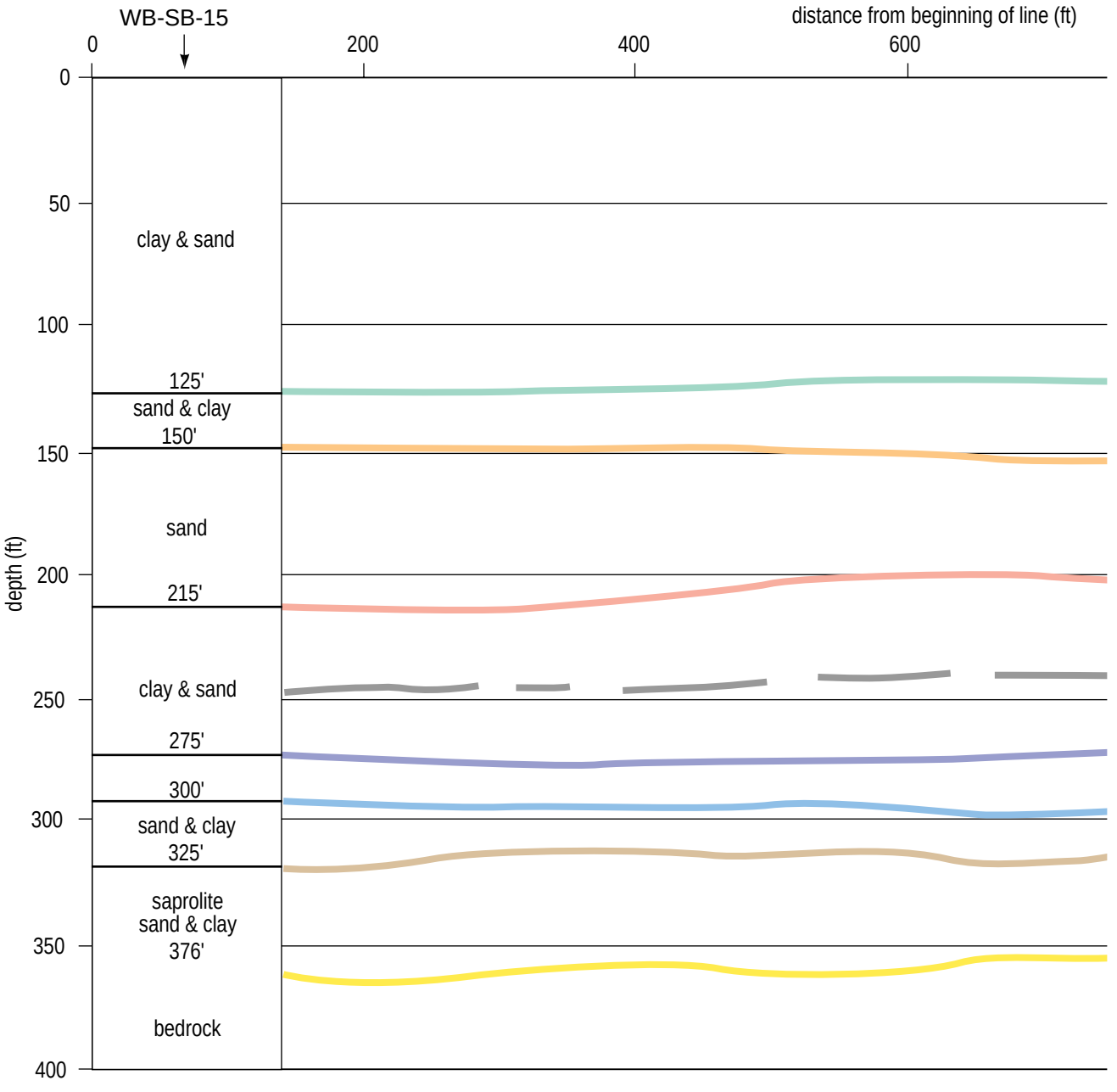

Figure 72a. Generalized geologic cross-section with lithologies interpreted from borehole geologic and geophysical logs near the airstrip line.

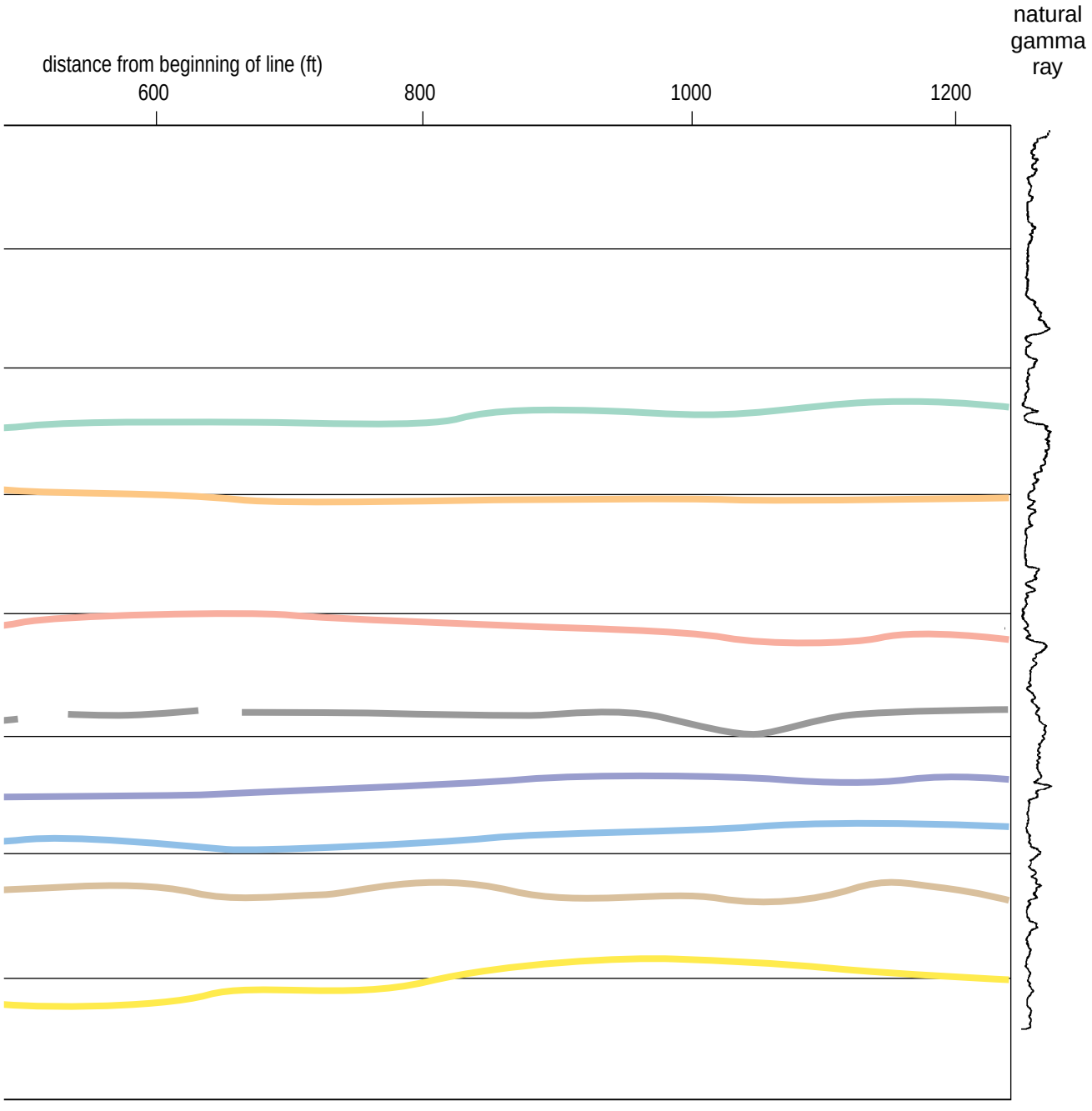
natural
gamma
ray
distance from beginning of line (ft)
600
800
1000
1200

Figure 72b.

represented on the seismic reflection section as two unique reflection wavelets. Tuning and wavelet interference phenomena become obvious as the bed thins to less than 1/2 wavelength. Continuity of this bed across the entire section can only be established through evaluation based on thin bed criteria (Widess, 1974; Gochioco, 1992). It appears likely the sand layer thins over the southern half of the line and then begins to thicken at the southernmost end. Careful analysis and correlation with existing borehole data suggests the practical resolution limits of data from this area is on the order of 1/4 wavelength, or 10 ft. Even considering the shorter line length, the horizontal variability of reflectors and the geometric complexity of bedding is significantly less along the airstrip line than the western boundary line.

The bedrock reflection (yellow) is very pronounced and in places possesses the same scalloped, broken coherency look pointed out on the western boundary line (Figure 71). Line-to-line consistency of this and other reflection characteristics allows considerable interpretation confidence. The bedrock surface is interpreted to have a topographic low beneath about CDP 12060 (Figure 72). The clay/sand/saprolite layer that directly overlays the bedrock surface has completely infilled the undulating bedrock surface. Only subtle topographic variations are interpretable in layers deposited above the bedrock surface.

Correlation of seismic reflection data to borehole #WB-SB-15 provides a uniform and horizontally continuous picture of the subsurface (Figure 72). The borehole was located about 150 ft off the southern end of the line. The geophysical logs and geologists log correlate excellently with the stacked reflection data. Generation of the geologic cross-section was based on a ray path model of reflection time and interval velocity. Interval velocities were established from NMO velocity, local borehole derived interval, and average velocities (Table 2). Some fine-tuning of interval velocities (i.e., < 5%) was necessary to optimize the correlation between the geologic cross-section and borehole lithologies.

Spesutie Island Line

Reflections on field files from Spesutie Island can be confidently identified and correlated to reflectors interpreted from geophysical logs of borehole HAR-Dg 3 (Figure 73). The thicker unconsolidated section present at Spesutie Island in comparison to the airstrip and western boundary is evident on the shot gather and modeled reflection arrivals (Figure 74). Reflections interpreted on field files have zero offset times from 50 to about 250 msec, which equates to a depth range from

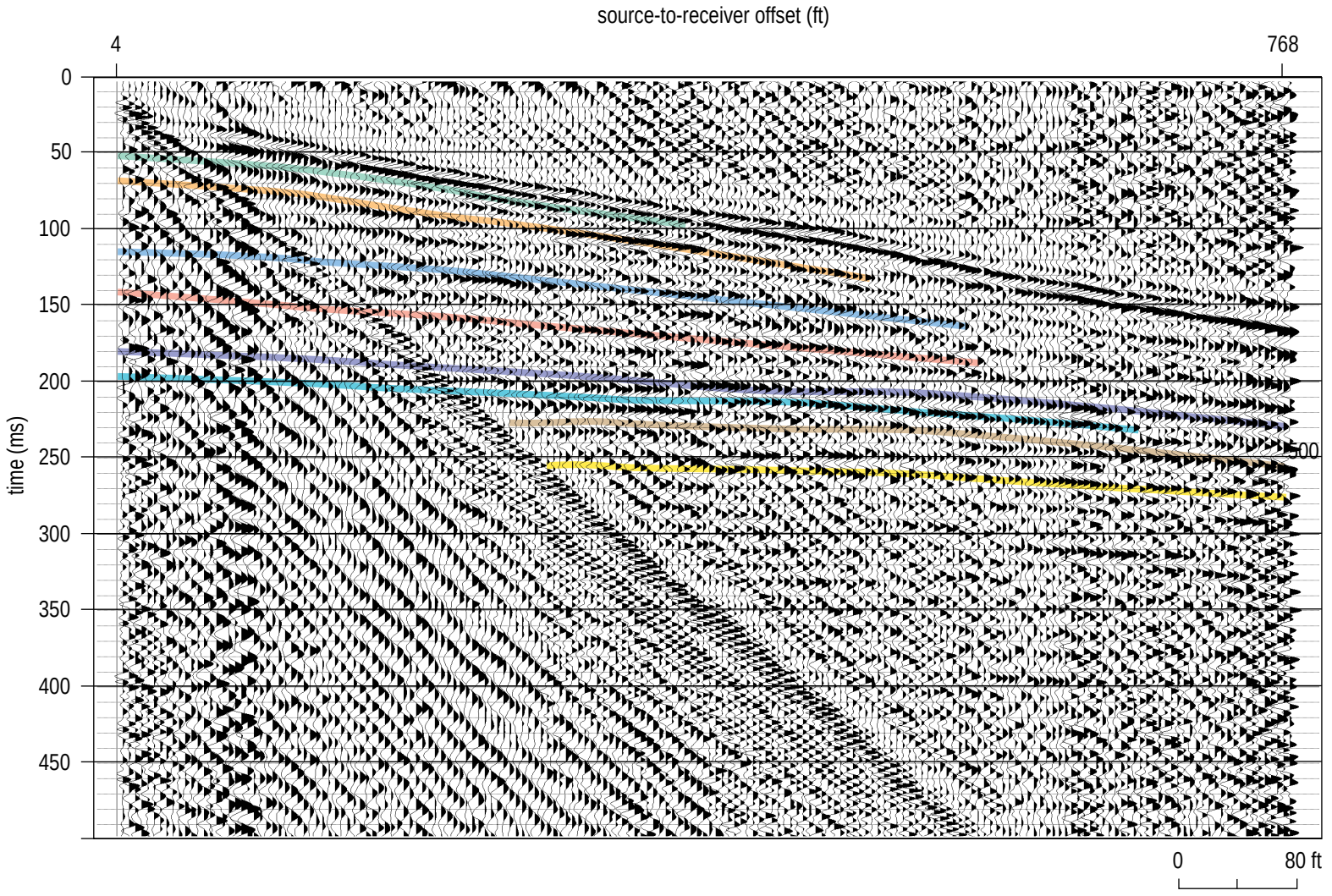

Figure 73. Shot gather with color interpreted reflection hyperbola from Spesutie Island.

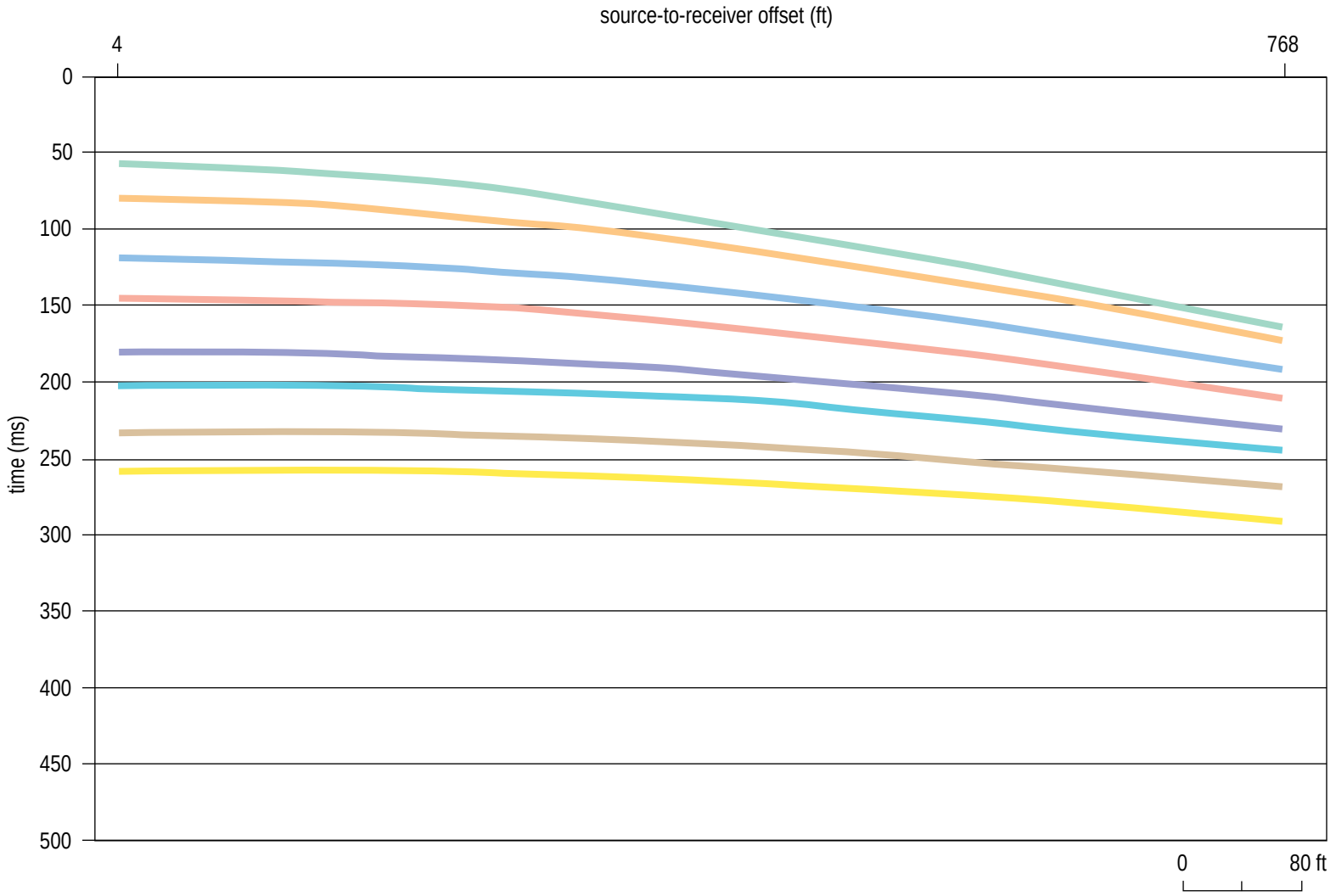

Figure 74. Ray trace model of reflection hyperbola with color interpreted from borehole data consistent with the shot gather in Figure 73 from Spesutie Island.

about 100 to over 750 ft. Reflections shallower than 100 ft can be effectively imaged at Spesutie Island by simply modifying the acquisition parameters to focus on the shallower depths. Modifying acquisition parameters to target shallower reflectors is possible but likely to be at the expense of deeper reflectors. The vertical offset in reflection coherency and/or wavelet consistency on field files at around a 400 ft source offset is related to changes in the source location (Figure 73). This type of source static is common on walkaways when more than one source location is included in a single shot gather. The reflector spacing at Spesutie Island seems to be greater (i.e., unit thickness) than observed at either the airstrip or the western boundary. This apparent thickening to the east is consistent with the borehole-interpreted geologic cross-section across APG.

The modeled shot gather (Figure 74) with hyperbola calculated based on reflection arrival times and apparent velocities matches extremely well with the trace of the actual reflection curves on shot gathers (Figure 73). The cycle repeat time between modeled reflection hyperbola ranges from 20 to 40 msec. The resolution potential (i.e., the dominant and upper corner frequency) of the shot gathers is consistent with the airstrip and western boundary. The quality of the match between the theoretical shot gather with modeled reflection hyperbola and the real shot gather allows a great deal of confidence in event identification and approximation of reflector depths.

The 24-fold CDP stacked section from Spesutie Island provides several interpretive challenges (Figure 75). The coherency and number of high amplitude reflections is measurably greater on stacked data from Spesutie Island than either the airstrip or western boundary. This apparent increase in coherency is at least in part related to the overall increase in signal-to-noise ratio and reflector consistency. Several subtle cut-and-fill type features are interpretable. The combined effects of wavelet tuning/interference with a high signal-to-noise ratio (which in this context lowers the threshold reflectivity detectable on a CDP stacked section) complicates differentiating each unique reflection wavelet. Individual reflection identification is necessary for the generation of a representative reflector cross-section.

In many cases an acoustic feature can be geologically interpreted in a variety of ways. Some interpretations are acoustically more reasonable while others may be geologically preferred. In the best of all worlds, the best acoustic interpretation is also the most likely/favorite geologic explanation. An integrated interpretation approach normally provides the most accurate geologic model.

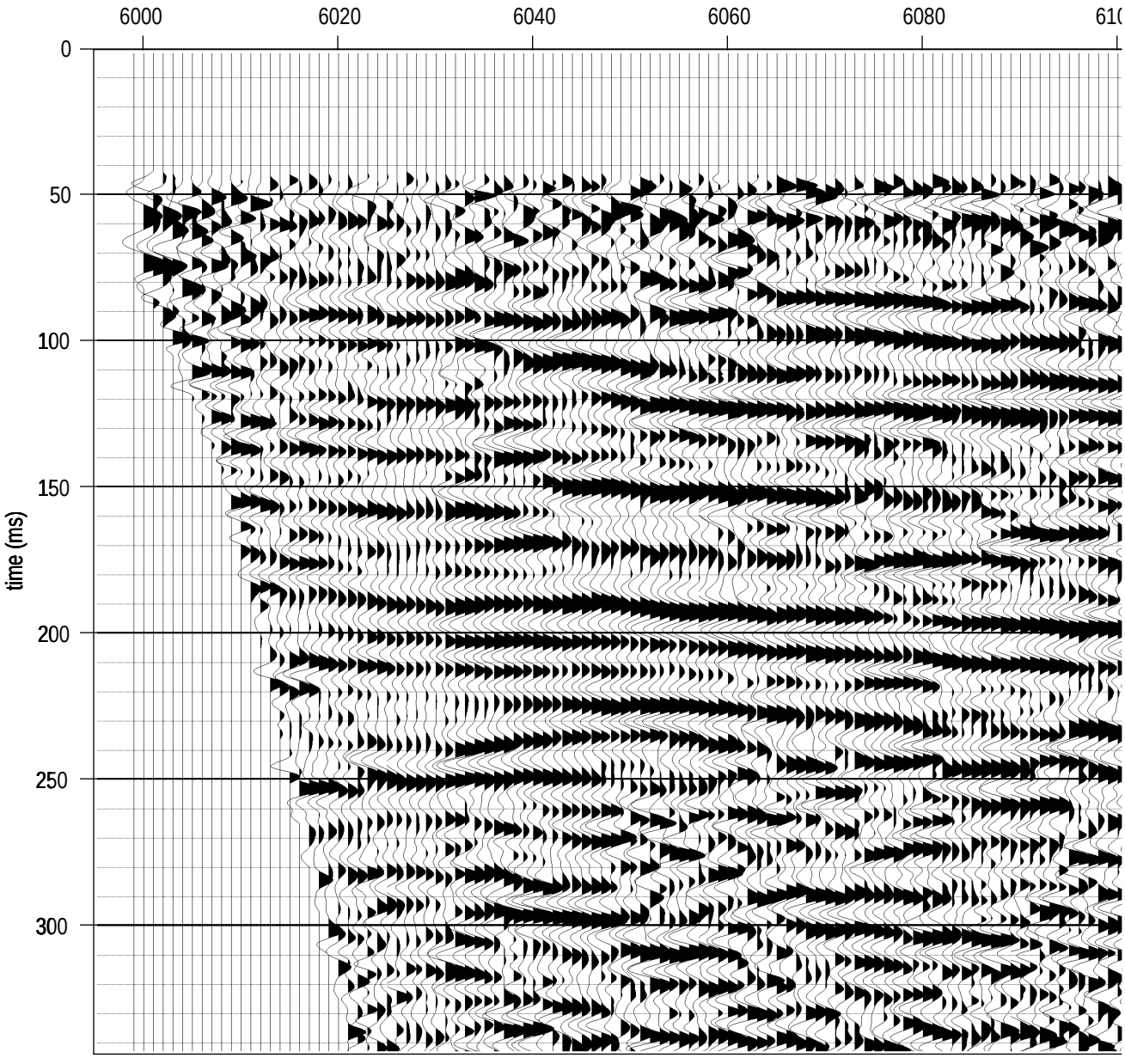

Figure 75a.CDP stacked section from Spesutie Island.

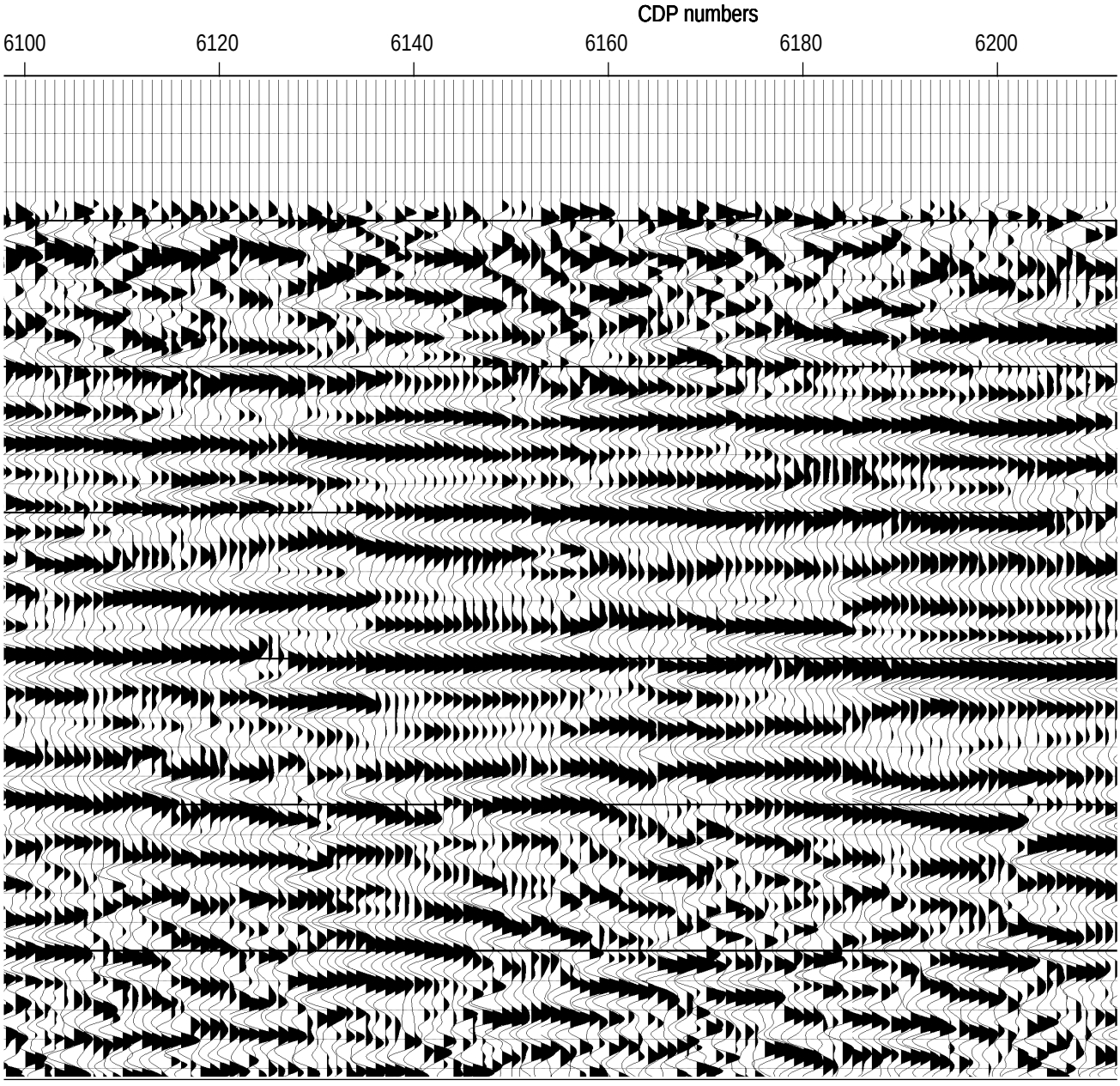

Figure 75b.

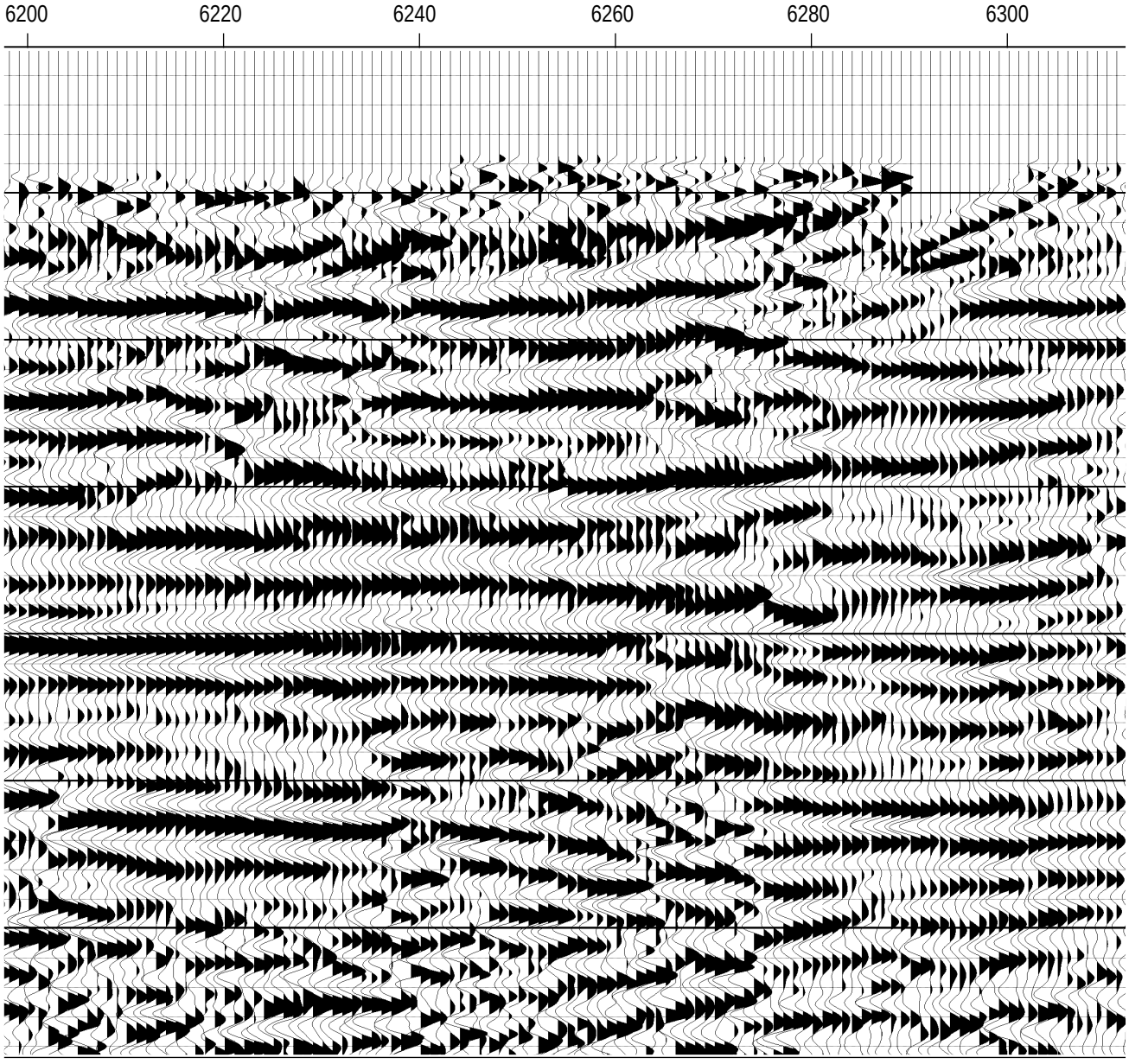

Figure 75c.

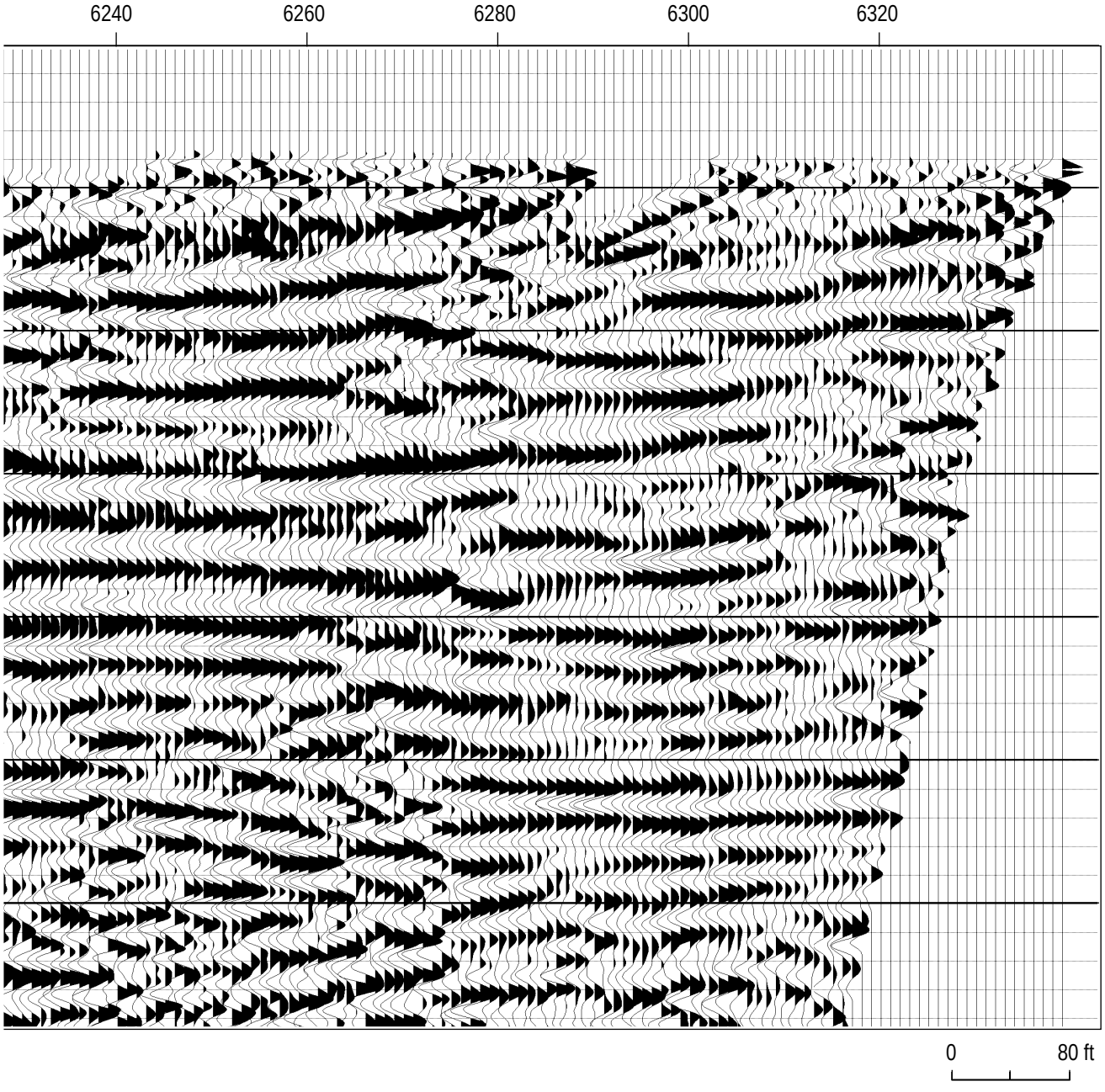

Figure 75d.

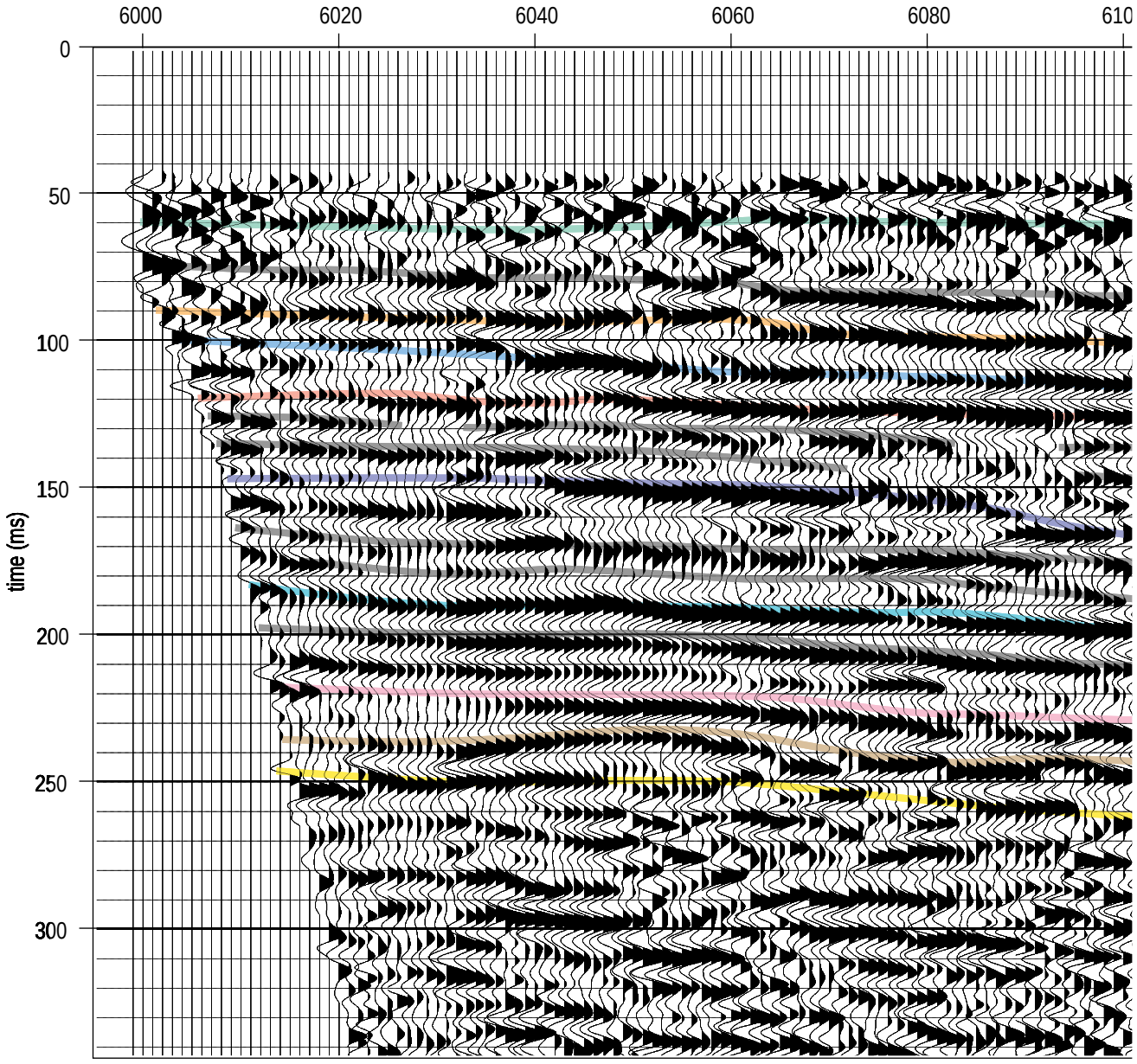

Figure 76a. Color interpreted CDP stacked section correlated to borehole data from Spesutie Island

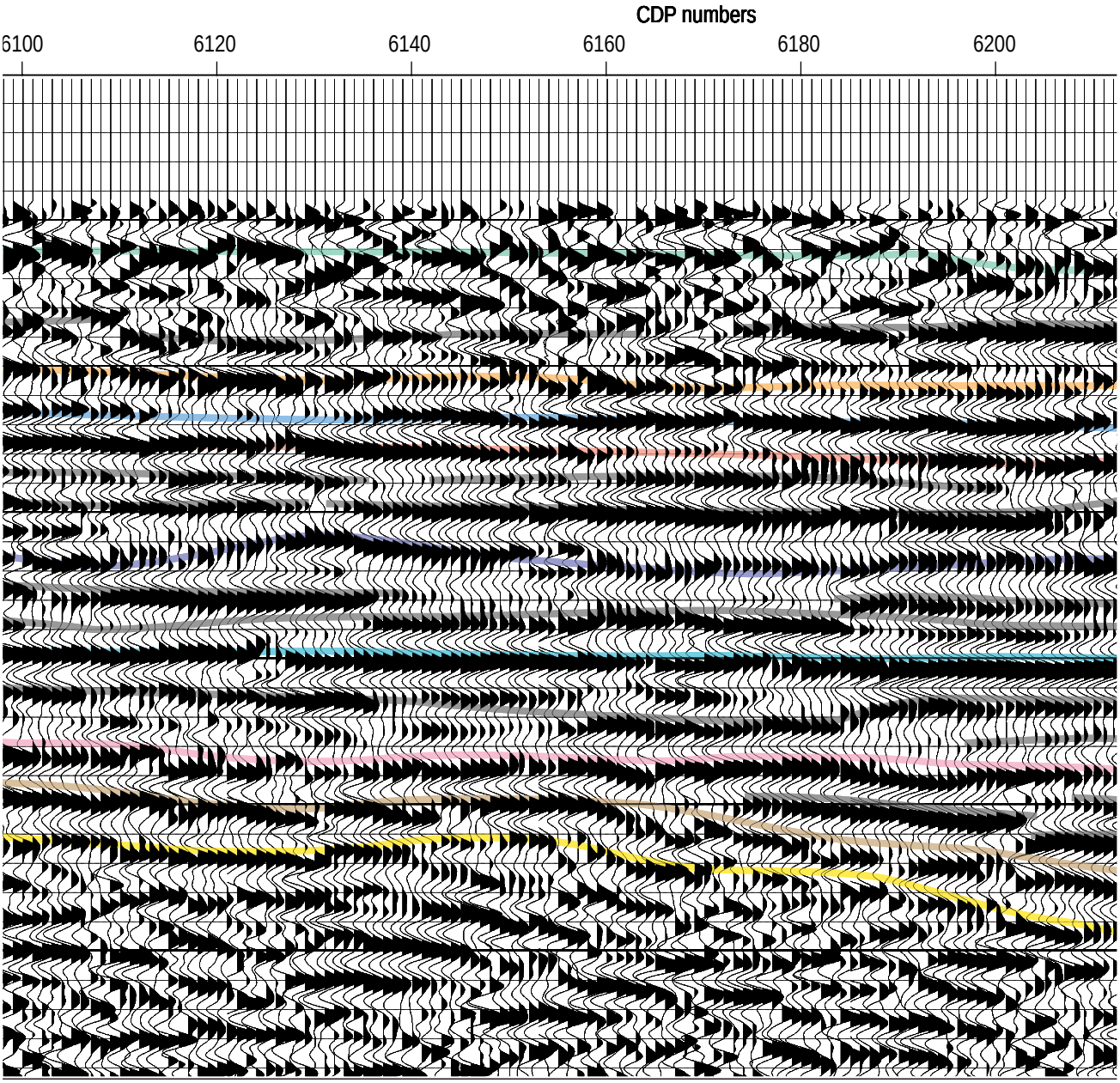

Figure 76b.

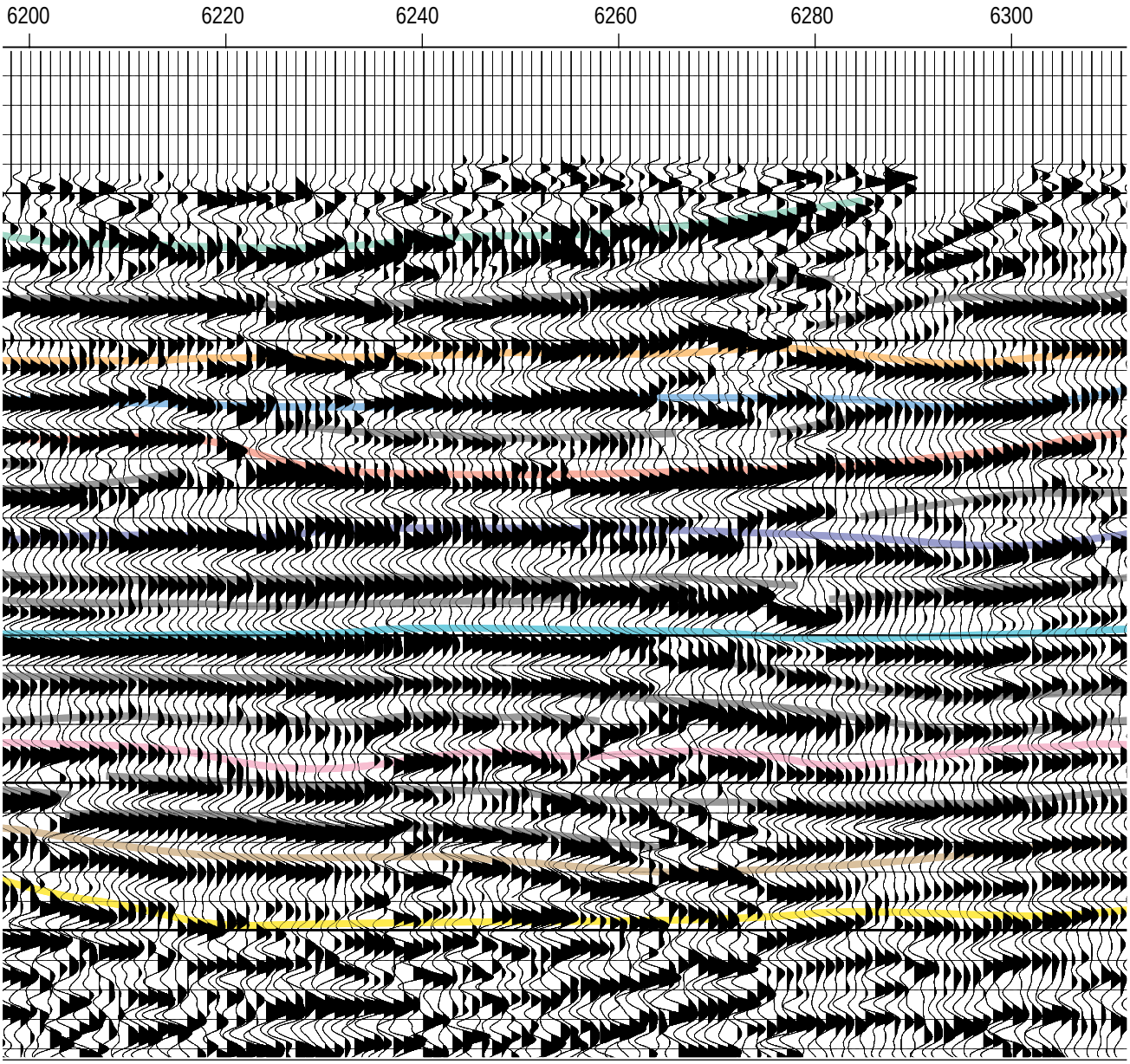

Figure 76c.

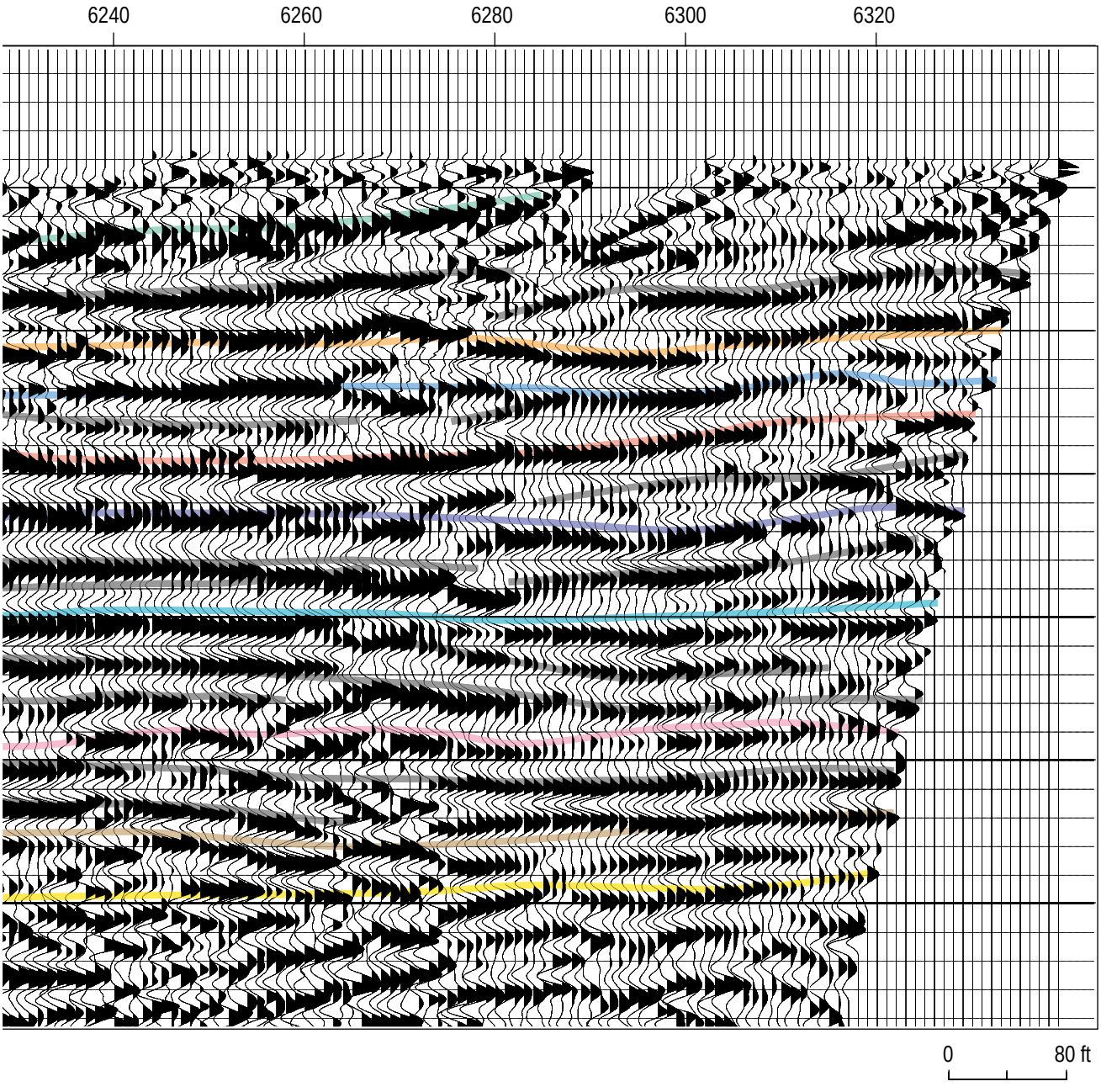

Figure 76d.

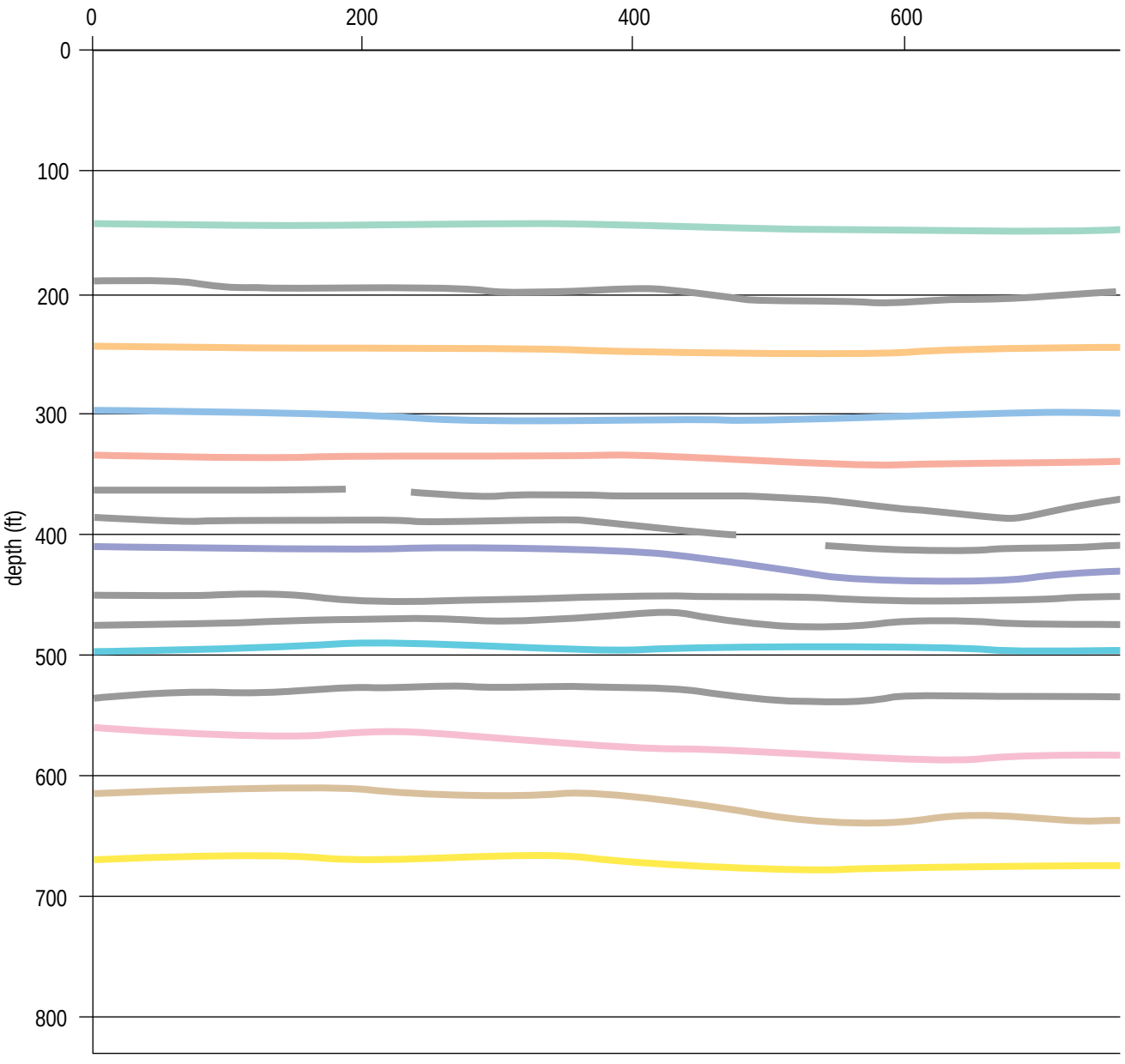

Figure 77a.Generalized geologic cross-section with lithologies interpreted from borehole geologic and geophysical logs on Spesutie Island.

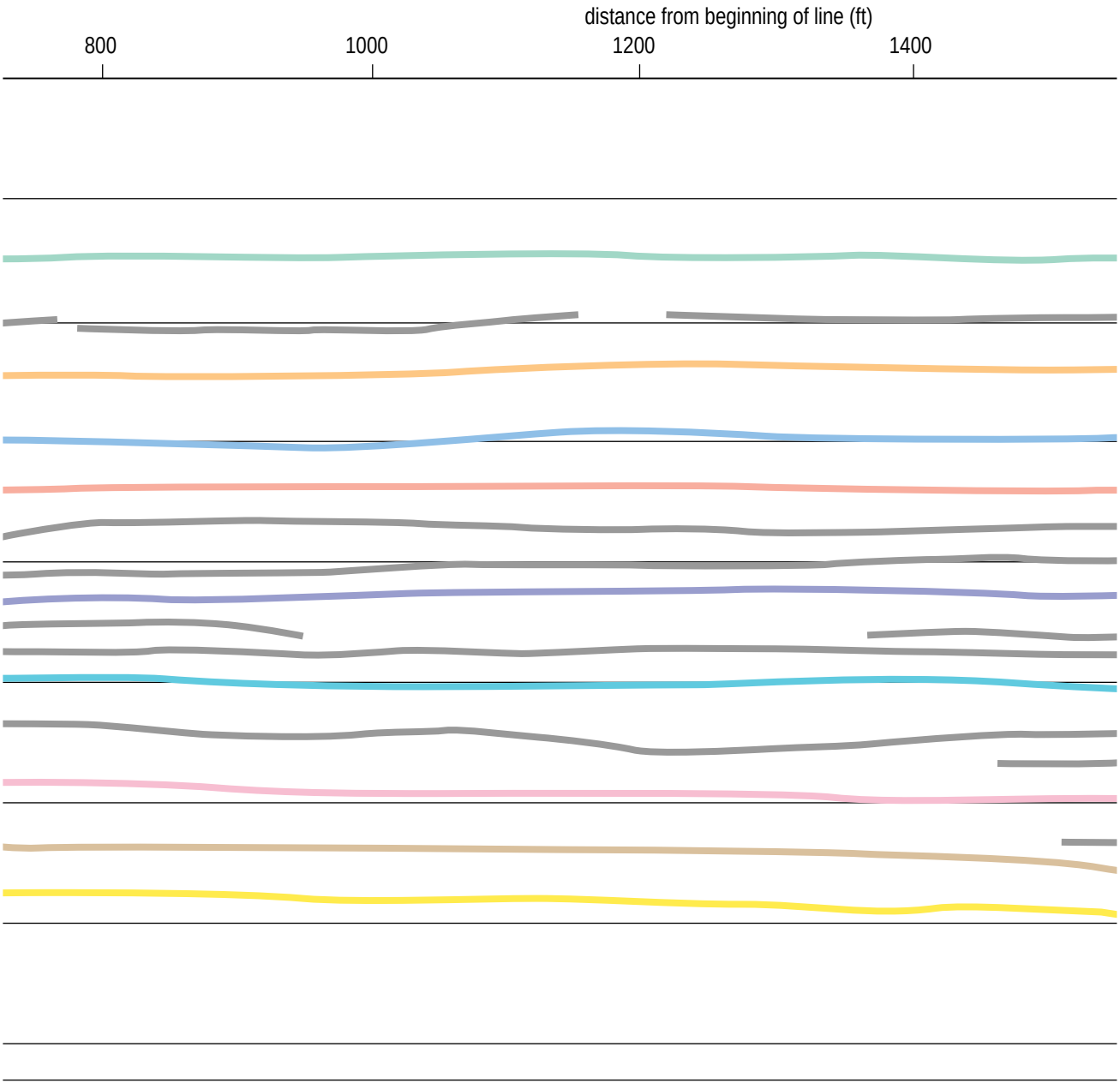

Figure 77b.

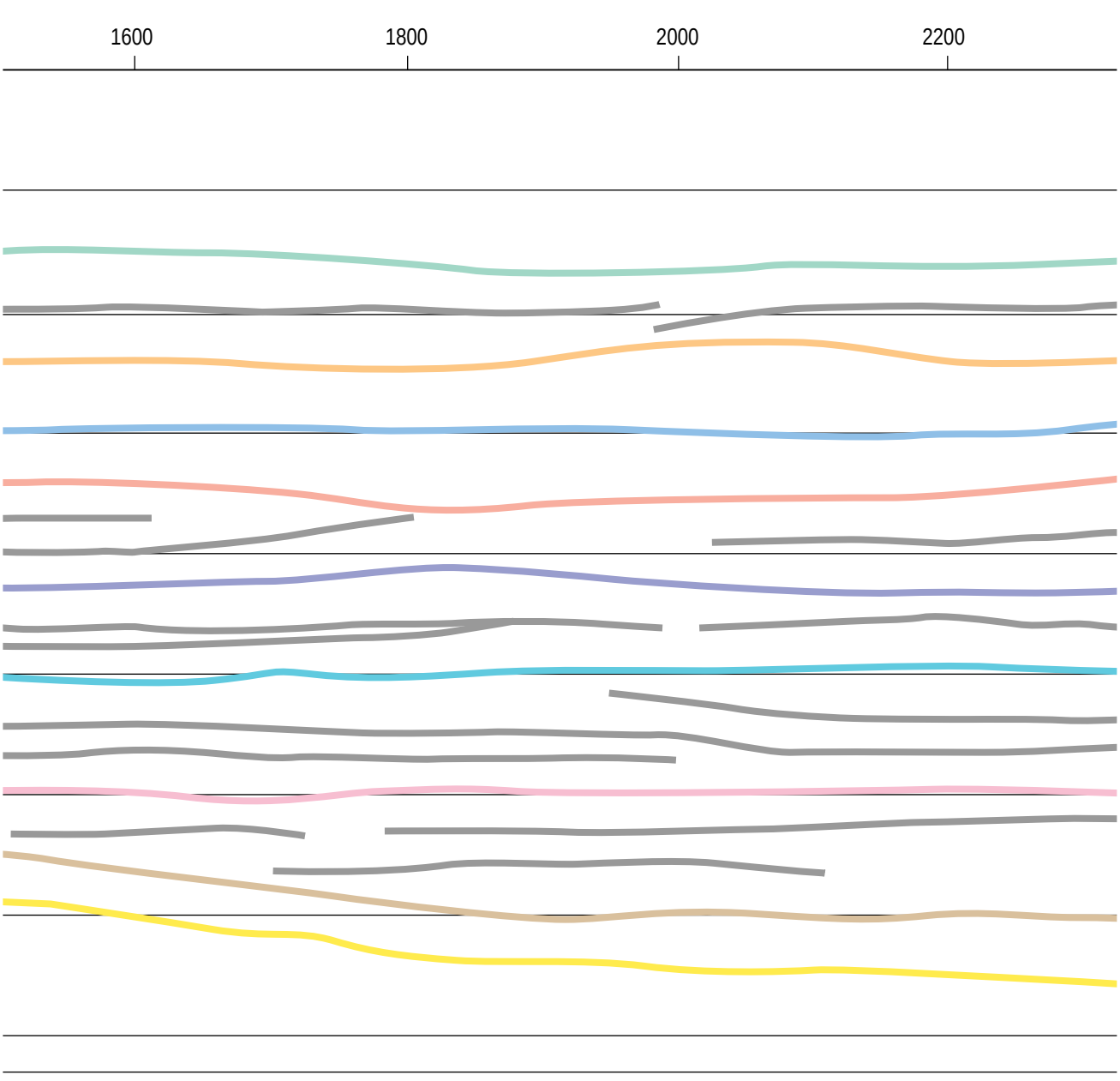

Figure 77c.

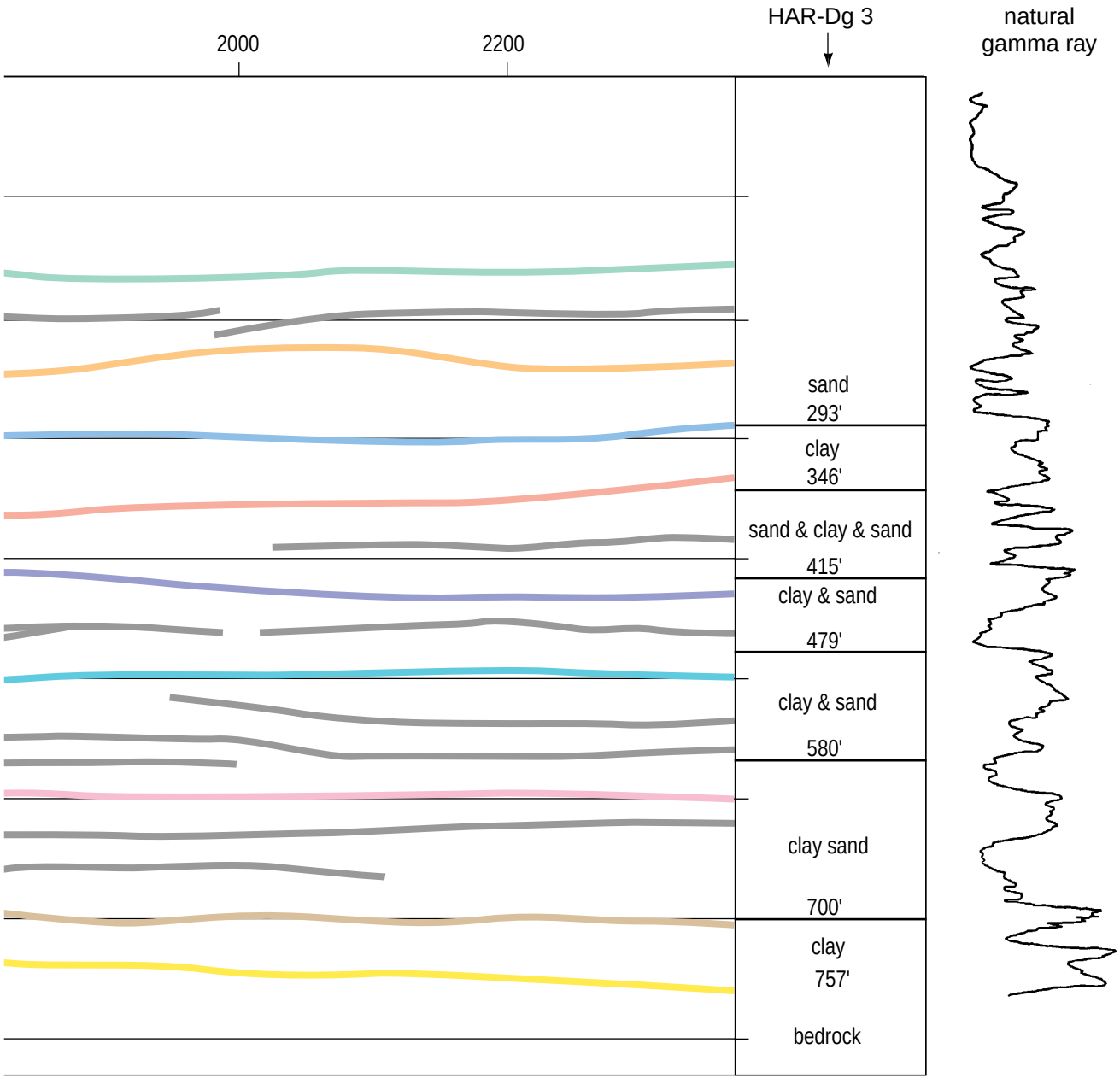
2000
2200
HAR-Dg 3
natural
gamma ray
sand
293'
clay
346'
sand & clay & sand
415'
clay & sand
479'
clay & sand
580'
clay sand
700'
clay
757'
bedrock

Figure 77d.

Accurate interpretation of all the minor changes in bed thickness and material types on CDP data from APG requires an integrated interpretation by both a geophysicist familiar with the seismic reflection data and a geologist with expertise in local geology and borehole information. From a geophysical perspective the half-dozen strong, coherent reflections interpreted on the Spesutie Island data are indicative of large acoustic impedance contrasts and probably represent abrupt vertical changes in material (Figure 76). Several anomalies interpreted as channel-like features are probably real and correspond to scour and infill episodes. Some of the apparent relative decrease in dominant frequency at Spesutie Island (in comparison to the other two sites) is due to increased depth of penetration, decreased lower corner frequency of the reflection bandwidth, and increased signal-to-noise ratio, making interference effects/tuning more evident (appear less like degradation in signal from noise).

The bedrock at Spesutie Island is very well defined with a scalloped/broken coherency similar to that observed at both the western boundary and the airstrip. From CDP 6020 south to about CDP 6180 the bedrock dips south at a rate of about 60 ft/mile, which is consistent with the regional 75 ft/mile (keeping in mind that the line orientation may not be perpendicular to strike). From about CDP 6180 to CDP 6270 a relatively steep-sided 40 ft deep channel feature appears to be cut into the bedrock surface. Based on average velocity estimations, the deepest part of this channel is about 750 ft below the ground surface. The shot gather used for parameter selection and field file event identification was acquired very near the north end the line, hence the 250 msec bedrock reflection hyperbola when maximum two-way travel time to bedrock on the south end of this line is almost 300 msec.

The geologic cross-section interpreted from the CDP stacked section presents a subsurface picture with excellent correlation to the borehole, but with a reduction in bed resolution as compared to the airstrip and western boundary lines (Figure 77). From the borehole lithology the interpreted interfaces correlate well with most of the described clay/sand contacts. Some contacts interpreted on borehole and geophysical logs are not clearly represented on the CDP stacked section. These missing units are likely due to either a conservative interpretation of interference effects or the abruptness and/or relative size of acoustic impedance contrast. A more aggressive interpretation would likely allow correlation of most, if not all, the borehole contacts with CDP stacked reflections.

Conclusions

Shallow seismic reflection is an effective technique at APG for imaging and nearly continuously mapping of contacts between different types of unconsolidated sediments and the sediment/bedrock contact. The detail and confidence provided by the shallow reflection data are not possible from drill data alone. Extrapolation of drill data from borehole to borehole prior to this reflection data set required significant speculation and assumptions about lithologic correlations. Extensive testing at APG was instrumental in fully evaluating the potential of the technique and optimum equipment and parameters necessary for acquiring multi-fold (redundant) profiles at several representative settings. Correlating the seismic reflection data borehole-to-borehole provided a high confidence continuous profile in areas previously requiring assumptions about and extrapolation of rapidly changing sedimentary sequences.

Subtle features of potential local hydrologic and geologic significance were identified with this 2-D seismic reflection survey that could not have been detected, much less imaged, with any other non-invasive method. Scour and infill patterns with a horizontal expanse of less than 200 ft and vertical extent of less than 20 ft were imaged at Spesutie Island. To even detect these features (and by no means fully image them) with drilling methods would have required closely spaced boreholes and significant expense. Horizontal resolution limits to depths of around 150 to 200 ft at APG averaged around 30 to 50 ft. Practical vertical bed resolution was around 10 to 15 ft at the three sites investigated during this study. While shallow seismic reflection is a very cost effective, non-invasive method of successfully imaging very detailed subsurface features and evaluating horizontal continuity of bedding (or at least acoustic impedance contrasts), it can not replace drilling and in the best of all worlds should be incorporated into a well orchestrated drilling program.

In this geometrically complex subsurface setting, accurate correlation of drill-determined geology with seismic reflection data requires a well defined velocity profile. The generalized geologic cross-sections constructed for this report were based on interval velocities calculated from average velocities which below about 170 ft were determined through curve fitting of reflection hyperbola. The largest potential source of error in both determining depth to reflectors and correlating reflecting events with drill-determined geologic contacts is the velocity function. For the geologic setting at APG and the type of problems to be solved there (both hydrologic and geologic) at minimum a velocity profile should be acquired in bore-

holes near any potential future seismic profile, and for maximum value, VSP and sonic log surveys should be acquired in as many existing boreholes as possible and should be part of all future drilling programs. With this type of information, future seismic reflection surveys will provide subsurface pictures with significantly less potential error associated with time-to-depth conversions and generalized geologic cross-sections.

Acknowledgments

This work was supported by the United States Army Corps of Engineers under Contract DACW39-94-C-0012. We graciously thank Jose Llopis for his valuable assistance during project preparation and data acquisition. We also thank P.Acker for graphics and Mary Brohammer for manuscript preparation and editorial suggestions.

References

Black, R.A., D.W. Steeples, and R.D. Miller, 1994, Migration of shallow seismic reflection data: *Geophysics,* 59, 402-410.

Crawford, J.M., W. Doty, and M.R. Lee, 1960, Continuous signal seismograph: *Geophysics*, 25, 95-105.

Gochioco, L.M., 1992, Modeling studies of interference reflections in thin-layered media bounded by coal seams: *Geophysics*, 57, 1209-1216.

Healey, J., J. Anderson, R.D. Miller, D. Keiswetter, D.W. Steeples, and B. Bennett, 1991, Improved shallow seismic-reflection source: Building a better Buffalo [Exp. Abs.]: Soc. Explor. Geophys. v. 1, p. 588-591.

Hunter, J.A., S.E. Pullan, R.A. Burns, R.M. Gagne, and R.S. Good, 1984, Shallow seismic-reflection mapping of the overburden-bedrock interface with the engineering seismograph—Some simple techniques: *Geophysics,* 49, 1381-1385.

Mayne, W.H., 1962, Horizontal data stacking techniques: Supplement to *Geophysics*, 27, 927-938.

Miller, R.D., 1992, Normal moveout stretch mute on shallow-reflection data: *Geophysics,* 57, 1502-1507.

Owens, J.P., 1969, Coastal Plain rocks of Hartford County; *In* The Geology of Hartford County, Maryland: Maryland Geological Survey.

Pullan, S.E., and J.A. Hunter, 1985, Seismic model studies of the overburden-bedrock reflection: *Geophysics*, 50, 1684-1688.

Sheriff, R.E., 1991, Encyclopedic dictionary of exploration geophysics: Geophysical Reference Series 1, Soc. of Explor. Geophys., Tulsa, Oklahoma.

Steeples, D.W., and R.D. Miller, 1990, Seismic-reflection methods applied to engineering, environmental, and ground-water problems: Soc. Explor. Geophys. Investigations in Geophysics, Investigations in Geophysics no. 5, Stan Ward, ed., *Volume 1: Review and Tutorial,* p. 1-30.

Swartzel, S., and P. Miller, 1992, Draft workplan for CERCLA remedial investigation feasibility study for Michaelsville Landfill: U.S. Army Corps of Engineers-Waterway Experiment Station (draft).

Vroblesky, D.A., and W.B. Fleck, 1991, Hydrogeologic framework of the coastal plain of Maryland, Delaware, and the District of Columbia: U.S. Geological Survey Professional Paper 1404-E.

Widess, M.D., 1973, How thin is a thin bed?: *Geophysics*, 38, 1176-1180.

Witten, C., S. Swartzel, and K. Blough, 1995, Aberdeen area conceptual hydro-geologic model: U.S. Army Corps of Engineers-Waterway Experiment Station. Technical report (draft).

Yilmaz, O., 1987, Seismic data processing; S.M. Doherty, Ed.; *in* Series: Investigations in Geophysics, no. 2, Edwin B. Neitzel, Series Ed.: Soc. of Explor. Geophys., Tulsa, Oklahoma.